The Design and Manufacture of Immediate-Release Optimal Solid Dosage Forms

by

Aron H. Blaesi

MSc, Mechanical Engineering
Swiss Federal Institute of Technology Zurich, 2009

Submitted to the
Department of Mechanical Engineering
in Partial Fulfillment of the Requirements for the Degree of

DOCTOR OF PHILOSOPHY IN MECHANICAL ENGINEERING

at the

MASSACHUSETTS INSTITUTE OF TECHNOLOGY

June 2014

Signature of Author: _____

Department of Mechanical Engineering
May 23, 2014

Certified by: _____

David E. Hardt
Ralph E. & Eloise F. Cross Professor of Mechanical Engineering
Doctoral Thesis Committee Chair

Accepted by: _____

David E. Hardt
Ralph E. & Eloise F. Cross Professor of Mechanical Engineering
Graduate Officer

This page is intentionally left blank.

The Design and Manufacture of Immediate-Release Optimal Solid Dosage Forms

by

Aron H. Blaesi

Submitted to the Department of Mechanical Engineering on May 23, 2014
in Partial Fulfillment of the Requirements for the Degree of
Doctor of Philosophy in Mechanical Engineering

ABSTRACT

Pharmaceutical manufacturing has traditionally been considered largely a matter of regulatory compliance. Consequently, it has been inefficient, but it is now increasingly being recognized as an opportunity for cost reduction. Recent initiatives by regulatory authorities, and by the industry, aim at easing regulations and encouraging process innovation. Even though significant improvements, especially in process control and minimization of process interruptions, have been achieved, the underlying process technology has not changed for decades. For example, typical process steps to produce the most common pharmaceutical products, immediate-release solid dosage forms, from drug substance and excipient are: blending, wet granulating, drying, milling and screening, blending, tableting, coating, and so on. A new process, such as blending combined with solvent-less, multi-component injection-molding could greatly simplify manufacturing. Injection-molding, however, yields a non-porous material, intrinsically different from the state-of-the-art powder-compacted, porous dosage forms. This may appear problematic, because current products rely on a large surface area-to-volume ratio to achieve immediate drug release. In addition, process rates previously achieved by injection-molding solid dosage forms have been comparably low—offsetting some of the benefits offered by that process.

In this thesis, an analytical approach is first developed to model drug release from non-porous dosage forms, comprising a fast eroding excipient and randomly distributed drug particles in it. The model considers the central role of microstructure in drug release. Particular importance is given to the role of clusters of connected, slowly eroding drug particles, and to the effect of drug particle protrusion, due to their slow erosion rate, from the eroding excipient surface. The model is validated by dissolution experiments. Good agreement is observed between the model and the experimental data. The drug release model is then used in product design for manufacturing as an optimization problem—with manufacturing performance as objective function and design specifications as constraints. It is found that the drug volume fraction needs to be about 0.5 to efficiently produce non-porous dosage forms in specification, which implies that an excessive amount of excipient material is required. Therefore, new product designs are proposed: a cellular excipient micro-structure with up to ten-fold reduction in excipient content. The new designs are further shown to allow injection-molding of immediate-release dosage forms that meet specifications with a three-fold increase in injection-molding process rate compared with conventional designs.

Doctoral Thesis Committee:

Prof. David E. Hardt (Committee chair)
Prof. Roger D. Kamm (Committee member)
Prof. Rohit Karnik (Committee member)
Prof. Charles L. Cooney (Committee member)

This page is intentionally left blank.

"Any intelligent fool can make things bigger, more complex, and more violent. It takes a touch of genius – and a lot of courage – to move in the opposite direction."

Albert Einstein

This page is intentionally left blank.

ACKNOWLEDGEMENTS

My time at MIT would not have been as wonderful and successful without the support of many people to whom I would like to express my deepest gratitude. First, I would like to thank my thesis committee, Prof. David Hardt (Chair), Prof. Charles Cooney, Prof. Roger Kamm and Prof. Rohit Karnik for their invaluable guidance, perspective, and insights. With knowledge, experience, and enthusiasm they rapidly identified gaps and limitations in my thinking processes, and helped me approach and solve the underlying challenging engineering problems. I am especially grateful to Prof. David Hardt, for forming and chairing a committee of such distinguished expertise. I am also very grateful to Dr. Nannaji Saka, for many helpful suggestions on several aspects of the thesis. Dr. Saka taught me how to think beyond what I learned in the classroom.

At its very beginnings, this thesis was supported by Novartis AG (Basel, Switzerland), which is gratefully acknowledged. I wish to thank Dr. Markus Krumme and Dr. Norbert Rasenack of Novartis AG for their insights and help in defining the topic of this work. I really enjoyed our meeting in Basel on the stunning Novartis campus.

Also, I am very grateful to Chancellor W. Eric L. Grimson for his kind advise and generous support during my stay at MIT.

I was further privileged to gain professional experience beyond my thesis project. I would like to thank Prof. Franz Hover and my colleagues in the teaching crew of the course *Dynamics and Controls II* for a very enriching and fun time. Also, I am very grateful to Prof. Cullen Buie, who encouraged me to apply to MIT, and together with his lab members greatly supported me in working on electrochemical problems.

For an amazing time at MIT of exchange, enriching discussions and collaborative learning I am particularly indebted to my ’mates in 35’, the ‘car-team of 2.810’, my quals study-groups, the ‘corporate entrepreneurship-team’, the ‘advanced corporate finance-team’, the ‘operations strategy-team’, the ‘biomedical inventions-team’ chaired by Dr. Warren Zapol and Dr. Rox Anderson, and the ‘Central machine shop-team’. Also, I am indebted to the Mechanical Engineering Graduate Office chaired by Leslie for administrative support during my time at MIT.

I would like to thank my friends of whom I would like to highlight the extended group of Martha boys and girls, my Swiss buddies in the area including SwissLinkBoston and Swissnexboston, Mr. Marc Redlich, Esq., and the ‘Legendaers’ for their help and making Cambridge such a great place to live in. My buddies back in Switzerland I would like to thank for staying close even though far away, and for keeping me updated on the good stories from home.

To my family, I would like to express my deepest gratitude for unlimited support in any matter. I would not be where I am without their tremendous help. Finally, I would like to thank Meryem for being simply the best!

CONTENTS

This page is intentionally left blank.

LIST OF FIGURES

LIST OF TABLES

CHAPTER I

INTRODUCTION

1.1 Background

The pharmaceutical industry, dedicated to producing medicines mainly in the form of tablets, capsules, injections, powders, syrups, and ointments, has been one of the most profitable and fastest growing industries for decades. It was ranked second by the Fortune magazine in terms of global industry profitability in 2009, just behind mining and crude oil production [1,2]. Global sales exceeded 950 billion USD in 2012. The economic success and the characteristics of the pharmaceutical industry are the legacy of several regulations and discoveries since the Great Depression.

Even though many drug products existed before the second world war, the number of basic medicines available was small and included mostly medicines that could relieve symptoms by easing pain or inducing sleep. A breakthrough that triggered the structural transformation of the industry from a manufacturing-focused producer of selected chemicals to a research-oriented sector was the discovery of antibiotics. Penicillin was the most important such molecule, and it became first available for practical purposes after 1940.

The scientific discoveries were followed by the decision of the US patent office that the use of molds to produce antibiotics could be patented. This incentivized drug companies to heavily invest in research to find treatments for the sheer magnitude of unmet medical needs. As a result, what is now called the period of ‘therapeutic revolution’ was launched and by 1950 well and truly under way. Corticosteroids, antihistamines, antidepressants, diuretics, and many other drug preparations helping to alleviate human ailment were discovered and developed during that time. The increase in drug discoveries was also reflected in patent activities. For example, the number of pharmaceutical patents, the majority product patents instead of process patents, grew from 138 in the period 1926-1930 to above 1500 in the period 1951-1955.

The rapid introduction of novel pharmaceutical products between 1940 and 1960 presented great social benefits in that great contributions to modern treatment of diseases were made. However, there were clear social costs offsetting these benefits to pharmaceutical innovation. Long-term adverse side effects of certain medicines, which could initially not be detected by physicians, patients, and often even the pharmaceutical firms, occasionally led to disastrous results. As a consequence of such social cost, national government regulation of product safety and efficacy has emerged in all developed countries. In the US, for example, a series of requirements have been issued since 1962, including regulations to specify good manufacturing practice (GMP), preclinical guidelines for toxicity testing, regulations that specify requirements for well-controlled investigations to produce substantial evidence of a product's efficacy, and others. Subsequent to the introduction of these regulations, the number of new drug approvals per year dropped significantly, and the industry was concentrated among larger firms. Competition in the industry, however, was still dominated by research and innovation in that a more efficacious or a better-marketed product would replace its predecessor [3-7].

A legislation introduced in 1984, which significantly changed the competitive dynamics of the pharmaceutical industry, was the Hatch-Waxman Act [8-14]. Hatch-Watchman amendments were released upon the continuous political debate on drug prices. They aimed at providing affordable, high-quality medicines by easing some of the previously made stringent product testing requirements for market entry by generic drugs. The generic drug industry developed since then has focused on producing off-patent drugs. The characteristics of the generic drug industry are fundamentally different from the innovator drug industry in that competition is to a large extent by product price instead of product innovation. Generics tended to enter the market at wholesale prices 40 - 70% of those prevailing before the original drug's patent expired, and the generic price could fall below 20% of the pre-competition price if more competitors entered. By 2005, the share of US generic prescription units (i.e., tablets) increased from about 19% to about 60%, whereas the generic market share in dollars was about 20% in 2005. As a result of such changes in regulations for market access of generic products, the pressure on drug prices has increased, saving the consumers double digit billions of dollars every year [15].

Apart from the availability of inexpensive generic substitutes, new managed care net-

works and governmental price regulations that emerged in the 1980s and 1990s further put drug prices under scrutiny. At the same time, research expenditures were growing at high rates, but the number of approved drugs per year did not increase. Still today, the pharmaceutical industry environment is characterized by increasing generic competition, increasing bargaining power of buyers, and declining R&D productivity. Consequently, both innovator and generic drug companies are forced to reduce the costs of their internal processes in order to maintain high profit margins [7].

The present cost structure in the pharmaceutical industry is illustrated in Fig. 1.1, with the costs of goods sold (COGS), general expenses (G. Exp.), and research and development expenses (R&D) as main cost drivers. The costs of goods sold account for about 24% of revenues of innovator pharmaceutical companies and about 50% of revenues of generic drug companies [16]. They consist to a large extent of the manufacturing costs, which in total (including upstream and downstream processes) today amount to about 200 billion USD per year. Reducing pharmaceutical manufacturing costs by pharmaceutical manufacturing process innovation therefore could free up resources for generic producers to strengthen their position, and for innovator companies to invest in marketing and research in order to capitalize on opportunities in emerging markets and unmet medical needs [17-19].

Excellence in manufacturing has in several industries led to superior performance far beyond the optimization of COGS [20-22]. Simplification of manufacturing operations has shown significant reductions in product and process development time and costs, reductions of the environmental footprint, and improvement of traceability and product quality, just to name a few. Moreover, excellence in manufacturing is difficult to imitate. The Toyota Motor Corporation, for example, which between 1950 and 1980 pioneered lean manufacturing (i.e., a new way of highly efficient manufacturing), still is one of the most successful car companies in the world. It showed the highest net profit as well as the highest market capitalization among global car companies by a considerable margin in 2005 [23].

Optimization of pharmaceutical manufacturing, however, was up to recently an expensive and risky undertaking. Particularly, extensive supplemental documentation, increased FDA inspection, and the risk of production delays were feared if changes in

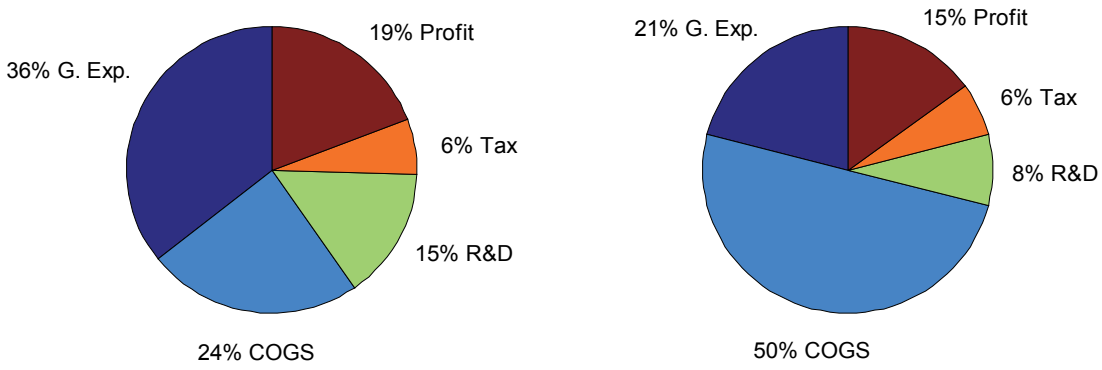

(a) (b)

Figure 1.1: Cost structure in percentage of total revenues: (a) patent-protected pharmaceuticals and (b) generic pharmaceuticals. The costs are subdivided into the units Costs of Goods Sold (COGS), General Expenses (G. Exp.), Research and Development (R&D), Tax, and Profit. (Data from Ref. [16]).

process technology were made in this highly regulated manufacturing environment. In 2000, GMPs that were considerably modified last in 1978, were still in use. Fundamental innovations in process technology have not been made in the period between 1978 and 2000. Consequently, the performance of traditional pharmaceutical manufacturing is below the one of other comparable industries, such as the food or chemical industries [24]. Most noticeably, it was found that the cycle time of traditional pharmaceutical downstream manufacturing, which simply consisted of the process steps to manufacture an oral pharmaceutical tablet out of the raw materials drug substance (i.e., active pharmaceutical ingredient (API)), excipients, and other processing aids, was above 25 days on the average with a standard deviation of the same order of magnitude [18,25]. It was further remarkable that the sum of the effective process times of the individual processes was just a small part of the measured, average cycle time, whereas most time was spent on off-line quality control (QC).

The inefficiencies in pharmaceutical manufacturing, and limited incentives for process innovation, have induced the FDA together with the industry to develop an important new initiative – Pharmaceutical cGMPs for the 21st Century: A Risk-Based Approach. This initiative simplifies regulations of process innovation if Quality by Design (QbD) principles are applied (i.e., product understanding, process understanding, and process control based on sound science and quality risk management) [26-29].

These new regulations have caused industry and academia to heavily devote resources to the optimization of pharmaceutical manufacturing, which currently is expensive and inefficient. The most important advances that have been made, and to a certain extent implemented since the release of the new initiative, are in in-process and online quality control. QbD principles together with process analytical technologies (PAT) even allowed the development of pharmaceutical processing in an integrated, continuous way. Continuous manufacturing can eliminate several inefficiencies intrinsic to the traditional batch processes. Most noticeably, equipment utilization and quality control processes are optimized resulting in the improvement of a variety of manufacturing performance measures [30-38]. The physical principles of the underlying pharmaceutical downstream manufacturing process technologies, however, to a large extent still have not been further developed. Optimization of pharmaceutical downstream manufacturing within the space of

traditional process technologies is limited, and a fundamental technological change is required to achieve significant improvements in pharmaceutical downstream manufacturing performance beyond the benefits of state-of-the-art continuous manufacturing.

1.2 Thesis Objective

The focus of this work is on the design and manufacture of immediate-release solid dosage forms. Immediate-release solid dosage forms belong to the most standard drug products. Most often, they are in the form of orally delivered pharmaceutical tablets or capsules. Moreover, immediate-release solid dosage forms are typically the first way to deliver a new drug that can be administered orally, and further are desirable for several therapeutic reasons, such as immediate pain relief or control of blood sugar levels.

It is well known that the manufacturing efforts required to produce a specific product are to a large extent determined by product design. Therefore, product design considered here is crucial to enable manufacturing improvement. Alternative designs of immediate-release solid dosage forms that are fundamentally different from the state-of-the-art are studied in this thesis. They consist of non-porous or cellular materials instead of the powder-based, porous bulk of current products. Consequently, a broad space of alternative manufacturing processes that could potentially be applied to produce such product designs is opened up. In turn, significant improvements in manufacturing efficiency are offered, far beyond the opportunities using state-of-the-art technologies.

The objective of this thesis is to develop a methodology which, based on the desired product properties, allows to determine the specifics of the non-porous or cellular drug design for optimal product performance at improved downstream manufacturing efficiency. Accordingly, the aspects emphasized on in this work are to: (a) investigate the relevant parameters that affect product performance, and the dependence of product performance on these parameters, (b) investigate the relevant parameters to affect manufacturing efficiency, and the dependence of manufacturing efficiency on these parameters, and (c) identify the optimal non-porous or cellular designs to improve product performance and manufacturing efficiency for given product requirements.

1.3 Thesis Outline

Chapter 2 presents the specifications of immediate-release solid dosage forms together with the state-of-the-art powder-based, porous immediate-release dosage form design and respective manufacturing technologies. Subsequently, non-porous immediate-release dosage forms are discussed, in terms of the process value stream map and manufacturing processes, and in terms of their performance and ability to meet the specifications of immediate-release dosage forms.

In Chapter 3, present drug release models of solid dosage forms are reviewed. First, drug release mechanisms that characterize the physical phenomena by which drug is released from the solid dosage form are given. State-of-the-art mathematical models to describe drug release, particularly for non-swellable matrix diffusion, matrix swellable, and surface erodible systems are then presented. Finally, the suitable mechanism for non-porous immediate-release dosage forms is identified.

A new model for drug release of non-porous immediate-release dosage forms based on mass transfer limited surface erosion is developed in Chapter 4. The erosion rate and mass transfer rate of a surface eroding disk is first derived for single-phase systems. The model is then extended to systems of multiple phases. Specifically, equations to describe drug release from a disk consisting of drug and excipient are developed. Moreover, effects of surface roughness which arise during erosion of the drug-excipient composite disk are discussed.

Chapter 5 addresses experimental validation of the non-porous, immediate-release model. Materials and methods applied for sample preparation and execution of erosion and dissolution experiments are first described. The experimental results so obtained are then presented and the immediate-release model developed for the rate of drug release, as well as erosion rate and dissolution time is validated based on the experimental data.

Immediate-release solid dosage forms must have satisfactory mechanical properties for processing and handling. Thus in Chapter 6, the mechanical properties of selected immediate-release excipients and composite materials are presented.

In Chapter 7, designs for optimal immediate-release solid dosage forms are developed. The design guidelines are found by combining manufacturing efficiency objective functions with design specifications along with the previously developed dissolution model. A set of optimal designs with unique features and manufacturing processes are presented. Finally, in Chapter 8 the salient conclusions of the present work are summarized.

References

[1] From the website: http://www.imshealth.com/deployedfiles/imshealth/Global/... Content/Corporate/Press%20Room/Total_World_Pharma_Market_Topline_... metrics_2012.pdf, as of February 1, 2014.

[2] From the website: http.//money.cnn.com/magazines/fortune/global500/2009/… performers/industries/profits, as of February 1, 2014.

[3] P. Temin, 1978, The evolution of the modern pharmaceutical industry, MIT Press, Cambridge, MA.

[4] P. Temin, 1980, Taking Your Medicine: Drug Regulation in the United States, Harvard University Press. Cambridge, MA.

[5] Committee on Technology and International Economic and Trade Issues of the Office of the Foreign Secretary, Commission on Engineering and Technical Science, National Research Council, 1983, The Competitive Status of the U.S. Pharmaceutical Industry: The Influences of Technology in Determining International Industry Competitive Advantage, National Academy Press, Washington, DC.

[6] W.D. Reekie, 1975, The Economics of the Pharmaceutical Industry, The Macmillan Press LTD, London, UK.

[7] G.P. Pisano, 1997, The Development Factory: Unlocking the Potential of Process Innovation, Harvard Business School Press, Boston, MA.

[8] R.E. Caves, M.D. Whinston, M.A. Hurwitz, Patent Expiration, Entry, and Competition in the U.S. Pharmaceutical Industry, Brooking Papers on Economic Activity: Microeconomics, 1991, 1-48.

[9] H. Grabowski, J.M. Vernon, Brand Loyalty, Entry, and Price Competition in Pharmaceuticals after the 1984 Drug Act, J. Law Econ., 1992, 35, 331-350.

[10] F.M. Scherer, The Pharmaceutical Industry, in A.L. Culyer, J.P. Newhouse, 2000, Handbook of Health Economics, Elsevier.

[11] R.G. Frank, D.S. Salkever, Generic Entry and the Pricing of Pharmaceuticals, Journal of Economics and Management Strategy, 1997, 6, 75-90.

[12] E.R. Berndt, The U.S. Pharmaceutical Industry: Why Major Growth in Times of Cost Containment?, Health Affairs, 20, 100-114.

[13] D. Reiffen, M.R. Ward, Generic Industry Dynamics, The Review of Economics and Statistics, 2005, 87, 37-49.

[14] T.L. Regan, Generic Entry, Price Competition, and Market Segmentation in the Prescription Drug Market, International Journal of Industrial Organization, 2008, 26, 930-948.

[15] A.A. Signore, T. Jacobs, 2005, Good Design Practices for GMP Pharmaceutical Facilities, Taylor & Francis Group, Boca Raton, FL.

[16] P. Basu, G. Joglekar, S. Rai, P. Suresh, J. Vernon, Analysis of Manufacturing Costs in Pharmaceutical Companies, J. Pharm. Innov., 2008, 3, 30-40.

[17] P. Suresh, P.K. Basu, Improving Pharmaceutical Product Development and Manufacturing: Impact on Cost of Drug Development and Cost of Goods Sold of Pharmaceuticals, J. Pharm. Innov., 2008, 3, 175-187.

[18] T. Friedli, M. Kickuth, F. Stieneker, P. Thaler, J. Werani, 2006, Operational Excellence in the Pharmaceutical Industry, Editio Cantor Verlag, Aulendorf, Germany.

[19] G.K.P. Raju, 1994, Pharmaceutical Manufacturing: Structuring Organizational Learning Through "Benchmarking", Master's Thesis, Massachusetts Institute of Technology, Cambridge, MA.

[20] R.H. Hayes, S.C. Wheelwright, 1984, Restoring our Competitive Edge Competing Through Manufacturing, John Wiley & Sons, Hoboken, NJ, USA.

[21] G.P. Pisano, Knowledge, Integration, and the Locus of Learning: An Empirical Analysis of Process Development, Strategic Management Journal, 1994, 15, 85-100.

[22] R.H. Hayes, G.P. Pisano, Manufacturing Strategy: At the Intersection of two Paradigm Shifts, Production and Operations Management, 1996, 5, 25-41.

[23] S.L. Beckman, D.B. Rosenfield, 2008, Operations Strategy Competing in the 21st Century, McGraw-Hill, New York, NY.

[24] L. Abboud, S. Hensley, New Prescription for Drug Makers: Update the Plants, The Wall Street Journal, September 3, 2003.

[25] G.K. Raju, Pharmaceutical Manufacturing: New Technology Opportunities, FDA Science Board Meeting, 2001.

[26] U.S. Department of Health and Human Services, 2004, Pharmaceutical cGMPs for the 21st century – A risk-based approach, Final report, Food and Drug Administration, Rockville, MD.

[27] U.S. Department of Health and Human Services, 2004, Guidance for industry: PAT – A framework for innovative pharmaceutical development, manufacturing, and quality assurance, Food and Drug Administration, Rockville, MD.

[28] A. Hussain, A Final Report on PAT and Manufacturing Science, FDA Science Board Meeting, 2004.

[29] M. Narhi, K. Nordstrom, National GMP Regulations and Codes and International GMP Guides and Guidelines: Correspondences and Differences, in S.C. Gad, 2008, Pharmaceutical Manufacturing Handbook: Regulations and Quality, John Wiley & Sons, Hoboken, NJ.

[30] H. Leuenberger, New Trends in the Production of Pharmaceutical Granules: Batch vs. Continuous Processing, Eur. J. Pharm. Biopharm, 2001, 52, 289-296.

[31] A.A. Signore, T. Jacobs, 2005, Good Design Practices for GMP Pharmaceutical Facilities, CRC Press, Boca Raton, FL.

[32] L. Pernenkil, C.L. Cooney, A review on the continuous blending of powders, Chem. Eng. Sci., 2006, 61, 720-742.

[33] R.P. Cogdill, T.P. Knight, C.A. Anderson, J.K. Drennen, The financial returns on investment in process analytical technologies and lean manufacturing: Bench marks and case study, J. Pharm. Innov., 2007, 2, 38-50.

[34] R. Singh, M. Ierapetritou, R. Ramachandran, An engineering study on the enhanced control and operation of continuous manufacturing of pharmaceutical tablets via roller compaction, Int. J. Pharm., 2012, 438, 307-326.

[35] K.V. Gernaey, A.E. Cervera-Padrell, J.M. Woodley, A perspective on PSE in pharmaceutical process development and innovation, Comput. Chem. Eng., 2012, 42, 15-29.

[36] G.M. Troup, C. Georgakis, Process systems engineering tools in the pharmaceutical industry, Comput. Chem. Eng., 2013, 51, 157-171.

[37] R.P Cogdill, Case for Process Analytical Technology: Regulatory and Industrial Perspectives, in S.C. Gad, 2008, Pharmaceutical Manufacturing Handbook: Regulations and Quality, John Wiley & Sons, Hoboken, NJ.

[38] T. Friedli, M. Goetzfried, P. Basu, Analysis of the Implementation of Total Productive Maintenance, Total Quality Management, and Just-In-Time in Phamaceutical Manufacturing, J. Pharm. Innov., 2010, 5, 181-192.

This page is intentionally left blank.

CHAPTER II

ON POROUS AND NON-POROUS IMMEDIATE-RELEASE DOSAGE FORMS

2.1 Introduction

In this chapter, the specifications of immediate-release solid dosage forms are first listed. State-of-the-art powder-based, porous immediate-release dosage form designs and manufacturing process technologies are then reviewed. Subsequently, the advantages and disadvantages of non-porous, immediate-release dosage forms are discussed in terms of the process value-stream map and manufacturing efficiency, and in terms of the non-porous immediate-release dosage form's performance and capability to meet the specifications.

2.2 Specifications of Immediate-Release Solid Dosage Forms

As with most pharmaceutical products, immediate-release solid dosage forms are assigned measurable technical specifications, which guarantee a product's efficacy and safety once the performance of the API it contains has been proven in clinical studies. The specifications are highly regulated. Detailed specifications of US-marketed immediate-release solid dosage forms are defined in the United States Pharmacopeia and in guidelines published by the International Conference on Harmonisation (ICH). They determine testing methods and acceptance criteria for drug product critical quality attributes [1-7]. Such attributes include the amount of active substance in the dosage form, uniformity of dosage units (i.e., the coefficient of variation in the amount of the active substance), dissolution time (i.e., the time it takes to dissolve the active ingredient contained in the drug product), level of impurities, hardness/friability, water content, and microbial limits. Table 2.1 lists an overview of testing methods and acceptance criteria that can be considered as reference standard for immediate-release tablets and capsules.

Table 2.1: Typical specifications of immediate-release solid dosage forms given by the regulator. The requirements are listed after the release of the batch as well as after the stability retest, where the product has been exposed to accelerated storage conditions for a prolonged period of time.

Test	Method	Requirements	Batch release	Stability retest
Description	Appearance by visual examination	Shape, color, surface according to product description	+	+
Identity	UV, HPLC	Corresponds to the reference	+	-
Mean mass	Weighing scale	According to USP	+	-
Dissolution	UV-Dissolution	Not less than 80% of the declared content in 30 mins, according to the acceptance table of USP	+	+
Water content	Karl Fischer titration	< 5%	+	
Water content	Karl Fischer titration	< 6%	-	+
Residual solvent	HPLC	According to the document ICH Q3C, depending on the class of the solvent	+	-
Degradation products	HPLC	According to the document ICH Q3B, depending on drug content	+	+
Uniformity of dosage units	Uniformity of dosage units by content uniformity	Coefficient of variation in drug content (CV) < 5%, or according to USP	+	-
Assay by HPLC	HPLC	95%-105% of the declared content	+	+
Microbial limits	Total aerobic microbial count, Total yeast and mold count, etc.	Meet the requirements of Ph. Eur., USP, and JP	+	-

It is possible though that the details of such testing methods and acceptance criteria deviate from the usual case presented in Table 2.1. This happens particularly if the manufacturer and regulatory agencies agree that different specifications or testing methods are to be used to guarantee the product's safety and efficacy (i.e., product quality).

The specifications need to be met throughout the shelf life of the drug product. At the time of registration, however, shelf-life stability testing is often not completed. Statistical extrapolation of limited stability data to the proposed shelf life is therefore the standard practice [8]. Finally, in addition to the specifications that guarantee a product's continuing safety and efficacy, the product needs to be patient compliant. Conventional tablets and capsules, for example, need to be of a certain size, shape, and taste in order to be appealing and easy to swallow.

2.3 State-of-the-Art Design and Manufacture of Immediate-Release Solid Dosage Forms

2.3.1 State-of-the-Art Design

Immediate-release solid dosage forms in the configuration of a tablet or capsule today are powder-based materials with porous bulk containing excipients and drug at the specified content [9-12]. The framework of state-of-the-art product designs is illustrated in Fig. 2.1, where the drug volume fraction, the product geometry, the drug particle size, the granulated excipient particle size, the porosity, and the coating formulation and thickness are design parameters. These parameters typically need to be within a moderately tight window in order for the product to satisfy the specifications. Drug volume fraction and drug particle size, for example, need to be such that the product contains the specified drug amount at the desired content uniformity. Physicochemical properties along with the porosity and size of granulated excipient particles and API particles must allow immediate dissolution of the API. Product size, shape and coating thickness must be within a range that gives a patient compliant product and sufficiently fast API dissolution.

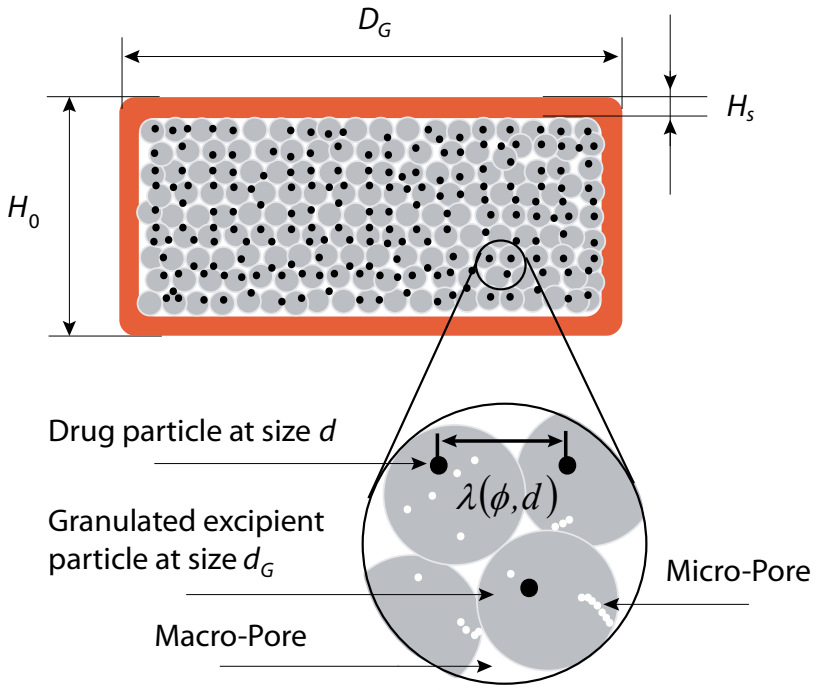

Figure 2.1: Schematic of the state-of-the-art design of a coated immediate-release tablet with drug particles embedded in compressed excipient granules giving a large surface area-to-volume ratio.

The state-of-the-art product design is well suited to meet the specifications of immediate-release solid dosage forms. Most importantly, the porous, hydrophilic nature of the state-of-the-art bulk material enables the dissolution medium to rapidly wet and penetrate the pores. Even though the compressed granulated particles are agglomerated in the dry state, they deagglomerate once in contact with the dissolution medium, causing the product to lose mechanical strength and disintegrate. This creates an extraordinarily large particle-dissolution medium interface (i.e. surface area), and it significantly reduces distances of drug mass transfer within the excipient matrix. Both the resulting large surface area and the reduced drug mass transfer distances within the excipient give a large surface area-to-volume ratio with fast dissolution rate to guarantee that the product meets specifications of immediate-release [13].

An additional advantage of current designs is their high flexibility in terms of drug content. Typically, constraints on dissolution, hardness/friability, and manufacturability currently limit the maximum drug mass- and volume fraction to a range of about 0.5 - 0.9, whereas the minimum drug mass- and volume fraction can be as low as 0.001. This allows the design of products with a large range in drug content, from less than 0.5 mg API to above 500 mg API, within the desired swallowable product dimensions.

2.3.2 State-of-the-Art Manufacturing Process Technologies

For most of the past, pharmaceutical manufacturing has been done by a batch process. The traditional batch process gives high flexibility in the equipment use and process parameters applied. However, it accounts for low equipment utilization and hence large equipment idle times, scale-up challenges, and often manual, time-consuming quality control. These inefficiencies, particularly in the manufacture of high volume products, have led the industry, with the support of regulatory authorities, to develop new process analytical technologies (PAT) that allow automated, integrated quality control. This opened opportunities for integrated, continuous pharmaceutical manufacturing systems that are now commercially available [14-18].

Even though tremendous improvements in equipment utilization, quality control processes, and scale up complications can be achieved by applying continuous manufactur-

ing technologies, manufacturing of the state-of-the-art immediate-release tablets is far from straightforward. The major reason for pharmaceutical manufacturing being a complicated process lies in the current product design. It relies, for example, on a material based on compressed powder, which prior to compression needs to be thoroughly prepared for it to possess the required properties on particle size, flowability, wettability, compressibility, and uniformity.

A value-stream map of the standard state-of-the-art pharmaceutical downstream manufacturing process is illustrated in Fig. 2.2. Raw API and excipient powder at the required particle size are fed into the manufacturing system which outputs a coated product, consisting of such unit operations as blending and granulating, drying, milling and screening, blending, tableting, and coating [5,19,20]. Further, solvents are usually added to the system to support the unit operations granulation and coating. The technical specifics of the present process steps are briefly outlined below. Table 2.2 gives an overview of state-of-the-art equipment used along with process times of the individual process steps of both batch and continuous processes.

Blending and Granulating: Blending and granulating is a crucial step in the manufacture of a drug product. It is accountable for mixing API and excipient to the required uniformity. Also, it provides the mixture the physical and physicochemical properties needed to achieve the desired product performance and efficient further downstream processing. Wet granulation, the most commonly applied granulation process, in most batch processing cases is done using a high shear granulator. High-shear granulators can also be used for powder blending prior to wet granulation. They consist of a mixing bowl with a main impeller revolving in the horizontal plane, an auxiliary chopper revolving in either the vertical or horizontal plane, and a nozzle that allows controlled solvent addition. Blending and wet granulation is a three-stage process comprising a dry powder blending stage, a solvent infusion stage, and a wet mass stage to generate granules of API and excipient at uniform size [21,22]. The total process time of blending and wet granulating using a high shear granulator is typically 20 – 90 minutes.

An alternative equipment technology that allows granulation in a continuous manner at minimum equipment idle time, hence high equipment utilization, is pharmaceutical extrusion [21]. Pharmaceutical extruders are typically designed as either single screw or twin

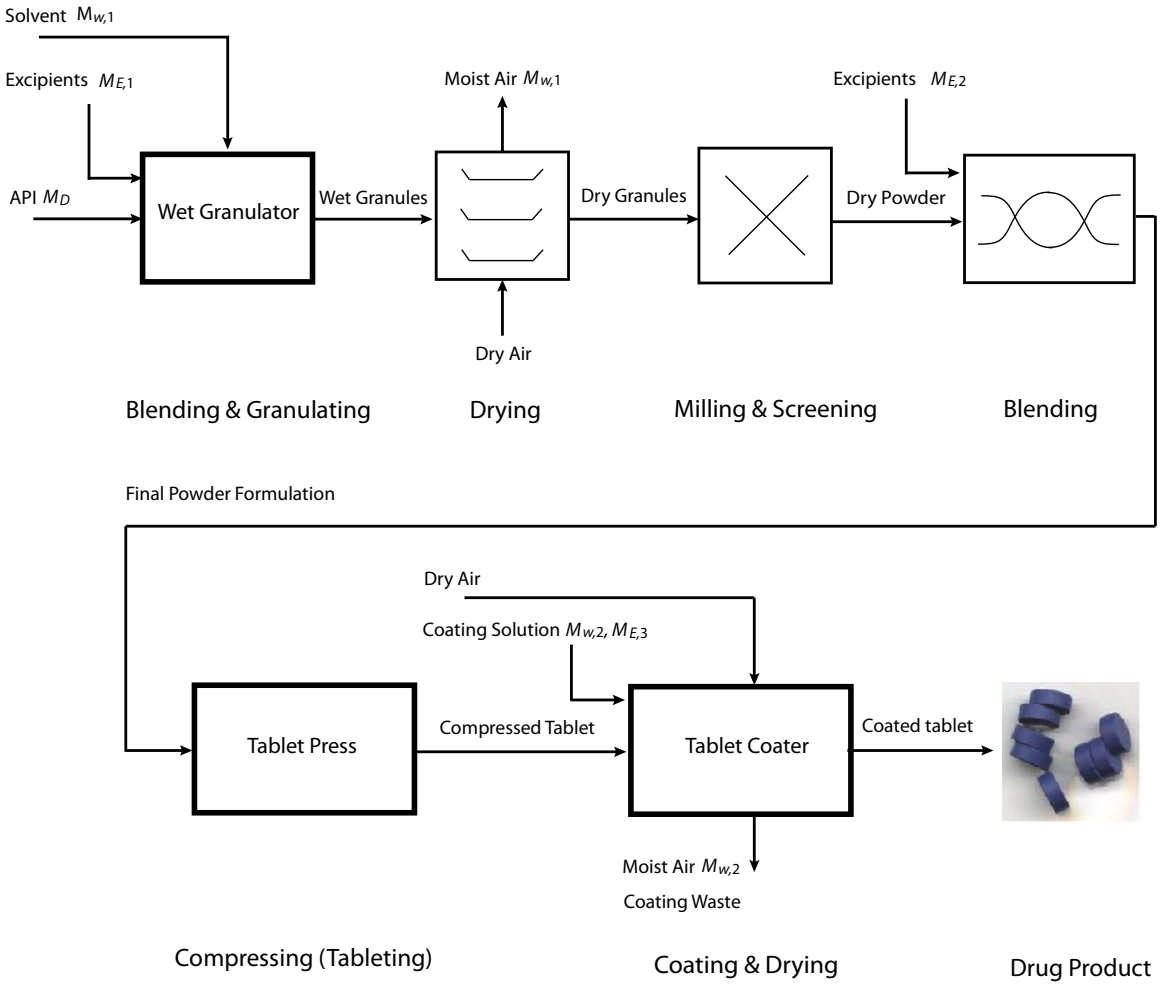

Figure 2.2: A typical value-stream map of the state-of-the-art pharmaceutical downstream manufacturing process to produce immediate-release solid dosage forms. It comprises the unit operations blending and granulating, drying, milling and screening, blending, compressing (tableting), and coating.

screw. Twin-screw extruders in combination with precise volumetric or gravimetric feeders have some mixing capability, however, a powder blending stage for mixing API and excipient is often required to precede extrusion. The residence time of the material in the extruder is determined by the screw geometry, the extruder aspect ratio, *L/D*, and the rotation rate of the screw(s). Generally, extruder residence times are 10 seconds – 15 minutes, and in combination with a continuous blending or feeding unit, process times of about 3-30 minutes can be achieved.

The nature of wet granulation to use a solvent for material plastification is one of the biggest drawbacks of this universally applied process. An amount of 0.7 – 1.1 weight % of solvent relative to the total amount of API and excipient is typically required, which is simply material waste that needs to be disposed of. Depending on the API and formulation, dry granulation (roller compaction) or hot melt granulation can also be used to serve the purpose of granulation [23-25]. The advantage of these technologies is that they are solventless, and hence produce no material waste in the granulation unit. Also, the need for a drying stage subsequent to the granulation step is obviated, saving a unit operation.

Drying: In the drying step subsequent to wet granulation, the solvent is removed from the granules. Conventional dryers are tray dryers, tumbling dryers, and fluid-bed dryers [26,27]. Fluid-bed dryers usually show the fastest drying rates and can be operated in either batch or continuous mode, whereas tray dryers typically show the slowest drying rate and can be operated in batch mode only. The process time is generally limited by mass transfer of liquid solvent in the granule to gaseous solvent in the gas phase. A process time of 2-20 minutes is easily achievable using a continuously operating fluid bed dryer with small lot size.

Milling and Screening: Milling and screening of granules serves the purpose of reducing the size and the variation in size of the granules to improve the ease of further downstream processing and the resulting product properties. The basic principle of mills is to apply a large enough force on the granules so that they crush. A number of process technologies can be used for milling, including hammer mills, ball mills, and edge and runner mills [28,29]. Typical unmilled pharmaceutical granules have a size of 400 – 800 μm, whereas a powder size of 100 – 400 μm is generally desirable for further downstream processing and to achieve the required product properties. A residence time between less

Table 2.2: Unit operations, typical equipment, and process times of the state-of-the-art batch (B) and continuous (C) pharmaceutical downstream processes.

Unit operation	Equipment	Process type (B/C)	Process time[a] (min)
Blending and granulating	High shear mixer	B	20 – 90
	Twin screw extruder	B/C	3 – 30[b]
	Roller compactor	-	-
Drying	Tray dryer	B	> 600
	Tumbling dryer	B	120 – 240
	Fluidized bed dryer	B	20 – 60
	Fluidized bed dryer	C	2 – 20
Milling & screening	Hammer mill	B/C	1 – 10
Blending	V-Blender	B	5 – 50
	Continuous Blender	C	1 – 10
Compressing/tableting	Tablet press	B/C	< 5
Coating	Pan coater	B	60 – 120
	Fluidized bed coater	B	60 – 120
	Continuous coater	C	6 – 30
	Total	B	107 – 875
	Total	C	14 – 105

[a] Depends on the underlying API and formulation, as well as the scale and type of the process. The numbers indicated represent values that apply to the manufacture of most standard products. Process time in the batch process is considered as the minimum time required to process an entire batch without considering times required for quality control, equipment setup, material transfer, etc. The process time in the continuous process is considered as the minimum residence time of the material in the system, without considering times for quality control, times the material waits in buffers, times for material transfer, etc.

than 1 minute and 10 minutes, for example, is typical for Hammer mills to achieve the desired size reduction.

Blending: In the blending unit, a small amount of lubricant (e.g. 1-5 wt% magnesium stearate) is added to the milled and screened powder to improve powder flowability and to reduce powder stickiness in the tablet press. Conventional blenders are V-blenders, double cone blenders, ribbon blenders, and low shear mixers. Continuous ribbon blenders, for example, are available that achieve a blending residence time of 1-10 minutes.

Tableting: Tablets are made by compression molding of the as-produced powder in a tablet press. Tablet presses are comparably expensive machines that require high maintenance. The pressure-time profile during compression is adjustable during the contact time, and it is a critical parameter to produce a product at the desired mechanical strength and porosity [30-32]. The maximum compaction pressure is of the order of 100 MPa, giving a compaction force above a ton for conventional tablet dimensions. The total material residence time to produce one tablet, including feeding time, contact time, and the ejection time, is typically less than 5 minutes. Process rates that are currently achieved with production-scale tablet presses are of the order of 200,000 – 1000,000 tablets per hour.

Coating: Coating of the tablets so produced is the final step in the manufacture of a product. Coating is typically done in the form of solvent-based film coating, where an atomized coating solution consisting of solvent and the coating formulation is sprayed on the target surface. In order for the coating solution to have the desired physical properties, the solid content in the liquid typically should be 10-20 wt%. Once the solution is on the target surface which is in continuous movement, the solvent is evaporated. A controlled balance between spray rate and solvent vaporization rate by concurrently applying heated air flow to the target surface is maintained. Conventional coating equipment examples are coating pans and fluidized bed coaters [33,34]. The minimum coating thickness is typically about 50-70 μm, which is required to achieve the desired contrast ratio in color.

Furthermore, in immediate-release solid dosage forms the coating must not cause significant delay in API dissolution. This can usually be achieved if the coating consists of a rapidly eroding material and has a thickness of less than 150 – 200 μm. The total amount of coating material deposited is hence equal to about 3-30 mg which is reflected in a weight gain per tablet due to the coating of about 2-5 wt%. The total material waste pro-

duced (i.e., solvent and coating waste) intrinsic to the solvent based coating process is of the order of 10 - 50% of the tablet weight. The rate of coating deposition along with the desired coating thickness determine the process time. Typically, the process time is about 1-2 hours in batch processes, and a deposition rate of about 4 μm/min is achieved in continuous coaters.

2.4 Non-Porous Immediate-Release Dosage Forms

2.4.1 Manufacturing Optimization by Thorough Removal of Waste

The overriding principle followed here to develop a new, optimized pharmaceutical downstream manufacturing system is elimination of waste – similar to the methods proposed previously aimed at manufacturing efficiency improvements in a variety of industries [35-37]. Waste includes anything other than the minimum of resources, in the form of equipment, materials, workers, etc., that are absolutely essential to manufacture products with the desired specifications. This implies, applied to the pharmaceutical downstream manufacturing process, the minimization of the number of processing steps, process time, amount of excipient used, amount of solvent used, and even equipment complexity.

The most crucial step in achieving manufacturing innovation is product design, as the number and type of process steps required to produce a product are determined largely by its design [38,39]. Instead of the state-of-the-art powder-based porous product design, which requires excessive resources to give a coated product, here immediate-release solid dosage forms based on much simpler non-porous material designs are considered. This opens a wide range of manufacturing processes which could fundamentally change the way pharmaceuticals are made and provide significant improvements in downstream manufacturing.

2.4.2 Value-Stream Map for the Manufacture of Non-Porous Immediate-Release Dosage Forms

The manufacture of non-porous products of the size of a conventional tablet or capsule can be done, for example, by several of the highly efficient processes currently used for forming operations in the plastics industry: injection-molding, hot-melt extrusion, and hot-melt casting. Injection-molding using a multi-shot injection-molding machine allows mixed API and excipient material, as well as the coating material, both in powder form, to be fed into it providing a coated finished product as output. Plastification of the pharmaceutical material to form the product, and subsequent solidification of the material is done via phase change within the material, instead of addition and removal of a solvent. This process opens opportunities for manufacturing optimization by reducing the number of unit operations, process time, and material waste. Fig. 2.3 illustrates a schematic of the value-stream map of such a downstream pharmaceutical manufacturing process with only 2 unit operations. Raw API and excipient are fed into a mixing unit which provides the required raw materials to be fed into the injection molding machine together with the coating formulation.

2.4.3 Mixing of API and Excipient

Mixing of API and excipient in powder form can be done using commercially available equipment, such as V-blenders, rotating cubes, or continuous ribbon blenders [19,20,29,40]. In order that powders may be mixed, the individual particles must move relative to each other. Mixing process rate is determined by the size of the equipment divided by the mixing time required to achieve the desired uniformity in content. Mixing time is an important variable for characterizing mixing performance and to optimize the process rate at a certain equipment size. Typically, the mixing residence time is of the order of 1-10 minutes using a continuous powder blender as shown in Fig. 2.4.

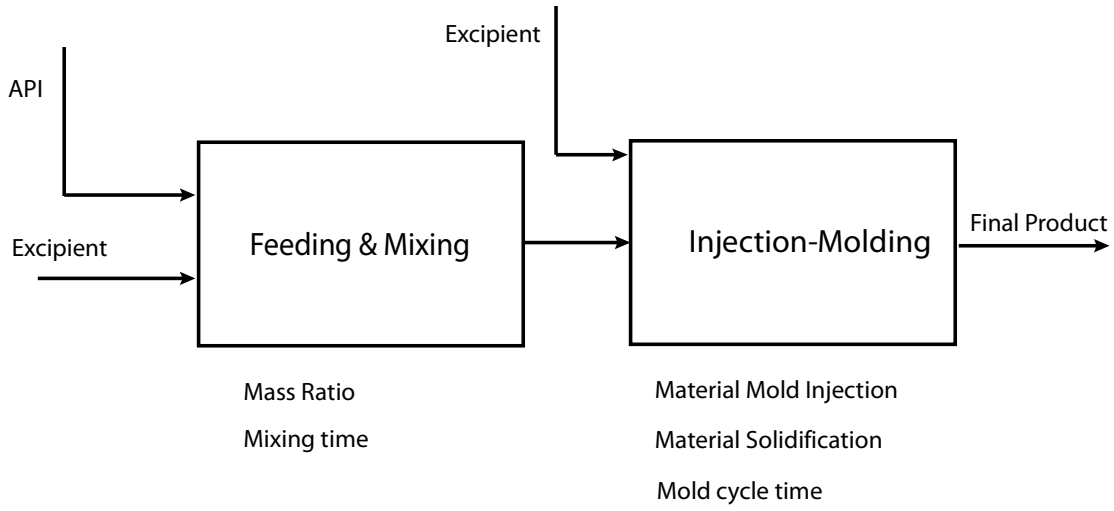

Figure 2.3: Value-stream map of the proposed pharmaceutical downstream manufacturing process to produce non-porous immediate-release dosage forms comprising the unit operations feeding and mixing, as well as injection-molding.

2.4.4 Injection-Molding to Manufacture Solid Dosage Forms

Also, it has been shown that single and multi-component injection-molding to produce solid dosage forms can be done using commercially available equipment [41-44]. The injection-molding process comprises solid material feeding, material plastification, melt distribution, melt injection, melt solidification, and part ejection. All these individual steps are typically done in a time of 2 – 10 minutes using a conventional injection-molding machine as shown in Fig. 2.5. The most relevant parameter in injection-molding is the rate at which a product can be produced determined by the mold cycle time, t_{cycle}, which is the sum of injection time, cooling time (i.e. solidification time) and mold resetting time (i.e. mold opening, part ejection, mold closing) [45-48]. Typical mold cycle times for tablets with conventional melt processable materials and geometries of thickness above 5 mm are above 15 seconds. This may be problematic, because even if the number of cavities in the mold is at the upper bound of 512, the number of dosage forms produced per hour will be less than 150,000, which is below the 200,000 – 1,000,000 tablets per hour that can be produced with a conventional powder compaction process [49].

2.4.5 Performance of Porous versus Non-Porous Immediate-Release Dosage Forms

It is shown above that, by just changing product design from the current powder-based, porous material structure to a simpler non-porous design, the number of unit operations is reduced from 6 to 2, process time is reduced from about 14 – 105 minutes (process time of state-of-the-art continuous systems) to about 3 – 20 minutes, and solvents are eliminated. Despite the technological maturity and the high manufacturing efficiency at which products comparable to solid dosage forms can be produced using the injection-molding process, it still is a niche process in pharmaceutical manufacturing in that it is applied to manufacture only certain types of long-term drug-releasing implants and controlled-release oral solid dosage forms. A compelling reason why injection-molding is not widespread in pharmaceutical manufacturing is that it has so far not been shown under what conditions immediate-release formulations could be produced using the injection molding process. A preliminary evaluation of injection-molding as a technology to produce tablets

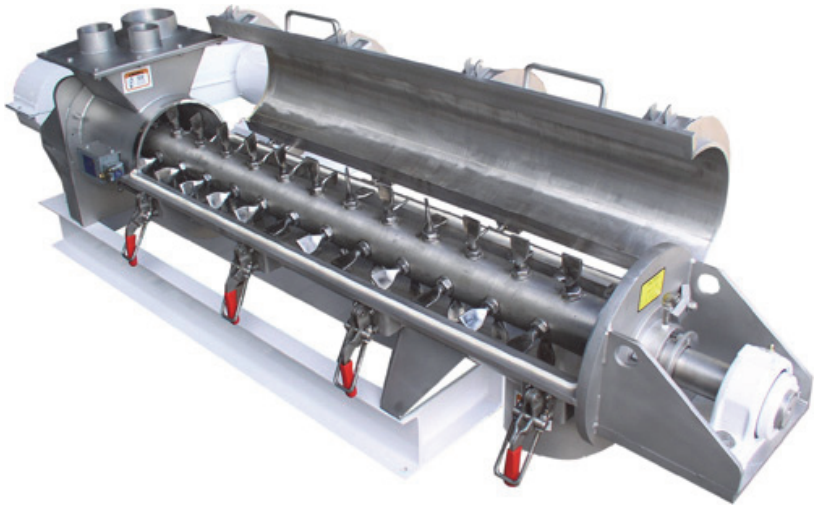

Figure 2.4: Illustration of a powder blender applicable for continuous mixing of pharmaceutical powders [source: http://www.scottequipment.com/HST-continuous-blender.html, as of February 4, 2014].

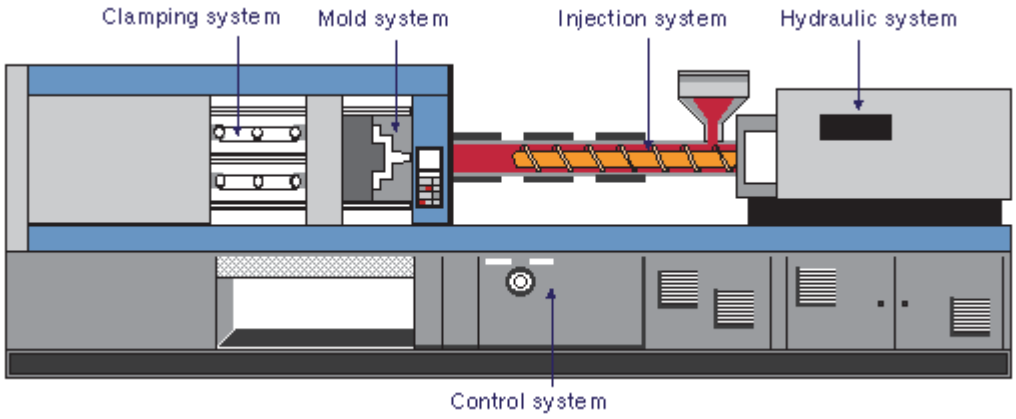

Figure 2.5: Schematic drawing of an injection molding machine with hydraulic injection actuation system applicable for producing solid dosage forms [source: http://www.dc.engr.scu.edu/cmdoc/dg_doc/develop/process/control/b1000001.htm, as of February 4, 2014].

was performed by Cuff et. al [49]. The formulation used was Polyethylene glycol 8000 (PEG 8000), an excipient with low melting temperature commonly used in immediate-release formulations, together with a small molecule API in the ratio 7:3 by weight. Excellent results in terms of the amount of chemical degradation products, drug content uniformity, and mechanical properties were achieved. However, only one formulation with one out of four APIs tested met the specifications on dissolution time.

Drug release from non-porous, injection-molded dosage forms is significantly different from the porous dosage forms produced by conventional powder-based forming processes. As illustrated in Fig. 2.6, soon after a porous dosage form is placed in the dissolution medium, the medium penetrates the pores. Upon penetration of the medium, the matrix becomes physically unstable. Initially, the size of the pores is increased, and eventually, the matrix loses its mechanical integrity and disintegrates into granules, aggregates, and fine particles. The large surface area-to-volume ratio that develops rapidly after the porous dosage form is placed into the dissolution medium is crucial for immediate drug release. Non-porous material, by contrast, prevents dissolution medium from rapidly penetrating through pores into the bulk of the matrix to disintegrate the dosage form into particles. The surface area-to-volume ratio is comparably small, and the release of drug from the core is intrinsically blocked. It is evident that this may be favorable for long-term release applications, but it is not obvious under what conditions immediate drug release is feasible (Fig. 2.7).

2.5 Problem Statement

It may be stated, therefore, that non-porous designs of immediate-release solid dosage forms offer manufacturing improvements, but the following issues must be addressed:
(1) *Drug release*—the conditions to achieve the desired immediate drug release profile using a non-porous dosage form, (2) *Excipients*—the type and amount of excipient needed for the product to have the required properties, and (3) *Process rate*— parameters that affect the rate of the new process and how process rate can be further optimized.

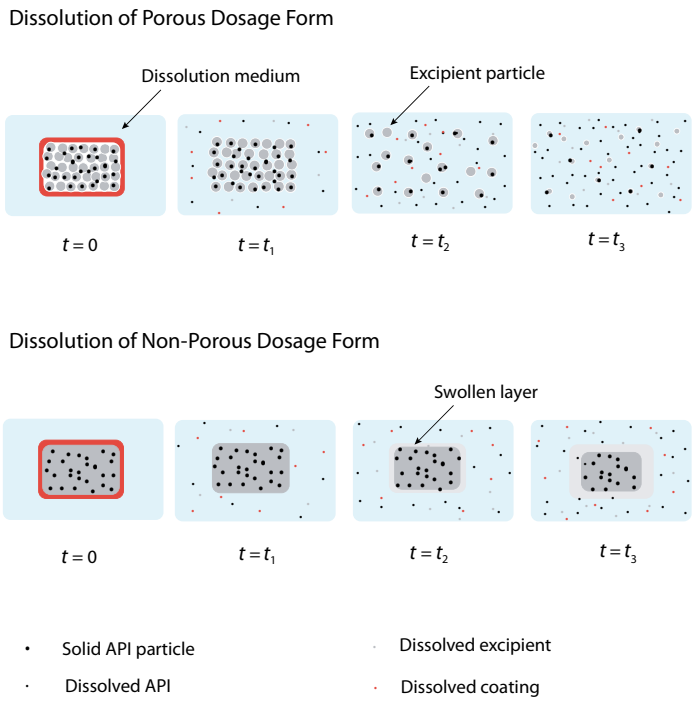

Figure 2.6: Dissolution of porous and non-porous dosage forms. Powder-based, porous immediate-release dosage forms are rapidly penetrated by dissolution medium causing the dosage form to disintegrate into small particles with large surface area-to-volume ratio for rapid drug release. Non-porous dosage forms, by contrast, do not disintegrate into small particles.

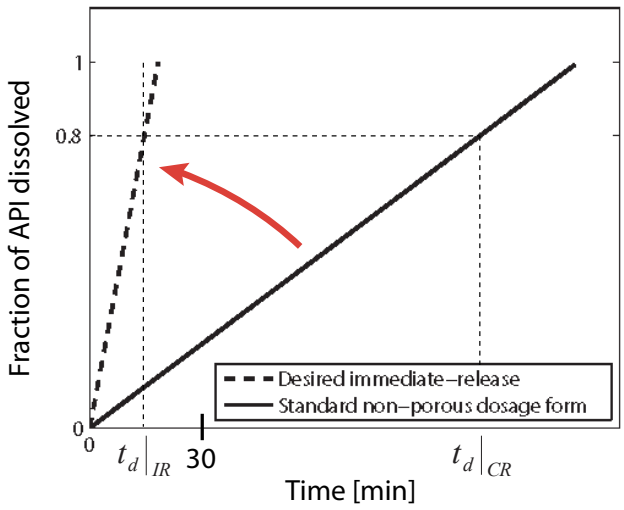

Figure 2.7: Dissolution profile of a standard non-porous dosage form and the desired profile of a non-porous immediate-release dosage form.

2.6 Summary

The state-of-the-art porous structure of the immediate-release dosage forms is well suited, due to the large surface area-to-volume ratio for rapid drug release. Manufacture of current porous dosage forms, however, is inefficient because a large number of unit operations and long process times are required to produce such products. A non-porous structure, which could be produced by simply mixing of API and excipient followed by injection-molding, for example, improves efficiency in manufacturing such products by reducing the number of unit operations from 6 to 2, process time from about 14 – 105 minutes to about 3 – 20 minutes, and eliminating solvents. Some of the benefits of manufacturing by using the injection-molding process, however, are inadequate because the process rates that can be achieved are currently lower than the rates of conventional powder compaction processes. Furthermore, the non-porous structure of injection-molded material does not allow rapid penetration of dissolution medium inside it. Therefore, non-porous dosage forms do not disintegrate into smaller units once they are put into the dissolution medium in contrast to the porous counterparts, resulting in a small surface area-to-volume ratio. This is advantageous for long-term drug release applications, but it may be problematic if immediate-release is the goal. Modeling of drug release from non-porous dosage forms tailored to immediate drug release is required to determine the parameters and conditions that must be satisfied so that non-porous immediate-release dosage forms could be produced. Knowledge of the design constraints given by such analytical dissolution models in turn could allow predictive product design for optimizing manufacturing.

References

[1] The U.S. Pharmacopeial Convention, US Pharmacopeia, USP 35-NF 30.

[2] ICH Working Group, Q6A Specifications: Test Procedures and Acceptance Criteria for New Drug Substances and New Drug Products: Chemical Substances, 1999, International Conference on Harmonisation of Technical Requirements of Phamaceuticals for Human Use.

[3] ICH Working Group, Q3B(R2) Impurities in New Drug Products, 2006, International Conference on Harmonisation of Technical Requirements of Pharmaceuticals for Human Use.

[4] W. Chen, S. Stithit, J.Y. Zheng, R. Hwang, Specification Setting and Manufacturing Process Control for Solid Oral Drug Products, in Y. Qiu, Y. Chen, G.G.Z. Zhang, L. Liu, W.R. Porter, 2009, Developing Solid Oral Dosage Forms Pharma ceutical Theory and Practice, Academic Press, Burlington, MA.

[5] M.E. Aulton, K.M.G Taylor, 2013, Aulton's Pharmaceutics The Design and Manufacture of Medicine, fourth edition, Churchill Livingstone Elsevier, London, UK.

[6] C.Y. Wu, L.Z. Benet, Predicting Drug Disposition via Application of BCS: Transport/Absorption/Elimination Interplay and Development of a Biopharmaceutics Drug Disposition Classification System, Pharmaceutical Research, 2005, 22, 11-23.

[7] M. Long, Y. Chen, Dissolution Testing of Solid Products, in Y. Qiu, Y. Chen, G.G.Z. Zhang, L. Liu, W.R. Porter, 2009, Developing Solid Oral Dosage Forms Pharmaceutical Theory and Practice, Academic Press, Burlington, MA.

[8] J.T. Carstensen, C.T. Rhodes, 2000, Drug Stability: Principles and Practices, Third Edition, Marcel Dekker, New York, NY.

[9] H.A. Lieberman, L. Lachman, 1980, Pharmaceutical Dosage Forms: Tablets, Volume 1, Marcel Dekker, New York, NY.

[10] L.L. Augsburger, S.W. Hoag, 2008, Pharmaceutical Dosage Forms: Tablets, Volume 1: Unit Operations and Mechanical Properties, Third Edition, Informa Healthcare, New York, NY.

[11] L.L. Augsburger, S.W. Hoag, 2008, Pharmaceutical Dosage Forms: Tablets, Volume 2: Unit Operations and Mechanical Properties, Third Edition, Informa Healthcare, New York, NY.

[12] L.L. Augsburger, S.W. Hoag, 2008, Pharmaceutical Dosage Forms: Tablets, Volume 3: Unit Operations and Mechanical Properties, Third Edition, Informa Healthcare, New York, NY.

[13] H.A. Lieberman, L. Lachman, 1981, Pharmaceutical Dosage Forms: Tablets, Volume 2, Marcel Dekker, New York, NY.

[14] G.K. Raju, Pharmaceutical Manufacturing: New Technology Opportunities, FDA Science Board Meeting, 2001.

[15] U.S. Department of Health and Human Services, 2004, Pharmaceutical cGMPs for the 21st century – A risk-based approach, Final report, Food and Drug Administration, Rockville, MD.

[16] U.S. Department of Health and Human Services, 2004, Guidance for industry: PAT – A framework for innovative pharmaceutical development, manufacturing, and quality assurance, Food and Drug Administration, Rockville, MD.

[17] A. Hussain, A Final Report on PAT and Manufacturing Science, FDA Science Board Meeting, 2004.

[18] J. Markarian, Optimizing Solid Dosage Manufacturing, Pharm. Tech., 2014, 38, 24-28.

[19] H.A. Lieberman, L. Lachman, 1981, Pharmaceutical Dosage Forms: Tablets, Volume 1, Marcel Dekker, New York, NY.

[20] H.A. Lieberman, L. Lachman, 1981, Pharmaceutical Dosage Forms: Tablets, Volume 3, Marcel Dekker, New York, NY.

[21] D.M. Parikh, 2010, Handbook of Pharmaceutical Granulation Technology, third edition, Informa Healthcare, New York, NY.

[22] L. Liu, M. Levin, P. Sheskey, Process Development and Scale-up of Wet Granulation by the High Shear Process, in Y. Qiu, Y. Chen, G.G.Z. Zhang, L. Liu, W.R. Porter, 2009, Developing Solid Oral Dosage Forms Pharmaceutical Theory and Practice, Academic Press, Burlington, MA.

[23] I. Ghebre-Sellassie, C. Martin, 2003, Pharmaceutical Extrusion Technology, Marcel Dekker, Basel, Switzerland.

[24] J. Breitenbach, Melt extrusion: from process to drug delivery technology, Eur. J. Pharm. Biopharm., 2002, 54, 107-117.

[25] M.M. Crowley, F. Zhang, M.A. Repka, S. Thumma, S.B. Upadhye, S.K. Battu, J.W. McGinity, C. Martin, Pharmaceutical Applications of Hot-Melt Extrusion: Part I, Drug Dev. and Ind. Pharm., 2007, 33, 909-926.

[26] T. J. Smith, G. Sackett, P. Sheskey, L. Liu, Development, Scale-up, and Optimization of Process Parameters: Roller Compaction, in Y. Qiu, Y. Chen, G.G.Z. Zhang, L. Liu, W.R. Porter, 2009, Developing Solid Oral Dosage Forms Pharmaceutical Theory and Practice, Academic Press, Burlington, MA.

[27] M.E. Aulton, Drying, in M.E. Aulton, K.M.G Taylor, 2013, Aulton's Pharmaceutics The Design and Manufacture of Medicine, fourth edition, Churchill Living stone Elsevier, London, UK.

[28] A.J. Hickey, D. Ganderton, 2001, Pharmaceutical Process Engineering, Marcel Dekker, Basel, Switzerland.

[29] J.T. Carstensen, 2001, Advanced Pharmaceutical Solids, Marcel Dekker, New York, NY.

[30] G.Alderborn, C. Nystrom, 1996, Pharmaceutical Powder Compaction Technology, Marcel Dekker, New York, NY.

[31] G. Alderborn, Tablets and compaction, in M.E. Aulton, K.M.G Taylor, 2013, Aulton's Pharmaceutics The Design and Manufacture of Medicine, fourth edition, Churchill Livingstone Elsevier, London, UK.

[32] D. Natoli, M. Levin, L. Tsygan, L. Liu, Development, Optimization, and Scale-up of Process Parameters: Tablet Compression, in Y. Qiu, Y. Chen, G.G.Z. Zhang, L. Liu, W.R. Porter, 2009, Developing Solid Oral Dosage Forms, Pharmaceutical Theory and Practice, Academic Press, Burlington, MA.

[33] S. Porter, G. Sackett, L. Liu, Development, Optimization, and Scale-up of Process Parameters: Pan Coating, in Y. Qiu, Y. Chen, G.G.Z. Zhang, L. Liu, W.R. Porter, 2009, Developing Solid Oral Dosage Forms Pharmaceutical Theory and Practice, Academic Press, Burlington, MA.

[34] S.C. Porter, Coating of tablets and multiparticulates, in M.E. Aulton, K.M.G Taylor, 2013, Aulton's Pharmaceutics The Design and Manufacture of Medicine, fourth edition, Churchill Livingstone Elsevier, London, UK.

[35] Y. Sugimori, K. Kusunoki, F. Cho, S. Uchikawa, Toyota production system and Kanban system Materialization of just-in-time and respect –for-human system' Int. J. Prod. Res., 1977, 15, 553-564.

[36] J.P Womack, D.T. Jones, 1996, Lean Thinking, Banish Waste and Create Wealth in your Corporation, Free Press, New York, NY.

[37] S.L. Beckman, D.B. Rosenfield, 2008, Operations Strategy Competing in the 21st Century, McGraw-Hill, New York, NY.

[38] G. Boothroyd, Product design for manufacture and assembly, Computer-Aided Design, 1994, 26, 505-520.

[39] G. Boothroyd, P. Dewhurst, W.A. Knight, 2011, Product Design for Manufacture and Assembly, Third Edition, CRC Press, Boca Raton, FL.

[40] L. Pernenkil, C.L. Cooney, A review on the continuous blending of powders, Chem. Eng. Sci., 2006, 61, 720-742.

[41] A. Rothen-Weinhold, K. Besseghir, E. Vuaridel, E. Sublet, N. Oudry, F. Kubel, R. Gurny, Injection-molding versus extrusion as manufacturing technique for the preparation of biodegradable implants, Eur. J. Pharm. Biopharm., 1999, 48, 113-121.

[42] T. Quinten, T. De Beer, C. Vervaet and J.P. Remon, Evaluation of injection moulding as a pharmaceutical technology to produce matrix tablets, Eur. J. Pharm. Biopharm., 2009, 71, pp. 145-154.

[43] T. Quinten, T. De Beer, F.O. Onofre, G. Mendez-Montealvo, Y.J. Wang, J.P. Remon, C. Vervaet, Sustained-Release and Swelling Characteristics of Xanthan Gum/Ethylcellulose-Based Injection Moulded Matrix Tablets: in Vitro and in Vivo Evaluation, J. Pharm. Sci., 2011, 100, 2858-2870.

[44] L. Zema, G. Loreti, A. Melocchi, A. Maroni, A. Gazzaniga, Injection Molding and its application to drug delivery, J. Contr. Rel., 2012, 159, 324-331.

[45] G. Boothroyd, P. Dewhurst, W.A. Knight, Design for Injection Molding, in G. Boothroyd, P. Dewhurst, W.A. Knight, 2011, Product Design for Manufacture and Assembly, Third Edition, CRC Press, Boca Raton, FL.

[46] I.I. Rubin, 1972, Injection Molding Theory and Practice, John Wiley & Sons, Hoboken, NJ.

[47] T. Osswald, L.S. Turng, P. Gramann, 2008, Injection Molding Handbook, Second Edition, Carl Hanser Verlag, Munich, Germany.

[48] Z. Tadmor, C.G. Gogos, 2006, Principles of Polymer Processing, John Wiley & Sons, Hoboken, NJ.

[49] G. Cuff, F. Raouf, A preliminary evaluation of injection molding as a technology to produce tablets, Pharmaceut. Tech., 1998, 22, 96-106.

CHAPTER III

REVIEW OF DRUG RELEASE MODELS OF SOLID DOSAGE FORMS

3.1 Introduction

In this chapter, the mechanisms by which drug release occurs are first reviewed. An overview of previous models of drug release is then given, and a drug release mechanism suitable for non-porous immediate-release dosage forms is selected. The limitations of the state-of-the-art models to describe drug release by this mechanism are then discussed and highlighted in the context of aiming to model drug release from non-porous immediate-release dosage forms for predictive product design.

3.2 Drug Release Mechanisms

Drug release is the process by which drug is transferred from the solid state inside the dosage form to the suspended or dissolved states in the dissolution medium. It is evident, therefore, that a necessary property of pure solid drug material is to dissolve when in contact with dissolution medium [1-4]. Further, the kinetics of pure drug dissolution, which depends on the intrinsic properties of the pure drug material and the dissolution medium, plays an important role in drug release. Pure drug is typically dissolved by erosion, where the surface of the solid material dissolves with no change in its composition. Modification of solubility and erosion characteristics of pure drug in the dissolution medium therefore allows to effect dissolution kinetics of the pure drug molecule.

Design and synthesis of the drug molecule is, however, beyond the scope of this thesis. Rather, the focus is on the role of dosage form design (i.e., formulation, geometry, microstructure, etc.) on drug release kinetics. Given the dissolution properties of the pure drug, the dosage form design determines the crucial characteristics of drug release, such as the rate at which dissolution medium can facilitate pure solid drug to be dissolved, or the ki-

netics by which dispersed drug in a matrix is released into the dissolution medium. The way the drug is transferred from the dosage form to the dissolution medium is the mechanism and is crucial for the kinetics of drug release.

Extensive reviews on the mechanisms of drug-release have been published by Langer and Peppas [6] for controlled-release systems, by Siepmann and Peppas for HPMC-based drug-release systems [7], and Wise [8] edited a book on controlled release where state-of-the-art models for various types of drug release systems are given, including matrices, membrane controlled reservoir systems, and erodible systems. Costa and Sousa Lobo reviewed mainly empirical models that have been developed so far to describe drug release [8]. Three major drug release mechanisms, and combinations thereof, are generally accepted to be dominant: erosion, swelling, and diffusion (Fig. 3.1).

In erodible systems, both the drug and the excipients dissolve into the dissolution medium. While dissolution of the drug, as mentioned above, usually does not include any changes in its composition, dissolution of the excipient can be either physical or chemical. Physically eroding systems do not comprise any change in material composition upon erosion. In chemically eroding excipients, on the other hand, material dissolution is induced by a chemical reaction (e.g. hydrolytic or enzymatic degradation) that converts the solid material into water soluble units when in contact with the dissolution medium.

The erosion mechanism of both physically and chemically eroding systems in turn can occur via two macroscopic phenomena: surface erosion and bulk erosion. Surface erosion occurs when the rate at which dissolution medium penetrates the dosage form is slower than the rate of conversion of the formulation into water soluble materials [9].

In surface erosion, only the surface of the dosage form, consisting of drug and excipient, dissolves into the medium causing drug to be released according to the continuous decrease of the size of the dosage form. Most phase-erodible systems, i.e. physically erodible crystalline solid materials with low solubility of the dissolution medium in the solid material, but high solubility of the material in the dissolution medium, erode by surface erosion. On the other hand, bulk erosion occurs when the rate at which the solvent penetrates the dosage form exceeds that at which the formulation is converted into water

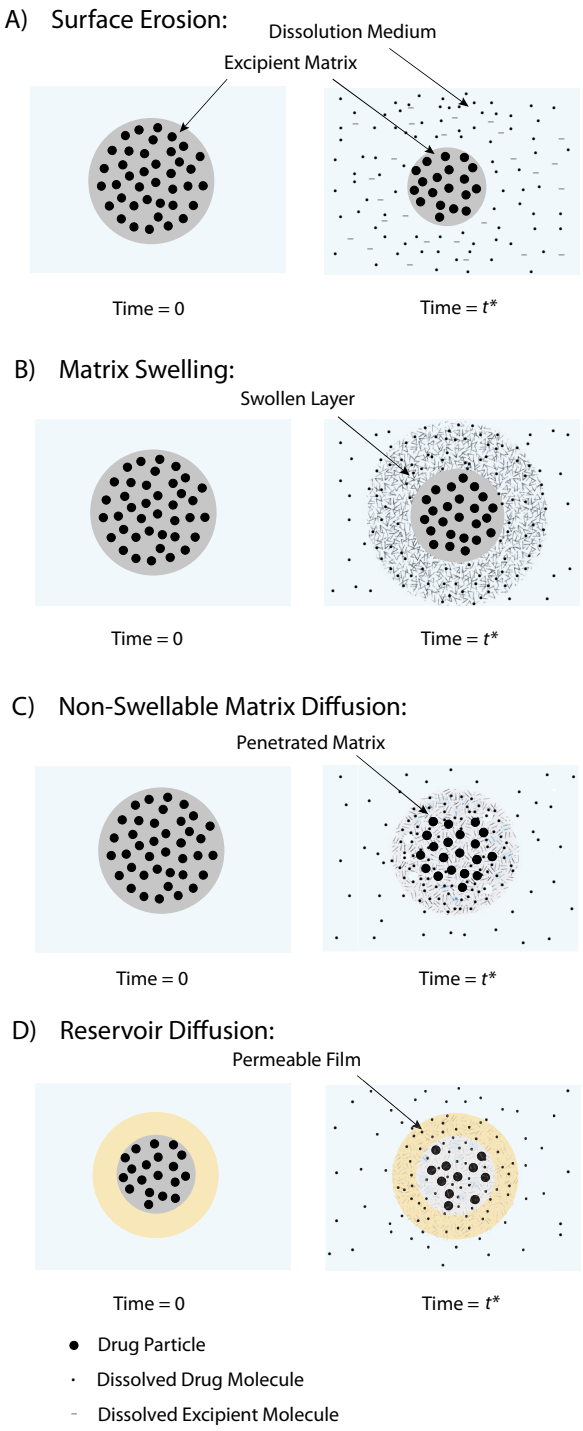

Figure 3.1: Common drug release systems. Dosage forms are illustrated at time $t = 0$ and at time $t = t^*$ in solution. (A) Surface erodible excipients where both drug and excipient dissolve into the dissolution medium, (B) Matrix-swellable excipients where drug diffuses through swollen excipient into the dissolution medium, (C) Non-swellable excipients where drug diffuses through non-swollen excipient into the dissolution medium and (D) Non-swellable excipients surrounded by a rate-limiting permeable membrane.

soluble materials [10]. In bulk erosion, the dosage form's matrix dissolves continuously.

Matrix-swellable systems comprise excipients that swell but do not erode when in contact with the dissolution medium. Dissolution medium penetrates the dosage form and causes the penetrated layer to swell as soon as the dosage form is put into the medium. Penetration of the medium is by diffusion and subsequent relaxation (swelling).

Three classes are distinguished according to the relative rates of diffusion and polymer relaxation: Case I or Fickian diffusion, where the rate of diffusion is much less than that of relaxation; Case II diffusion, where diffusion is very rapid compared with the relaxation process; Case III diffusion where diffusion and relaxation rates are comparable. Once in contact with the penetrated dissolution medium, the drug dissolves inside the dosage form. Subsequently, the drug diffuses out of the swollen layer to be released into the free-flowing dissolution medium.

Diffusion-systems have been formulated in two basic configurations: reservoirs and matrices. In both configurations, dissolution medium first penetrates the dosage form by diffusion. Drug in contact with the dissolution medium dissolves inside the dosage form, and subsequently diffuses out of the matrix. Excipients neither substantially swell, nor erode in the process of drug release. Matrix systems consist of uniformly distributed drug particles within an excipient matrix, and diffusion through this excipient matrix typically is the rate-limiting step. In reservoir systems, a core of drug is surrounded by a film, and the diffusion of the drug through this film determines the rate of release.

The dominant drug release mechanism can be identified, for example, by the drug release profile which may be different for different drug release mechanisms [11]. Common release profiles are '$t^{1/2}$ release', 'zero order release', and 'drug release according to 1-$exp(-t/\tau)$' (Fig. 3.2).[11] The '$t^{1/2}$ release' occurs in matrix diffusion controlled systems, in physically erodible systems that are mass transfer limited in unstirred solution, and in case I swelling controlled systems. In '$t^{1/2}$ release', the rate of drug release is proportional to $t^{-1/2}$ and the accumulated drug amount released is proportional to $t^{1/2}$, revealing that a transient diffusion process is rate-determining. (A transient diffusion process can be rate-determining in non-swellable diffusion systems, matrix swellable systems, but also in erodible systems.) In 'zero order release', the rate of drug release is constant (i.e.,

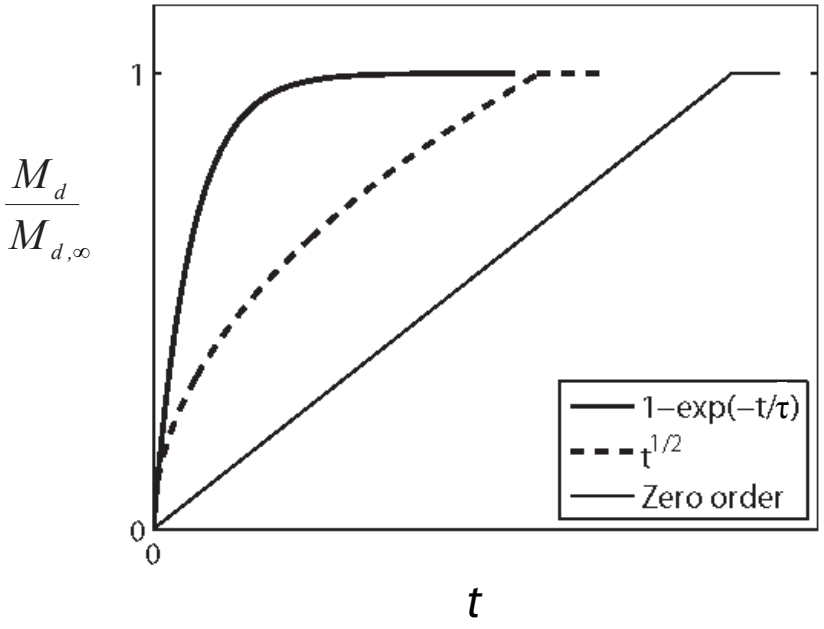

Figure 3.2: Common drug release profiles illustrating the normalized accumulated mass of drug released versus time. The rate of drug release, the slope of the curves, is constant in the case of 'zero order release', proportional to $t^{-1/2}$ in the case of '$t^{1/2}$ release', and equal to $\tau*exp(-t/\tau)$ in drug release according to $1-exp(-t/\tau)$.

proportional to t^0) such that the drug concentration in the dissolution medium increases linearly with time. This type of release occurs for example in surface erodible systems with constant surface area and erosion rate, and in reservoir (membrane) systems with large initial drug concentration (i.e., the concentration of drug inside the reservoir is much larger than its solubility). Drug release according to $1\text{-}exp(-t/\tau)$ occurs in reservoir (membrane) systems at low initial drug concentration, i.e., the concentration of drug inside the reservoir is lower than its solubility. Since the rate of drug release is proportional to $exp(-t/\tau)$ in these systems, the amount of drug released, M_d, varies with time as $M_d(t) = M_{d,\infty}(1\text{-}exp(-t/\tau))$ where $M_{d,\infty}$ is the content of drug initially contained in the dosage form and τ is the time constant of the system.

3.3 Previous Models of Drug-Release

Drug release can be modeled as a transport problem, comprising the equation of continuity for species i (i can be either drug or excipient), the equation of continuity for the dissolution medium of constant mass density, and the Navier-Stokes equation for Newtonian fluid and incompressible flow as [12,13]:

$$\frac{\partial c_i}{\partial t} = \nabla \cdot \left(D \nabla c_i\right) - \nabla \cdot c_i v + r_i \tag{3.1}$$

$$\nabla \cdot v = 0 \tag{3.2}$$

$$\rho\left(\frac{\partial v}{\partial t} + v \cdot \nabla v\right) = -\nabla P + \mu_f \nabla^2 v + f \tag{3.3}$$

Boundary conditions for Eq. (3.1) include the solubilities of the individual components, as determined by the kinetics of the interfacial "reaction" of solid state to dissolved state of component i. Boundary conditions for Eq. (3.2) and Eq. (3.3) are given by the conditions that govern fluid flow in proximity to the solid pharmaceutical components. The above transport equations are hard to solve in full, and hence are simplified for various

specific cases to account only for the relevant and rate-determining phenomena. An overview of the models developed so far is presented below. For further insight, the reviews by Langer and Peppas, 1981, Costa and Sousa Lobo, 2001, Siepmann and Peppas, 2001, Siepmann and Goepferich, 2001, Langer and Peppas, 2003, and Siepmann and Siepmann 2008 may be consulted. A historical perspective of dissolution research, which started for pharmaceutical applications after it was recognized in 1951 that dissolution rate can be the rate-determining step controlling the appearance of orally-delivered drug in the human body, was published by Dokoumetzidis and Macheras in 2006 [6,8,9,14-16].

3.3.1 Non-Swellable Matrix Diffusion Systems

The first and probably the most famous model of drug release from non-swellable matrix diffusion systems was developed by Higuchi in 1961 [17,18]. He formulated a 1-d equation to describe drug release from an ointment matrix with drug diffusion through the ointment being the rate determining step of drug release. Three zones, depending on drug concentration in the ointment matrix were defined: zone I where the drug concentration is at the constant value c_0 above its solubility in the ointment matrix, zone II where drug is partially depleted from the ointment matrix to a concentration below its solubility, and zone III at the interface between the ointment matrix and the skin where the drug concentration is approximately equal to zero. Furthermore, it is assumed: (a) the suspended drug is in a fine state such that the drug particles are much smaller than the thickness of the applied layer, (b) the drug concentration in the matrix is initially much higher than its solubility, i.e. $c_0 >> c_s$, and (c) the interface between ointment matrix and skin is assumed to be a perfect sink. Under these conditions, the time for drug dissolution is much greater than the time for drug diffusion to reach steady state, i.e. $t_d >> \tau_{ss}$, which allows the transport equations to be reduced to the following quasi steady-state problem:

$$\frac{\partial^2 c}{\partial x^2} = 0 \tag{3.4}$$

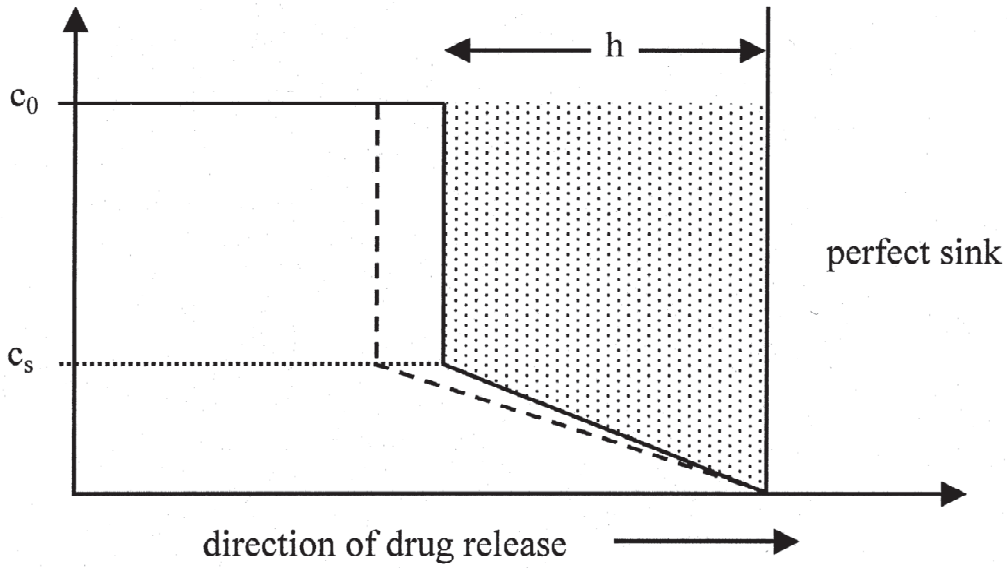

Figure 3.3: Illustration of the Higuchi quasi-steady state model with moving boundary. The drug concentration is initially at the constant value c_0, which is larger than its solubility in the ointment matrix, c_s. The zone where drug is partially depleted from the ointment matrix is moving inwards into the center of the ointment matrix. In this zone, the concentration profile is assumed linear with the boundary conditions $c = c_s$ at the moving boundary and $c = 0$ on the fixed surface of the dosage form (from Ref. [5]).

This gives a linear drug concentration profile with boundary condition $c = 0$ at the interface between ointment matrix and the skin, and $c = c_s$ at the moving boundary between zones I and II, where zone II is moving inwards into zone I (Fig. 3.3). The final equations obtained for the dissolution time, t_d, and the accumulated amount of drug released are:

$$t_d = \frac{H_0^2}{4Dc_s}\left(2c_0 - c_s\right) \qquad for \qquad c_0 > c_s \tag{3.5}$$

$$M_d\left(t\right) = A\sqrt{\left(2c_0 - c_s\right)c_s Dt} \qquad for \qquad c_0 > c_s \tag{3.6}$$

where c_0 is the initial concentration of drug in the ointment matrix in [kg/m^3], c_s the solubility of drug as [kg/m^3], D the diffusion coefficient of drug in the external phase of the ointment matrix, t is the time, and A is the surface area of the matrix. The accumulated amount of drug released is proportional to the square-root of time, which gives an explanation for the famous '$t^{1/2}$ release profile' of this type of systems.

Numerous refinements and extensions of such quasi steady-state solutions have been reported since Higuchi's publication of his equation. An overview of models based on simplified solutions to the diffusion equation developed after Higuchi's model can be found in the work by Baker and Lonsdale [19]. Disadvantages of models using 1-d quasi steady-state solutions compared with the transient diffusion equation are inaccuracies, particularly if the geometry cannot be reduced to a 1-d model with the drug dispersed as fine particles in the matrix, or if the time for drug dissolution is of the order of the time for drug diffusion to reach steady state.

Equations for solute release from various geometries based on solutions to the transient diffusion equation are reported by Crank in 1975 [20]. In one dimension, the transient diffusion equation is:

$$\frac{\partial c}{\partial t} = D\frac{\partial^2 c}{\partial x^2} \tag{3.7}$$

For a sheet with thickness equal to $2l$, the accumulated fraction of solute released is:

$$\frac{M_d(t)}{M_{d,\infty}} = 1 - \frac{8}{\pi^2}\sum_{n=0}^{\infty}\frac{1}{(2n+1)^2}\exp\left\{-D(2n+1)^2\pi^2 t/l^2\right\} \tag{3.8}$$

Fu et al. developed a similar model in 1976 using the three-dimensional transient diffusion equation to describe drug transport through polymer composite tablets [21]. In cylindrical coordinates the equation reads:

$$\frac{\partial c}{\partial t} = D\left(\frac{\partial^2 c}{\partial r^2} + \frac{1}{r}\frac{\partial c}{\partial r} + \frac{\partial^2 c}{\partial z^2}\right) \tag{3.9}$$

Solutions to this transient problem were adapted from the book on conduction heat transfer in solids by Carslaw and Jaeger, and on the theory of Bessel functions by Watson [22,23]. The general solution for the fraction of drug released at a time *t* by the model of Fu et al. is:

$$\frac{M_d(t)}{M_{d,\infty}} = 1 - \frac{8}{l^2 a^2}\sum_{m=1}^{10}\exp\left(-D\alpha_m^2 t\right)\alpha_m^{-2}\sum_{n=1}^{10}\exp\left(-D\beta_n^2 t\right)\beta_n^{-2} \tag{3.10}$$

In 1985, Bawa et al. published an analytical explanation, supported by experiments, for drug release in controlled-release systems comprising macromolecules in hydrophobic polymer matrices as published earlier by Langer and Folkman [24,25]. It has been shown that even though diffusion of large molecules in this type of polymers is very slow, these systems can act as drug delivery devices. Drug only minimally diffuses along the polymer backbone while being released from the matrix. In fact, it has been shown that the drug is released mainly via diffusion through interconnected pores formed by dissolved drug particles. The solutions for the accumulated amount of drug released were similar to the model developed earlier by Crank [20], with the exception that the effective diffusivity was used as diffusion coefficient.

Ritger and Peppas described, in 1987, models based on the transient diffusion equation for different geometries [26]. The solutions derived for the accumulated amount of drug released are again similar to the model developed earlier by Crank [20].

3.3.2 Matrix Swellable Systems

The swelling behavior of polymeric systems has been extensively studied in the 1950s and the 1960s. Excellent reviews of the outcome of these endeavors are given in the book *Diffusion in Polymers* edited by Crank and Park in 1968, and in the second edition of the book *The Mathematics of Diffusion* by Crank in 1975 [20,27]. Transport of solvent (i.e. dissolution medium) into a number of swellable polymers may not be described adequately by Fick's law. Deviations from Fickian behavior are considered to be associated with the finite rates at which the polymer structure may change in response to the sorption or desorption of penetrant molecules. This behavior is said 'anomalous'. Anomalous effects may be directly related to the influence of the changing polymer structure on diffusional mobility of the medium inside the polymer, or they may result from the internal stresses exerted by the medium on the polymer as diffusion proceeds. A generalized diffusion equation highlighted here takes anomalous effects into account while sorption as follows [20]:

$$\frac{\partial c}{\partial t} = \frac{\partial}{\partial x}\left\{ D(c,x,t)\frac{\partial c}{\partial x} - B(c,x,t)sc \right\} \tag{3.11}$$

where D is the diffusion coefficient of the penetrant in the polymer, B is a mobility coefficient and s is a constant related to the partial stress tensor in one dimension. Clearly, Fickian diffusion is dominant if the first term on the right hand side of Eq. (3.11) (the diffusion term) is rate-limiting. If the second term (the relaxation term) is rate-limiting, Case II diffusion will be seen. The so-called case III diffusion occurs when the diffusion and the relaxation terms are of the same order of magnitude. The classification of different cases can also be done by the Deborah number, which is the characteristic stress relaxation time divided by the characteristic diffusion time. Generally, case II or case III diffu-

sion is observed in glassy polymers that swell extensively and have a small Deborah number.

A 1-d drug release model that takes into account penetration of dissolution medium into the dosage form based on Fick's law, volumetric expansion of the polymer due to swelling, and drug release by diffusion through the swollen layer, similar to the illustrations in Fig. 3.4, has been presented by Peppas et al. in 1980 [28]. The diffusion coefficient in the swollen layer was assumed constant in this analysis. Reasonable agreement with experimental data was obtained. The model developed by Peppas was expanded by Korsmeyer et al. and others to account for the effects of porosity and penetrant concentration-dependent drug diffusion coefficients in the polymer [29,30]. The model was presented in non-dimensional form and for the diffusion of the penetrant (i.e., water) it was written as:

$$\frac{\partial C_1}{\partial \tau} = \frac{\partial}{\partial \xi}\left(D_1 \frac{\partial C_1}{\partial \xi} \right) \tag{3.12}$$

where $C_1 = c_w/c_{w,max}$, time was scaled according to the diffusion coefficient of water in the fully swollen polymer, $D_{1,s}$, and the dry length of the slab, L, as $\tau = D_{1,s}t/L^2$, and the nondimensional length was chosen as $\xi = x/L$. For drug diffusion through the polymer it was given that:

$$\frac{\partial C_2}{\partial \tau} = \frac{\partial}{\partial \xi}\left(D_2 \frac{\partial C_2}{\partial \xi} \right) \tag{3.13}$$

where $C_2 = c_d/c_{d,max}$. The boundary conditions at the two surfaces of the slab, given by $\xi = 0$ and $\xi = \xi'$ (moving boundary) are:

$$C_1(0,\tau) = C_1(\xi',\tau) = 1 \tag{3.14}$$

$$C_2(0,\tau) = C_2(\xi',\tau) = 0 \tag{3.15}$$

The diffusion coefficients were written according to the free volume theory as follows, where $D_{2,d}$ represents the diffusion coefficient of the drug in the fully swollen gel:

$$D_1 = \exp\left(-\beta_1\left(1 - C_1\right)\right) \tag{3.16}$$

$$D_2 = D_{2,d}\exp\left(-\beta_1\left(1 - C_1\right)\right) \tag{3.17}$$

β_1 and β_2 are parameters defining the concentration dependence of D_1 and D_2. Volumetric expansion of the slab due to swelling was taken into account as follows, where ξ' is equal to L initially ($\xi'_0 = L$):

$$\xi' = \sum_{i=1}^{n} \Delta\xi_i = \sum_{i=1}^{n} \frac{\Delta\xi_0}{1 - \nu_{1,e}C_{1,i}} \tag{3.18}$$

Singh and Fan expanded the above model to account for non-Fickian behavior of penetrant transport on the basis of Eq. (3.11) in 1986 [31].

Analytical approximations to the solution of a similar model were given by Cohen and Erneux in 1988. Fig. 3.4 illustrates the underlying drug release model with Fickian diffusion determining the transport rates of both penetrant and solute [32,33].

It is, however, difficult to formulate exact analytical drug release models from matrix swellable systems, and thus numerical methods are typically required to obtain an accurate solution, though a simple, empirical model may be beneficial in some situations. A famous empirical model to describe drug release from hydrophilic matrices has been given by Korsmeyer et al. as:

$$\frac{M_d}{M_{d,\infty}} = kt^n \tag{3.19}$$

The rate-limiting drug release mechanism can be identified by the exponent *n.* If *n* is 0.5, Fickian diffusion determines drug release, whereas if *n* is equal to 1, it is case II diffusion rate-limiting [34,35].

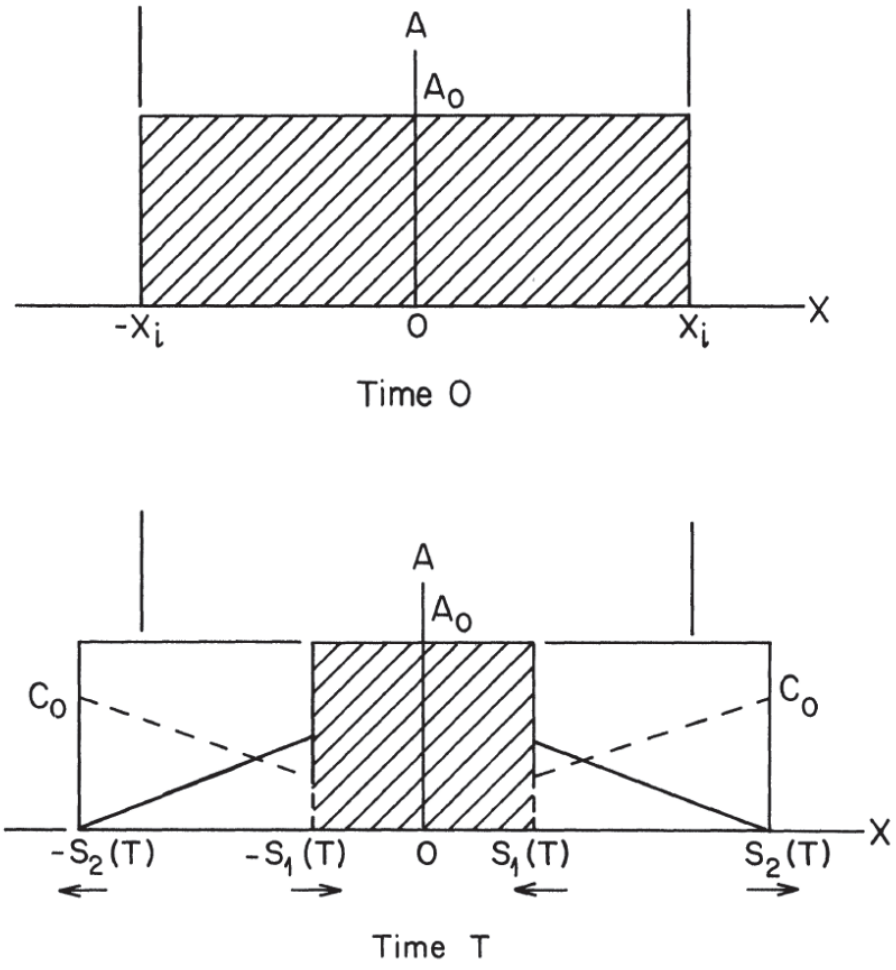

Figure 3.4: Illustration of drug release from a swellable matrix. Dissolution medium at a concentration c_0 on the surface of the dosage form penetrates the dosage form and causes the excipient to swell. Drug on the other hand, which is initially solid at a concentration A_0, dissolves upon penetration of the dissolution medium and diffuses through the swollen excipient outside of the dosage form into the dissolution medium (from Ref. [32]).

3.3.3 Surface Erodible Systems

Surface erodible systems in agitated solution have been modeled first by Noyes and Whitney in 1897 [36]. They presented a general equation to describe the rate of dissolution of solid substances in their own solutions as:

$$\frac{dc_\infty}{dt} = C\left(c_s - c_\infty\right) \tag{3.20}$$

where c_∞ represents the concentration in the dissolution medium, t the time, c_s the solubility of the substance, and C a constant. The equation was developed for solubility determinations and it was experimentally validated on dissolution of benzoic acid and lead chloride cylinders. Nernst and Brunner expanded the model by Noyes and Whitney in 1904 [37,38]. It was recognized that the constant C is in fact proportional to the surface area, A, with a proportionality constant equal to the diffusivity of the species in the medium divided by the concentration boundary layer thickness, D/δ, giving:

$$\frac{dc}{dt} = \frac{DA}{\delta}\left(c_s - c\right) \tag{3.21}$$

Without being able to directly calculate the concentration boundary layer thickness, it was already then recognized by Nernst and Brunner that the concentration boundary layer thickness decreases in length with increasing fluid velocity. The 'convective diffusion theory' has later been further developed by Levich, who provided approximate solutions for the concentration boundary layer thickness to solve specific problems in electrochemistry [13,39].

Based on Eq. (3.20) and Eq. (3.21), Hixson and Crowell developed a model for dissolution of a crystal, taking into account the fact that the surface area of the crystal decreases upon erosion [40]. It was assumed that the surface area varies as the two-thirds power of its volume, owing to the condition of similar geometrical solids. If the concentration change in the dissolution medium is negligible, they showed that:

$$w_0^{1/3} - w^{1/3} = kt \tag{3.22}$$

w_0 is the initial weight of the crystal, w is the weight of the crystal at time t, and k is a rate constant proportional to D/δ.

Even though it is was not known until 1951 that the drug dissolution rate can be the rate-controlling step which controls the appearance of orally delivered drug in the human body, and both the Noyes-Whitney and the Hixson-Crowell models have not been developed for pharmaceutical applications, they are still being used today for drug dissolution modeling, particularly to describe the dissolution rate of solid drug particles that dissolve after the break-up of a direct compressed tablet.

Cooney in 1972 and Hopfenberg in 1976 studied the effect of geometry on the dissolution of pharmaceutical solids [41,42]. The underlying equation was similar to the one used by Hixson and Crowell with the only exception that different laws for the calculation of the eroding surface area were applied. An addition to Cooney's and Hopfenberg's models was made by Katzenhendler et al. in 1997 [43]. They took different rate constants k of different eroding surfaces into account. Analytical models to describe erosion of multi-phase systems, as solid dosage forms generally are, however have not been developed so far.

3.3.4 Recent Advanced Models of Drug Release

Recent advanced models of drug release were based on: (a) Monte Carlo simulations to describe the diffusion of drug out of an erodible excipient matrix, (b) dissolution models for diffusional drug release from erodible matrices, and (c) numerical simulations of the underlying model for systems with polymer swelling and dissolution. Advanced models for erosion of polymer-drug matrices based on Monte Carlo simulations were first developed by Zygourakis in 1989. They were later refined by Goepferich and Langer in 1995, and Siepmann et al. in 2002 [44-47].

The major idea of Monte Carlo based models for the simulation of drug diffusion out of erodible matrices is to represent the matrices as 2-dimensional grid, similar to the illus-

tration in Fig. 3.5. Each pixel in the grid represents one of the system's components which can be either drug, polymer, filler, or pore. To simulate drug or excipient erosion, a life expectancy is defined for each type of pixel. As soon as a pixel comes into contact with the solvent, there is a characteristic time until the pixel dissolves. After this characteristic time expires, the pixel is assumed to dissolve instantaneously and diffuse out of the matrix. The transient diffusion equation is applied to describe transport of the solute through the generated pores out of the remainder of the matrix. It is possible to adjust the characteristic time to dissolve a pixel based on solubility and concentration of the respective solute in the pores of the excipient matrix. Note that the solubility of the solute may depend on pH, which may again be affected by the concentration of the eroded solutes.

A drug release model for diffusional drug release from erodible matrices is presented by Lee in 1980 [48]. The drug release model is based on movements of two fronts: a diffusing front, and an eroding front, as illustrated in Fig. (3.6). Drug diffusion out of the matrix is the rate-determining step, and it occurs between the diffusing front and the eroding front. Determination of the erosion rate was based on empirical observations.

Ju et al. developed a new analytical model to determine the erosion rate of hydrophilic polymers that can both swell and erode in stirred dissolution medium [49-51]. Polymer dissolution is modeled as mass-transfer flux under forced convection around an object, J_p, according to the equation:

$$J_p = f_p \left\langle D_p \right\rangle^{2/3} \left(\frac{\mu_f}{\rho_f} \right)^{-1/6} \omega_{app}^{1/2} c_0 \tag{3.23}$$

where f_p is a fitting constant, D_p is the polymer diffusivity, μ_f/ρ_f is the dynamic viscosity of the dissolution medium, ω_{app} is the rotation rate, and c_0 is the disentanglement concentration of the polymer. The polymer disentanglement concentration was estimated based on the postulate that the characteristic dependence on molecular weight of the concentration where polymer molecules overlap is similar to that of the disentanglement concentration. The diffusion coefficient of polymer in the dissolution medium was estimated based

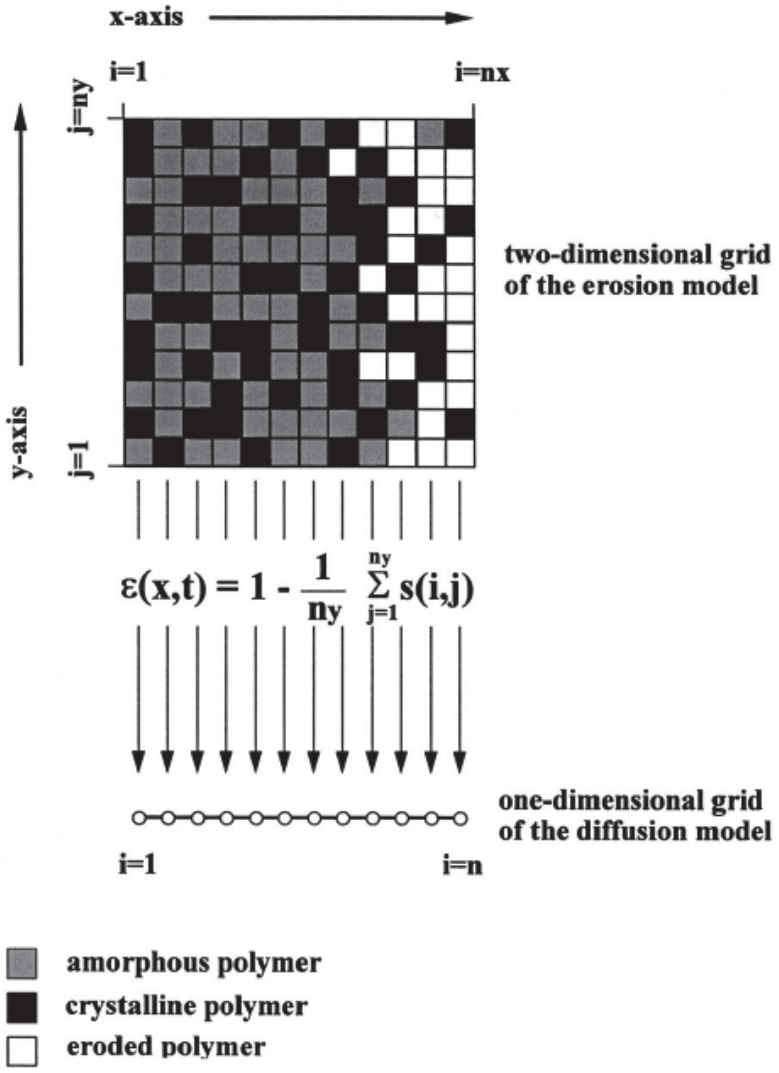

Figure 3.5: Model to simulate erosion of polymer matrices using Monte Carlo techniques. The microstructure of the eroding polymer, consisting of amorphous and crystalline units, is illustrated in a two-dimensional grid. A life expectancy is defined for each unit in the grid, and as soon as a unit comes into contact with the solvent, there is said to be a characteristic time until the unit dissolves. After this characteristic time expired, the unit is assumed to dissolve instantaneously and diffuse in positive x-direction out of the matrix (from Ref. [46]). The model is not only applicable to describe combined erosion of multi-phase polymers, but also for multi-phase systems comprising excipient, drug, pores, etc.

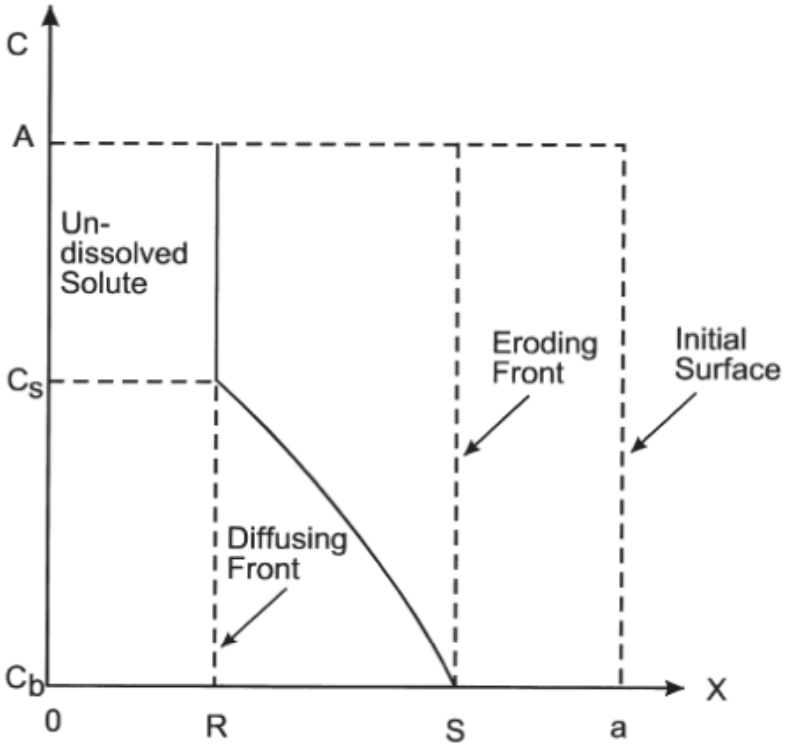

Figure 3.6: Schematic of diffusional drug release from erodible matrices. *A* is the initial concentration of solid drug inside the dosage form, c_s is the solubility of drug inside the dosage form that is penetrated by dissolution medium, *R(t)* is the time-dependent position of the moving diffusion front, *S(t)* is the time-dependent position of the moving erosion front, and *a* is the initial position of the eroding surface (from Ref. [48]).

on previous models summarized by Doi and Edwards [52,53]. The following scaling law was obtained:

$$J_p \propto M_n^{-1.15} \tag{3.24}$$

The release of drug from these matrices was however determined based on empirical observations, instead of an underlying analytical model. It was observed that:

$$\frac{M_d(t)}{M_{d,\infty}} \propto M_n^{-0.48} \tag{3.25}$$

Finally, a comprehensive analytical model for HPMC-based sustained release devices has been developed by Siepmann et al [54-57]. The underlying matrix is subdivided into sequential layers consisting of drug and HPMC for numerical analysis. The model takes into account the diffusion of water and drug in the matrix, non-constant diffusivities, moving boundary conditions, the swelling of the system, polymer and drug dissolution, and radial and axial mass transfer in cylindrical geometries. Transport of drug and water in the matrix were modeled using the diffusion equation:

$$\frac{\partial c_k}{\partial t} = \frac{1}{r}\left\{\frac{\partial}{\partial r}\left(r D_k \frac{\partial c_k}{\partial r}\right) + \frac{\partial}{\partial z}\left(r D_k \frac{\partial c_k}{\partial z}\right)\right\} \tag{3.26}$$

The fact that the drug concentration in the matrix may be above its solubility, as drug is dispersed in the matrix as solid particles, was taken into account by considering only the concentration below the solubility to be available for diffusion. The excess drug was considered as not dissolved and not available for diffusion. For the diffusion coefficients it was written as a function of the concentration of water in the matrix, c_1, and the water concentration in the fully swollen matrix, $c_{1,crit}$:

$$D_k = D_{k,crit} \exp\left\{-\beta_k \left(1 - \frac{c_1}{c_{1,crit}}\right)\right\} \tag{3.27}$$

Clearly, the diffusion coefficients increase as swelling and porosity of the matrix increase. It is noted here that porosity is based on the initial porosity and the dissolved drug particles (i.e. the amount of drug depleted from the matrix). Drug release was modeled to be limited by diffusion through the swollen matrix. A perfect sink for drug molecules was assumed on the device surface. The volume of the device was calculated based on the volume of penetrant and the volume of polymer dissolved. Polymer dissolution was taken into account using the following equation describing the mass of solid polymer:

$$M_p(t) = M_{p,0} - k_{diss} A t \tag{3.28}$$

where k_{diss} is a dissolution constant that can be calculated based on the theory developed by Doi and Edwards [52,53]. The fitted model agrees well with experimental data of drug release obtained from HPMC matrix tablets.

3.4 Drug Release Mechanism for Non-Porous IR Dosage Forms

Because non-porous dosage forms cannot rely on a large surface area-to-volume ratio to achieve immediate drug release, the mechanism by which drug is transferred from the solid state inside the dosage form to the dissolved state in the dissolution medium is crucial for the drug to be released rapidly. It is evident that in drug release by matrix swelling, non-swellable matrix diffusion, and reservoir diffusion, the excipient imposes a barrier to drug release and slows it down. In drug release by surface erosion, however, excipients that potentially hold up drug release can be eroded (i.e., dissolved) rapidly. This mechanism can therefore give the fastest drug release rate, and is chosen here for non-porous immediate-release dosage forms.

Prior models of drug release by surface erosion have been described for single-phase systems and for multi-phase systems using an empirically derived erosion rate. The very

important effects of material microstructure on surface erosion are, however, not taken into account in previous models. This limits their applicability for product design, because the material structure is a very important design parameter of solid dosage forms. A new model needs to be developed that allows quantification of such effects for predictive product design.

3.5 Summary

Drug release is a complex combination of interfacial dissolution reactions and transport phenomena, which vary in rate and characteristics based on the underlying system. A number of drug release systems with different drug release mechanisms have been developed so far, including erodible systems, matrix swellable systems, and non-swellable diffusion systems. Models that rely on the transport equations have been developed in the past to describe drug release. Most of the recent models are for sustained or controlled-release applications. They assume that material transport from the surface of the dosage form into the dissolution medium is rapid compared with the rate-determining drug transport inside the solid unit. Hence, perfect sink conditions are assumed on the surface of the solid matrix.

Since non-porous dosage forms, in contrast to current porous immediate-release dosage forms, do not rapidly disintegrate into small solid particles, they cannot rely on short mass transfer distances in the solid matrix and large surface area-to-volume ratios to achieve immediate drug release. A drug release mechanism is desirable for non-porous immediate-release dosage forms where drug release is not held up by the solid matrix. If the interfacial conversions of solid material into water soluble products are fast, drug release is limited by mass transfer from the surface of the dosage form into the dissolution medium, which potentially is much faster than mass transfer inside the dosage form, as diffusivities are large in the dissolution medium and concentration boundary layer thicknesses are comparably small. Hence, the drug release mechanism favored here for non-porous immediate-release dosage forms is surface erosion.

Analytical models for surface erosion of single-phase material are available, but it is difficult to formulate the erosion of multi-phase material, as the transport equations need to be adapted to account for the effect of material microstructure. Prediction of drug release for the case where drug particles are dispersed in a rapidly surface eroding excipient matrix cannot be done satisfactorily with any of the analytical models that are currently available. In fact, it is currently not clear what the impact of various design parameters is on surface erosion and drug release in a multi-phase system.

Nomenclature

A	characteristic surface area of the dosage form [m^2]
A_0 or A	concentration of drug in the dosage form [kg/m^3]
a	constant characteristic to a particular process
B	mobility coefficient [m/s]
c or c_∞	concentration of a particular species in the dissolution medium [kg/m^3]
c_0	solid-liquid interface concentration of an eroding polymer [kg/m^3]
c_0	concentration of drug in the dosage form [kg/m^3]
c_s	solubility of a particular species in dissolution medium [kg/m^3]
C	rate constant for dissolution of a solid [1/s]
C_i	non-dimensional concentration of species i
k	rate constant for drug dissolution [kg/s]
k_{diss}	mass flux of eroding polymer [kg/m^2s]
D	diffusion coefficient [m^2/s]
D_p	polymer center of mass diffusion coefficient [m^2/s]
f	body forces on a fluid element [N/m^3]
f_p	fitting constant

H_0	characteristic thickness of the dosage form [m]
J_p	mass flux under convection [kg/m^{2}s]
L	characteristic length of slab [m]
l	half thickness of a sheet [m]
M_n	number averaged molecular weight [kg/mol]
M_d	accumulated amount of drug released [kg]
$M_{d,\infty}$	drug content initially in the dosage form [kg]
dM_d/dt	drug release rate [kg/s]
$M_p(t)$	mass of solid polymer during polymer dissolution [kg]
n	constant characteristic to a particular process
P	fluid pressure [Pa]
r_i	rate at which species i is produced [kg/m^3]
s	constant to quantify anomalous effects of diffusion in polymers
w	mass of solid material [kg]
Re	Reynolds number
t	time [s]
t_d	drug dissolution time [s]
v	fluid velocity [m/s]
α	constant characteristic to a particular process
β	constant characteristic to a particular process
δ	concentration boundary layer thickness [m]
ξ	nondimensional length
ρ_f	fluid density [kg/m^3]
ρ_d	densidy of solid drug [kg/m^3]
τ	time constant of a particular process [s]

v	constant to describe volumetric expansion due to swelling
μ	viscosity [Pa·s]
μ_f	viscosity of dissolution medium [Pa·s]
ω_{app}	angular velocity of the eroding material [rad/s]

References

[1] The U.S. Pharmacopeial Convention, US Pharmacopeia, USP 35-NF 30.

[2] C.Y. Wu, L.Z. Benet, Predicting Drug Disposition via Application of BCS: Transport/Absorption/Elimination Interplay and Development of a Biopharmaceutics Drug Disposition Classification System, Pharmaceutical Research, 2005, 22, 11-23.

[3] US Food and Drug Administration (FDA), in Guidance for Industry PAT – A Framework for Innovative Pharmaceutical Development, Manufacturing, and Quality Assurance, Pharmaceutical CGMPs, 2004.

[4] S.C. Gad, 2008, Pharmaceutical Manufacturing Handbook: Production and Processes, Wiley Interscience, Hoboken, N.J.

[5] R.S. Langer, N.A. Peppas, 1981, Present and future applications of biomaterials in controlled drug delivery systems, Biomaterials, 2, pp. 201-214.

[6] J. Siepmann and N.A. Peppas, 2012, Modeling of drug release from delivery systems based on hydroxypropyl methylcellulose (HPMC), Adv. Drug Del. Rev., 64, pp. 163-174.

[7] D.L. Wise, 2001, Handbook of Pharmaceutical Controlled Release Technology, CRC Press.

[8] P. Costa, J.M. Sousa Lobo, 2001, Modeling and comparison of dissolution profiles, Eur. J. Pharm. Sci., 13, 123-133.

[9] R.S. Langer, N.A. Peppas, 2003, Advances in Biomaterials, Drug Delivery, and Bionanotechnology, AIChE Journal, 49, pp. 2990-3006.

[10] J.C. Middleton, A.J. Tipton, 2000, Synthetic biodegradable polymers as orthopedic devices, Biomaterials, , 21, pp. 2335-2346.

[11] E.L. Cussler, 1997, Diffusion Mass Transfer in Fluid Systems, Cambridge University Press, Cambridge, UK.

[12] R.B. Bird, W.E. Stewart and E.N. Lightfoot, 2002, Transport Phenomena, Second Edition, John Wiley & Sons, New York.

[13] S.M. Diebold, Physiological Parameters Relevant to Dissolution Testing: Hydrodynamic Considerations, in J. Dressman, J. Kraemer, 2005, Pharmaceutical Dissolution Testing, Taylor & Francis Group, Boca Raton, FL, USA.

[14] J. Siepmann, A. Goepferich, 2001, Mathematical modeling of bioerodible, polymeric drug delivery systems,, Adv. Drug Del. Rev., 48, 229-247.

[15] J. Siepmann, F. Siepmann, 2008, Mathematical modeling of drug delivery, Int. J. Pharm., 364, 328-343.

[16] A. Dokoumetzidis, P. Macheras, 2006, A century of dissolution research: From Noyes and Whitney to the Biopharmaceutics Classification System, Int. J. Pharm., 321, 1-11.

[17] T. Higuchi, 1961, Rate of Release of Medications from Ointment Bases Containing Drugs in Suspension, J. Pharm. Sci., 52, 1145-1149.

[18] T. Higuchi, Mechanism of Sustained-Action Medication, 1963, J. Pharm. Sci., 50, 874-875.

[19] R.W. Baker, H.K. Lonsdale, 1974, Controlled release: mechanism and rates, in A.C. Tanquary, R.E. Lacey (Eds.), Controlled Release of Biologically Active Agents, Plenum Press, New York, pp. 15-72.

[20] J. Crank, 1975, The Mathematics of Diffusion, Second Edition, Oxford University Press, Oxford, UK.

[21] J.C. Fu, C. Hagemeir, D.L. Moyer, E.W. Ng, 1976, A unified mathematical model for diffusion from drug-polymer composite tablets, J. Biomed. Mater. Res., 10, 743-758.

[22] H.S. Carslaw and J.C. Jaeger, 1959, Conduction of Heat in Solids, Oxford University Press, Oxford, UK.

[23] G.N. Watson, 1966, A treatise on the theory of Bessel functions, Cambridge University Press, Cambridge, UK.

[24] R. Bawa, R.A. Siegel, B. Marasca, M. Karel, R. Langer, 1985, An Explanation for the Controlled Release of Macromolecules from Polymers, J. Contr. Rel., 1, pp. 259-267.

[25] R. Langer and J. Folkman, 1976, Polymers for the sustained release of proteins and other macromolecules, Nature, 263, pp. 797-800.

[26] P.L. Ritger, N.A. Peppas, 1987, A simple equation for description of solute release I. Fickian and non-Fickian release from non-swellable devices in the form of slabs, spheres, cylinders or disks, J. Contr. Rel., 5, 23-36.

[27] J. Crank, G.S. Park, 1968, Diffusion in Polymers, Academic Press, New York, NY.

[28] N.A. Peppas, R. Gurny, E. Doelker, P. Buri, 1980, Modelling of drug diffusion through swellable polymeric systems, J. Membr. Sci., 7, 241-253.

[29] R.W. Korsmeyer, S.R. Lustig, N.A. Peppas, 1986, Solute and penetrant diffusion in swellable polymers. I. Mathematical modeling, J. Polym. Phys. Ed, 24, 395-408.

[30] R.W. Korsmeyer, E. von Meerwall, N.A. Peppas, Solute and penetrant diffusion in swellable polymers. II. Verification of Theoretical Models, 1986, J. Polym. Phys. Ed, 24, 409-434.

[31] S.K. Singh, L.T. Fan, 1986, A generalized model for swelling-controlled release systems, Biotechnol. Prog. 2, 145-156.

[32] D.S. Cohen, T. Erneux, 1988, Free boundary problems in controlled release pharmaceuticals. I. Diffusion in glassy polymers, SIAM J. Appl. Math., 48, 1451-1465.

[33] D.S. Cohen, T. Erneux, 1988, Free boundary problems in controlled release pharmaceuticals. II. Swelling-controlled release, SIAM J. Appl. Math., 48, 1466-1474.

[34] R.W. Korsmeyer, R. Gurny, E. Doelker, P. Buri, and N.A. Peppas, 1983, Mechanisms of solute release from porous hydrophilic polymers, Int. J. Pharm, 15, 25-35.

[35] P.L. Ritger, N.A. Peppas, 1987, A simple equation for description of solute release II. Fickian and anomalous release from swellable devices, J. Contr. Rel., 5, 37-42.

[36] A.A. Noyes, W.R. Whitney, 1897, The Rate of Solution of Solid Substances in their Own Solutions, J. Am. Chem. Soc., 19, 930-934.

[37] E. Brunner, Reaktionsgeschwindigkeit in heterogenen Systemen, 1904, Z. Phys. Chem., 47, 56-102.

[38] W. Nernst, Theorie der Reaktionsgeschwindigkeit in heterogenen Systemen, 1904, Z. Phys. Chem., 47, 52-55.

[39] V.G. Levich, 1962, Physicochemical Hydrodynamics, second edition, Prentice Hall, Upper Saddle River, NJ.

[40] A.W. Hixson, J.H. Crowell, 1931, Dependence of Reaction Velocity upon Surface and Agitation, Ind. and Eng. Chem, 23, 923-931.

[41] D.O. Cooney, 1972, Effect of Geometry on the Dissolution of Pharmaceutical Tablets and Other Solids: Surface Detachment Kinetics Controlling, AIChE Journal, 18, 446-449.

[42] H.B. Hopfenberg, 1976, Controlled Release from Erodible Slabs, Cylinders, and Spheres, In Controlled Release Polymeric Formulations, Paul, D., et al., ACS Symposium Series; American Chemical Society, Washington, DC.

[43] I. Katzenhendler, A. Hoffman, A. Goldberger, M. Friedman, 1997, Modeling of Drug Release from Erodible Tablets, J. Pharm. Sci., 86, 110-115.

[44] K. Zygourakis, 1989, Discrete simulation and bioerodible controlled release systems, Polym. Prep. ACS, 30, 456-457.

[45] A. Goepferich, R. Langer, 1995, Modeling of Polymer Erosion in Three Dimensions: Rotationally Symmetric Devices, AIChE Journal, 41, 2292-2299.

[46] A. Goepferich, R. Langer, 1995, Modeling monomer release from bioerodible polymers, J. Contr. Rel., 33, 55-69.

[47] J. Siepmann, N. Faisant, J.P. Benoit, 2002, A New Mathematical Model Quantifying Drug Release from Bioerodible Microparticles Using Monte Carlo Simulations, Pharmaceutical Research,, 19, 1885-1893.

[48] P.I. Lee, 1980, Diffusional release of a solute from a polymeric matrix - Approximate analytical solutions, J. Membrane Sci., 7, 255-275.

[49] R.T.C. Ju, P.R. Nixon, M.V. Patel, 1995, Drug release from hydrophilic matrices. 1. New scaling laws for predicting polymer and drug release based on the polymer disentanglement concentration and the diffusion layer, J. Pharm. Sci., 84, 1455-1463.

[50] R.T.C. Ju, P.R. Nixon, M.V. Patel, D.M. Tong, 1995, Drug release from hydrophilic matrices. 2. A mathematical model based on the polymer disentanglement concentration and the diffusion layer , J. Pharm. Sci., 84, 1464-1477.

[51] R.T.C. Ju, P.R. Nixon, M.V. Patel, 1997, Diffusion coefficients of polymer chains in the diffusion layer adjacent to a swollen hydrophilic matrix, J. Pharm. Sci., 86, 1293-1298.

[52] M. Doi and S.F. Edwards, 1986, The Theory of Polymer Dynamics, Oxford University Press, Oxford, UK.

[53] M. Doi, 1996, Introduction to Polymer Physics, Oxford University Press, Oxford, UK.

[54] J. Siepmann, H. Kranz, N.A. Peppas, R. Bodmeier, 2000, Calculation of the required size and shape of hydroxypropyl methylcellulose matrices to achieve desired drug release profiles, Int. J. Pharm., 201, 151-164.

[55] J. Siepmann, H. Kranz, R. Bodmeier, N.A. Peppas, 1999, HPMC-matrices for controlled drug delivery: a new model combining diffusion, swelling and dissolution mechanisms and predicting the release kinetics, Pharm. Res., 16, 1748-1756.

[56] J. Siepmann, K. Podual, M. Sriwongjanya, N.A. Peppas, R. Bodmeier, 1999, A new model describing the swelling and drug release kinetics from hydroxypropyl methylcellulose tablets, J. Pharm. Sci., 88, 65-72.

[57] J. Siepmann, N.A. Peppas, 2000, Hydrophilic matrices for controlled drug delivery: an improved mathematical model to predict the resulting drug release kinetics (the 'sequential layer' model), Pharm. Res., 17, 1290-1298.

This page is intentionally left blank.

CHAPTER IV

DRUG DISSOLUTION MODELING OF NON-POROUS, IMMEDIATE-RELEASE DOSAGE FORMS

4.1 Introduction

In this chapter, an analytical model is developed to describe erosion and drug release from a two-phase material comprising drug particles embedded in an excipient matrix. First, an overview of mass transfer limited surface erosion is given and equations are developed to describe the erosion rate of a single-phase system. A second phase is then added to the single-phase material in the form of slowly eroding particles, and the model is extended to predict erosion of such materials. This allows calculation of the rate and time of drug release. For simplicity, the geometry of a flat disk is used to represent the dosage form for most part of the analysis.

4.2 Mass Transfer Limited Surface Erosion

One of the most basic equations of a model for drug release by surface erosion is that for the rate of material transferred from the eroding surface into the dissolution medium. For a dosage form with a flat surface, where the roughness is much smaller than the dosage form's thickness, the rate of material transferred, *dM/dt*, can be expressed, similar to the prior models of drug release by surface erosion developed by Cooney in 1972 and Katzenhendler et al. in 1997 [1,2]:

$$\frac{dM}{dt} = \frac{dm}{dt} A(t) = \rho_s \frac{dH}{dt} A(t) \tag{4.1}$$

where *dm/dt* is the average mass flux from the eroding surface, *A(t)* is the eroding surface area, ρ_s is the average density of the solid material, and *dH/dt* is the erosion rate in units

of meters per second. Note that the erosion rate in turn is equal to the average material flux removed from the dosage form divided by the density of the solid material in Eq. (4.1). If the erosion rate, dH/dt, of a material comprising either randomly dispersed drug particles or dissolved molecules uniformly distributed in the excipient matrix at a given drug volume fraction, φ, is known, the drug release rate can be calculated. The rate of drug released, dM_d/dt, then is:

$$\frac{dM_d}{dt} = \frac{dm_d}{dt} A(t) = \frac{dH}{dt} \rho_d \phi A(t) \tag{4.2}$$

where dm_d/dt is the drug release flux, and ρ_d is the density of the drug material. The normalized accumulated amount of drug released versus time, as the relevant property when considering the aim of controlling drug concentrations in the human body by the dosage form's dissolution properties, can be calculated by integration of Eq. (4.2) to give:

$$\frac{M_d}{M_{d,\infty}} = \frac{\rho_d \phi}{M_{d,\infty}} \int_0^t \frac{dH}{dt} A(t) dt \tag{4.3}$$

It is evident that the initial dosage form geometry, the drug volume fraction in case the drug units are randomly distributed in the excipient matrix, as well as the erosion rate (i.e. material removal rate) play major roles in describing drug release by surface erosion.

Similarly, the time it takes to disintegrate the dosage form, t_d, which is simply the time for the drug to be released from the dosage form, can be derived from the initial characteristic thickness of the dosage form, H_0, and the erosion rate, dH/dt. If the dosage form is a flat disk eroding at steady-state conditions (e.g. steady-state convection), the time to disintegrate the dosage form is:

$$t_d = \frac{H_0}{2\dot{H}} \tag{4.4}$$

Again under the condition of surface erosion of a flat disk at steady-state (e.g. steady-state convection), both *dH/dt* and *A(t)* are constant and time-independent. Hence, if the drug is randomly distributed in the excipient matrix, the accumulated amount of drug released can be characterized by a linear, 'zero-order' profile of drug concentration versus time as follows:

$$\frac{M_d}{M_{d,\infty}} = \frac{A}{M_{d,\infty}} \frac{dm_d}{dt} t = \frac{A \phi \rho_d}{M_{d,\infty}} \frac{dH}{dt} t \tag{4.5}$$

The erosion rate, *dH/dt*, is the only parameter which cannot be directly read out of the properties of material and geometry of the dosage form in the set of equations given above. It must be derived from the laws of mass transfer of the eroding solid material into the dissolution medium. Emphasis is given in this work to a typical case of pharmaceutical material comprising randomly distributed drug particles embedded in an excipient matrix, as shown in Fig. 4.4. In this configuration, material microstructure is an important parameter that affects the rate of surface erosion. However, analytical models that account for such microstructural effects on drug release by surface erosion have not been developed so far. The equations to describe erosion of single-phase systems are first derived in the next section and microstructural effects are added to the model subsequently.

4.3 Erosion of Single-Phase Systems

4.3.1 Erosion of Single-Phase Material in Agitated Medium

The mass transfer mechanism of single-phase surface-eroding systems depends on the conditions the eroding material is exposed to. Since the focus of this work is on immediate-release solid dosage forms which in the majority of cases are delivered orally for dissolution in the stomach, emphasis is given in this work to the calculation of erosion rate under such conditions as found in the gastrointestinal system. Fluid velocity in the stomach during digestion is reported to be in the range of about 0.001 m/s – 0.1 m/s. Such

conditions of fluid flow in the gastrointestinal system after intake of a solid dosage form are incorporated in the USP-standardized dissolution test protocols where the specified dissolution medium is typically stirred with either paddles or baskets at rates between 50 and 200 revolutions per minute [3-6].

Assuming the fluid velocities just given, the Peclet number, which describes the ratio of the rate of mass transfer by convection divided by the rate of mass transfer by diffusion as $Pe = v_\infty L/D$, is for such a typical system with a characteristic length, L, of 0.01 m, and a diffusivity of the eroding material, D, of $8\text{x}10^{-10}$ m^2/s, of the order of $10^4 - 10^6$. Therefore, convective mass transfer from the surface of the dosage form to the free-flowing dissolution medium is the dominant mass-transfer mechanism to describe surface erosion in such a case [7]. The relevant variable, dH/dt, can hence be derived from the equations of continuity and motion of the medium, as well as the equation of continuity of the erodible species giving the following three equations [7]:

$$\frac{\partial v_x}{\partial x} + \frac{\partial v_y}{\partial y} = 0 \tag{4.6}$$

$$\rho_f \left(v_x \frac{\partial v_x}{\partial x} + v_y \frac{\partial v_y}{\partial y} \right) = -\frac{\partial P}{\partial x} + \mu_f \frac{\partial^2 v_x}{\partial y^2} \tag{4.7}$$

$$v_x \frac{\partial c}{\partial x} + v_y \frac{\partial c}{\partial y} = D \frac{\partial^2 c}{\partial y^2} \tag{4.8}$$

The equations above are difficult to solve analytically for the entire system. The relevant behavior near the wall, however, can be described using the boundary-layer theory to obtain approximate solutions to Eq. (4.6) – Eq. (4.8) for velocity and concentration in a very thin layer near the wall. Because the time-scale for erosion of the dosage form is much larger than the time-scale for the velocity and concentration profile in the boundary layer to reach steady-state conditions, the problem is reduced to a steady-state problem with momentum and concentration boundary layer thicknesses as illustrated in Fig. 4.1.

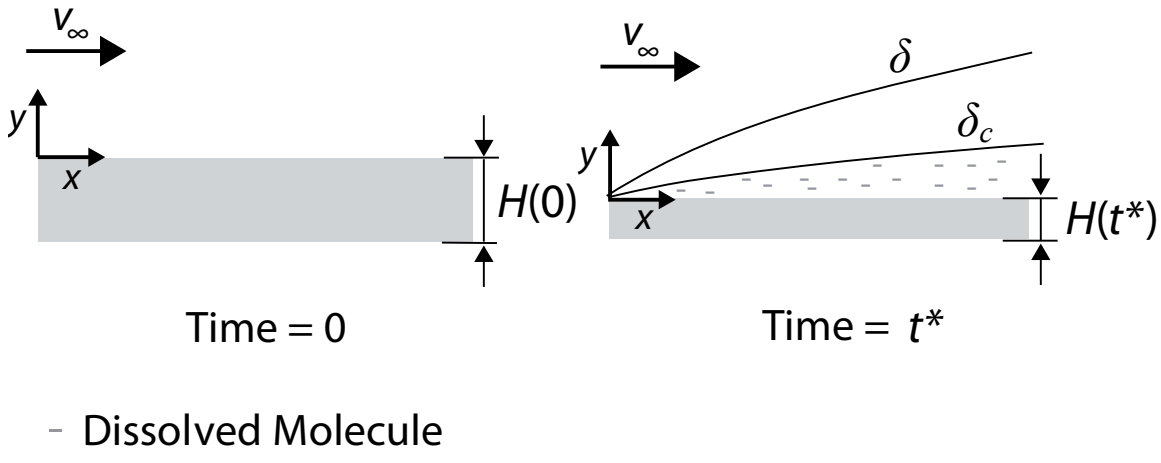

Figure 4.1: Erosion of single-phase material. At time $t = 0$, the dosage form is immersed in the dissolution medium. The velocity relative to the dosage form is set to a value equal to v_∞, and the viscous boundary layer and the concentration boundary layer develop.

Boundary conditions applied for the velocity to solve Eq. (4.6) – Eq. (4.8) within the boundary layer are $v_x = 0$ at the solid surface and $v_x = v_\infty$ at the outer edge of the momentum boundary layer. The velocity, v_∞, is constant for all values of x, and hence the pressure gradient, dP/dx is equal to zero. The corresponding boundary conditions for the concentration are $c = c_0$ at the eroding surface and $c = 0$ at the outer edge of the concentration boundary layer.

Using the equation of continuity, both the equation of motion of the fluid and the equation of continuity of the eroding species can be formally integrated, with the boundary conditions just given, to yield the following set of boundary layer balances:

$$\mu_f \left.\frac{\partial v_x}{dy}\right|_{y=0} = \frac{d}{dx}\int_0^\infty \rho_f v_x \left(v_\infty - v_x\right) dy \tag{4.9}$$

$$\rho D \left.\frac{\partial c}{dy}\right|_{y=0} = -\frac{d}{dx}\int_0^\infty \rho_f v_x c \, dy \tag{4.10}$$

Eq. (4.9) and Eq. (4.10) are extensions of the *von Karman* balances, which are transformations of the original Prandtl boundary layer equations [7]. Solutions to Eq. (4.9) and Eq. (4.10) are called 'approximate boundary layer solutions', because they are based on reasonable guesses for the velocity and the concentration profile. The solutions for the cumulative mass transferred obtained from 'approximate boundary layer solutions' have the same form as the respective exact solution. In fact, the approximate and the exact solutions for the accumulated mass transferred only vary by a constant factor. Thus, the 'approximate boundary layer solutions' allows one to obtain the correct dependence of the erosion rate, dH/dt, on the relevant variables and parameters.

In systems with large Schmidt numbers ($Sc = \mu/\rho D$), which is typical in erosion of pharmaceutical material, the concentration boundary layer thickness is small compared with the momentum boundary layer thickness. This allows to approximate the velocity profile with a simple linear function while safely guaranteeing accuracy of the underlying model. Also for the concentration profile within the concentration boundary layer, a simple linear form is assumed here. This improves simplicity of the model, but still allows to

obtain correct dependence of the solutions for erosion rate on the relevant variables and parameters. The solutions will be off by a constant factor, but this is acceptable considering the purpose of the analysis performed here. The assumed forms of the velocity and the concentration profile are:

$$\frac{v_x}{v_\infty} = \begin{cases} \dfrac{y}{\delta(x)} & y \le \delta \\ 1 & y \ge \delta \end{cases} \tag{4.11}$$

$$\frac{c}{c_0} = \begin{cases} 1 - \dfrac{y}{\delta_c(x)} & y \le \delta_c \\ 0 & y \ge \delta_c \end{cases} \tag{4.12}$$

Eq. (4.9) – Eq. (4.12) can then be solved to give for the momentum and concentration boundary layer thicknesses as [7-9]:

$$\delta(x) = \sqrt{12\frac{\mu_f x}{\rho_f v_\infty}} \tag{4.13}$$

$$\delta_c(x) = \delta(x)\left(\frac{\rho_f D}{\mu_f}\right)^{\frac{1}{3}} \tag{4.14}$$

Because the concentration profile in the concentration boundary layer is linear, the local mass flux on the eroding surface for a flat diskin stirred solution can be written as:

$$\frac{dm}{dt}(x) = \frac{M_n D c_0}{\delta_c(x)} = M_n c_0 D^{\frac{2}{3}} \sqrt{\left(\left(\frac{\rho_f}{\mu_f}\right)^{\frac{1}{3}} \frac{v_\infty}{12x}\right)} \tag{4.15}$$

Integration of Eq. (4.15) over the eroding surface and division by the eroding surface area allows derivation of the erosion rate of the flat disk:

$$\frac{dH}{dt} = \frac{1}{\rho_s}\frac{dm}{dt} = \frac{M_n c_0 D^{\frac{2}{3}}}{\rho_s} \sqrt{\left(\left(\frac{\rho_f}{\mu_f}\right)^{\frac{1}{3}} \frac{v_\infty}{3L}\right)} \tag{4.16}$$

where M_n is the number averaged molecular weight of the eroding component, ρ_s is its density in the solid state, D the component's diffusion coefficient in the dissolution medium, and c_0 is its concentration in the dissolution medium at the solid-liquid interface which is equal to the component's solubility, c_s. Eq. (4.16) is an important result, as it shows the correct dependence of the erosion rate on the relevant parameters for a single-phase system. It is evident that the geometry may be more complex than a flat disk. Dosage form geometry affects fluid flow in the vicinity of the eroding surface, and this causes the solution for the erosion rate to change by a geometry-dependent factor without affecting the rest of the solution.

If again the geometry of a flat disk is considered with constant eroding surface area, then accumulated amount of drug embedded in a single-phase material can be calculated by combining Eq. (4.5) with Eq. (4.16). Such material structures are, for example, observed if drug is in the amorphous form dissolved in the excipient matrix, and the cumulative amount of drug released is:

$$\frac{M_d}{M_{d,\infty}} = \frac{A\phi}{M_{d,\infty}} M_n c_0 D^{\frac{2}{3}} \sqrt{\left(\left(\frac{\rho_f}{\mu_f}\right)^{\frac{1}{3}} \frac{v_\infty}{3L}\right) \cdot t} \tag{4.17}$$

It may be noted that the relevant variables to model the systems considered here are the solubility of the eroding material in the dissolution medium, $M_n c_0$, its diffusion coefficient, D, the fluid density, ρ_f, the fluid viscosity, μ_f, and the fluid velocity, v_∞. Eroding solids consisting of small molecules typically show a sharp solid-liquid interface that can be characterized, for example, by a step function of viscosity with constant finite value equaling the viscosity of the medium on the liquid side and infinite value on the solid side. In this case, the solid/liquid interface and all the relevant variables required for the calculations above are easy to determine. In polymer-solvent systems, however, viscosity depends on polymer concentration, which causes the equation of motion, Eq. (4.7) to become nonlinear within the concentration boundary layer [10]. Furthermore, the solid/liquid interface is relatively diffuse, and thus it is not obvious which values to choose for both c_0 and D because D in dilute solutions is different from that in concentrated solutions. Because polymeric excipients are widely used for the formulation of a variety of solid dosage forms, a model to describe erosion of such materials is developed and shown below.

4.3.2 Erosion of Single-Phase Polymers in Agitated Medium

The concentration-dependence of the viscosity in the polymer-solvent system causes the equation of fluid motion in Eq. (4.7) to become nonlinear within the concentration boundary layer. This affects calculation of the viscous boundary layer thickness which in turn affects the thickness of the concentration boundary layer. The problem needs to be solved numerically if a precise solution is desired. In the context of this work, however, the focus is on the identification of scaling laws and upper- and lower-bound solutions to determine the relevant design and formulation parameters that affect drug release. The upper bound of viscosity is at the concentration c_0 and the lower bound equals the viscosity of the dissolution medium as illustrated in Fig. 4.2. If upper and lower bound of viscosity are applied in Eq. (4.7) and Eq. (4.9), an upper and a lower bound for the viscous boundary layer is obtained. This allows derivation of the range and the correct dependence on relevant parameters of the concentration boundary layer thickness, δ_C, to calculate dm/dt and dH/dt provided that c_0 and D are known and constant (Fig. 4.3).

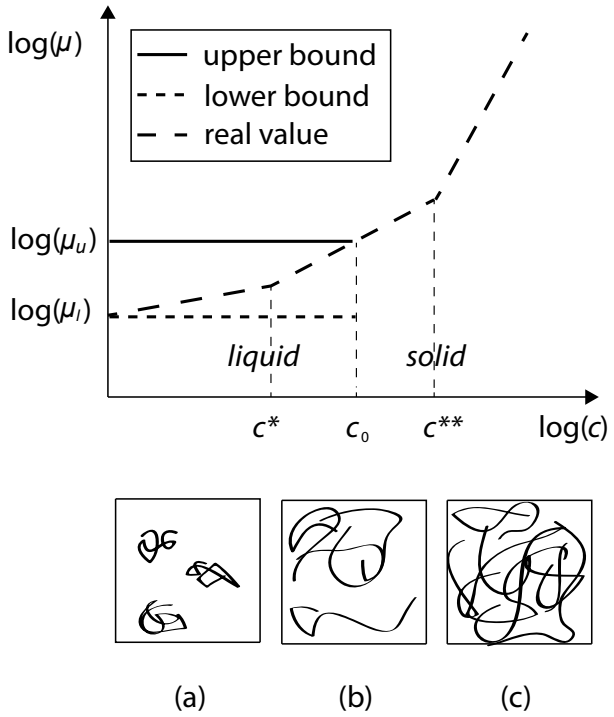

Figure 4.2: Viscosity as a function of polymer concentration. The region with polymer concentration below c^* refers to dilute solution (a), a polymer concentration between c^* and c^{**} refers to semi-dilute solution (b), and a polymer concentration above c^{**} refers to concentrated solution (c). Also illustrated are the upper and the lower bounds of viscosity in the concentration boundary layer with a solid-liquid interface concentration equal to c_0 (adapted from Ref. [10] and Ref. [11]).

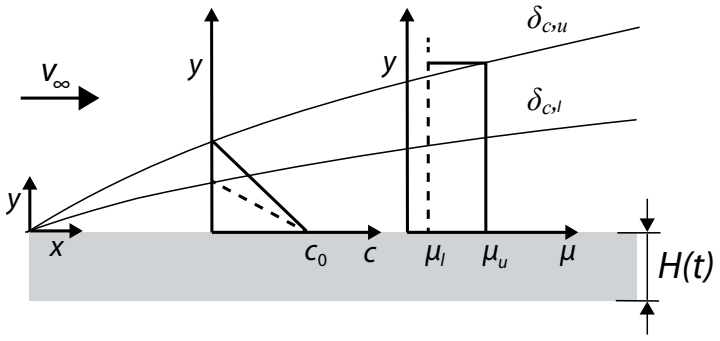

Figure 4.3: Illustration of upper and lower bounds of concentration boundary layer thickness, concentration gradient, and liquid solution viscosity. Solid and dashed lines represent upper bound and lower bound of viscosity.

However, c_0 and D are difficult to determine precisely, because swelling is another phenomenon that complicates modeling. Even though the rate at which the medium penetrates the dosage form in surface erosion is per definition much smaller than the rate at which material is converted into dissolved molecules, the solid/liquid interface still is relatively diffuse in polymeric systems. In fact, the interface can be characterized by viscosity, which is a continuous function of distance starting with the value of the medium on the far liquid side and ending with the highest value deep inside the solid on the solid side. Therefore, it is not obvious which values to choose for both c_0 and D (D in dilute solutions is different from D in concentrated solutions). To elucidate this problem, theories and concepts of polymer dynamics developed by polymer physicists are applied.

The interfacial region of eroding polymers can be subdivided into three regions, each with its unique characteristics. These are: dilute region, semi-dilute region, and the concentrated region (Fig. 4.2) [11,12]. The polymer concentration c^* that separates the dilute from the semi-dilute region is defined as the concentration above which polymer molecules overlap where the spherical radius that each polymer on average occupies scales as:

$$R_g \propto N^{\nu} b \tag{4.18}$$

This gives for c^*:

$$c^* \cong \frac{3}{4\pi N_A R_g^3} \tag{4.19}$$

The semi-dilute region still retains some of the characteristics of dilute solutions, such as large and strongly correlated fluctuations in the segment density. If the polymer concentration is sufficiently large, the fluctuations become small and can be treated by a simple mean field theory. Such a solution is called concentrated, and the concentration that separates the semi-dilute from the concentrated region is denoted c^{**}.

As shown in Fig. 4.2, erosion of polymeric systems is modeled by Eq. (4.16) and assuming c_0 to lie within the semi-dilute region. The argument for this assumption is that

both polymer diffusion and fluid flow are negligibly small in concentrated solution compared with dilute or semi-dilute solution. Hence, c_0 can be written as:

$$c_0 = ac^* \qquad 1 < a < \frac{c^{**}}{c^*} \tag{4.20}$$

Further assuming that D can be described by Zimm's model for dilute solutions [11,12]:

$$D_g = 0.203 \frac{k_B T}{\sqrt{6}\mu_f R_g} \propto \frac{1}{M_n^{\nu}} \tag{4.21}$$

where k_B is Boltzmann's constant, T is the temperature, and μ_f is the solvent viscosity. Combining Eq. (4.16), and Eq. (4.18) – Eq. (4.21) the scaling laws for mass flux and the erosion rate become as follows, similar to the results obtained by Ju et al. [13-15]:

$$\frac{dm}{dt} \propto M_n^{-3.66\nu+1} \tag{4.22}$$

$$\frac{dH}{dt} \propto M_n^{-3.66\nu+1} \tag{4.23}$$

4.3.3 Erosion of Single-Phase Material in Still Medium

A different kinetics of the erosion rate is obtained when the dissolution medium is still and not agitated. In this case, the Peclet number is low and only diffusion is relevant. Hence, only the equation for the continuity of the species, Eq. (4.8), needs to be solved with $v = 0$, boundary conditions $c = c_0$ at the surface and $c = 0$ at infinity, and an initial condition of $c = c_0$ on the eroding surface and $c = 0$ in the solution infinitely far away from the eroding surface. The inverse of this problem has extensively been studied in electrochemical systems with the Cottrell equation describing the flux of species to an electrochemical electrode in unstirred solution [16,17]. The erosion rate, dH/dt, is still

dependent on the solubility of the material in the dissolution medium and its diffusion coefficient in this case and can be written as:

$$\frac{dH}{dt} = \frac{1}{\rho_s}\frac{dm}{dt} = \frac{1}{\rho_s}\frac{M_n c_0 \sqrt{D}}{\sqrt{\pi t}} \tag{4.24}$$

The accumulated amount of material released versus time can be calculated by combining Eq. (4.3) with Eq. (4.24), and it is consequently proportional to $t^{1/2}$ in this case.

4.4 Erosion of Two-Phase Systems

4.4.1 Relevant Characteristics of Microstructure in Erosion of Two-Phase Material

Most pharmaceutical dosages are not single-phase, but consist of a multi-phase material that can be characterized by randomly distributed drug particles in an excipient matrix. In contrast to the homogeneous case analyzed in the previous section, the eroding surface considered here is heterogeneous consisting of both drug and excipient. Because drug particles are randomly distributed, the location of drug and excipient phase on the eroding surface changes with time as the dosage form erodes, causing the spatial concentrations of drug and excipient to change. In the analysis performed here, it is assumed that the time-scale of changing the structure of the eroding surface is much larger than the time scale for mass transfer to reach steady state. The problem is therefore reduced to a steady-state problem.

Further, a parameter that may be affected by the presence of multiple components (i.e. drug and excipient), is the diffusion coefficient [17]. Here, a dilute solution assumption is made where diffusion coefficients are uncoupled. Consequently, Eq. (4.6) – Eq. (4.8) can be applied to calculate convective mass transfer rates and erosion rates of the individual phases. If Eq. (4.11) and Eq. (4.12) are again used to describe the postulated velocity and concentration profiles, then Eq. (4.13) and Eq. (4.14) give the thicknesses of the viscous

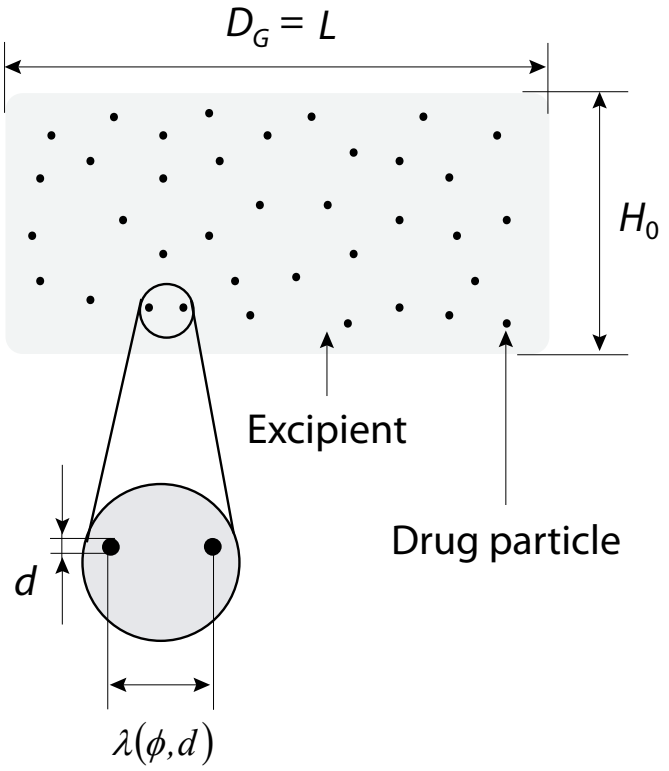

Figure 4.4: Illustration of the design of a disk-shaped dosage form comprising randomly distributed drug particles embedded in a non-porous excipient matrix.

and concentration boundary layers. Boundary conditions of the surfaces covered by excipient and drug, respectively, are set equal to the solubilities of the individual phases (i.e. excipient and drug) in the dissolution medium. If the concentration boundary layer thickness is averaged over the entire area of the surface, Eq. (4.15) and Eq. (4.16) are obtained to describe the convective mass flux and erosion rate of the pure excipient phase, $dm_{e,0}/dt$ and $dH_{e,0}/dt$, as well as the mass flux and the erosion rate of the pure drug phase, $dm_{d,0}/dt$ and $dH_{d,0}/dt$, respectively. Therefore, the convective mass fluxes and erosion rates of the individual phases in 2-phase material with heterogeneous eroding surface are modeled to follow the same equations as if they were embedded in a single-phase material with homogeneous surface.

The erosion rate of the two-phase pharmaceutical dosage form, dH/dt, depends, however, not only on erosion rates of the individual phases, but also on the details of how the underlying microstructure is arranged. In the present case with randomly distributed drug particles in an excipient matrix, the microstructure is characterized by the drug volume fraction, φ, and the particle size, d. Both φ and d define the distribution of the interparticle distance, λ (Fig. 4.4). In the present case, because a rapidly eroding excipient is used for fast disintegration of the dosage form, the drug particles typically erode at a slower rate than the excipient phase. They can therefore block erosion of the excipient. Depending on the microstructure of the underlying sample, two different mechanisms by which such slowly eroding particles can block erosion of the faster eroding phase are distinguished: (a) blockage of excipient erosion by isolated, slowly eroding drug particles and (b) blockage of excipient erosion by interconnected clusters of slowly eroding drug particles.

A cluster of an individual phase, in agreement with the definition by Stauffer and Aharony, is referred here to a group of nearest neighboring sites occupied by the same phase in the lattice [18]. If the lattice is, for example, made up of an array of squares, then squares with one common side are considered nearest neighbors, and squares that touch each others corner are called next nearest neighbors. The cluster is considered interconnected if it extends from one side of the system to the other. It can be shown that there are two drug volume fractions in the infinitely large square lattice to characterize such interconnected clusters of drug and excipient: these are the percolation threshold of the drug

phase, φ^{*}, and the percolation threshold of the excipient phase, φ^{**}. In the infinite square lattice, the volume fraction above which the drug phase forms an interconnected cluster is 0.59, and the volume fraction below which the excipient phase forms an interconnected cluster is 0.41. Fig. 4.5 presents finite square lattices of randomly distributed drug particles and excipient at various drug volume fractions. It is evident that an excipient cluster exists that spans the size of the system at a drug volume fraction of 0, 0.2, and 0.4, whereas a drug cluster exists that spans the size of the system at a drug volume fraction of 0.6, 0.8, and 1. It may be noted, however, that percolation thresholds change as the underlying lattice or the definition of a cluster is changed. In an infinite simple cubic lattice, for example, with a cluster defined by cubes that are next nearest neighbor, the drug phase forms an interconnected cluster at a drug volume fraction above 0.31. On the other hand, excipient phase forms an interconnected cluster up to a drug volume fraction of 0.69 in this lattice.

Moreover, the probability that an interconnected cluster of a phase exists depends on the size of the system. In an infinite system, the probability that an interconnected cluster of an individual phase exists versus the volume fraction of the phase is a step function, (i.e. equal to 1 above the percolation threshold, φ_c, and equal to zero below φ_c). The systems considered here, however, are of finite size. In finite systems, the lattice may start to percolate at a different volume fraction than the percolation threshold. It is generally accepted that the average percolation threshold, φ_{av}, can be described as a function of the system size, L, as:

$$\phi_{av} - \phi_c \propto L^{-\frac{1}{\upsilon}} \tag{4.25}$$

The proportionality constant of this function is smaller than 1, and for the exponent, the equation $1/\upsilon \geq 1$ is valid. In the present case, the drug particle size is of the order of 20 μm - 100 μm, and the system size is about 1 mm – 20 mm. Therefore, for the present case, the equation $|\varphi_{av} - \varphi_c| \leq 0.1$ is valid. Consequently, the average percolation threshold of the finite system considered here is reasonably close to the value of the infinite system, and the values obtained for the infinite system are therefore used to guide the model.

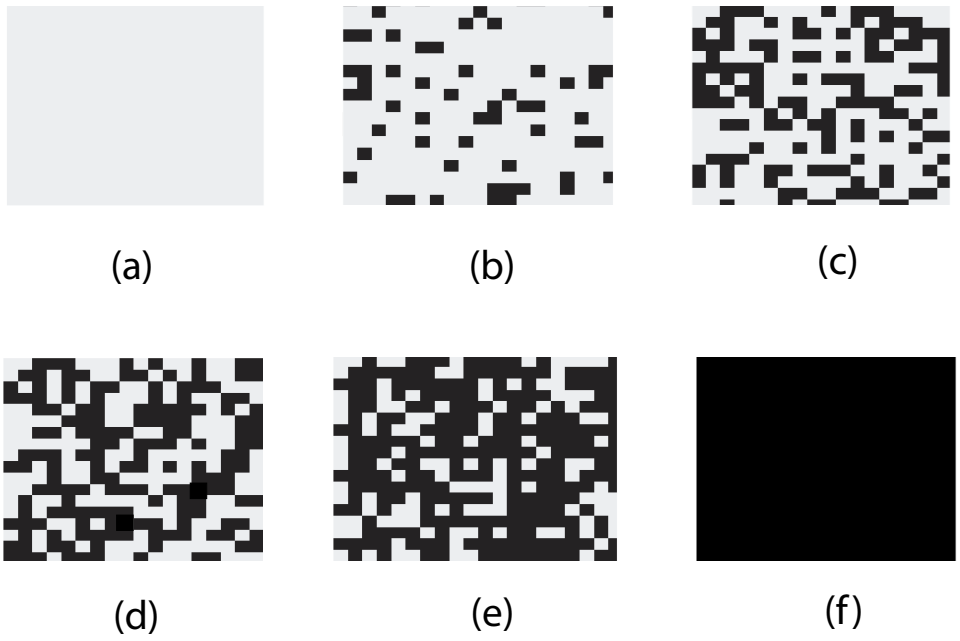

Figure 4.5: Illustration of relevant microstructures of two-phase material with faster eroding phase (gray) and slower phase (black): (a) $\varphi = 0$, (b) $\varphi = 0.2$, (c) $\varphi = 0.4$, (d) $\varphi = 0.6$, (e) $\varphi = 8$, and (f) $\varphi = 1$.

Since dosage forms are 3-d systems, the drug volume fraction above which drug particles form at least one cluster that is interconnected in the infinite lattice, i.e. the percolation threshold of the drug phase, φ^*, is considered to be about 0.31. The drug volume fraction below which the excipient phase forms an interconnected cluster in the infinite lattice, i.e. the percolation threshold of the excipient phase, φ^{**}, is considered to be about 0.69. In the present model, accordingly, three regimes based on the characteristics of the clusters of the individual phases are distinguished. In the first regime, the drug volume fraction is between $\varphi = 0$ and $\varphi = \varphi^*$, where no cluster of interconnected drug particles is formed. Drug particles are embedded in the excipient matrix as isolated particles in this case. The second regime spans drug volume fractions between $\varphi = \varphi^*$ and $\varphi = \varphi^{**}$, with a microstructure characterized by clusters of both excipient phase and drug phase. The drug phase is partially interconnected in this regime. Finally, the third regime is at a drug volume fraction above φ^{**} where no interconnected excipient cluster is found in the infinite lattice. The drug phase is therefore fully interconnected in this case.

4.4.2 Erosion of Two-Phase Material, $\varphi < \varphi^*$

In the first regime where the drug volume fraction is so low that excipient is well-interconnected and drug particles are isolated in the excipient, fast-eroding excipient can erode around the drug particles, and simply wash them off once their surrounding eroded. The rate of excipient mass released from the dosage form, dM_e/dt, can, according to the schematic in Fig. 4.6, be modeled as follows:

$$\frac{dM_e}{dt} = A_e \frac{dm_e}{dt} = A_{e,p} \frac{dm_{e,0}}{dt} = A_{e,p} \frac{M_n D c_0}{\bar{\delta}_e} = A_{e,p} M_n c_0 D^{\frac{2}{3}} \sqrt{\left(\left(\frac{\rho_f}{\mu_f} \right)^{\frac{1}{3}} \frac{v_\infty}{3L} \right)} \tag{4.26}$$

where A_e is the excipient surface area, i.e. the area covered by excipient at the position of the excipient-medium interface, dm_e/dt is the excipient flux with respect to A_e, $A_{e,p}$ is the projected surface area of the excipient accounting for the fact that part of the excipient

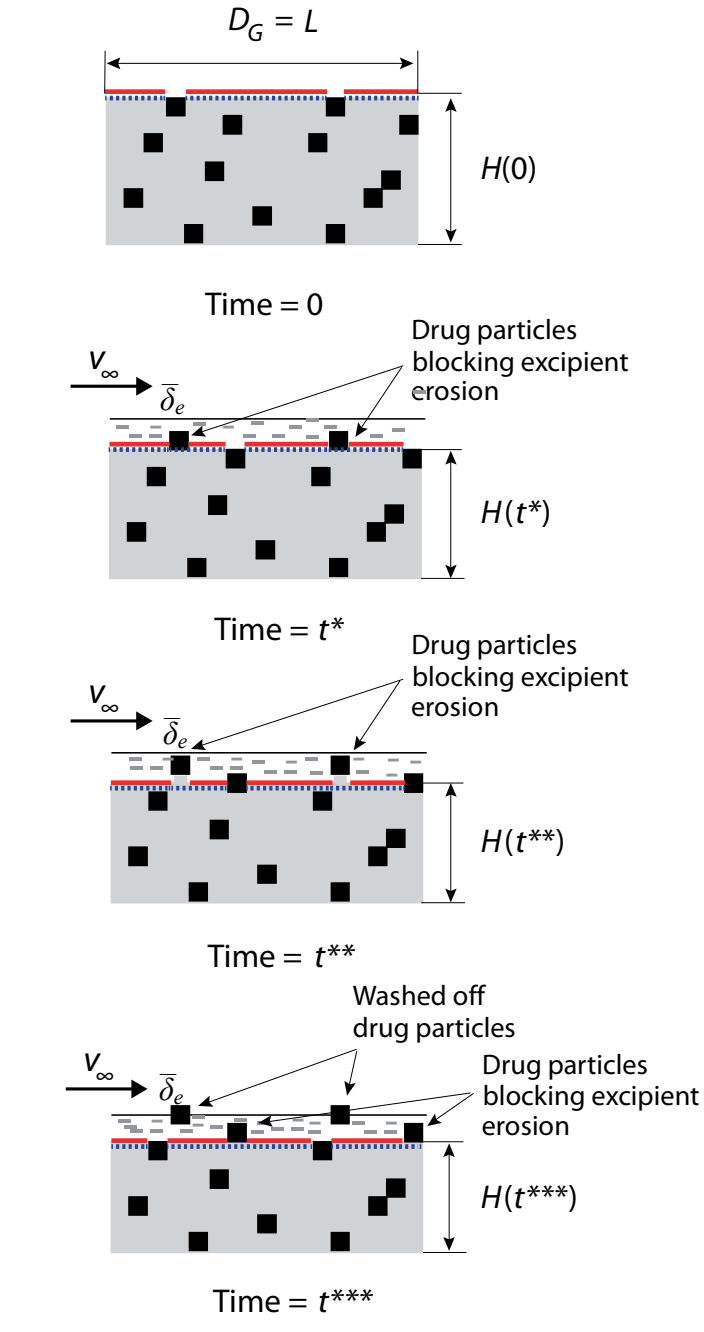

Figure 4.6: Erosion of 2-phase material comprising slowly eroding particles embedded in a rapidly eroding matrix at $\varphi < \varphi^*$.

surface area is blocked by protruding drug particles, and $dm_{e,0}/dt$ is the excipient flux with respect to $A_{e,p}$. $dm_{e,0}/dt$ can be described by Eq. (4.15). Since the drug volume fraction equals the drug area fraction, the excipient surface area, A_e, can be described as a function of the total surface area, A, and the drug volume fraction as:

$$A_e = (1-\phi)A \tag{4.27}$$

The projected surface area covered by excipient, $A_{e,p}$, is typically smaller than A_e, because protruding drug particles block part of the excipient surface area. If the protruding drug particles do not form any clusters along the direction of erosion, and the particles are washed off in the time during which the thickness of a particle size is eroded, then the excipient surface area that is blocked by such drug particles is equal to the area fraction of the drug, as illustrated in Fig. 4.6. Therefore, again because the drug area fraction is equal to the drug volume fraction:

$$A_{e,p} = (1-\phi)^2 A \tag{4.28}$$

This result allows derivation of the excipient mass flux, which at such low drug volume fractions determines the erosion rate of the dosage form, dH/dt. It can be written:

$$\frac{dm_e}{dt} = (1-\phi)\frac{dm_{e,0}}{dt} \tag{4.29}$$

$$\frac{dH}{dt} = \frac{dH_e}{dt} = (1-\phi)\frac{dH_{e,0}}{dt} \tag{4.30}$$

Therefore, even though the erosion rate is determined by the erosion rate of the excipient at low drug volume fractions because excipient can erode the surrounding of drug particles to wash them off, protruding drug particles affect the erosion rate of the excipient and the dosage form by reducing the surface area available for excipient mass transfer. Therefore, even if drug particles are dispersed in the excipient matrix at a drug volume

fraction below φ^*, the erosion rate of the excipient and the dosage form of such a system is smaller than the erosion rate of a sample consisting of pure excipient.

4.4.3 Erosion of Two-Phase Material, $\varphi > \varphi^{**}$

As the drug volume fraction is increased above φ^*, and the drug particles become interconnected, the mechanism of washing-off drug particles by excipient erosion around the particle's surrounding is increasingly suppressed. It is modeled that in the third regime, at a drug volume fraction above the second percolation threshold where the excipient does not form an interconnected cluster, washing-off drug particles by excipient erosion around the particle's horizontal surrounding becomes negligible. Erosion is then considered as a 1-d problem, where the dosage form is considered as an array of infinitesimally small units that erode unaffected by their surrounding. As shown in Fig. 4.7, the infinitesimally small unit alternately consists of drug and excipient units. Using the condition that length fraction is equal to volume fraction, it is derived that the drug units make up a length fraction equal to φ of the total length of the unit, whereas the excipient length fraction is 1-φ of the total length of the unit. The erosion rate of the unit depends on the phase that is on its surface. If it is the drug, then the unit erodes at the rate of the drug, and if it is excipient, then the unit erodes at the rate of the excipient. The time-averaged erosion rates of all the infinitesimally small units that make up the dosage form are identical, as they are composed of the same ratios of drug and excipient. The time-averaged erosion rate of the dosage form can therefore be written as:

$$\frac{dH}{dt} = \left(\frac{\dot{H}_{d,0}\dot{H}_{e,0}}{(1-\phi)\dot{H}_{d,0} + \dot{H}_{e,0}\phi} \right) \tag{4.31}$$

Eq. (4.31) is simply the harmonic mean of drug erosion rate and excipient erosion rate with respect to the drug volume fraction.

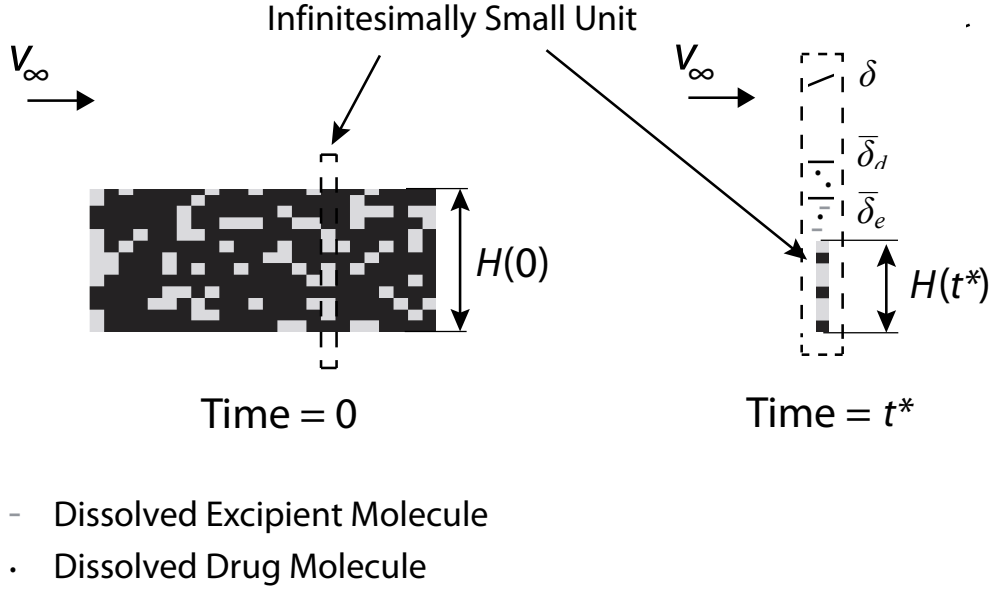

Figure 4.7: Surface erosion of two-phase dosage form at high drug volume fraction. Drug particles cannot be washed off by erosion of their surrounding. An infinitesimally small unit is extracted, and the erosion rate of this infinitesimally small unit follows the erosion rate of the phase on the surface. The average erosion rate of the dosage form equals the average erosion rate of the infinitesimally small unit.

4.4.4 Summary of Erosion and Drug Release of Two-Phase Dosage Forms

If a linear interpolation with respect to drug volume fraction in the interval φ^* and φ^{**} is applied, based on Eq. (4.30) and Eq. (4.31) the erosion rates can be expressed as:

$$\frac{dH}{dt} = \begin{cases} (1-\phi)\dfrac{dH_{e,0}}{dt} & \phi \le \phi^* \\ \left.\dfrac{dH}{dt}\right|_{\phi=\phi^*}\left(\dfrac{\phi^{**}-\phi}{\phi^{**}-\phi^*}\right)+\left.\dfrac{dH}{dt}\right|_{\phi=\phi^{**}}\left(\dfrac{\phi-\phi^*}{\phi^{**}-\phi^*}\right) & \phi^* < \phi < \phi^{**} \\ \dfrac{\dot{H}_{e,0}\dot{H}_{d,0}}{\phi\dot{H}_{e,0}+(1-\phi)\dot{H}_{d,0}} & \phi \ge \phi^{**} \end{cases} \quad (4.32)$$

From the erosion rate, it is possible to derive the drug release rate by Eq. (4.2), the drug release flux by multiplying with the density of the drug and the drug volume fraction, dosage form disintegration time by Eq. (4.4), and the accumulated amount of drug released by Eq. (4.3). For a flat disk, the asymptotic value of normalized accumulated amount of drug released, by combining Eq. (4.32) with Eq. (4.5) can be written as:

$$M_d = \begin{cases} A\rho_d\phi(1-\phi)\dfrac{dH_{e,0}}{dt}t & \phi \le \phi^* \\ A\rho_d\phi\left.\dfrac{dH}{dt}\right|_{\phi=\phi^*}\left(\dfrac{\phi^{**}-\phi}{\phi^{**}-\phi^*}\right)\cdot t + A\rho_d\phi\left.\dfrac{dH}{dt}\right|_{\phi=\phi^{**}}\left(\dfrac{\phi-\phi^*}{\phi^{**}-\phi^*}\right)\cdot t & \phi^* < \phi < \phi^{**} \\ A\rho_d\phi\dfrac{\dot{H}_{e,0}\dot{H}_{d,0}}{\phi\dot{H}_{e,0}+(1-\phi)\dot{H}_{d,0}}t & \phi \ge \phi^{**} \end{cases} \quad (4.33)$$

It must be noted, however, that the equations provided here to describe the erosion rate

and the normalized amount of drug released only give asymptotic values. They do not, for example, account for the effect of surface roughness on erosion. A surface profile develops due to the heterogeneous erosion rates of drug and excipient, and its effect on erosion is discussed next.

4.5 Effect of Surface Roughness on Erosion of Two-Phase Materials

It is evident that the slower eroding phase not only blocks surface area for erosion of the faster eroding phase, but also protrudes from the surface to form a rough profile. Surface roughness affects fluid flow in the vicinity of the surface, and it can therefore affect mass transfer and erosion. Surface roughness can, for example, induce turbulence, and turbulence increases mass transfer rates and erosion rates. The Reynolds number in the current problem, however, is about 3 orders of magnitude below the critical Reynolds number, and turbulence is therefore neglected.

In laminar flow, fluid that flows towards a protruding surface element adheres to the wall it hits. Consequently, the direction of the fluid velocity changes in the vicinity of this wall. This causes a rise in fluid pressure in the vicinity of the wall facing upstream. The same pressure gradient initially develops locally behind the protruding element. However, if the uphill pressure gradient behind the protruding element is so large that the flow next to the wall facing downstream reverses direction, the flow separates from this wall. 'Standing' eddies appear in this case behind the element, and these eddies act like 'fluiddynamic' rollers over which the main stream flows, Fig. 4.8. The average velocity in these 'standing' eddies is small compared with the velocity in the fluid stream [19-23].

Clearly, the effect of these 'standing' eddies on fluid flow near the top surface of the slower eroding drug component, which resembles the protruding surface elements, is minimal. However, the effect of these 'standing' eddies on fluid flow near the eroding surface of the faster eroding excipient can be significant. Fluid flow is reduced in the 'standing' eddies, and this causes convective mass transfer to be decreased. The 'standing' eddies therefore act as a barrier for mass transfer of the excipient, and cause an increase in the thickness of the respective excipient concentration boundary layer.

The erosion rate of the faster eroding excipient can hence be written as:

$$\frac{dH_{e,r}}{dt} = f\frac{dH_e}{dt} \tag{4.34}$$

where dH_e/dt is the erosion rate of the excipient phase. The extent by which these 'standing' eddies affect mass flux from the excipient surface to the fluid stream, and hence erosion rate of the excipient component, can be characterized by two non-dimensional variables: the average height of the protruding surface elements divided by the average excipient concentration boundary layer thickness of the smooth surface, $\delta_e/(\delta_e+h)$, and the fraction of the excipient surface which is covered by 'standing' eddies, l/λ. The parameter f can therefore be written as:

$$f = f\left(\frac{\delta_e}{\delta_e + h}, \frac{l}{\lambda}\right) \tag{4.35}$$

The first variable, $\delta_e/(\delta_e+h)$, gives a measure of the maximum factor by which the average excipient concentration boundary layer thickness is increased due to 'standing' eddies. The average height of the protruding elements, h, is of the order of the the drug particle size, which typically is in the range between 20 μm and 200 μm. The rationale behind such a particle size range is that very small drug particles are difficult to produce, whereas large particles may exhibit unfavorable dissolution characteristics or not allow production of a dosage form with the desired content uniformity (i.e. the desired variation in drug content). The excipient concentration boundary layer of the smooth surface, δ_e, can be calculated using Eq. (4.14), and it is of the order of 20 μm - 50 μm for candidate excipients, such as PEG, PEO, sugars, or polyols under typical fluid flow conditions. Therefore, as in a typical case, the boundary layer thickness of the smooth surface is 50 μm, and the drug particle size is 100 μm, the maximum factor by which the erosion rate can be reduced due to surface roughness effects is two. Consequently, surface roughness effects are usually secondary compared with the effects of interconnected clusters of an individual phase or the effect of slowly eroding, protruding drug particles blocking excip-

ient area for erosion discussed in the previous section, which can reduce the erosion rate of the two-phase sample compared with the pure excipient by orders of magnitude.

The second variable, l/λ, gives a measure of the fraction of the maximum factor, by which the average excipient concentration boundary layer thickness is increased due to the 'standing' eddies, Fig. 4.8. Two regimes based on the value of l/λ are distinguished. In regime 1, the fluid flow in the valleys between the excrescences of the surface is only minimally affected by their presence. The fluid penetrates the gaps between the excrescences of the surface, and hence provides for convective mass transfer near the eroding excipient surface ($l < \lambda$). In regime 2, however, the fluid does not penetrate the gaps between the excrescences of the surface ($l \geq \lambda$). The maximum increase in the excipient concentration boundary layer thickness is achieved if the fluid between the excrescences is stagnant. The increase of the excipient concentration boundary layer thickness is of the order of the drug particle size. The erosion rate of the excipient is therefore modeled as follows for rough surfaces:

$$\frac{dH_{e,r}}{dt} = \begin{cases} f\left(\frac{h}{\delta_e}, \frac{l}{\lambda}\right)\frac{dH_e}{dt} & l < \lambda \\ \frac{\delta_e}{\delta_e + h}\frac{dH_e}{dt} & l \geq \lambda \end{cases} \tag{4.36}$$

Here, $1 > f > \delta_e/(\delta_e+h)$ is valid, and exact values of f must be determined experimentally. The length l of the surface between two particles which is covered by the 'standing' eddy is hard to determine analytically. It can, however, be characterized based on previous observations made on flow past objects. Characteristics of vortices behind an object have for example been extensively studied for flow over a circular cylinder. In this case, the wake develops if the Reynolds number is above 4, and stays completely laminar if the Reynolds number is below 40 [19]. The eddies get longer as the Reynolds number is increased. In fact, the length of the eddies depends on Re_h for any geometry. Therefore, also in the present case where the flow is affected by the wall upstream and downstream the protruding element, Re_h acts as a good non-dimensional parameter to characterize the

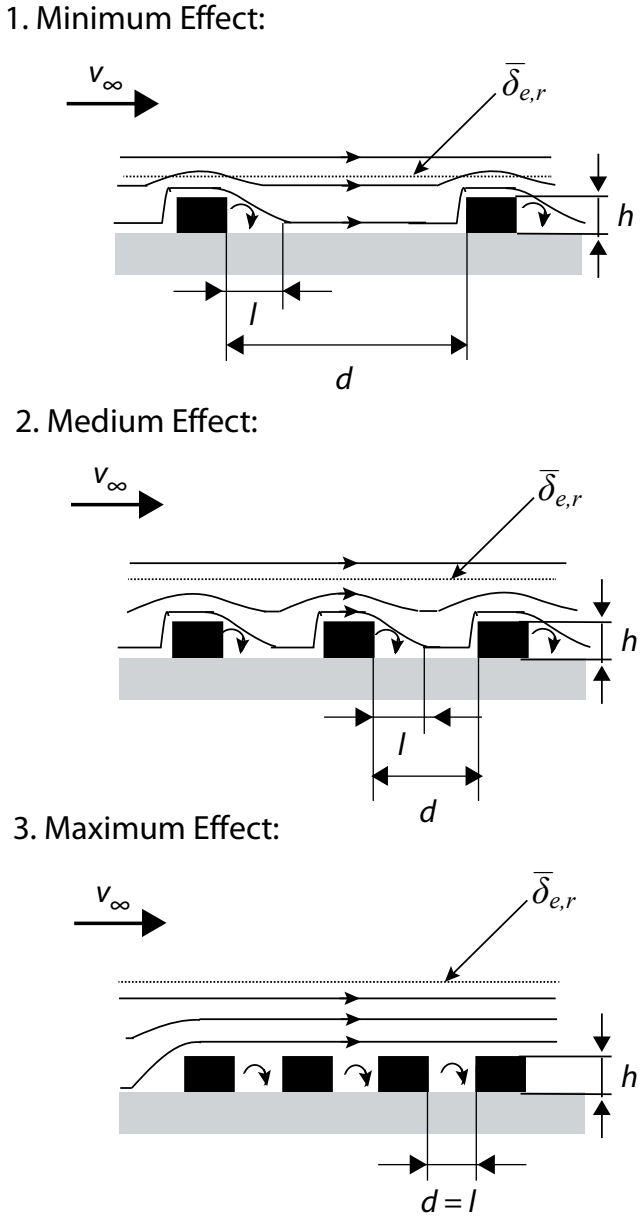

Figure 4.8: Ilustration of the different characteristics of fluid flow in the vicinity of the eroding surface and average excipient concentration boundary layer thickness of the rough surface. The schematics above have been drawn based on visualized experimental results of fluid flow around such surface profiles presented in Ref. [24].

extent of l. Hence, the equation $l = const.\ Re_h h$ is proposed for the calculation of l, with *const* being a geometric factor. The inter-particle distance can be estimated from the drug volume fraction and the drug particle size to be about $d(1/\varphi\text{-}1)$ where d is the size of an individual particle.

4.6 Summary

A model for the erosion rate of a single-phase non-porous material under the conditions of a typical dissolution test for immediate-release solid dosage forms is first developed using convective mass transfer equations along with the Navier-Stokes equations to describe fluid flow. In addition to the conditions and properties of flow and fluid such as v_∞, ρ_f, and μ_f, the erosion rate depends on diffusivity, D, of the eroding component in the dissolution medium, as well as the solid-liquid interface concentration, c_0. If the eroding material has a sharp solid-liquid interface, both c_0 and D are easy to derive. Polymers, which are heavily used as pharmaceutical excipients, however, usually exhibit swelling resulting in a diffuse solid-liquid interface, which may even depend on the conditions of fluid flow. This makes it difficult to determine D and c_0 in such materials. Here, Zimm's model for dilute solution is applied to determine D, and for c_0, the equation $c_0 = ac^*$ is used with c^* being the concentration above which polymer molecules overlap and a being a proportionality constant.

The model for the erosion rate of a single-phase material is then expanded to account for the effects of material microstructure on erosion in two-phase systems comprising a fast eroding excipient phase with randomly distributed drug particles that erode slowly. Two microstructural effects are given particular importance: the effect of blockage of excipient erosion by isolated, slowly eroding drug particles, and the effect of blockage of excipient erosion by interconnected clusters of slowly eroding drug particles. The two cases can be distinguished by the drug volume fraction of the randomly distributed particles in the excipient matrix, with two percolation thresholds that can be derived from the percolation theory.

In the new model, accordingly, three regimes with different laws for the erosion rate based on drug volume fraction are differentiated. In the first regime, the drug volume fraction is below φ^*, where φ^* is the drug volume fraction below which the drug particles are isolated in the excipient matrix. The erosion rate of the dosage form is modeled to follow the erosion rate of the excipient phase, but taking into account the excipient surface area that is blocked by the isolated drug particles. In contrast, if the drug volume fraction is above φ^{**}, where φ^{**} is the drug volume fraction above which there is no cluster of interconnected excipient phase, the erosion rate of the dosage form is modeled to follow the weighted harmonic mean of the individual phase's erosion rates. If the drug volume fraction is between the first and the second percolation threshold, the erosion rate is linearly interpolated between the value obtained at φ^* and the value obtained at φ^{**}.

A further effect that is discussed is the effect of surface roughness that develops due to the heterogeneous erosion rates, which is affected by the ratio of the average height of the protruding surface elements and the average excipient concentration boundary layer thickness of the smooth surface, h/δ_e, and the fraction of the excipient surface which is covered by 'standing' eddies, l/λ. Taking this effect into account, the erosion rate of the excipient is calculated as $dH_{e,r}/dt = f^*dH_e/dt$. The parameter f depends on the variables stated above, and a range for f is defined as $1 < f < \delta_e/(\delta_e+h)$. The exact value of f in between this range, however, needs to be fitted to experimental data.

Nomenclature

A	eroding surface area [m^2]
A_e	excipient area at the position of the eroding surface [m^2]
$A_{e,p}$	projected excipient surface area [m^2]
a	proportionality constant to determine the solid-liquid interfacial concentration
b	bond length within the polymer chain [m]
c	concentration of a particular species in dissolution medium [mol/m^3]
c_0	concentration of a particular species at solid-medium interface [mol/m^3]

c_s	solubility of a particular species in dissolution medium [mol/m^3]
c^*	polymer concentration at the boundary of dilute and semi-dilute region [mol/m^3]
c^{**}	polymer concentration at the boundary of semi-dilute and concentrated region [mol/m^3]
D	diffusion coefficient [m^2/s]
D_g	diffusion coefficient of the polymer's center of mass [m^2/s]
d	particle size [m]
f	factor by which the erosion rate is decreased due to surface roughness
H	thickness of sample [m]
H_0	initial thickness of sample [m]
dH/dt	erosion rate of the sample [m/s]
$dH_{d,0}/dt$	erosion rate of pure drug phase [m/s]
dH_e/dt	erosion rate of excipient phase [m/s]
$dH_{e,0}/dt$	erosion rate of pure excipient phase [m/s]
$dH_{e,r}/dt$	erosion rate of excipient phase of a rough surface [m/s]
h	surface roughness or profile height [m]
k_B	Boltzmann's constant [J/K]
L	characteristic length of eroding surface [m]
l	length of a standing eddy [m]
M_0	initial sample mass [kg]
M_d	accumulated amount of drug released [kg]
$M_{d,\infty}$	drug content initially in the dosage form [kg]
M_n	number averaged molecular weight [g/mol] or [kg/mol]
dM/dt	rate of mass released [kg/s]

dM_d/dt	drug release rate [kg/s]
dm/dt	mass flux [kg/m^{2}s]
dm_d/dt	drug release flux [kg/m^{2}s]
N	number of bonds along the polymer chain
N_A	Avogadro's number
P	fluid pressure [Pa]
R_g	polymer radius [m]
T	temperature [K]
Re	Reynolds number
t	time [s]
t_d	disintegration time to erode sample [s]
v	fluid velocity [m/s]
v_∞	maximum fluid velocity [m/s]
δ	viscous boundary layer thickness [m]
δ_c	concentration boundary layer thickness [m]
δ_e	excipient concentration boundary layer thickness [m]
λ	interparticle distance [m]
ρ_f	fluid density [kg/m^3]
ρ_d	solid density of drug [kg/m^3]
ρ_s	average density of solid sample [kg/m^3]
μ	viscosity [Pa·s]
μ_f	viscosity of dissolution medium [Pa·s]
ν	Flory exponent
φ	drug volume fraction
φ^*	drug volume fraction below which there is no interconnected drug cluster

φ^{**} drug volume fraction above which there is no interconnected excipient cluster

References

[1] D.O. Cooney, 1972, Effect of Geometry on the Dissolution of Pharmaceutical Tablets and Other Solids: Surface Detachment Kinetics Controlling, AIChE Journal, 18, 446-449.

[2] I. Katzenhendler, 1997, A. Hoffman, A. Goldberger, M. Friedman, Modeling of Drug Release from Erodible Tablets, J. Pharm. Sci., 86, 110-115.

[3] M.J. Ferrua, R.P. Singh, 2010, Modeling the Fluid Dynamics in a Human Stomach to Gain Insight of Food Digestion, Journal of Food Science, 75, R151-R162.

[4] J.B. Dressmann, G.L. Amidon, C. Reppas, V.P. Shah, 1998, Dissolution Testing as a Prognostic Tool for Oral Drug Absorption: Immediate Release Dosage Forms, Pharmaceutical Research, 15, pp. 11-22.

[5] The U.S. Pharmacopeial Convention, US Pharmacopeia, USP 35-NF 30.

[6] S.M. Diebold, Physiological Parameters Relevant to Dissolution Testing: Hydrodynamic Considerations, in J. Dressman, J. Kraemer, 2005, Pharmaceutical Dissolution Testing, Taylor & Francis Group, Boca Raton, FL, USA.

[7] R.B. Bird, W.E. Stewart and E.N. Lightfoot, 2002, Transport Phenomena, Second Edition, John Wiley & Sons, New York.

[8] E. Brunner, 1904, Reaktionsgeschwindigkeit in heterogenen Systemen, Z. Phys. Chem., 47, 56-102.

[9] W. Nernst, 1904, Theorie der Reaktionsgeschwindigkeit in heterogenen Systemen, Z. Phys. Chem., 47, 56-102.

[10] M. Rubinstein, 2003, in Polymer Physics, Oxford University Press, Oxford, UK.

[11] M. Doi and S.F. Edwards, 1986, The Theory of Polymer Dynamics (Eds: J. Birman, S.F. Edwards, C. H. Llewellyn Smith and M. Rees), Oxford University Press, Oxford, UK.

[12] M. Doi, 1996, Introduction to Polymer Physics, Oxford University Press, Oxford, UK.

[13] R.T.C. Ju, P.R. Nixon, M.V. Patel, 1995, Drug release from hydrophilic matrices. 1. New scaling laws for predicting polymer and drug release based on the polymer disentanglement concentration and the diffusion layer, J. Pharm. Sci. 84, 1455-1463.

[14] R.T.C. Ju, P.R. Nixon, M.V. Patel, D.M. Tong, 1995, Drug release from hydrophilic matrices. 2.A mathematical model based on the polymer disentanglement concentration and the diffusion layer , J. Pharm. Sci. 84, 1464-1477.

[15] R.T.C. Ju, P.R. Nixon, M.V. Patel, 1997, Diffusion coefficients of polymer chains in the diffusion layer adjacent to a swollen hydrophilic matrix, J. Pharm. Sci. 86, 1293-1298.

[16] A.J. Bard, L.R. Faulkner, 2001, Electrochemical Methods, Second Edition, John Wiley & Sons, New York.

[17] E.L. Cussler, 1997, Diffusion Mass Transfer in Fluid Systems, Cambridge University Press, Cambridge, UK.

[18] D. Stauffer, 1986, Introduction to Percolation Theory, Taylor & Francis Ltd, London UK and Philadelphia USA.

[19] P. Kundu, I.M. Cohen, 2012, Fluid Mechanics, Fifth Edition, Academic Press, Oxford, UK.

[20] H. Schlichting, 1936, Experimentelle Untersuchungen zum Rauhigkeitsproblem, Ingenieur-Archiv 7, pp. 1-34.

[21] H. Schlichting, 1987, Boundary Layer Theory, 7th edition, Mc-Graw-Hill, New York, NY.

[22] P.R. Owen, W.R. Thomson, 1962, Heat transfer across rough surfaces, Fluid Mech. 15, pp. 321-334.

[23] A. Niavarani, N.V. Priezjev, 2009, The effective slip length and vortex formation in laminar flow over a rough surface, Physics of Fluids, 21, 052105-1 - 052105-10.

[24] S. Taneda, 1979, Visualization of Separating Stokes Flows, J. Phys. Soc. Jpn., 46, 1935-1942.

This page is intentionally left blank.

CHAPTER V

EXPERIMENTAL VALIDATION OF THE NON-POROUS, IMMEDIATE-RELEASE MODEL

5.1 Introduction

The model developed in Chapter IV for the dissolution kinetics of non-porous immediate-release dosage forms is experimentally validated using suitable excipient and API materials, and the findings of these efforts are presented in this chapter. Erosion experiments have been performed where the thickness of the eroding dosage form, a thin circular disk, is measured versus time. Further, dissolution tests have been conducted where the concentration of the dissolved API is measured versus time under specified conditions. The results obtained are first used to derive empirical equations to determine the dependence of erosion rate on the relevant variables. Calculated values using the model introduced in Chapter IV and measured values of erosion rate and drug release flux are then compared to determine the validity and limitations of the model.

5.2 Materials and Methods

5.2.1 Material Selection for Model Validation

The excipients chosen for model validation belong to the group of polyethylene glycols (PEGs) and polyethylene oxides (PEOs). The PEGs and PEOs have the same molecular structures, as illustrated in Fig. 5.1. They therefore differ only in molecular weight, which for PEGs is below 100,000 g/mol and for PEOs above 100,000 g/mol. PEGs and PEOs were selected because they are linear polymers with high solubility that are surface-eroding (i.e. phase-eroding). Further, due to their low melting temperatures, below 70°C, and good melt stability, they are well suited to be hot-melt processed. PEGs and PEOs are available in a variety of molecular weights, and hence properties of the material can

be changed just by altering the molecular weight, without changing the underlying repeat unit of the material [1-4].

The API selected here to validate the model is aspirin, which has a chemical structure as shown in Fig. 5.2. Aspirin is chosen because it is inexpensive and has low potency. Also, with a solubility of about 4 mg/ml in the dissolution medium, orders of magnitude lower than the solubility of PEGs, it well represents most of the small-molecule APIs that erode at a significantly slower rate than the fast eroding excipient [5,6].

5.2.2 Materials for Sample Preparation

All the materials used to formulate the samples to perform erosion and dissolution experiments were purchased from Sigma-Aldrich (St. Louis, MO). They include aspirin (USP-grade), PEG 1,500 (Fluka), PEG 6,000 (Fluka), PEG 8,000 (Fluka), PEG 20,000 (Fluka), PEG 35,000 (Fluka), and PEO 100,000 (Fluka). The medium to perform erosion tests was tap water, whereas the dissolution medium was prepared using glacial acetic acid, sodium acetate trihydrate, and deionized water according to the USP monograph for aspirin tablets. Glacial acetic acid (USP-grade) and sodium acetate trihadrate (USP-grade) were purchased from Sigma-Aldrich (St. Louis, MO), whereas the deionized water used was purified by a water filtration station (Milli-Q, 18.2 MΩ, Millipore, Billerica, MA).

5.2.3 Sample Preparation by Hot-Melt Casting

Samples prepared by hot melt casting were single-phase consisting of excipient only. The first step to prepare such a hot-melt cast sample was to heat up the raw excipient material in powder form to obtain a uniform, homogeneous melt at a temperature of 90°C. This melt was then filled into a pre-heated plastic syringe. An aliquot of the melt was afterwards placed on the surface of the bottom mold cavity which was at a temperature of 25°C. Subsequently, the aliquot was compressed with the top mold, where a hand press with maximum force of 2,500 N was used to apply the compressive force (Fig. 5.3).

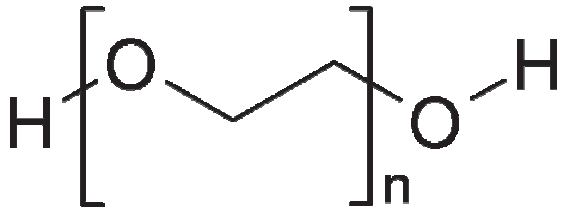

Figure 5.1: Structural formula of polyethylene glycol (PEG) and polyethylene oxide (PEO). PEGs have a molecular weight below 100,000 g/mol, whereas the molecular weight of PEOs is above 100,000 g/mol.

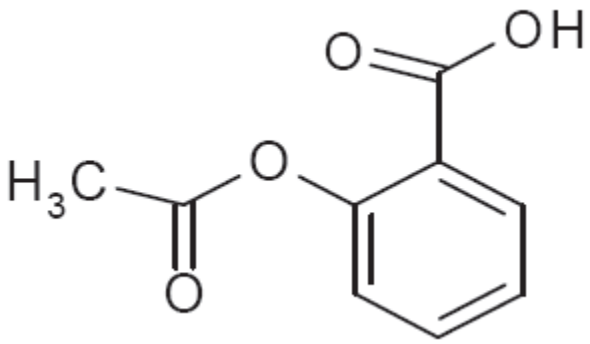

Figure 5.2: Structural formula of aspirin. The molecular weight of aspirin is 180 g/mol.

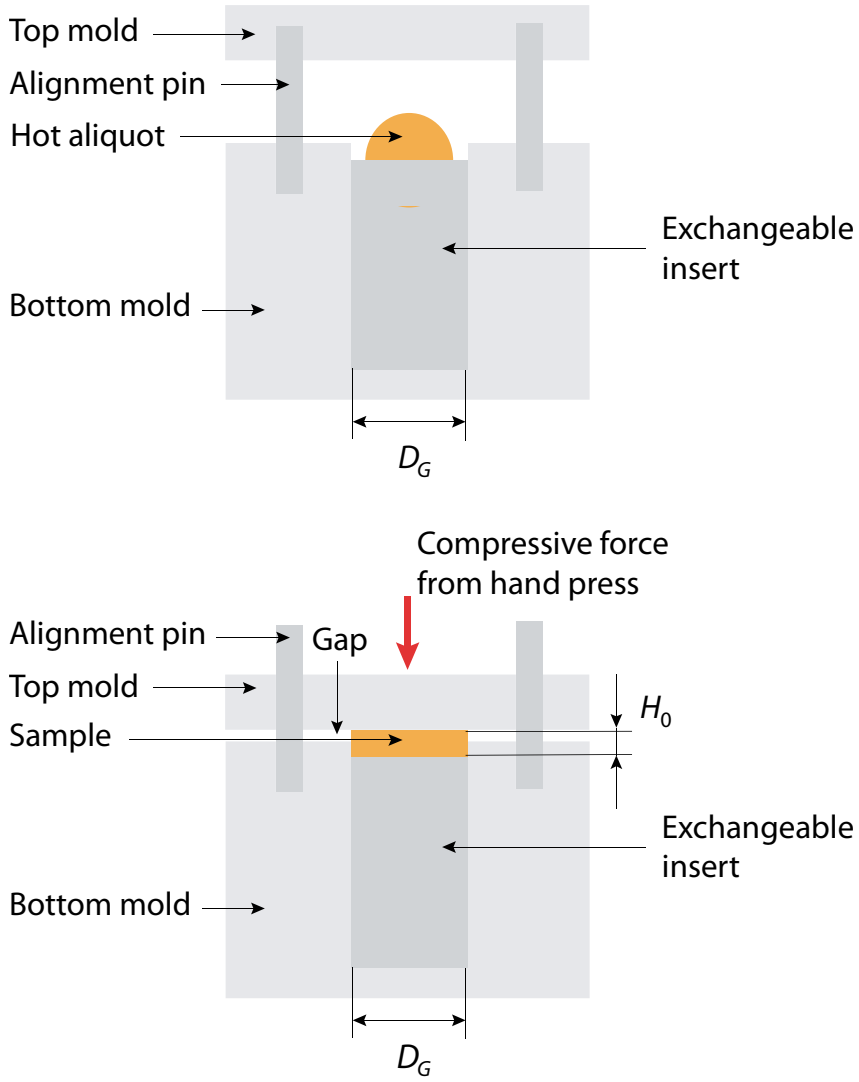

Figure 5.3: Illustration of the hot-melt casting setup for sample preparation. Top: A hot aliquot which has been placed on the bottom mold. Bottom: The aliquot is compressed, cooled, and solidified to form the finished sample.

The cooling time was 30 seconds. The samples so prepared had a thickness of 1.5 mm and a diameter of 12.7 mm (Table 5.1).

5.2.4 Setup for Preparing Injection-Molded Samples

All the injection-molded samples were prepared using a home-made, laboratory-scale injection-molding machine, as shown in Fig. 5.4. The major components of this machine are a linear actuator, an injection piston, a melting chamber, temperature controlled molds, a mold clamp, and a mechanical frame. The linear actuator is an electrical drive that allowed control of position and velocity up to a load of 1.5 tons (Tritex II AC Linear Actuator, Exlar, Chanhassen, MN) to operate the injection piston (a 1 cm diameter class Z gage pin, Meyer Gage Company, South Windsor, CT). The melting chamber plasticizes the raw material and allows it to be pressurized by the piston. It is, for the main part, a stainless-steel annulus with an inner diameter of 10 mm and an outer diameter of 50 mm surrounded by a band heater for temperature control. Its inner tube is manufactured at a tolerance that gives a maximum gap-size between piston and die of 10 μm. Near the interface to the mold, the inner diameter of the melting chamber is decreased to 1.5 mm to give an analog to a hot runner. Also the temperature-controlled molds are made of stainless steel. They constitute the gate, the mold cavity, and cooling channels. The gate, which is simply the inlet channel of plasticized material into the mold cavity, is 1.5 mm in diameter. The mold cavity is a hole with diameter D equal to 12.7 mm and a length of 30 mm. It is possible to insert pins into the mold cavity to adjust the length of the cavity, such that samples at different thicknesses can be produced. Temperature control of the molds is by water circulation through the integrated cooling channels using a fluid temperature control unit (Lauda-Brinkmann, Lauda-Koenigshofen, Germany). The mold clamp guarantees that the molds stay closed during injection and can be opened upon injection and solidification of the sample to be produced. A linear pneumatic actuator with bore diameter 250 mm and a stroke of 125 mm (Festo, Esslingen am Neckar, Germany) is used. Finally, the mechanical frame comprises four shafts, four plates, sleeve bearings for the movable plates, and bushings for the fixed plates. The shafts are hardened and have a diameter of 1.5 inches and a length of 60 inches (McMaster-Carr, Elmhurst, IL).

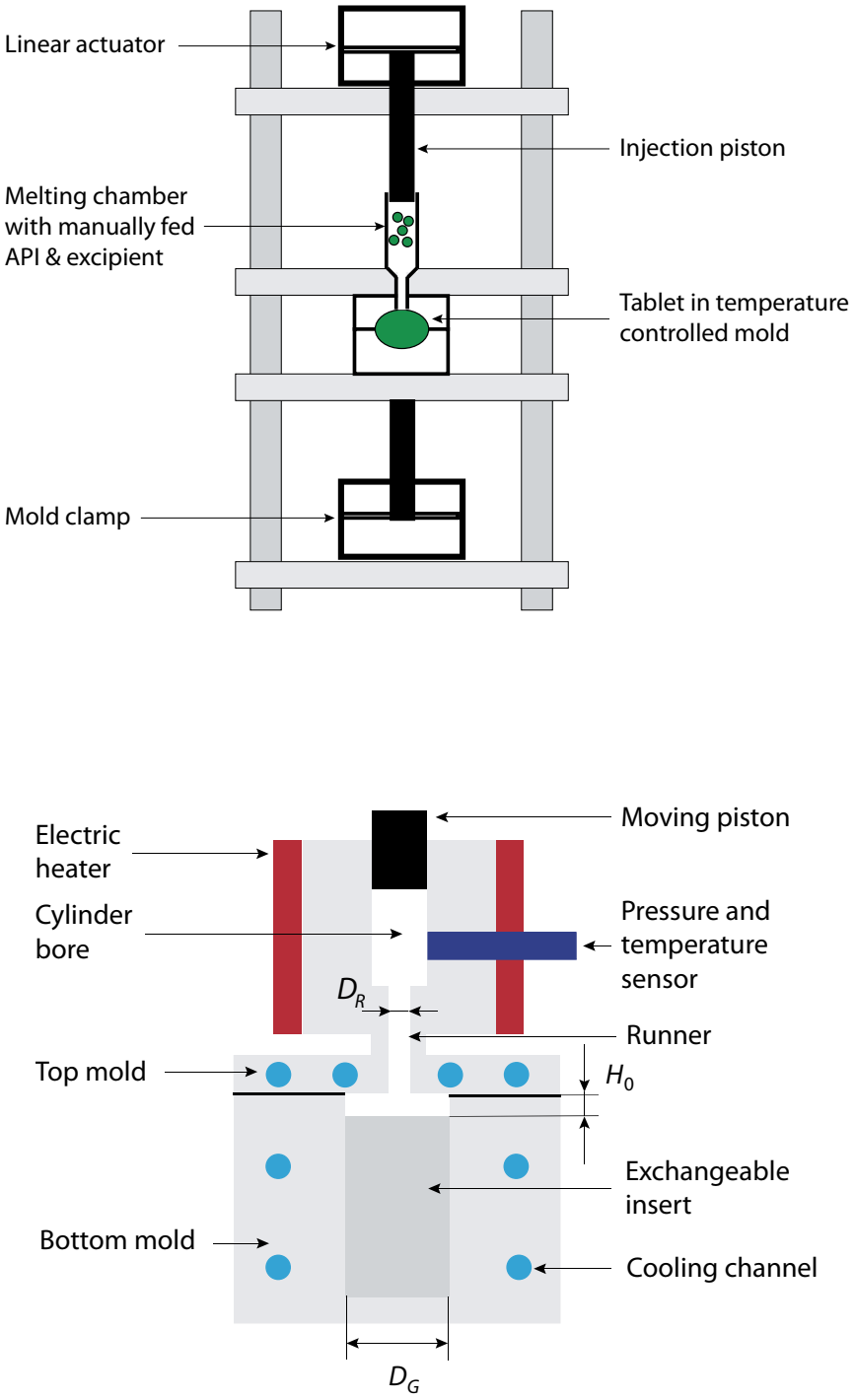

Figure 5.4: Illustration of the injection-molding setup for sample preparation. Top: Schematic of the injection-molding machine. Bottom: Schematic of the melting chamber with injection piston and mold.

The plates are made out of 4140 alloy steel, they are surface-ground and have dimension 16.5 x 13.75 x 1.25 inch (Precision Grinding, Birmingham, AL). Bronze bearings (McMaster-Carr, Elmhurst, IL) are used for the movable plates and B-Loc keyless bushings (Fenner Drives, Manheim, PA) are used to fix the non-movable plates. A photograph of the injection-molding machine is given in Appendix B.

5.2.5 Preparation of Injection-Molded Samples

Samples prepared by injection-molding were either single-phase consisting of excipient only or two-phase consisting of both excipient and drug. For preparation of the injection-molded samples, the raw material in powder form first needed to be prepared if the material consisted of multiple components. This step initially comprised reduction of particle size of the individual components using a mortar and a pestle. Then these particles were sieved with a mesh 70 and mesh 270 sieves such that particles size between 50 μm and 150 μm was obtained. Powders of individual components were then added into a glass jar at the determined ratio. Then, the powder was mixed for 60 minutes using a Turbula mixer (Willy A. Bachofen AG, Muttenz, Switzerland) to give a random mixture. No previous preparation of the powder was required if the sample to prepare was made of a single component.

The powder (either a single component or a mixture prepared as described above) could then be filled into the heated 10 mm diameter hollow cylinder of the laboratory-scale injection-molding machine. The melting chamber was at melt temperature, and the material was left in this chamber for 15 minutes after powder filling to guarantee that the temperature was uniform to give a well-plasticized material. Then, the molten material was injected into the mold using the piston-injector, which was driven by the electrical drive. The mold geometry which determines the geometry of the specific sample, could be adjusted by using different mold inserts. The material was then allowed to cool and solidify after the injection process-step was terminated. Finally, the non-porous sample was ejected from the mold. A picture of a sample so produced is presented in Fig. 5.5. The process parameters were volumetric flow rate, holding pressure, holding time,

Table 5.1: Material, geometric, and process parameters for sample preparation of erosion and dissolution tests. Erosion test samples were cast, whereas samples for dissolution tests were injection-molded (IM). Aspirin was used as API.

Parameter	**Erosion test (Casted sample)**	**Dissolution test (IM sample)**
Materials	PEG/PEO	API & PEG/API & PEO
Sample diameter (mm)	12.7	12.7
Sample thickness (mm)	1.5	0.5/1/1.8
Melt Temperature (°C)	90	75
Mold Temperature (°C)	25	25
Injection Flow Rate (cm^3/s)	-	5
Hold Pressure (MPa)	-	40
Casting pressure (MPa)	15	-
Cooling Time (s)	30	30

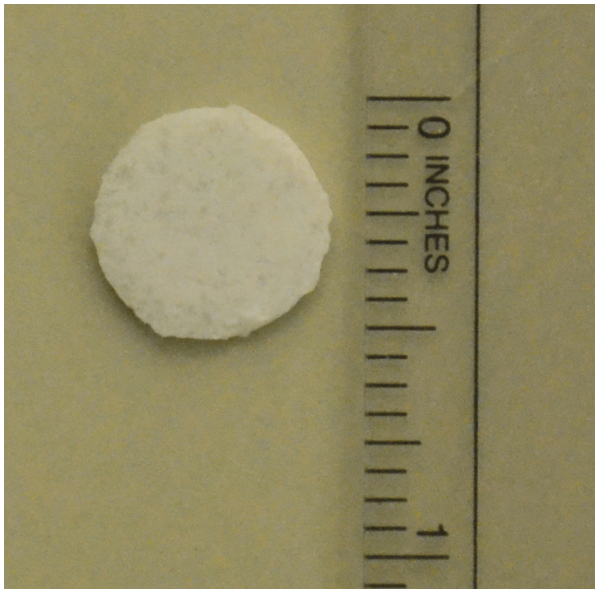

Figure 5.5: PEG-aspirin sample, 1 mm thick and with an aspirin volume fraction of 0.45.

melt temperature, mold temperature, and the cooling time. Different process parameter values were applied for samples with different geometry and material (Table 5.1).

5.2.6 Erosion Tests

Erosion tests were conducted using the home-built setup illustrated in Fig. 5.6. The sample was glued to a magnetic disk, which was attached to a rotating cylinder driven by an adjustable speed rotator (Bodine Electric Company, Chicago, IL, USA). The distance between the center of rotation of the cylinder and the outer edge of the sample, R_p, was 16.2 mm. A rotation rate of 50 rpm was applied, resulting in a maximum velocity of the medium relative to the sample of about 0.0848 m/s. The test was stopped as soon as the sample was eroded, the thickness of the sample measured, and the time recorded. The erosion rate was determined by dividing the eroded thickness by the erosion time (i.e., erosion rate = (initial thickness - final thickness) / erosion time). Table 5.2 summarizes the parameters used for the erosion test.

5.2.7 Dissolution Tests

Dissolution tests of the non-porous pharmaceutical samples at various aspirin loadings were performed according to the USP-Monograph for aspirin tablets [7]. A dissolution bath (Varian VK 7025, Agilent, Santa Clara, CA) and a Cary 50 Bio UV spectrophotometer (Agilent, Santa Clara, CA) comprised the equipment used to perform the dissolution tests (Fig. 5.7). The dissolution medium consisted of 500 ml deionized water with 1.49 g of sodium acetate trihydrate and 0.83 ml glacial acetic acid. The pH of the medium was 4.5, and it was kept at a temperature of 25˚C during the time-scale of the experiment. The dissolution bath was equipped with baskets (apparatus I), and the rotation rate of the baskets was set to 50 revolutions per minute (Fig. 5.8). The UV-measurements were done at a wavelength of 265 nm. The UV-absorption data obtained during the measurements were compared with the UV-absorption data obtained from the standard solution, such that the concentration of aspirin in the dissolution medium could be calculated for

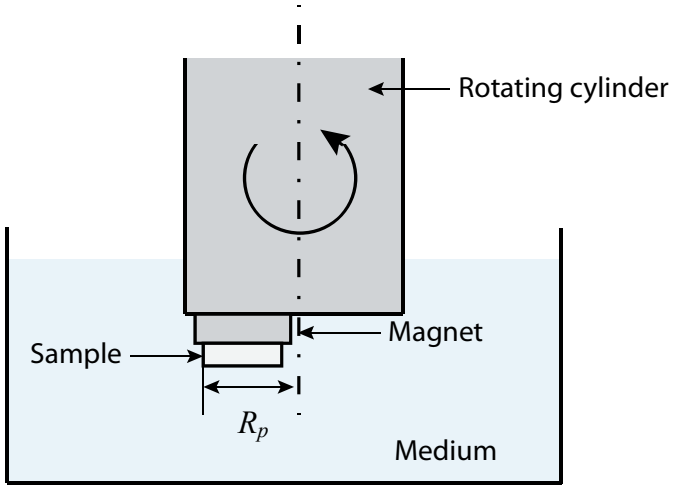

Figure 5.6: Schematic drawing of the erosion test setup. Also shown is the distance of the outer edge of the sample to the center of rotation. This distance is considered here as sample position.

Table 5.2: Experimental conditions of erosion and dissolution tests.

Parameter	Erosion test	Dissolution test
Apparatus	Adjustable speed rotator	UV Fiber optic dissolution
Type		Basket apparatus
Basket diameter		2 cm, according to USP
Measured value	Eroded thickness per time	API concentration
Erosion	From 1 side	From 2 sides
Sample position (outer edge)[a]	16.2 mm from cent. of rot.	10 mm from cent. of rot.
Rotation rate	50 rpm	50 rpm
Estimated max. fluid velocity[a]	0.0848 m/s	0.052 m/s
Medium	Tap water	According to USP
Medium volume	500 ml	500 ml
Medium pH	7	4.5

[a] Estimated max. fluid velocity = 2 x pi x Sample position x Rotation rate

Figure 5.7: Dissolution test setup (source: www.agilent.com/lifesciences/UVdissolution, as of February 4, 2014).

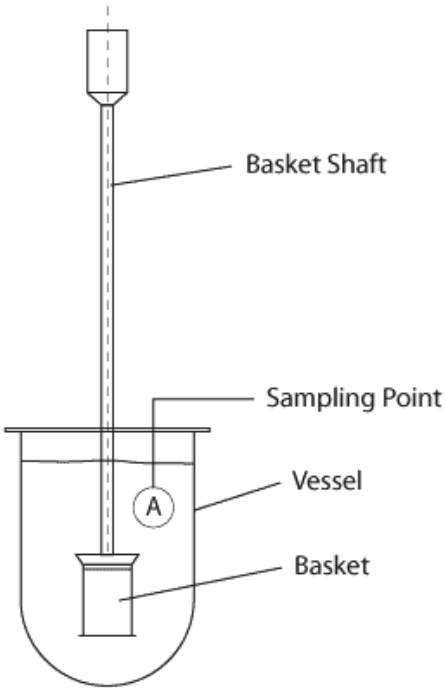

Figure 5.8: Rotating basket setup for dissolution test. (Adapted from www.tabletdissolution.com, as of February 4, 2014)

any data point. The absorption of the excipients at the wavelength chosen and at the given concentrations was found to have no significant effect on the signal. A UV-measurement was taken every minute during the time-frame of the experiment by probes inserted into the bath connected to the spectrophotometer by fiber optic cables.

5.3 Results

5.3.1 Erosion Data

Results of the erosion tests on pure, single-phase PEG and PEO excipients are presented in Table 5.3. The initial thickness of the hot-melt cast samples was between 1.4 mm and 1.6 mm, whereas the eroded thickness was between 1.02 mm and 1.35 mm. Erosion times varied between 11 min for PEG 6,000 and 105 min for PEO 100,000, which results in the erosion rate to be reduced by a factor of 9 if the number averaged molecular weight is increased by a factor of about 16.5 (i.e. from 6,000 g/mol to 100,000 g/mol). Fig. 5.9 shows a log-log plot of measured erosion rate versus excipient number averaged molecular weight. It is found, by linear regression, that the dependence of erosion rate on molecular weight under the experimental conditions studied can be written as $dH_{e,0}/dt = 1.75\text{x}10^{6}M_n^{-0.8}$. It may be noted that this equation is obtained at the velocity, $v_\infty = 0.0848$ m/s. If v_∞ is 0.052 m/s, the erosion rate of PEG, using $dH_{e,0}/dt \sim v_\infty^{0.5}$, can be calculated to follow the equation $dH_{e,0}/dt = 1.37\text{x}10^{6}M_n^{-0.8}$.

5.3.2 Dissolution Data

Dissolution data obtained from aspirin-PEG 8,000 samples that show the accumulated amount of drug released at a drug volume fraction of 0.45 are illustrated in Fig. 5.10 for sample thicknesses of 0.5, 1, and 1.8 mm. All three curves are close to linear with constant slope from $t = 0$ up to a time where the drug mass released is above 80% of the drug mass initially contained in the dosage form. The curves plateau, and the final cumulative

Table 5.3: Erosion time and erosion rate of pure PEG and PEO.

Excipient	Molecular weight (g/mol)	Sample thickness (mm)	Eroded thickness[a] (mm)	Erosion time[a] (min)	Erosion rate[b] (nm/s)
PEG 6k	6,000	1.55	1.19	12	1658
PEG 6k	6,000	1.45	1.09	11	1655
PEG 8k	8,000	1.40	1.14	14	1361
PEG 8k	8,000	1.60	1.19	13	1531
PEG 20k	20,000	1.50	1.09	27	674
PEG 20k	20,000	1.55	1.27	33	641
PEG 20k	20,000	1.60	1.35	35	641
PEG 35k	35,000	1.40	1.02	37	458
PEG 35k	35,000	1.50	1.14	46	405
PEO 100k	100,000	1.50	1.14	105	181

[a] "Eroded thickness" is defined as the thickness eroded during the "Erosion time".

[b] Erosion rate = eroded thickness/ erosion time

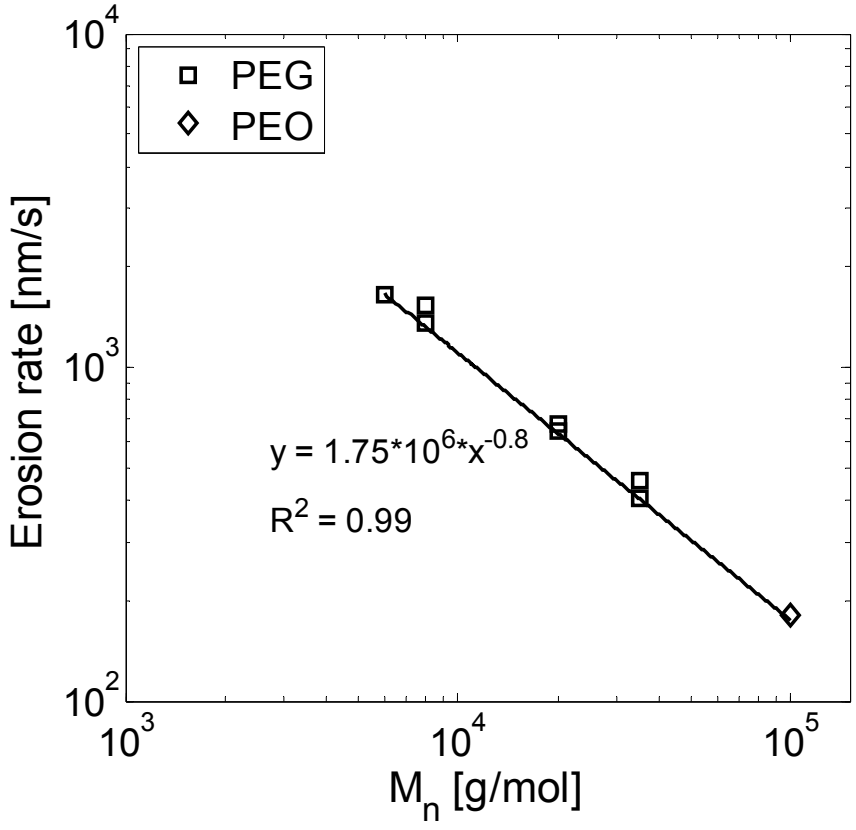

Figure 5.9: Measured erosion rate versus molecular weight of pure PEG and PEO.

amounts of drug released are consistent with a linear increase in drug content with thickness. 40, 80, and 144 mg were the final drug amounts released for the 0.5, 1, and 1.8 mm thick sample, respectively. The average slope of the curves, the drug release rate, is between 0.048 and 0.053 mg/s. Since these slopes do not change with time and are almost identical, it can be inferred that the drug release rate is: (a) at steady-state and (b) does not depend on sample thickness for the geometries studied. The erosion rates of the samples studied eroding from two sides can hence be calculated as $H_0/2t_{0.8}$, where $t_{0.8}$ is the dissolution time. The dissolution time considered here is the time it takes to dissolve 80% of the initial drug mass contained in the dosage form. The dissolution time is equal to the time to release 80% of the drug from the dosage form, if the drug dissolves immediately once it is released to the free flowing dissolution medium. Due to the small drug particle size together with the physicochemical properties of aspirin, it is assumed here that the drug dissolves immediately after it is released from the dosage form. The erosion rates of the 0.5, 1, and 1.8 mm thick sample are 303, 333, and 308 nm/s, respectively, and do not change as the sample thickness is changed.

Fig. 5.11 illustrates dissolution data obtained from 1 mm thick aspirin-PEG 8,000 samples at different aspirin volume fractions. The values of the linear slopes of the curves, the drug release rates, are of the same order of magnitude for a drug volume fraction of 0.17, 0.3, and 0.45, with values of 0.05, 0.065, and 0.053 mg/s, respectively. These values are significantly larger than the value of the slope at 0.76 aspirin volume fraction, which is 0.019 mg/s. Consequently, the drug release rate at 0.76 aspirin volume fraction is significantly reduced compared with the values obtained for 0.17, 0.3, and 0.45 drug volume fraction. The erosion rates are continuously decreasing as the drug volume fraction is increased, with values of 833, 606, 333, and 69 nm/s at drug volume fractions of 0.17, 0.30, 0.45, and 0.76.

The dependence of aspirin-PEG and aspirin-PEO dissolution curves on excipient molecular weight is presented in Fig. 5.12. The samples that belong to the curves shown are 1 mm thick and contain an aspirin volume fraction of 0.17, whereas PEG 8,000, PEG 20,000, and PEO 100,000 are used as excipient.

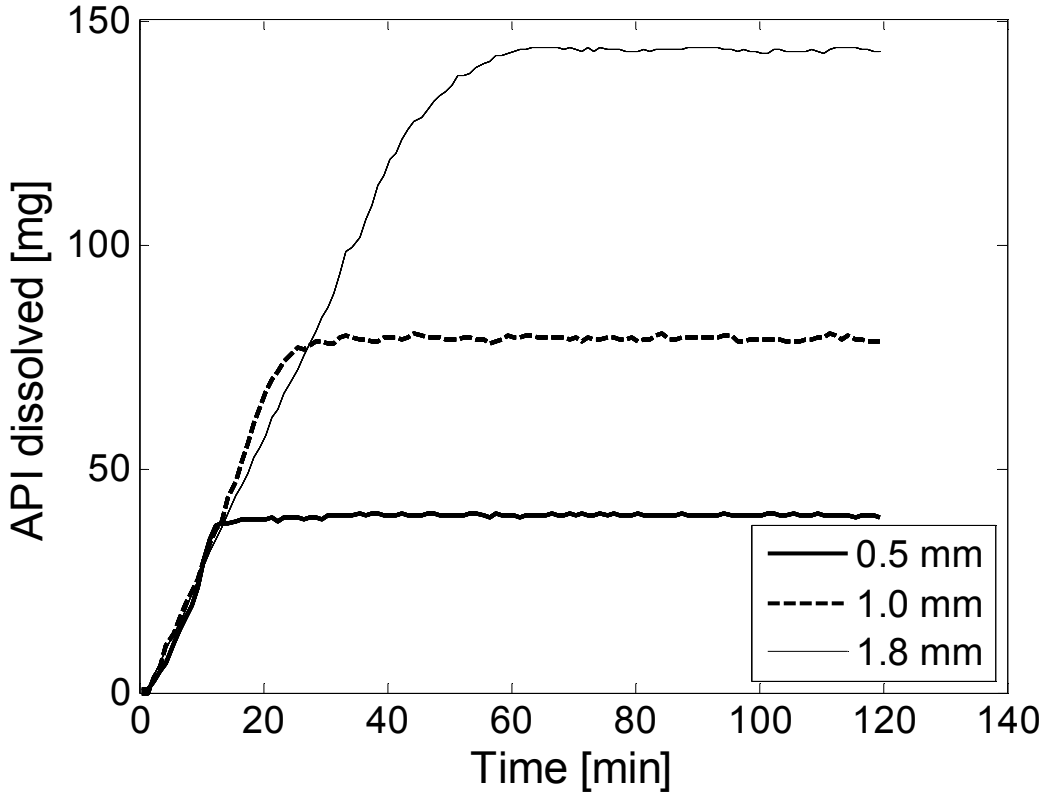

Figure 5.10: Amount of API dissolved versus time for disks of various thicknesses with a PEG 8,000 matrix at 0.45 API volume fraction.

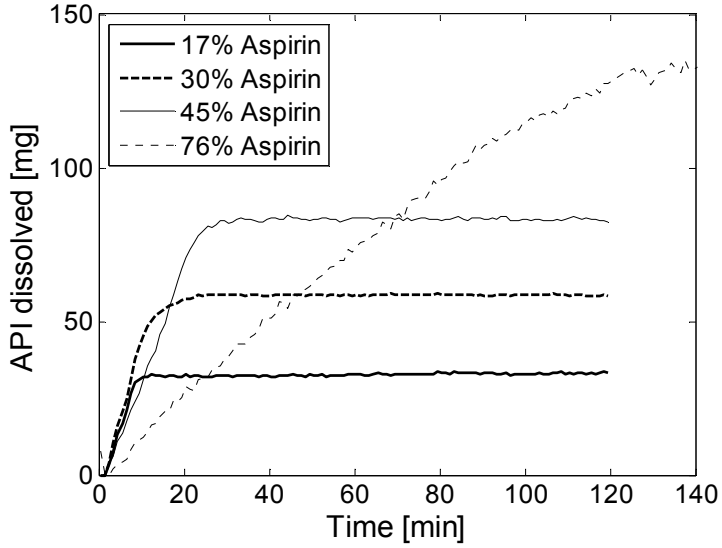

Figure 5.11: Amount of API dissolved versus time of 1 mm thick disks with a PEG 8,000 excipient matrix at various API volume fractions.

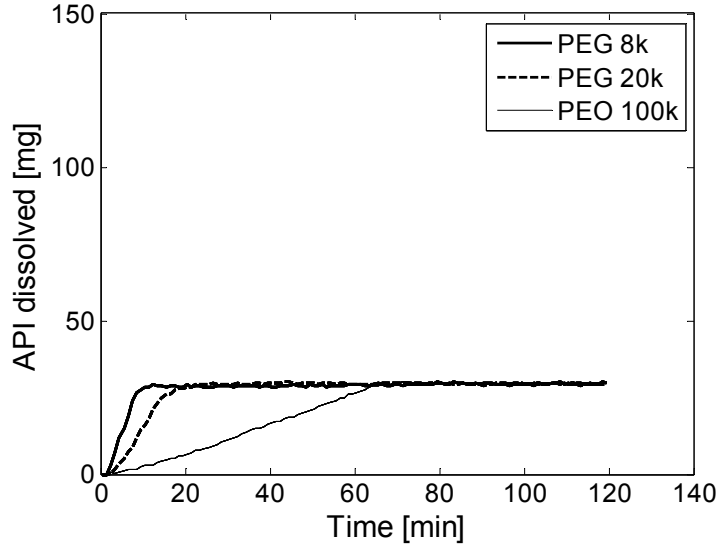

Figure 5.12: Amount of API dissolved versus time for disks 1 mm thick with 0.17 API volume fraction at various PEG molecular weight excipient matrices.

Table 5.4: API release time, erosion rate, and API release flux of PEG/PEO–aspirin solid dosage forms.

Excipient	Molecular weight (g/mol)	API volume fraction	Sample thickness (mm)	API release time[a] (min)	Erosion rate[b] (nm/s)	API release flux[c] (mg/m^2s)
PEG 8k	8,000	0.04	1.0	7	952	53
PEG 8k	8,000	0.04	1.8	12	1000	56
PEG 8k	8,000	0.17	0.55	5	733	175
PEG 8k	8,000	0.17	1.0	8	833	198
PEG 8k	8,000	0.17	1.8	14	857	204
PEG 8k	8,000	0.30	1.0	11	606	255
PEG 8k	8,000	0.30	1.8	23	522	219
PEG 8k	8,000	0.45	0.5	11	303	191
PEG 8k	8,000	0.45	1.0	20	333	210
PEG 8k	8,000	0.45	1.8	39	308	194
PEG 8k	8,000	0.76	1.0	96	69	74
PEG 8k	8,000	0.76	1.0	97	69	73
PEG 20k	20,000	0.17	0.6	10	400	95
PEG 20k	20,000	0.17	1.0	14	476	113
PEG 20k	20,000	0.17	1.8	30	400	95
PEG 20k	20,000	0.45	1.0	27	247	156
PEO 100k	100,000	0.17	0.6	34	118	28
PEO 100k	100,000	0.17	1.05	56	125	30

[a] "Release time" is defined as the time required to dissolve 80% of the API content. Note that drug is released from both sides of the disk sample.

[b] Erosion rate = (0.8 x sample thickness)/ (2 x release time)

[c] API release flux = API density x API volume fraction x erosion rate,
The density of the API, aspirin, is 1400 kg/m^3.

It is clearly shown that the slope of the curves decreases with increasing polymer molecular weight, and therefore, the drug release rate decreases with decreasing excipient erosion rate due to increased PEG molecular weight.

Results of the dissolution experiments are summarized in Table 5.4, with emphasis on API release time, erosion rate, and API release flux. A plot of the measured erosion rate versus drug volume fraction is shown in Fig. 5.13. The erosion rates at a volume fraction equal to zero were calculated based on the linear regression obtained from the erosion tests normalized with the square-root of the ratio of the maximum velocities applied in the dissolution test and the erosion test, respectively. For all the cases studied, the erosion rate decreased with increasing drug volume fraction. Linear regression analysis gives empirical equations for the dependence of erosion rate on drug volume fraction. For the PEG 8000 – aspiring system, the erosion rate versus drug volume fraction could be written as $y = -1415x + 1043$ with $R^2 = 0.95$, whereas the equations $y = -581x + 517$ with $R^2 = 0.92$ and $y = -121x + 142$ with $R^2 = 0.92$ were obtained if PEG 20,000 and PEO 100,000 were used as excipient, respectively. These trends show that both the erosion rate at zero drug volume fraction and the slope of the erosion rate versus drug volume fraction decrease when the excipient molecular weight is increased. Fig. 5.14 illustrates the curves of $-dH/dtd\varphi$ versus excipient molecular weight. A dependence of $y = 8.96x10^6x^{-0.97}$ is obtained by linear regression.

The drug release flux, the product of erosion rate, drug volume fraction, and the drug density, is illustrated in a 3-d plot versus drug volume fraction and excipient molecular weight in Fig. 5.15. Consistent with the erosion rate, the drug release flux increases with decreasing excipient molecular weight. It is further small at low drug volume fractions of 0.04, but increases when the drug volume fraction is increased to 0.3. If the drug volume fraction is increased above 0.3 to a value of 0.45, the drug release flux is again decreased, and it further decreases if the drug volume fraction is increased to a value of 0.76.

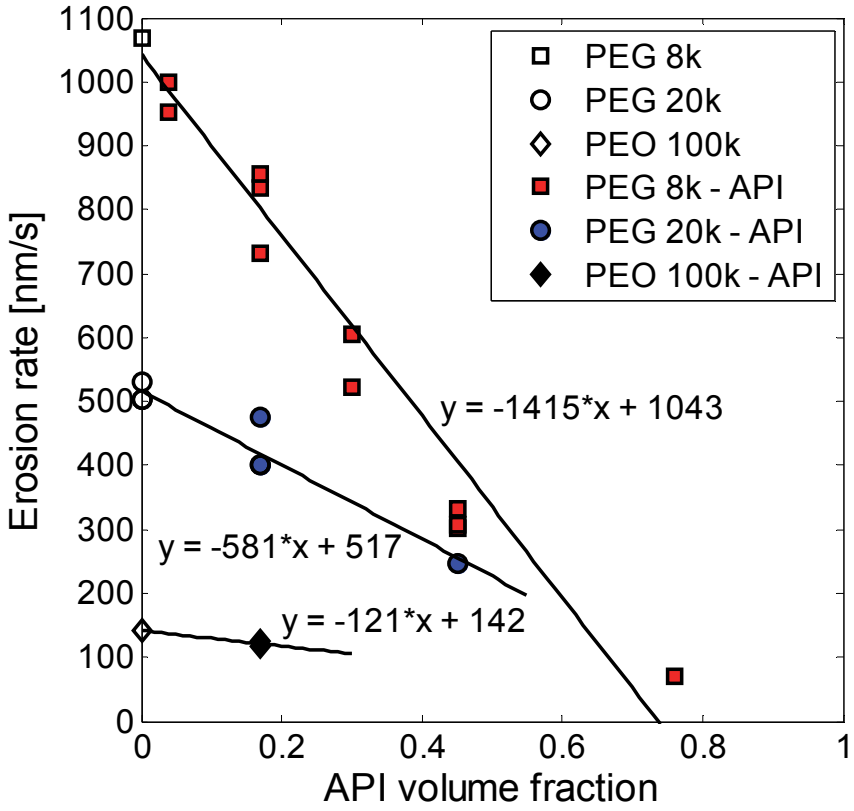

Figure 5.13: Measured erosion rate versus drug volume fraction for the PEG 8k – aspirin, the PEG 20k – aspirin, and the PEO 100k – aspirin system. The data are fitted by linear regression, and the curves have the following R^2 values: PEG 8k - aspirin $R^2 = 0.95$, PEG 20k – aspirin $R^2 = 0.92$, PEO 100k - aspirin $R^2 = 0.92$.

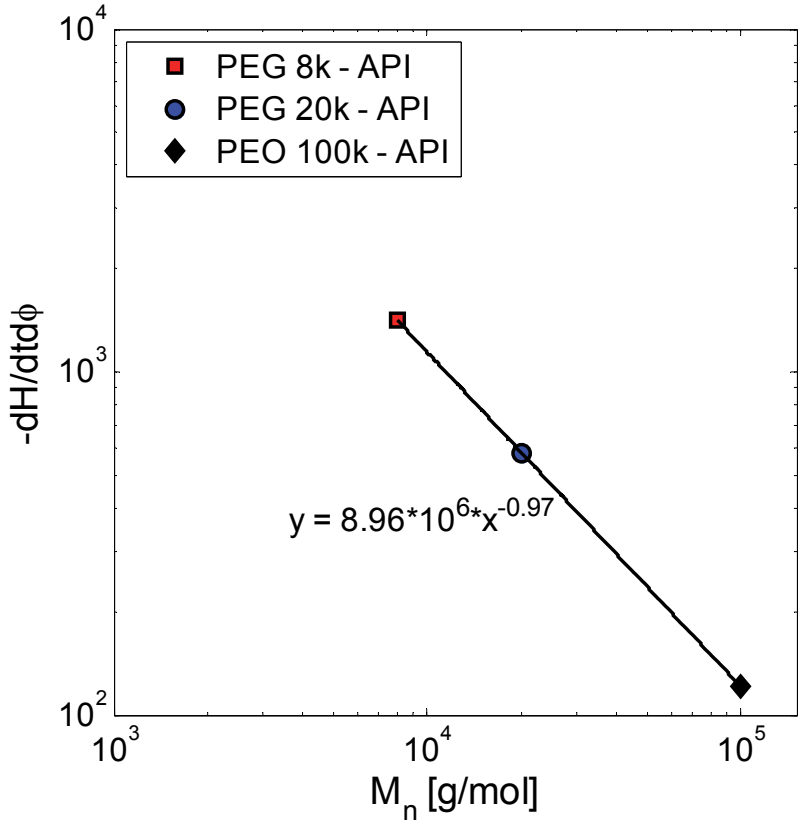

Figure 5.14: Negative value of Δ Erosion rate/ Δ API volume fraction (*-dH/dtdφ*) obtained from the linear regression curves versus PEG molecular weight.

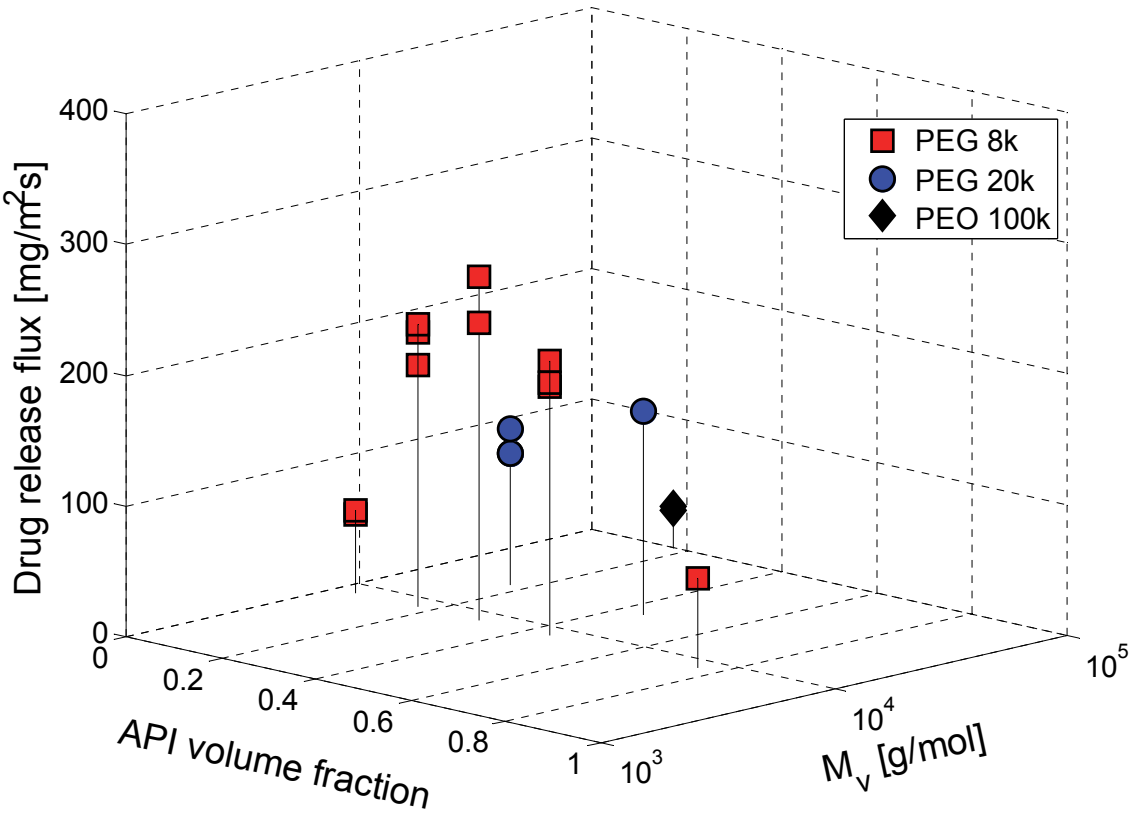

Figure 5.15: 3-D plot of measured drug release flux versus API volume fraction and PEG molecular weight.

5.4 Model Validation

5.4.1 Erosion Rate of PEG

The erosion rate values of PEG and PEO allow determination of two important constants: the Flory exponent, v, and the proportionality constant, a, to determine the effective solubility of the polymer in the dissolution medium. Note that by Eq. (4.20), the effective solubility is modeled as $M_n c_0 = a M_n c^*$, c^* being the PEG concentration above which PEG molecules overlap as:

$$c^* \cong \frac{3}{4\pi N_A R_g^3} \propto M_n^{-3v} \tag{5.1}$$

where $R_g \sim M_n^{\,v}$ [8]. The Flory exponent can be derived from the scaling law obtained from erosion experiments giving that $dH_{e,0}/dt \sim M_n^{-0.8}$. If this scaling law is compared with Eq. (4.23), which predicts that $dH_{e,0}/dt \sim M_n^{-3.66v+1}$, it is found that v is equal to 0.492. This is an important result, because the value for the Flory exponent is in good agreement with the value of the Flory exponent used in Zimm's model for diffusion of linear polymers in dilute solutions, which predicts the Flory exponent as $v = 0.5$.

If the Flory exponent is known, only one parameter is left unknown in the equation to model erosion rate, and this is the proportionality constant a to determine the effective solubility of the polymer as $M_n c_0 = a M_n c^*$. The equation to model the erosion rate of excipient in stirred solution is restated here as:

$$\frac{dH_{e,0}}{dt} = \frac{M_n c_0 D_e^{\frac{2}{3}}}{\rho_e} \sqrt{\left(\frac{\rho_f}{\mu_f}\right)^{\frac{1}{3}} \frac{v_\infty}{3L_0}} \tag{5.2}$$

where the values of known constants on the right hand side of Eq. (5.2) are given in Table (5.6), and the diffusivity of the polymer can be calculated according to Zimm's law:

$$D_g = 0.203 \frac{k_B T}{\sqrt{6}\mu_f R_g} \tag{5.3}$$

with the radius of the polymer molecule being equal to about:

$$R_{g,} \propto N^{\nu} b \tag{5.4}$$

N is the number of bonds in the polymer chain proportional to the polymer molecular weight and b is the bond length in the chain. The value of N for selected PEG molecules is given in Table 5.5 whereas the C-C bond length of 1.54 A is used for the value of b. It may be noted that a proportionality constant equal to $1/\sqrt{6}$ is typically applied on the right hand side of Eq. (5.4).

The unknown effective solubility of PEG in the dissolution medium is derived by comparing Eq. (5.2) with the linear regression equation of erosion data giving that $dH_{e,0}/dt = 1.37\text{x}10^6 M_n^{-0.8}$ for $v_\infty = 0.052$ m/s. It can then be obtained, with the properties and conditions of the dissolution medium given in Table 5.6 for the effective solubility of PEG and PEO in units [g/m^3] or [kg/m^3], as:

$$M_n c_0 = 0.13 D_g^{-\frac{2}{3}} M_n^{-0.8} \tag{5.5}$$

By Eq. (4.20) the value on the right-hand side of Eq. (5.5) is equal to $aM_n c^*$. If c^* is calculated by Eq. (5.1) and Eq. (5.4), and D_g is calculated by Eq. (5.3) and Eq. (5.4), then using the values given in Table 5.5 and Table 5.6 for the properties and conditions of the polymer and the dissolution medium, the proportionality constant can be derived as $a = 6.72$. This means that the effective solubility of PEG is, under the conditions studied, by a reasonable factor of 6.72 greater than the polymer concentration above which polymer molecules overlap. Finally, the values of diffusivity and effective solubility of selected PEG and PEO excipients so derived with a Flory exponent of 0.5 are also listed in Table 5.5.

Table 5.5: Properties of selected polyethylene glycols.

Excipient	Number of repeat units	Number of bonds	Density (kg/m^3)	Solubility (kg/m^3)	Diffusivity (m^2/s)
PEG 1.5k	33	99	1120	994	$23.10*10^{-11}$
PEG 4k	91	273	1125	636	$13.90*10^{-11}$
PEG 6k	136	408	1125	525	$11.40*10^{-11}$
PEG 8k	181.4	544.2	1125	459	$9.87*10^{-11}$
PEG 12k	272.7	818.2	1125	380	$8.05*10^{-11}$
PEG 20k	450	1350	1127	298	$6.27*10^{-11}$
PEG 35k	795	2385	1127	231	$4.71*10^{-11}$
PEO 100k	2275	6825	1130	141	$2.79*10^{-11}$

Table 5.6: Relevant parameters and their values used for model validation.

Parameter	Value
Aspirin solubility (kg/m^3)	4
Aspirin diffusivity (m^2/s)	$1x10^{-9}$
Aspirin density (kg/m^3)	1400
Aspirin particle size (µm)	100
1^{st} percolation threshold	0.31
2^{nd} percolation threshold	0.69
Medium density (kg/m^3)	1000
Medium viscosity (Pas)	0.001
Medium velocity (m/s)	0.052
Medium temperature (°C)	37°C
Tablet disk diameter (mm)	12.7
C-C bond length (A)	1.54

5.4.2 Erosion Rate of the PEG-Aspirin System

The model developed in Chapter IV to describe dissolution of API mixed with a rapidly eroding excipient constitutes three different laws, depending on drug volume fraction, to describe the erosion rate of the composite material. The critical drug volume fractions that subdivide the laws are derived from the percolation theory, and are determined by two percolation thresholds. If the drug volume fraction is below the first percolation threshold, φ^*, no interconnected cluster of drug particles exists in the infinite lattice provided that the drug particles are of uniform size and shape. Drug particles are isolated in the excipient matrix. At a volume fraction above φ^*, drug particles are at least partially interconnected forming an interconnected cluster in the infinite lattice. Similarly, if the drug volume fraction is above the second percolation threshold, φ^{**} (= 1 – φ^*), no interconnected cluster is formed by the excipient in the infinite lattice, provided excipient particles are of uniform size and shape. The drug phase is fully interconnected in this case.

At a drug volume fraction below φ^*, the model predicts that the erosion rate of the composite material follows the erosion rate of the excipient, taking into account that part of the excipient surface area is blocked by isolated, protruding, slowly eroding drug particles. At a drug volume fraction above φ^{**}, the erosion rate is predicted to approach the harmonic mean of the erosion rate of the excipient phase and the erosion rate of the drug phase. If the drug volume fraction is between φ^* and φ^{**}, a linear interpolation is made which gives:

$$\frac{dH}{dt} = \begin{cases} (1-\phi)\dfrac{dH_{e,0}}{dt} & \phi \le \phi^* \\ \left.\dfrac{dH}{dt}\right|_{\phi=\phi^*}\left(\dfrac{\phi^{**}-\phi}{\phi^{**}-\phi^*}\right) + \left.\dfrac{dH}{dt}\right|_{\phi=\phi^{**}}\left(\dfrac{\phi-\phi^*}{\phi^{**}-\phi^*}\right) & \phi^* < \phi < \phi^{**} \\ \dfrac{\dot{H}_{e,0}\dot{H}_{d,0}}{\phi\dot{H}_{e,0} + (1-\phi)\dot{H}_{d,0}} & \phi \ge \phi^{**} \end{cases} \quad (5.6)$$

where the erosion rate of the pure, individual phase for both the drug and the excipient may be calculated as:

$$\frac{dH_{i,0}}{dt} = \frac{M_n c_{0,i} D_i^{\frac{2}{3}}}{\rho_i} \sqrt{\left(\frac{\rho_f}{\mu_f}\right)^{\frac{1}{3}} \frac{v_\infty}{3L_0}} \qquad i = e,d \tag{5.7}$$

with $M_n c_0$ being the effective solubility of the component in the dissolution medium in units kg/m^3, D the diffusion coefficient of the dissolved component, ρ_i the density of the solid material, ρ_f the density of the dissolution medium, μ_f the viscosity of the dissolution medium, and v_∞ the velocity of the dissolution medium at infinity.

Erosion rates of the PEG-aspirin disks are then calculated using Eq. (5.6) and Eq. (5.7), with the parameter values presented in Table 5.5 and Table 5.6. A comparison of erosion rate with measured values is listed in Table 5.7. The average and standard deviation of the percent difference (100 x (Measured rate – Calculated rate)/ Calculated rate) is -3% and 21.9%, respectively. A plot of the measured erosion rate versus calculated rate is shown in Fig. 5.16. Further, the line $y = x$ is drawn into the figure representing the line of "excellent" agreement between model and experiment. An R^2 value of 0.9 is observed when comparing the data points with this linear curve, which proves that the agreement between model and experiment is reasonably good.

Finally, Fig. 5.17 illustrates the model and measured values of the erosion rate versus drug volume fraction. The calculated curves show a linear decay up to the first percolation threshold, which is due to the fact that the excipient surface area is blocked by the protruding drug particles, linearly with increasing drug volume fraction. If the drug volume fraction is between the first and the second percolation thresholds, the erosion rate of the composite material is further decreased as the connectivity of drug particles increases and the connectivity of excipient units decreases. Finally, if the drug volume fraction is above the second percolation threshold, the negative slope of the calculated erosion rate versus drug volume fraction is significantly smaller than what it is if the drug volume fraction is below the second percolation threshold. Excipient particles in this case show a

Table 5.7: Measured and calculated erosion rates of PEG/PEO–aspirin dosage forms.

Excipient	Molecular Weight (g/mol)	API Volume Fraction	Sample Thickness (mm)	Measured rate (nm/s)	Calculated rate (nm/s)	Percent difference
PEG 8k	8,000	0.04	1.0	952	992	-4
PEG 8k	8,000	0.04	1.8	1000	992	0.8
PEG 8k	8,000	0.17	0.55	733	858	-14.6
PEG 8k	8,000	0.17	1.0	833	858	-2.9
PEG 8k	8,000	0.17	1.8	857	858	-0.1
PEG 8k	8,000	0.30	1.0	606	724	-16.3
PEG 8k	8,000	0.30	1.8	522	724	-27.9
PEG 8k	8,000	0.45	0.5	303	470	-35.5
PEG 8k	8,000	0.45	1.0	333	470	-29.1
PEG 8k	8,000	0.45	1.8	308	470	-34.5
PEG 8k	8,000	0.76	1.0	69	49	40.8
PEG 8k	8,000	0.76	1.0	69	49	40.8
PEG 20k	20,000	0.17	0.6	400	412	-2.9
PEG 20k	20,000	0.17	1.0	476	412	15.5
PEG 20k	20,000	0.17	1.8	400	412	-2.9
PEG 20k	20,000	0.45	1.0	247	236	4.7
PEO 100k	100,000	0.17	0.6	118	114	3.5
PEO 100k	100,000	0.17	1.05	125	114	9.6
					Average	-3
					Std. Dev.	21.9

Percent difference = 100 x (Measured rate – Calculated rate)/ Calculated rate

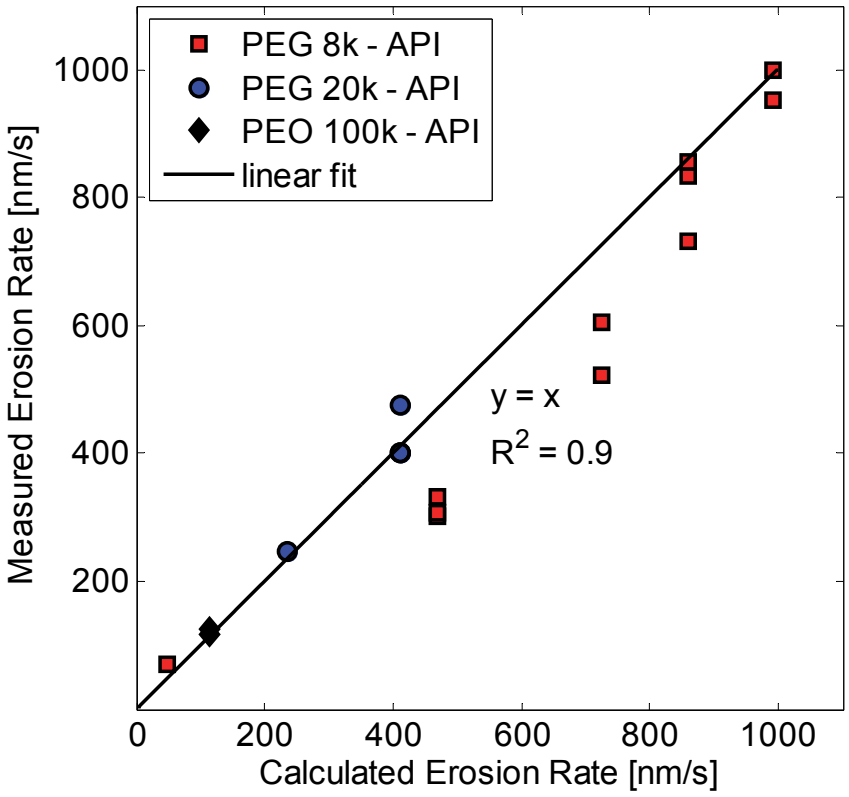

Figure 5.16: Measured erosion rate versus the calculated rate of the PEG-aspirin system.

low level of connectivity, and hence have limited effect on erosion rate of the composite material.

The measured values of erosion rate follow the calculated curves reasonably well, which indicates that the simple, analytical model is capable of taking the relevant physical phenomena into account accurately, without using any empirical fitting parameters. This result, however, does not mean that the model could not be improved further. The deviation of modeled and experimental values is, using PEG 8,000 as excipient at drug volume fractions between about 0.3 and 0.5, observed to be about 15 - 36%. The experimentally derived erosion rate has a lower value than what is calculated in this case. Further, the experimentally derived erosion rate at a drug volume fraction of 0.76 is by about 40% above the calculated value.

Such deviations of experimental data from calculated values, particularly at drug volume fractions between about 0.3 and 0.5 have their origin in multiple sources. Most importantly, as shown in Chapter IV, protruding slowly eroding drug particles can change fluid flow conditions in the vicinity of the eroding excipient surface, increasing the excipient concentration boundary layer thickness, and decreasing the erosion rate of the excipient phase. Further, the model assumes that isolated, protruding drug particles blocking excipient surface area for erosion are washed off in the time the excipient is eroded by the thickness of one particle size. This assumption may not be quite correct, however. Moreover, the percolation thresholds applied in the model are valid for an infinite cubic lattice with excipient and drug units with a cubic shape and uniform size. It is evident that such a case is only partially resembled in the dosage forms. Finally, the model assumes that the drug particles are randomly distributed in the excipient. This may not be fully achieved in the sample preparation. Deviations of experimental data from the calculated values at drug volume fractions above the second percolation threshold may be due to the fact that excipient cannot wash off any drug particles in this regime. This may not be entirely true in a real system; hence, the calculated values of erosion rate at a drug volume fraction above the second percolation threshold resemble the lower-bound of erosion rate.

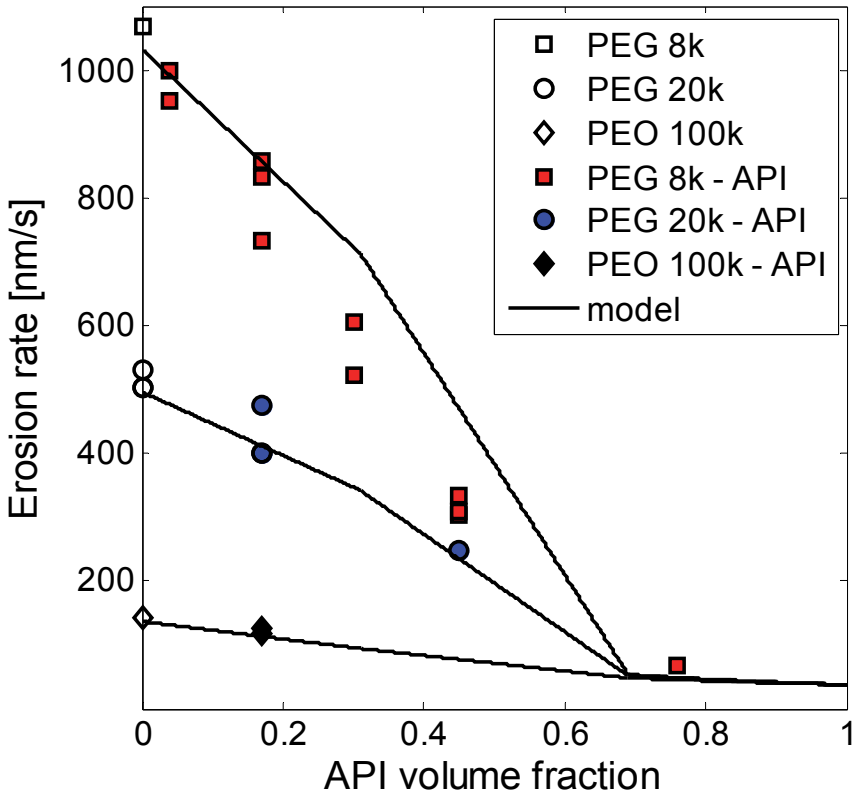

Figure 5.17: Measured and modeled values of erosion rate versus API volume fraction of the PEG-aspirin system.

5.4.3 Drug Release Flux

The mass flux of drug released is the fundamental property of a dosage form. For the case of the surface eroding non-porous dosage forms, it can be expressed as:

$$\frac{dm_d}{dt} = \rho_d \phi \frac{dH}{dt} \tag{5.8}$$

where ρ_d is the density and φ is the volume fraction of the drug. The drug release flux in Eq. (5.8) is the sum of the convective mass flux of dissolved drug molecules and of the mass particles washed off by the faster eroding excipient phase. For the calculation of the erosion rate of the dosage form, Eq. (5.6) and Eq. (5.7) can be applied using the parameter values listed in Tables 5.5 and 5.6.

Table 5.8 shows the measured and calculated drug release fluxes together with the percent difference An average difference of -3.1% with a standard deviation of 22% is obtained, with reasonably good agreement between the measured and the calculated values by the model. Measured values of drug release flux versus calculated values are illustrated in Fig. 5.18. Again, the line $y = x$ represents perfect agreement between model and experiment, and an R^2-value of 0.56 is obtained if the entire data set is compared with this line. However, Fig. 5.18 reveals that the values at high drug release flux show particularly large deviation from the linear trend. These points have a large effect on the R^2-value obtained, and if they are discarded, the coefficient $R^2 = 0.95$.

Finally, the model and experimental values of the drug release flux are plotted against drug volume fraction in Fig. 5.19. If the drug volume fraction is increased, it increases to its maximum value, which is observed at a drug volume fraction between 0.3 and 0.4. The drug release flux then decreases with increasing drug volume fraction until the second percolation threshold is reached. If the drug volume fraction is above the second threshold, the release flux can be changed only marginally by increasing the volume fraction.

Table 5.8: Measured and calculated API release flux of PEG/PEO–aspirin solid dosage forms.

Excipient	Molecular Weight (g/mol)	API Volume Fraction	Sample Thickness (mm)	Measured flux (mg/m^2s)	Calculated flux (mg/m^2s)	Percent difference
PEG 8k	8,000	0.04	1.0	53	56	-5.4
PEG 8k	8,000	0.04	1.8	56	56	0
PEG 8k	8,000	0.17	0.55	175	204	-14.2
PEG 8k	8,000	0.17	1.0	198	204	-2.9
PEG 8k	8,000	0.17	1.8	204	204	0
PEG 8k	8,000	0.30	1.0	255	304	-16.1
PEG 8k	8,000	0.30	1.8	219	304	-28
PEG 8k	8,000	0.45	0.5	191	296	-35.5
PEG 8k	8,000	0.45	1.0	210	296	-29.1
PEG 8k	8,000	0.45	1.8	194	296	-34.5
PEG 8k	8,000	0.76	1.0	74	52	42.3
PEG 8k	8,000	0.76	1.0	73	52	40.4
PEG 20k	20,000	0.17	0.6	95	98	-3.1
PEG 20k	20,000	0.17	1.0	113	98	15.3
PEG 20k	20,000	0.17	1.8	95	98	-3.1
PEG 20k	20,000	0.45	1.0	156	149	4.7
PEO 100k	100,000	0.17	0.6	28	27	3.7
PEO 100k	100,000	0.17	1.05	30	27	11.1
					Average	-3.1
					Std. Dev.	22

Percent difference = 100 x (Measured flux – Calculated flux)/ Calculated flux

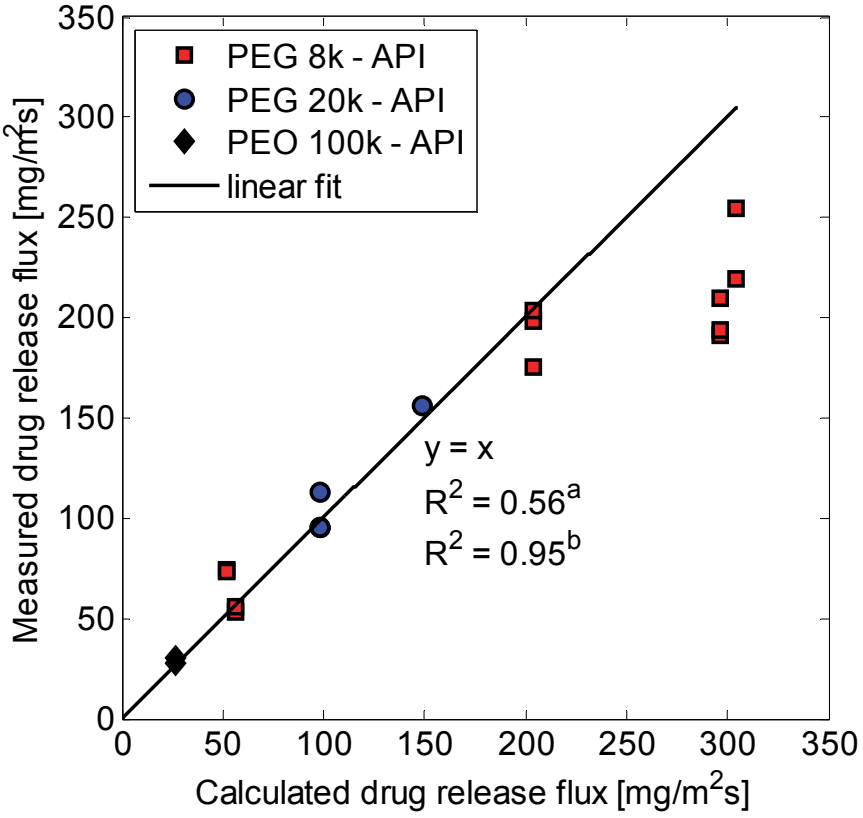

Figure 5.18: Measured drug release flux versus calculated drug release flux of the PEG-aspirin system. The coefficient of determination of data points versus linear curve is derived by (a) using all data points (b) excluding data points with calculated drug release flux above 250 mg/m^{2}s.

It is again observed that the measured data follow the calculated curves reasonably well. However, it is seen that the measured data deviate from the calculations, and the case with PEG 8,000 as excipient at a drug volume fraction between about 0.3 and 0.5 is again highlighted, as the measured values are between 15% and 36% lower than the calculated ones. These deviations are attributed to the same causes as mentioned in the previous section (section 5.4.2), and include the effect of increased excipient concentration boundary layer thickness due protruding drug particles affecting fluid flow in the vicinity of the excipient surface, the assumption that the time during which isolated drug particles that block excipient surface area for erosion are eroded is equal to the time to within which the excipient erodes by the thickness of a particle size, the fact that the percolation thresholds applied are for an idealized, infinite system, and the assumption that drug particles are randomly distributed in the excipient.

Although the model does not account for such sources of error as listed above, the curves of drug release flux versus drug volume fraction show interesting characteristics. They provide insights into: (a) what excipient is required such that a specific drug release flux is achieved and (b) how much excipient is required to achieve a given drug release flux. Therefore, the drug release flux, with typical curves for a system with rapidly eroding excipient and slowly eroding drug, illustrated in Fig. 5.19, presents a tool to guide the design of non-porous, immediate-release dosage forms with specified properties.

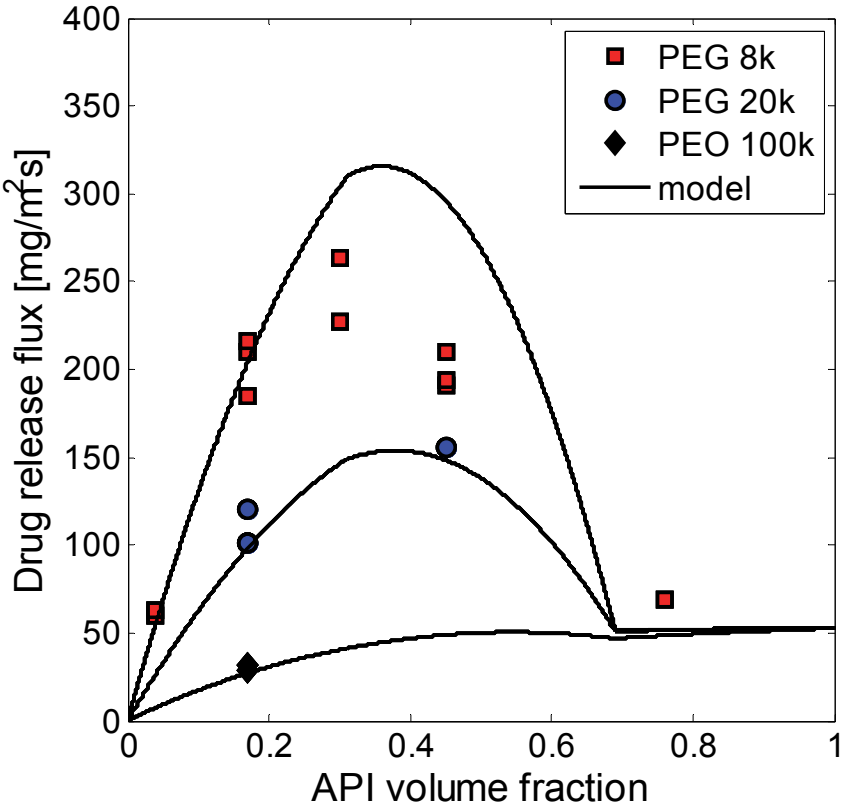

Figure 5.19: Measured and modeled drug release flux versus API volume fraction of the PEG-aspirin system.

5.5 Summary

The dosage form chosen here for model validation is a PEG-aspirin composite. PEG (or PEO) is selected as the excipient for its high solubility and diffusivity in the dissolution medium and favorable properties for hot-melt processing. For the API, aspirin is selected because it is inexpensive and has low potency. Due to the low solubility (orders of magnitude lower than the that of PEG) it also well represents most APIs which erode at a much slower rate than the excipients desired.

Erosion tests were conducted first on pure PEG and PEO of various molecular weights. They show that $dH_{e,0}/dt \sim M_n^{-0.8}$, which is consistent with the model describing the erosion rate of pure polymeric excipient with a Flory exponent of 0.492. Further, the erosion tests on pure, single-phase PEG and PEO allow derivation of the effective solubility of PEG to be applied in the equation for the erosion rate of pure excipient phase. It is found that the effective solubility of PEG and PEO under the conditions studied is 6.72 times the concentration c^*, above which the PEG molecules overlap.

Dissolution tests were then performed on the PEG-aspirin dosage form. It is shown that the erosion rate decreases with increasing API volume fraction. If the drug volume fraction is below the second percolation threshold, the results of erosion rate versus drug volume fraction can be well fitted to a straightline. It is found by linear regression of experimental data that the slope of the linear fit further depends on the molecular weight of the PEG excipient as: $dH/dtd\varphi = -8.96\text{x}10^{-3}M_n^{-0.97}$.

The model accounts for the effect of blockage of excipient erosion by the slowly eroding drug phase, either as isolated drug particles or as interconnected clusters, shows to agree well with experimental results. An average percent error of measured versus calculated erosion rate of -3% is obtained with a standard deviation of 21.9%. Further, a linear plot of measured versus calculated erosion rate gives an R^2 value of 0.9, confirming good agreement between model and measured values. Also, the modeled drug release flux agrees well with measured values. An average percent error of measured versus calculated drug release flux of -3.1% is obtained at a standard deviation of 22%. Both erosion rate versus φ and drug release flux versus φ curves have a unique shape for the systems

studied, with slowly eroding drug particles embedded in a rapidly eroding excipient matrix. The model is capable of serving as a valuable design tool for the formulation of immediate-release dosage forms with predictive properties.

Nomenclature

A	eroding surface area [m^2]
a	proportionality constant to determine the solid-liquid interfacial concentration
b	bond length within the polymer chain [m]
c	concentration of a particular species in dissolution medium [mol/m^3]
c_0	concentration of a particular species at solid-medium interface [mol/m^3]
c_s	solubility of a particular species in dissolution medium [mol/m^3]
c^*	polymer concentration at the boundary of dilute and semi-dilute region [mol/m^3]
c^{**}	polymer concentration at the boundary of semi-dilute and concentrated region [mol/m^3]
D	diffusion coefficient [m^2/s]
D_G	diameter of the dosage form [m]
D_g	diffusion coefficient of the polymer's center of mass [m^2/s]
D_R	diameter of the runner in the injection system [m]
d	particle size [m]
H	thickness of sample [m]
H_0	initial thickness of sample [m]
dH/dt	erosion rate of the sample [m/s]
$dH_{d,0}/dt$	erosion rate of pure drug phase [m/s]
dH_e/dt	erosion rate of excipient phase [m/s]

$dH_{e,0}/dt$	erosion rate of pure excipient phase [m/s]
k_B	Boltzmann's constant [J/K]
L	characteristic length of eroding surface [m]
M_d	accumulated amount of drug released [kg]
M_n	number averaged molecular weight [g/mol] or [kg/mol]
dM_d/dt	drug release rate [kg/s]
dm_d/dt	drug release flux [kg/m^{2}s]
N	number of bonds along the polymer chain
N_A	Avogadro's number
P	fluid pressure [Pa]
R_g	polymer radius [m]
R_p	Sample position in the erosion test [m]
T	temperature [K]
Re	Reynolds number
t	time [s]
t_d	disintegration time to erode sample [s]
v	fluid velocity [m/s]
v_∞	maximum fluid velocity [m/s]
δ	viscous boundary layer thickness [m]
δ_c	concentration boundary layer thickness [m]
δ_e	excipient concentration boundary layer thickness [m]
λ	interparticle distance [m]
ρ_f	fluid density [kg/m^3]
ρ_d	solid density of drug [kg/m^3]
ρ_s	average density of solid sample [kg/m^3]

μ	viscosity [Pa·s]
μ_f	viscosity of dissolution medium [Pa·s]
v	Flory exponent
φ	drug volume fraction
φ^*	drug volume fraction below which there is no interconnected drug cluster
φ^{**}	drug volume fraction above which there is no interconnected excipient cluster

References

[1] R.C. Rowe, S.C. Owen, P.J. Sheskey, 2006, Handbook of Pharmaceutical Excipi ents, fifth edition, published by the American Pharmaceutical Association.

[2] G. Cuff, F. Raouf, 1998, A preliminary evaluation of injection molding as a technology to produce tablets, Pharmaceut. Tech. 22, 96-106.

[3] K. Kolter, M. Karl, A. Gryczke, 2012, Hot-Melt Extrusion with BASF Pharma Polymers, BASF extrusion compendium, second edition.

[4] A.T.M. Serajuddin,1999, Solid Dispersions of Poorly Water-Soluble Drugs: Early Promises, Subsequent Problems, and Recent Breakthroughs, J. Pharm. Sci., 88, 1058-1066.

[5] M.J. O'Neil, P.E. Heckelman, C.B. Koch, K.J. Roman, 2006, Merck Index: An Encyclopedia of Chemicals, Drugs, and Biologicals, 14th edition, Merck Research Laboratories, Merck & Co Inc., Whitehouse Station, NJ.

[6] R.T. Rosenberg, N.R. Dan, 2010, Controlling surface porosity and release from hydrogels using a colloidal particle coating, Journal of Colloid and Interface Science, 349, 498-504.

[7] The U.S. Pharmacopeial Convention, US Pharmacopeia, USP 35-NF 30.

[8] M. Doi and S.F. Edwards, 1986, The Theory of Polymer Dynamics (Eds: J. Birman, S.F. Edwards, C. H. Llewellyn Smith and M. Rees), Oxford University Press, Oxford, UK.

This page is intentionally left blank.

CHAPTER VI

MECHANICAL PROPERTIES OF SELECTED IMMEDIATE-RELEASE EXCIPIENTS

6.1 Introduction

Immediate-release solid dosage forms must possess sufficient mechanical strength for the product to be processable and resist the stresses they are exposed to before being swallowed. Accordingly, compression tests have been performed to evaluate the mechanical properties of selected PEG and PEO excipients that have been tested for dissolution properties in Chapter V. Additionally, nanoindentation tests are also performed, mainly on Kollicoat IR – mannitol composite material. This allows identification of the effect of mannitol volume fraction on Young's modulus and hardness of the composite material system.

6.2 Materials and Methods

6.2.1 Materials for Sample Preparation

The materials used to formulate the samples for compression tests were all purchased from Sigma-Aldrich (St. Louis, MO), and included PEG 1,500 (Fluka), PEG 8,000 (Fluka), PEG 20,000 (Fluka), PEG 35,000 (Fluka), and PEO 100,000 (Fluka). The samples for nanoindentation tests were formulated using Kollicoat IR (USP-grade), which was a gift of BASF (Ludwidgshafen, Germany), and mannitol (USP-grade) which was purchased from Sigma-Aldrich (St. Louis, MO). Furthermore, nanoindentation tests were conducted on PEO 100,000 (Fluka), as well as Eudragit L100-55, which was a gift of Evonik (Essen, Germany), mixed with triethylcitrate purchased from Sigma-Aldrich (St. Louis, MO).

6.2.2 Sample Preparation

Samples for compression tests were prepared either by hot-melt casting or by injection-molding, as described in chapter 5, the only differences being that cooling times were changed to 60 seconds for either process and the sample size was adjusted to fit the requirements of the compression test. Hot-melt cast samples had a diameter of 12.7 mm and a thickness of 18 mm, whereas injection-molded samples were 23 mm thick at a diameter of 12.7 mm. A summary of process parameters for preparing the samples is given in Table 6.1, and Fig. 6.1 shows a picture of a sample so prepared.

Samples for nanoindentation tests were prepared by injection-molding, as described in Chapter V. Process parameters were adapted to comply with the properties of the underlying formulation. For example, since mannitol has a melting temperature of 162°C-167°C, and process temperatures for solventless Kollicoat IR processing are reported to be 165°C-190°C, a melt temperature of 185°C was chosen for such Kollicoat IR-mannitol formulations. Also the hold pressure was increased to 100 MPa if the mannitol volume fraction was below 0.3, as the increased viscosity compared with PEG and PEO of the material with high Kollicoat IR content required processing at increased pressures. Process parameters employed to prepare samples for nanoindentation tests are also presented in Table 6.1, and Fig. 6.1 gives a picture of the as-prepared sample.

6.2.3 Compression Tests on PEG and PEO

Compression tests were conducted on pure PEG and PEO specimens, and the ASTM standard test method for compressive properties of rigid plastics, ASTM D695-10, was used as the protocol [1]. The testing machine was a Zwick Roell Z2.5 with a 2.5 kN load cell (Zwick GmbH & Co. KG, Ulm, Germany), equipped with compression platens. A speed of 1.3 mm/min was applied for the platens to move towards each other. Fig. 6.2 shows the setup with compression platens and a test specimen, and Table 6.2 summarizes the parameters of the compression tests.

Table 6.1: Material, geometric, and process parameter values applied for sample preparation. Aspirin was used as API.

Parameter	Compression test (Cast sample)	Compression test (IM sample)	Nanoindentation (IM sample)
Materials	PEG or PEO	PEG or PEO	KCIR & Mann., others[a]
Diameter (mm)	12.7	12.7	12.7
Thickness (mm)	18	23	2
Melt Temperature (°C)	90	75	185, 75, 170[b]
Mold Temperature (°C)	25	25	25
Injection Flow Rate (cm^3/s)	-	5	5
Hold Pressure (MPa)	-	40	100
Casting pressure (MPa)	15	-	-
Cooling Time (s)	60	60	30

[a] "Others" refers to the excipients PEO 100k, and 75% Eudragit L100-55 25% triethylcitrate

[b] The melt temperature of the Kollicoat IR – mannitol sample was 185°C, the melt temperature of PEO 100k 75°C, and the melt temperature of 75% Eudragit L100-55 25% triethylcitrate was 170°C.

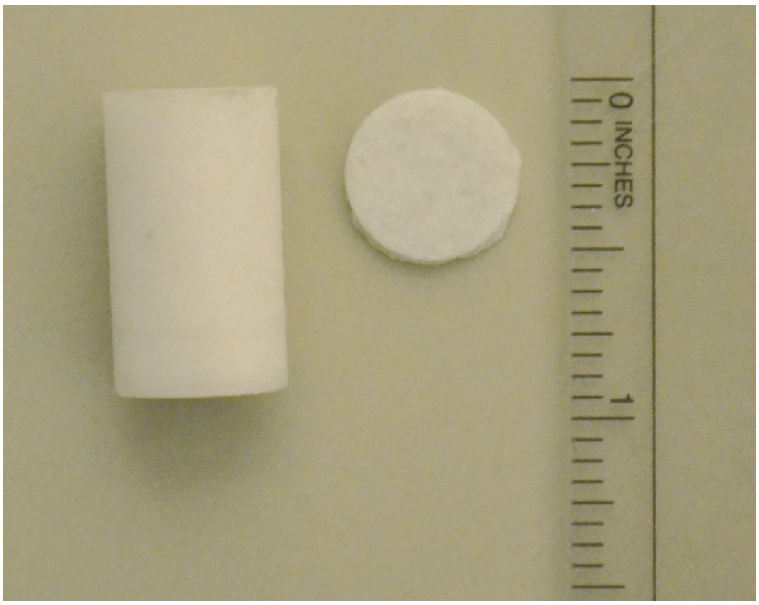

Figure 6.1: Illustration of samples for compression test (left) and nanoindentation test (right).

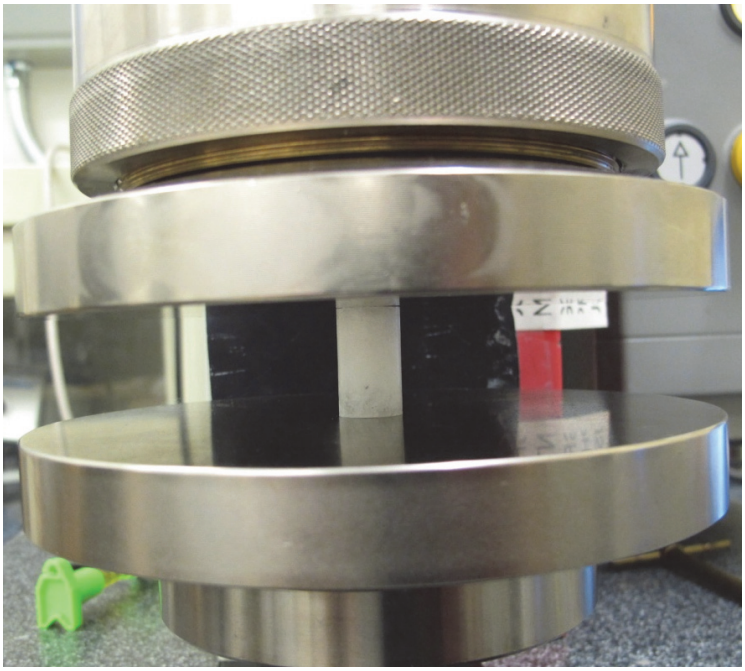

Figure 6.2: Compression test setup with a sample between the compression platens.

Table 6.2: Experimental parameters of the compression test.

Parameter	Compression test
Apparatus	Zwick Roell Z2.5
Load cell	Max force: 2500 N
Measured values	Compressive force & distance travelled by platen
Velocity of platen	1.3 mm/min
Strain rate	9.4×10^{-4} s^{-1} [a], 1.2×10^{-3} s^{-1} [b]

[a] Strain rate of cast sample with 18 mm length.

[b] Strain rate of injection-molded sample with 23 mm length.

Table 6.3: Experimental parameters of the nanoindentation test.

Parameter	Nanoindentation test
Apparatus	Hysitron triboindenter
Tip type	Berkovich
Measured values	Force & distance travelled by tip
Loading curves	Depth control
Maximum depth	2500 nm
Loading time	10 seconds
Hold time	3 seconds
Unloading time	10 seconds
Methods	Oliver-Pharr for calculation of *E* and *H*

6.2.4 Nanoindentation Tests

Nanoindentation tests were performed using a TriboIndenter (Hysitron, Eden Prairie, MN) equipped with a Berkovich tip. The Oliver-Pharr method was used to determine the reduced elastic modulus and the hardness from the initial part of the unloading curve where elastic relaxation occurs [2,3]. Loading was by depth control with a peak depth of 2500 nm, and 10 seconds loading, 3 seconds hold, and 10 seconds unloading were applied. The sample surface was flat and polished. Table 6.3 lists the experimental parameters used for nanoindentation testing.

6.3 Results

6.3.1 Compression Tests

Results of compression tests in the form of engineering stress – engineering strain curves are presented in Fig. 6.3 for specimens with various PEG molecular weights [4-6]. The curve is linear at small strains , which allows the calculation of the elastic modulus of the materials as $E = \Delta\sigma/\Delta\varepsilon$. Further the yield strength, which is defined as the point at which a linear curve parallel to the elastic region of the stress-strain curve offset by a strain of 0.002 intersects with the stress-strain curve, is calculated. Finally, for materials that are comparably brittle, values for the compressive strength and for the compressive strain at fracture were determined. The compressive strength is defined as the peak stress, whereas the strain at fracture is the strain at which the stress-strain curve decayed by 10% from the peak value. Table 6.4 together with Fig. 6.4 – Fig. 6.7 provide a summary of the mechanical properties of the various PEGs.

As shown in Fig. 6.3, the slopes of the stress-strain curves of PEG and PEO in the elastic range are of the same order of magnitude, and hence, the elastic moduli do not vary much if the PEG molecular weight is changed. Fig. 6.4 illustrates that a dependence of

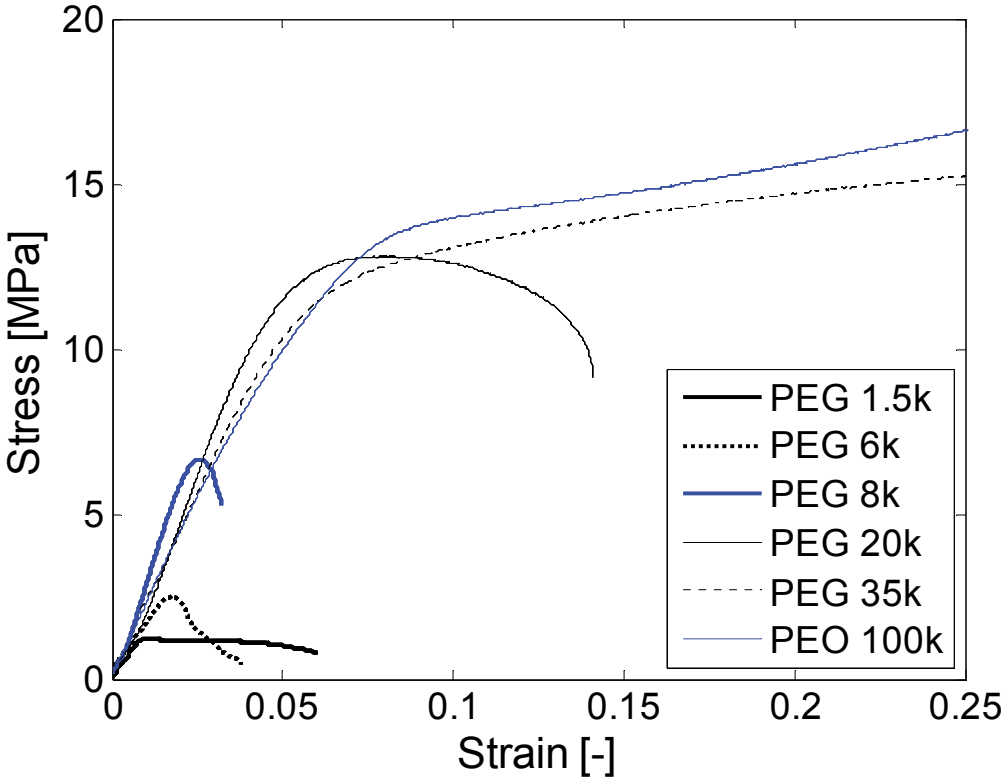

Figure 6.3: Engineering stress versus engineering strain curves from compression tests of melt-processed PEGs and PEO. PEG 1.5k and PEG 8k samples were injection-molded, all others were cast.

Table 6.4: Mechanical properties of PEG and PEO from compression tests.

Material	Molecular weight (g/mol)	Young's modulus (GPa)	Yield strength (MPa)	Compressive strength (MPa)	Strain at fracture (-)
PEG 1.5k[a]	1,500	0.14	1.2	1.2	0.04
PEG 6k[b]	6,000	0.13	2.5	2.5	0.03
PEG 6k[b]	6,000	0.15	2.5	2.5	0.02
PEG 8k[a]	8,000	0.34	6.1	6.5	0.03
PEG 8k[b]	8,000	0.18	4.5	4.6	0.04
PEG 20k[b]	20,000	0.23	9.0	10.4	0.09
PEG 20k[b]	20,000	0.26	8.2	9.6	0.11
PEG 20k[b]	20,000	0.29	10.2	12.8	0.13
PEG 35k[b]	35,000	0.22	10.2	>17.6	>0.5
PEG 35k[b]	35,000	0.21	10.8	>17.6	>0.5
PEG 35k[b]	35,000	0.24	10.4	13.6	0.29
PEG 35k[c]	35,000	0.30	11.0	>17.6	>0.5
PEO 100k[a]	100,000	0.31	7.5	>17.6	>0.5
PEO 100k[b]	100,000	0.23	9.1	>17.6	>0.5
Mannitol[d]	182	-	-	0.8	<0.02

[a] Based on injection-molded sample

[b] Based on casted sample

[c] Based on strain-hardened casted sample

[d] Based on compression-molded sample. The material could not be manufactured defect free and appropriately tested for Young's modulus and Yield strength.

the elastic modulus on PEG molecular weight of $y = 3.2x10^{-2}x^{0.19}$ is obtained by linear regression. The results are in agreement with data from the literature, which report a value of 0.3 GPa for the Young's modulus of bulk PEO [7,8]. The yield strength and compressive strength show a stronger dependence on the molecular weight of PEG. The yield strength, based on linear regression, increases from 1.2 MPa at a molecular weight of 1,500 g/mol up to 11.8 MPa at a molecular weight of 35,000 g/mol. A dependence of yield strength on molecular weight as $y = 6.3x10^{-3}x^{0.72}$ can be derived by linear regression for the range 1,500 g/mol to 35,000 g/mol. No increase in yield strength is observed if the molecular weight is increased from 35,000 g/mol to 100,000 g/mol. Similarly, the compressive strength shows a dependence of molecular weight as $y = 1.6x10^{-3}x^{0.89}$ by linear regression for the PEG molecular weight range 1,500 g/mol to 35,000 g/mol. For the molecular weight above 35,000 g/mol, the compressive strength could not be measured, because the material was too ductile for it to rupture in the compression test. Finally, the strain at fracture presents the highest dependence on the molecular weight of PEG; at low molecular weight it is comparably brittle with a strain at fracture of 0.04 or less. If the molecular weight is increased to 35,000 g/mol or above, the material becomes ductile and tough, so that it does not rupture in the compression test.

A mannitol sample was also tested for its mechanical properties under compression. The stress-strain curve, however, did not present a clear elastic regime, and it was too brittle to determine the mechanical properties based on compression tests.

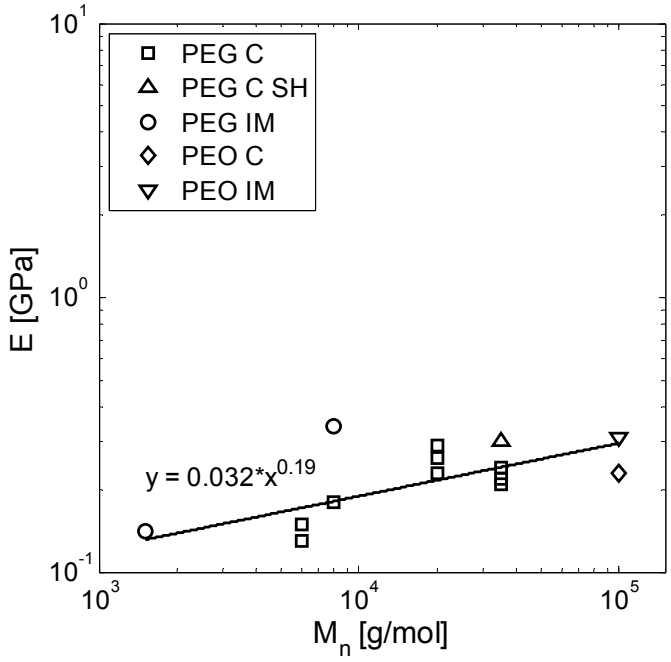

Figure 6.4: Log-log plot of Young's modulus versus molecular weight for selected injection-molded (IM), cast (CM), and cast and strain-hardened (SH) PEGs and PEOs. The data point for injection-molded PEG 8000 is not considered in the regression analysis.

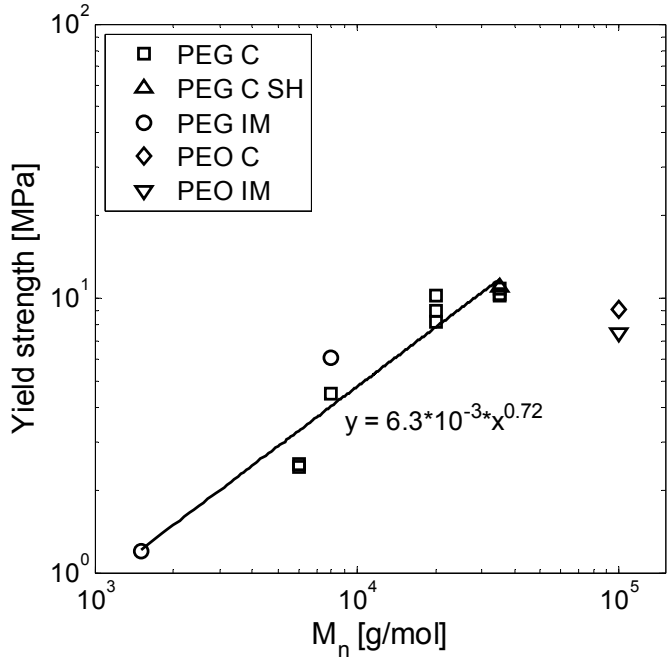

Figure 6.5: Log-log plot of yield strength versus molecular weight for selected injection-molded (IM), cast (CM), and cast and strain-hardened (SH) PEGs and PEOs.

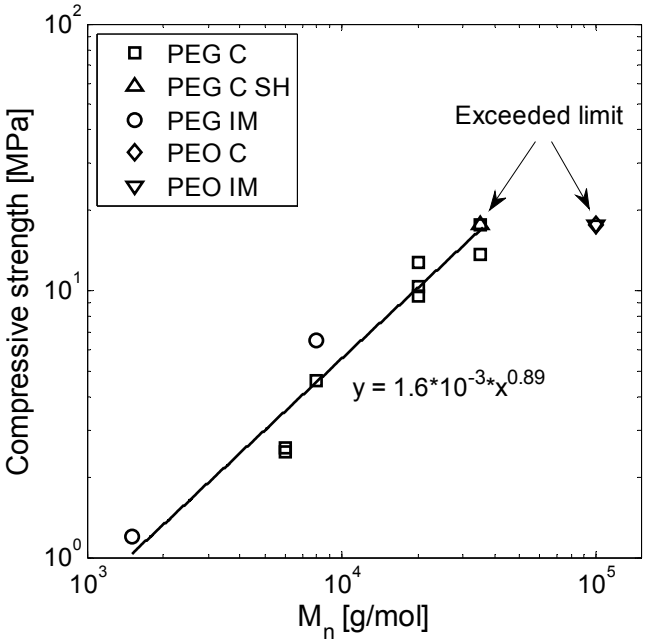

Figure 6.6: Log-log plot of compressive strength versus molecular weight for selected injection-molded (IM) cast (CM), and cast and strain-hardened (SH) PEGs and PEOs.

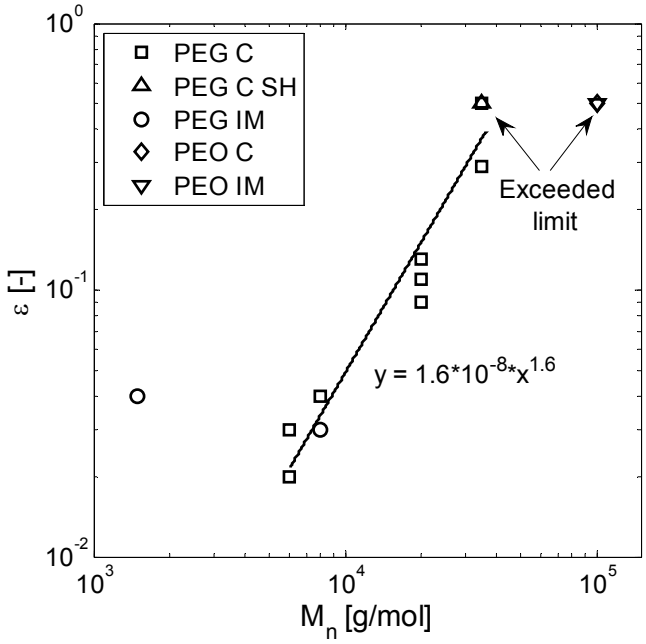

Figure 6.7: Log-log plot of strain at fracture versus molecular weight of selected injection-molded (IM), cast (CM), and cast and strain-hardened (SH) PEGs and PEOs.

6.3.2 Nanoindentation Tests

The results of nanoindentation tests, Young's modulus, hardness, and H/E ratio are listed in Table 6.5. Nanoindentation tests were performed to determine the mechanical properties, mainly of the Kollicoat IR-mannitol composite system. (Due to the moisture protective properties of Kollicoat IR (a PEG-polyvinylpyrrolidone copolymer with a molecular weight of about 35,000 g/mol) and the taste masking properties of mannitol, this may be a candidate for a hot-melt processed immediate-release coating formulation.) Figs. 6.8 and 6.9 show the elastic modulus and hardness versus drug volume fraction, with mannitol being stiffer and harder than Kollicoat IR. Both curves have similar shapes. It is observed that at a mannitol volume fraction below 0.2, both elastic modulus and hardness of the composite material are barely affected by the presence of mannitol. If the mannitol volume fraction is between 0.2 and 0.4, the elastic modulus and hardness are slightly increased compared with the properties of pure Kollicoat IR. If the mannitol volume fraction is increased from 0.4 to 0.6, a significant increase of elastic modulus and hardness is seen. From 60% mannitol to 100% mannitol, elastic modulus and hardness increase further, but less significantly to reach their respective values of the pure mannitol component.

In addition to the measured data, the upper and lower bounds of the properties of the are plotted in Fig. 6.8 and Fig. 6.9. The upper bound is

$$Q_{avg} = \phi_{Mann} Q_{Mann} + (1 - \phi_{Mann}) Q_{KCIR} \tag{6.1}$$

whereas the lower bound is

$$\frac{1}{Q_{Havg}} = \frac{1}{\phi_{Mann} Q_{Mann}} + \frac{1}{(1 - \phi_{Mann}) Q_{KCIR}} \tag{6.2}$$

with Q being the property, either the elastic modulus E or the hardness H [5]. As illustrated in Fig. 6.8 and Fig. 6.9, up to a mannitol volume fraction of about 0.3, the measured

data follow the lower bound, whereas at a volume fraction above about 0.7, the measured data are close to the upper bound. Between a mannitol volume fraction of 0.3 and 0.7, the measured data 'jump' upward. These results indicate that, for the Kollicoat IR-mannitol system with randomly distributed mannitol units, elastic modulus and hardness follow, at a mannitol volume fraction below 0.3, the same curve that is seen when the two components are aligned perpendicular to the applied force (lower bound). If the mannitol volume fraction is above 0.7, elastic modulus and hardness follow the trend that is seen when the two components are aligned parallel to the applied force (upper bound). The ratio of hardness to Young's modulus is plotted in Fig. 6.10. A value of 0.036 is obtained by linear regression.

An observation that is further highlighted is that the Young's modulus of PEO 100k derived from nanoindentation tests is about 3 times larger than the value obtained by compression testing. A similar trend has also been observed by other researchers [9].

Table 6.5: Young's modulus and hardness of selected melt-processed excipients and composites with mannitol, which here represents API.

Material	Molecular weight (g/mol)	API volume fraction	Young's modulus (GPa)	Hardness (MPa)	Ratio H/E (-)
PEO 100k	100,000	0.00	1.14[a]	60	5.26×10^{-2}
Eudragit L100-55*	320,000	0.00	2.64	138	5.23×10^{-2}
Kollicoat IR	45,000	0.00	0.77	36	4.68×10^{-2}
Kollicoat IR	45,000	0.08	0.38	26	6.84×10^{-2}
Kollicoat IR	45,000	0.16	0.82	36	4.39×10^{-2}
Kollicoat IR	45,000	0.24	1.52	52	3.42×10^{-2}
Kollicoat IR	45,000	0.34	2.23	70	3.14×10^{-2}
Kollicoat IR	45,000	0.43	3.65	104	2.85×10^{-2}
Kollicoat IR	45,000	0.63	9.98	460	4.61×10^{-2}
Mannitol	182	-	18.69	642	3.43×10^{-2}

* Eudragit L100-55 was mixed with 25% triethylcitrate by weight.

[a] Note that the Young's modulus of the surface of PEO 100k tested by nanoindentation may differ significantly from the modulus of the bulk material (see Table 6.4). This is in agreement with Ref. [9].

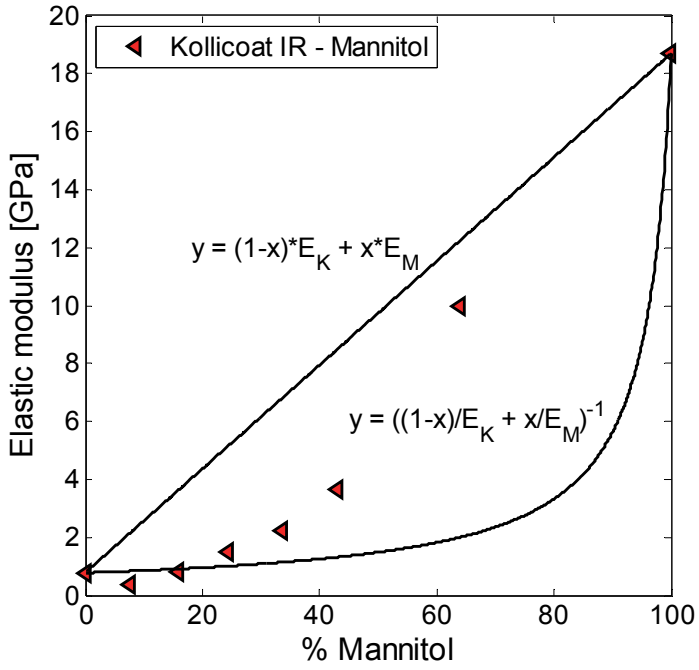

Figure 6.8: Elastic modulus versus mannitol volume fraction of the Kollicoat IR - mannitol composite material.

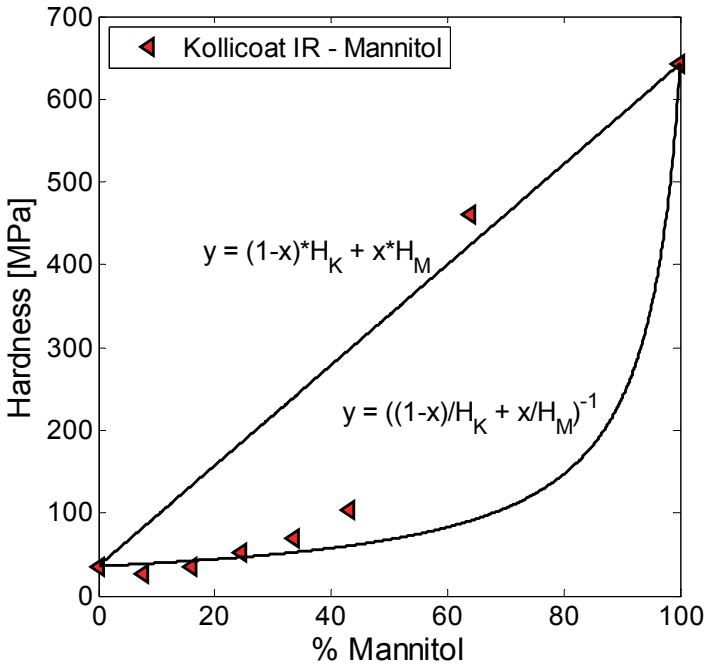

Figure 6.9: Hardness versus mannitol volume fraction of the Kollicoat IR - mannitol composite material.

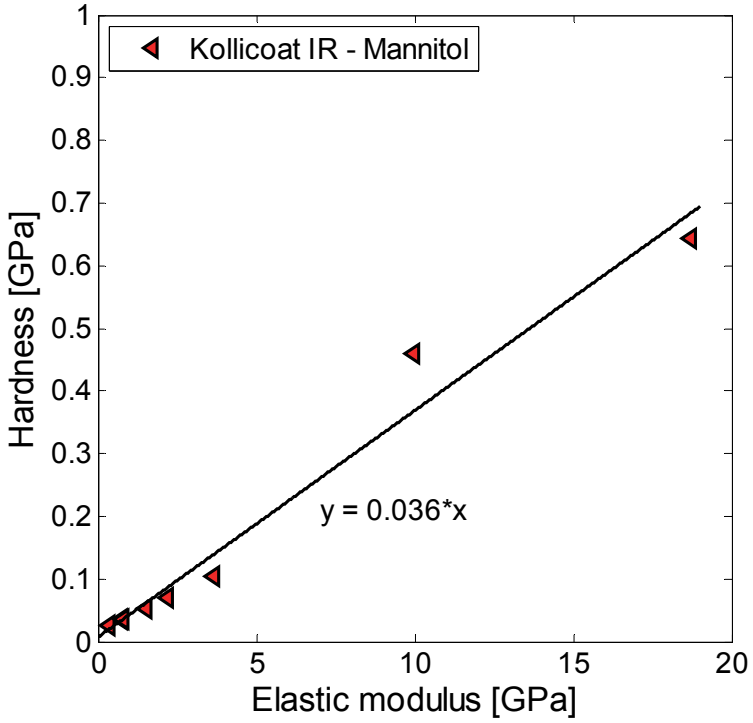

Figure 6.10: Hardness versus elastic modulus of the Kollicoat IR - mannitol formulation at various mannitol volume fractions.

6.4 Summary

Compression tests on PEGs and PEO of various molecular weights show that the mechanical properties of PEGs are, with exception of the elastic modulus, highly dependent on molecular weight. The yield strength ranges from 1.2 MPa for PEG 1,500 to 11.7 MPa for PEG 35,000. The strain at fracture is 0.04 or below if the molecular weight of PEG is low, and if the molecular weight is increased to 35,000 g/mol, the material becomes so ductile that this property cannot be measured anymore by a compression test.

Interesting results are obtained from nanoindentation tests of the Kollicoat IR-mannitol composite system. It is also shown that mechanical properties highly depend on the volume fractions of the individual components. It is found that if the volume fraction of mannitol, which is the stiffer and harder material, is kept below 0.3, the elastic modulus and hardness values of the composite material follow the lower bound. On the other hand, if the volume fraction of mannitol is above 0.7, the elastic modulus and hardness values of the composite material follow the upper bound.

References

[1] ASTM International, Standard Test Method for Compressive Properties of Rigid Plastics, Designation: D695-10, ASTM International, West Conshohocken, PA, USA.

[2] W.C. Oliver, G.M. Pharr, 2004, Measurement of hardness and elastic modulus by instrumented indentation: Advances in understanding and refinements to methodology, J. Mater. Res., 19, 3-20.

[3] W.C. Oliver, G.M. Pharr, 1992, An improved technique for determining hardness and elastic modulus using load and displacement sensing indentation experiments, J. Mater. Res., 7, 1564-1583.

[4] N.E. Dowling, 2012, Mechanical Behavior of Materials, fourth edition, Prentice Hall, Upper Saddle River, NJ.

[5] M.A. Meyers, K.K. Chawla, 2008, Mechanical Behavior of Materials, second edition, Cambridge University Press, Cambridge, UK.

[6] R.C. Rowe, S.C. Owen, P.J. Sheskey, 2006, Handbook of Pharmaceutical excipients, fifth edition, published by the American Pharmaceutical Association.

[7] R.W. Warfield, F.R. Barnet, 1972, Elastic Constants of Bulk Polymers, Angewandte Makromolekulare Chemie, 27, 215-217.

[8] L.M. Bellan, J. Kameoka, H.G. Craighead, 2005, Measurement of the Young's moduli of individual polyethylene oxide and glass fibres, Nanotechnology, 16, 1095-1099.

[9] H.-Y. Nie, M. Motomatsu, W. Mizutani, H. Tokumoto, 1997, Observation of modification and recovery of local properties of polyethylene oxide, J. Vac. Sci. Technol, B, 15, 1388-1393.

CHAPTER VII

OPTIMAL DESIGN AND MANUFACTURING METHODOLOGIES

7.1 Introduction

This chapter addresses the design and manufacture of immediate-release optimal solid dosage forms. First, the design problem with design variables, design objectives, and design constraints is stated for non-porous dosage forms. The dosage form design is then reduced to a two-phase disk-shaped device comprising drug particles embedded in an excipient matrix. Subsequently, an optimization problem, with manufacturing performance objective function and the product's specifications as functional design constraints, is formulated. The solution to this optimization problem allows identification of the design point (i.e., the excipient to use, drug volume fraction, drug particle size, and dosage form geometry) best for efficient manufacturing of non-porous immediate-release dosage forms. Moreover, the insights gained from the analysis allow derivation of novel product geometries and material structures for further optimizing manufacturing performance. Concepts for manufacturing such uncoated and coated optimal dosage forms by injection-molding are then presented. Finally, the manufacturing performance in terms of relevant performance measures is compared for dosage forms with a variety of drug contents.

7.2 Overview of the Design Problem

7.2.1 Problem Statement

Properties and specifications of immediate-release dosage forms are tight and highly regulated [1,2]. Accordingly, it is the goal of this chapter to develop a method that allows specification of the design variables of the dosage form so that (a) product performance related requirements are satisfied and (b) the manufacturing efficiency to produce the

Table 7.1: Overview of the design problem with design variables, design objectives, and design constraints for producing non-porous immediate-release dosage forms.

Design Variables:

- Drug volume fraction (φ)
- Drug particle size (d)
- Excipient(s)
    - Number of excipients and respective volume and mass fractions
    - solubility and diffusivity (c_0, D)
    - Process temperature (plasticizer melt temperature) (T_p, T_m)
    - Chemical stability (e.g. concentration of reactive degradation products)
    - Physical stability (e.g. hygroscopicity) (RH_{crit})
    - Thermal properties (e.g.thermal diffusivity) (α)
    - Plasticizer's tendency to solidify
- Geometry of the dosage form (D_G, H_0)

Design Objectives:

- Minimize material cost
- Minimize mixing time (t_m)
- Minimize mold cycle time per dosage form (t_{cycle})

Design Constraints:

- Drug content in the dosage form ($M_{d,\infty}$)
- Drug content uniformity in the dosage form (CV)
- Dissolution time of the dosage form (t_d)
- Concentration of degradation products in the dosage form (c_{deg})
- Physical and chemical stability of the dosage form
- Mechanical properties of the dosage form (E, σ_y, σ_c, ε)
- The dosage form is appealing to swallow (size and shape, color, taste, surface properties, etc.)

product is optimized. Design is where the most relevant decisions are made to affect product manufacturing, and hence can be considered the first and most important manufacturing step. The overriding principle followed here towards manufacturing optimization is waste reduction, based on the arguments stated by the proponents of lean manufacturing concepts (Sugimori et al. [3], Womack and Jones [4], and Couper et al. [5]). Waste, as articulated in chapter 2, is considered here as anything not essential to produce a product that meets the specifications and the needs of the consumer, characterized by excess unit operations (processing steps), excess process time, excess process rate, and excess material costs (i.e. excess amounts of solvent and excipient materials required). Since the process has been determined previously to comprise solvent-less injection-molding, the number of unit operations, process time, and solvent requirements are considered here as given. Material costs, driven by the amount of excipient material required, and process rate for a given equipment size, driven by the mixing time and the mold cycle time, however, are variable manufacturing performance measures and subjected to optimization. Accordingly, the design problem to produce such non-porous immediate-release optimal dosage forms is stated as shown in Table 7.1, with design variables being the parameters to affect the product's functional and manufacturing performance, design objectives being manufacturing performance measures to optimize, and the design constraints being the functional requirements that the dosage form must satisfy.

7.2.2 Reduction of the Design Problem

Design requirements can be integrated into the following formulation, as *'to produce a consumer-compliant, physically and chemically stable dosage form that dissolves the desired amount of drug in the desired time, whereas the dosage form does not contain any substantial amounts of toxic impurities or degradation products*'. In the light of this requirement, the excipient is a discontinuous, but highly critical design variable. It serves as release aid, processing aid, and mechanical binder. It further affects physical and chemical stability of the dosage form. Considering the requirements of immediate-release solid dosage forms, an excipient is desired that: (a) does allow processing of the API without degrading, (b) erodes rapidly for immediate drug release, (c) does not impair API stabil-

ity during storage and (d) does have mechanical properties sufficient for dosage form handling. It is the aim of this section to find an excipient family that satisfies the above criteria reasonably well. Specifying the excipient allows not only to reduce the number of design variables in the design and optimization problem introduced in Table 7.1, but also to eliminate the design constraints that are automatically satisfied if the proper excipient is used. The following paragraphs are devoted to guide the selection of suitable excipients for the present design.

First, most small molecule APIs, which are the focus of the present work, do not degrade substantially within the 2-20 minute time scale of the injection-molding process, if process temperature is kept below the melting temperature of the API. If the API, however, is molten during injection-molding processing, the kinetics of API degradation may become so fast that the level of impurities is out of specification after the material has been processed. This is because chemical kinetics of API degradation processes is increased by orders of magnitudes if the API is in liquid form compared with solid API. Since most small molecule APIs have a melting temperature between 75°C and 200°C, melting and degradation of the API can generally be avoided if the process temperature is kept below 75°C. An excipient as processing plasticizer is desired that melts below this temperature, but is solid up to temperatures above 45°C. Fig. 7.1 illustrates the melting temperatures versus molecular weight of excipients which have sufficient thermal stability to be commonly used for state-of-the-art immediate-release solid dosage forms processed by hot-melt extrusion. PEGs, PEOs, and selected poloxamers are crystalline, and they have their melting temperature within the desired temperature range [7,8].

Second, it is inferred from the analysis shown in chapters 4 and 5 that the rate at which the excipient erodes in a given environment is determined by the parameter solubility x diffusivity$^{2/3}$. Poloxamers and PEGs/PEOs are related in that poloxamers are triblock copolymers consisting of a central hydrophobic block of polypropylene glycol flanked by two hydrophilic blocks of polyethylene glycol. Due to the hydrophobic block, solubility of poloxamers in aqueous solution is lower than the solubility of PEGs/PEOs. PEGs are preferred here over poloxamers, because their higher solubility x diffusivity$^{2/3}$ gives a higher excipient erosion rate. Fig. 7.2 shows the solubility x diffusivity$^{2/3}$ versus

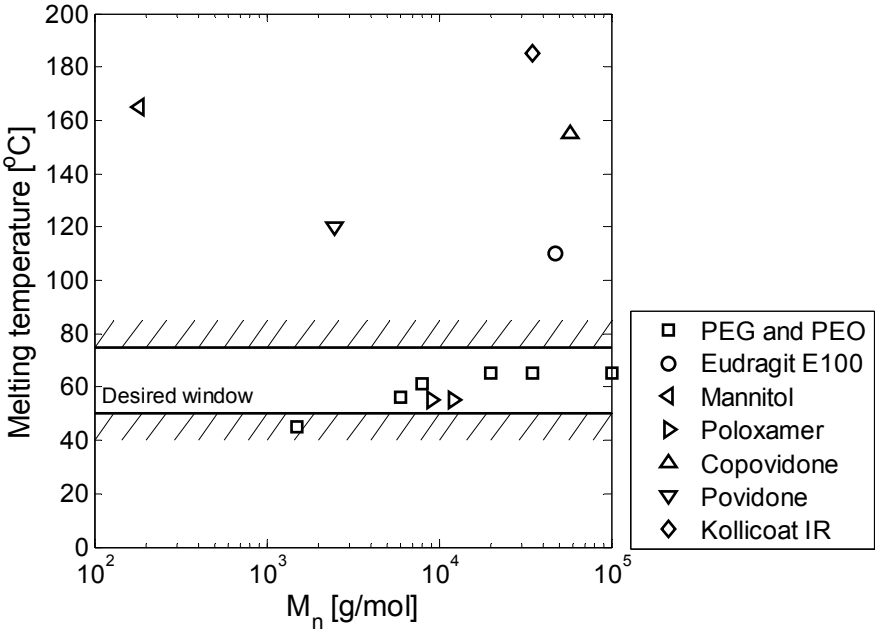

Figure 7.1: Melt temperature versus molecular weight of selected excipients commonly used for hot-melt extrusion (Data from Ref. [7] and Ref. [8]).

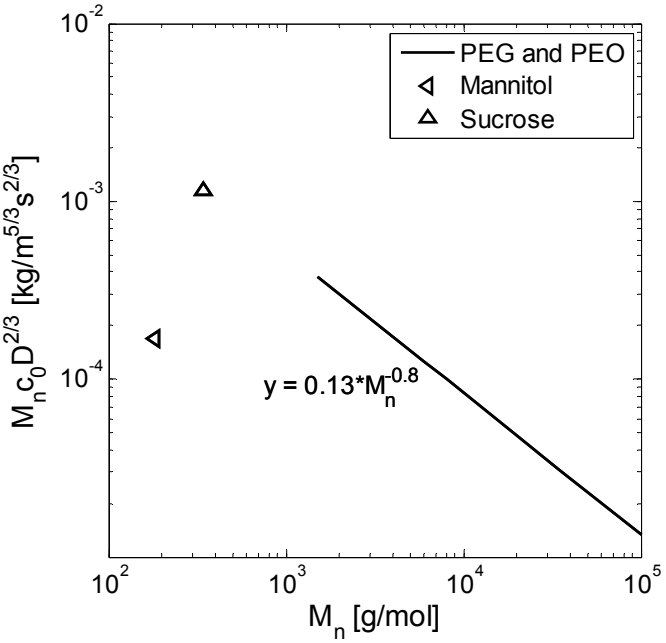

Figure 7.2: Solubility x diffusivity$^{2/3}$ of PEGs at various molecular weight, together with sucrose and mannitol. Data of mannitol and sucrose are from Ref. [7] and data of PEG are from chapter 5.

molecular weight for PEGs and PEO for the molecular weight range of 1,500-100,000 g/mol. Further illustrated is the solubility x diffusivity$^{2/3}$ of various polyols and sugars, which belong to the category of excipients with the highest solubility x diffusivity$^{2/3}$. PEG at low molecular weight has a solubility x diffusivity$^{2/3}$ of the order of mannitol, and slightly below the value of sucrose. PEGs, particularly at low molecular weight, hence belong to the fastest eroding excipients available.

Third, the favorable properties for fast erosion of low molecular weight PEGs, however, are also associated with the drawback that they may impair API stability during storage. As the length of the chains decreases, the density of the hydroxyl groups at the tails of the PEG molecule increases. This causes an increase in the content of free hydroxyl groups in the excipient, which may accelerate degradation of the API. The amount of free hydroxyl groups is quantified by the hydroxyl value, which for PEG is illustrated as a function of molecular weight in Fig. 7.3a. It is shown that the hydroxyl value is inversely proportional to the PEG molecular weight, suggesting that higher molecular weight PEG is preferred for APIs sensitive to free hydroxyl groups. A strategy which in some cases, however, has proven successful in reducing the number of free hydroxyl groups in low molecular weight PEGs, is the addition of stabilizers in the form of hydroxyl group scavengers. Moreover, PEGs at low molecular weight are hygroscopic. For example, at a temperature of 40°C, PEG 1,450 has shown a sharp increase in water content at 49% relative humidity. PEG 3,350 showed a sharp increase in water content at 71% relative humidity, whereas higher molecular weight PEG, such as PEG 6,000 and PEG 8,000, showed a sharp increase in water content at 75% relative humidity at the same temperature (Fig. 7.3b). PEG with molecular weight above 4,000 is therefore desired if the API chemical or physical stability exhibits water sensitivity.

Fourth, an overview of mechanical properties of PEGs within the selected range of molecular weights is given in Fig. 7.4a – Fig. 7.4d. Mechanical properties improve as the molecular weight of PEG is increased. For the entire chosen range of molecular weights of PEG, however, mechanical properties are sufficient to produce and handle non-porous dosage forms comprising a material structure with homogeneously distributed drug particles in the excipient matrix at conventional geometries.

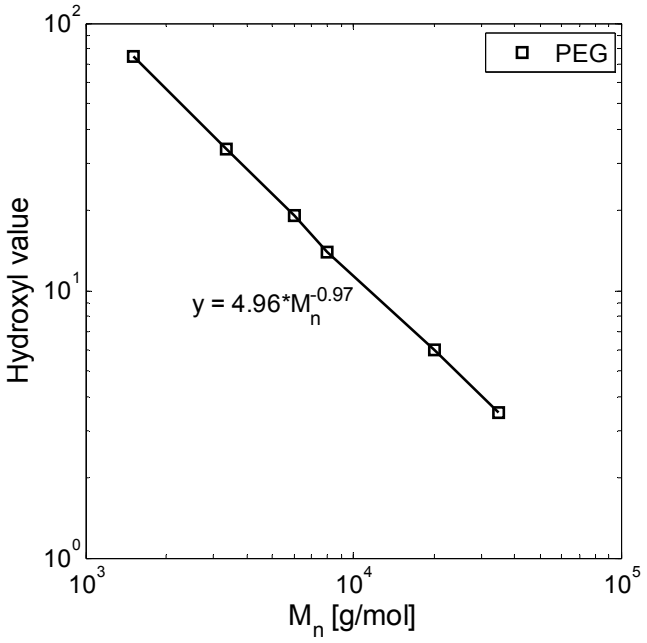

(a)

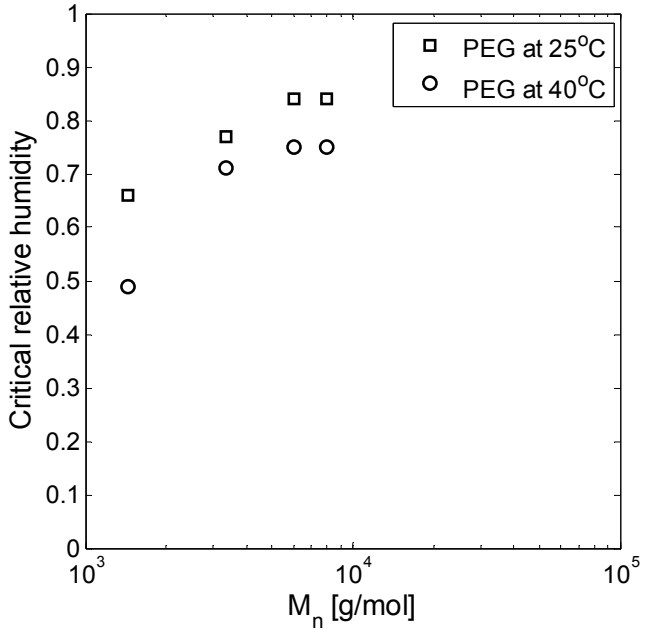

(b)

Figure 7.3: Properties of PEG relevant for dosage form stability. (a) Hydroxyl value of PEGs versus molecular weight (Data from Ref. [9]). (b) Critical relative humidity, determining the humidity above which water sorption becomes imminent, of selected PEGs (Data from Ref. [10]).

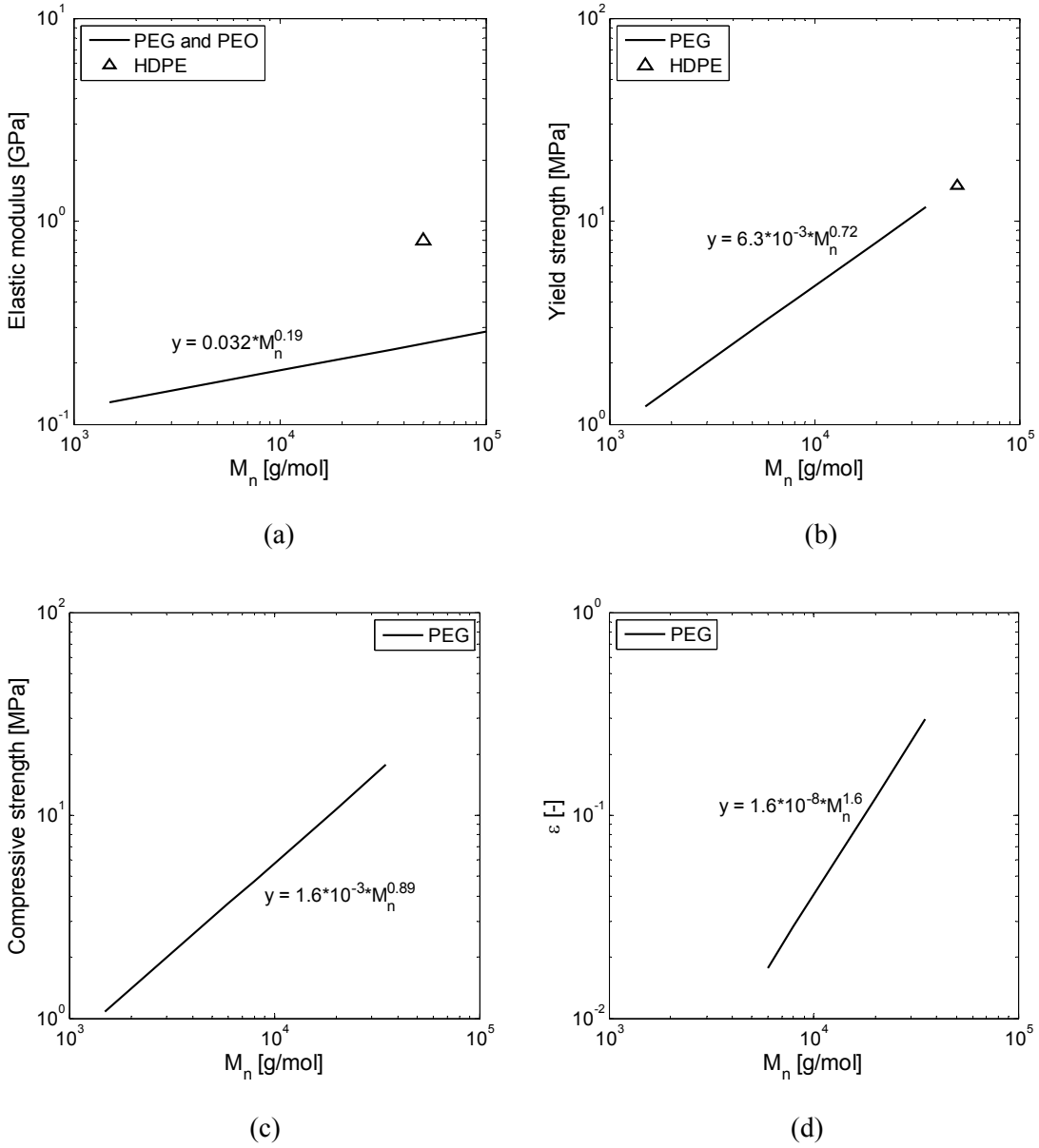

Figure 7.4: Mechanical properties of PEG (data from chapter 6). (a) Elastic modulus versus molecular weight of PEGs along with the elastic modulus of HDPE at a molecular weight of 50,000 g/mol from Ref. [11]. (b) Yield strength versus molecular weight of PEGs along with the yield strength of HDPE at a molecular weight of 50,000 g/mol from Ref. [11]. (c) Compressive strength versus molecular weight of PEGs and (d) strain at fracture versus molecular weight of PEGs.

Consequently, even if there may be materials or material combinations which in certain aspects may outperform PEG as an excipient for the present application, single-phase PEG is a viable excipient for non-porous immediate-release dosage forms containing a large range of small-molecule APIs. PEGs have a processing temperature below the melting temperature of most small-molecule APIs, high solubility x diffusivity$^{2/3}$, acceptable mechanical properties, and in the case of higher molecular weight PEGs (above about 4,000 g/mol) also good chemical and physical stability. The design of the dosage form is therefore reduced here to a two-phase system comprising API particles embedded in a PEG excipient matrix, with: (a) the drug volume fraction, (b) drug particle size, and (c) PEG molecular weight as formulation parameters. Design constraints are reduced simply to the requirements on (i) drug content in the dosage form, (ii) dissolution time of the dosage form, and (iii) dosage form geometry, because all the other constraints are automatically satisfied if PEG at the proper molecular weight is used. The dosage form geometry is further reduced to disk-shape in this work, as this geometry resembles the basic shape on which most conventional dosage form geometries are based. Continuous geometric variables are then the dosage form diameter, D_G, and the dosage form thickness, H_0, as presented in Fig. 7.5.

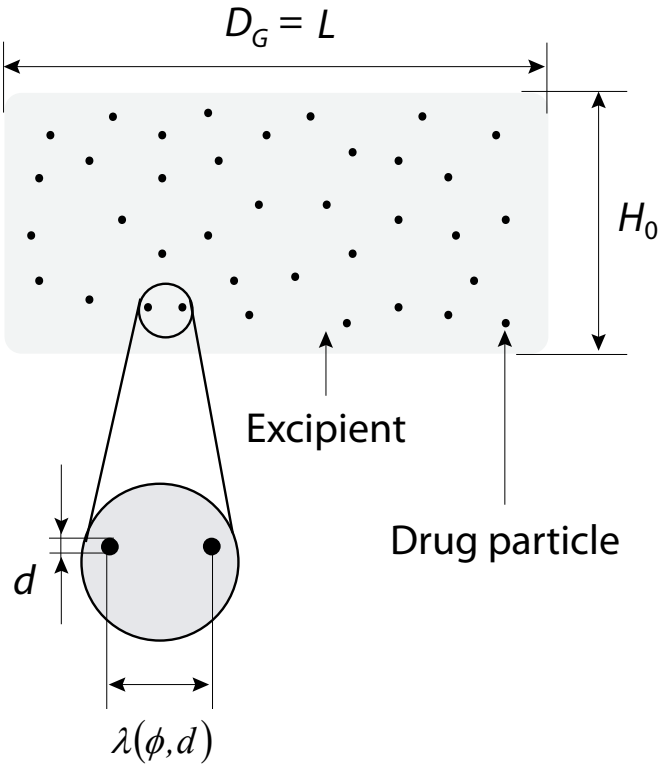

Figure 7.5: Design of a disk-shaped non-porous dosage form with drug volume fraction, drug particle size, and dosage form geometry as relevant design parameters.

7.3 Relevant Objective Functions and Constraints

It is evident based on the aim of this work that the design point must be so chosen that the dosage form meets specifications while manufacturing performance is optimized. A set of equations that describe design objectives and constraints as a function of design variables is, however, required before a mathematical optimization problem can be stated and solved. Such equations for the reduced design problem are developed in this section.

7.3.1 Mixing Time

Mixing of API and excipient aims at reducing the standard deviation of an individual component's content in a sample taken from the mixture. Generally, the standard deviation of a sample taken from the mixture comprising such an individual component's content, decreases with increasing mixing time. Mixing therefore must be carried on at least until the dosage form meets specifications on drug content uniformity [12,13]. Assuming that API and excipient are mixed as non-adherent powders, the standard deviation in API content of a sample taken can be described as a function of mixing time as [12,13]:

$$s = s_0 \exp\left(-\frac{t}{\tau_m}\right) \tag{7.1}$$

where

$$s_0 = \phi(1-\phi) \tag{7.2}$$

The mixing time constant, τ_m, depends on a variety of parameters, such as the size, density, and shape of the individual particles, the type of mixer, and the mixing process conditions. Eq. (7.1) allows derivation of the mixing time:

$$t_m = -\tau_m \ln\left(\frac{s_{final}}{s_0}\right) \tag{7.3}$$

The mixing endpoint, characterized by the standard deviation in API content of the sample at the endpoint, s_{final}, can be determined based on the specifications on content uniformity given by regulatory authorities, which require that the coefficient of variation (CV) in API content must be smaller than about 5% [1,2]. It hence can be written for the standard deviation in API content of the sample at the end point:

$$s_{final} = \frac{CV}{\phi} \tag{7.4}$$

Combining Eq.(7.1) – Eq.(7.4) then gives for the mixing time:

$$t_m = -\tau_m \ln\left(\frac{CV}{1-\phi}\right) \tag{7.5}$$

Eq. (7.5) is simply a function of the mixing time constant, the coefficient of variation at the mixing endpoint, and the drug volume fraction. In fact, the mixing time decreases monotonically with increasing drug volume fraction. Therefore, the mixing time is minimal if the drug volume fraction is maximal if both the mixing time constant and the coefficient of variation at the mixing endpoint are given.

The above presented result on required mixing time, however, must be interpreted with care. If the drug volume fraction assumes a large value approaching 1, the mixing time according to Eq. (7.5) decreases to zero. This result, however, is deceiving, as also the excipient phase must, for the dosage form to possess the desired properties, to a certain extent be uniformly distributed in the dosage form.

7.3.2 Mold Cycle Time

The mold cycle time, t_{cycle}, is the most relevant parameter that determines the rate at which a product can be produced by injection-molding at a given machine size [14]. It is composed of the injection time, t_{inj}, the cooling time, t_{cool}, and the mold resetting time, t_r (i.e. the time to open the mold, eject the part, and close the mold), and can be written as:

$$t_{cycle} = t_{inj} + t_{cool} + t_r \tag{7.6}$$

The injection time can be calculated from the average flow rate and the shot size. It is proportional to the shot volume and inversely proportional to the average flow rate. Typically, the injection time is between 0.5 and 1.5 seconds, which in general is small compared with the cooling time and the mold resetting time. If the material shows high tendency to solidify if it is at the temperature of the mold wall, the cooling time is the time required for the part to become sufficiently rigid such that it can be ejected from the mold without distortion or damage. Deciding when to demold a part on the basis of the minimum permitted rigidity is, however, complicated and impractical. Instead, the cooling time can be derived from the heat transfer equations using a demolding temperature. If the heat of fusion is negligible in heat transfer analysis, which is typical in common injection-molded polymers, the heat transfer equation reduced to one dimension is:

$$\frac{\partial^2 T}{\partial x^2} = \frac{1}{\alpha}\frac{\partial T}{\partial t} \tag{7.7}$$

Since the mold can be extensively cooled, and the thermal diffusivity of the mold material is typically orders of magnitude larger than the one of the polymeric material processed by injection molding, a constant wall temperature, T_w, can be set as boundary condition. The following solution to this problem has been proposed by Carslaw and Jaeger, with T_0 being the initial temperature of the melt [15]:

$$\frac{T - T_w}{T_0 - T_w} = \frac{4}{\pi}\sum_{n=0}^{\infty}\frac{1}{(2n+1)}\exp\left(-\frac{\kappa(2n+1)^2\pi^2 t}{H_0^2}\right)\sin\frac{(2n+1)\pi x}{H_0} \tag{7.8}$$

If this solution is truncated to just the first term, the following approximation can be derived for the cooling time:

$$t_{cool} = \frac{H_0^2}{\pi^2 \alpha} \ln\left(\frac{4}{\pi} \frac{(T_0 - T_w)}{(T_{\max} - T_w)}\right) \tag{7.9}$$

where T_{max} is the temperature in the center of the piece when the part can be ejected, i.e., the demolding temperature that is to be determined experimentally for a given system. The mold resetting time can be calculated based on estimates for the times of such individual steps as mold opening, mold closing, part ejection, as well as mold pull-back and mold rotation applicable in certain multi-component injection-molding systems. Rough estimates of the times required to execute the individual molding steps are summarized in Table 7.2.

Based on this analysis, the mold cycle time of a system with a melt temperature of 75°C, a mold temperature of 5°C, a demolding temperature of 65°C, and the geometry of a conventional solid dosage form with thickness above 5 mm is expected to be above 13.5 seconds. This may be problematic, because even if the number of cavities per mold plate applied in the injection molding system is at the upper bound, which today is 256-512, the cycle time per mold cavity is above 26 ms, which is significantly larger than the 2-20 ms cycle time per mold cavity that can be achieved with conventional powder compaction equipment.

7.3.3 Excipient Cost

Excipients account for a significant part of downstream manufacturing costs. The cost of the excipient contained in the dosage form is composed of the excipient mass multiplied with the unit cost of the excipient:

$$Excipient\ cost = c_e M_e = c_e \frac{\rho_e (1-\phi) \pi H_0 D_G^2}{4} \tag{7.10}$$

Table 7.2: Estimated times required for the individual molding steps.

Process step	Time (s)
Injection	0.5
Solidification	Cooling time
Mold opening	0.75
Mold rotation	1
Mold closing	1.5
Mold pull back	0.5
Part ejection	0.75

If the cost per unit of excipient is constant, the minimum excipient cost is observed when the drug volume fraction is maximal.

7.3.4 Drug Content

Similar to the amount of the excipient in the dosage form, the dosage form's drug content is simply the volume occupied by the drug phase multiplied with its density:

$$M_{d,\infty} = \frac{\pi \rho_d \phi H_0 D_G^2}{4} \tag{7.11}$$

The drug content in the dosage form is considered here as a given constraint, which depending on the potency of the active ingredient can range from less than 0.5 mg up to more than 500 mg.

7.3.5 Dissolution Time

Assuming that the disk-shaped dosage form erodes from both faces, the constraint equation for the dissolution time is

$$t_d = \frac{H_0}{2\dot{H}} \tag{7.12}$$

where dH/dt is the erosion rate of one face of the dosage form, and H_0 is the dosage form's initial thickness. It is shown in chapters 4 and 5 that interconnected excipient clusters must exist for the excipient to be capable of having any substantial effect on erosion rate. Since the pure drug phase generally erodes at a much smaller rate than what is required for a conventional dosage form to meet specifications of immediate-release, the maximum drug volume fraction is limited to the second percolation threshold. The dissolution model developed in chapters 4 and 5, and the experimental results show that the dependence of erosion rate on drug volume fraction is reasonably well approximated by a

linear fit if the drug volume fraction is below the second percolation threshold. Hence, for simplicity, the empirical equations presented in Fig. 5.9, Fig. 5.13, and Fig. 5.14 for the PEG-aspirin system are used to describe the erosion rate as a function of drug volume fraction as:

$$\frac{dH}{dt} = \frac{dH_{e,0}}{dt}\left(1 - c\phi\right) \tag{7.13}$$

$$\frac{dH_{e,0}}{dt} = 1.75 * 10^{-3} M_n^{-0.8} \sqrt{\frac{v_\infty}{0.0848} \frac{L_0}{L}} \tag{7.14}$$

$$c = -\left(\frac{dH_{e,0}}{dt}\right)^{-1} \frac{dH}{dt d\phi} = 6.36 M_n^{-0.17} \tag{7.15}$$

where the velocity v_∞ is 0.052 m/s and the length L_0 = 12.7 mm with L = 12 mm are used. Combining Eq. (7.13) – Eq. (7.15) gives for the dissolution time of the disk:

$$t_d = \frac{H_0}{1.41 * 10^{-3} M_n^{-0.8}\left(1 - 6.36 M_n^{-0.17}\phi\right)} \tag{7.16}$$

The maximum acceptable dissolution time, $t_{d,max}$, is considered here as 30 minutes. Note: the lower bound of the erosion rate can be calculated by the harmonic mean with respect to the drug volume fraction of the erosion rate of the pure excipient and pure drug phase, Eq. 4.3. From this equation, the dissolution time, drug release flux, etc. can be calculated particularly if the drug volume fraction is above the second percolation threshold.

7.3.6 Geometric Constraints

Solid dosage forms do not have any fixed dimensional constraints, rather their shape and size must allow easy to handling and swallowing. A reasonable range of dimensions of state-of-the-art disk-shaped dosage forms is as follows $D_{G,min}$ = 3 mm, $D_{G,max}$ = 21 mm, $H_{0,min}$ = 1.5 mm, $H_{0,max}$ = 10 mm [16-20].

7.4 The Design of Non-Porous, Immediate-Release Dosage Forms

7.4.1 Statement of the Optimization Problem

With the objective to design the dosage form for manufacturing optimization, an optimization problem is stated that has manufacturing performance parameters as objective function and product specifications as constraints. The problem is formulated similar to a typical problem in engineering optimization that is to minimize the effort required to achieve a given goal [21] as follows:

Find **x = [φ, H, D, M_n]** **that minimizes:**

Excipient mass
$$M_e = \frac{\pi \rho_e (1-\phi) H_0 D_G^2}{4} \tag{7.17}$$

Cooling time
$$t_{cool} = \frac{H_0^2}{\pi^2 \alpha} \ln\left(\frac{4}{\pi} \frac{(T_0 - T_w)}{(T_{\max} - T_w)}\right) \tag{7.18}$$

Mixing time
$$t_m = -\tau_m \ln\left(\frac{CV}{(1-\phi)}\right) \tag{7.19}$$

Subject to:

Drug content
$$M_{d,\infty} = \frac{\pi \rho_d \phi H_0 D_G^2}{4} \tag{7.20}$$

Dissolution time
$$t_{d,\max} > \frac{H_0}{1.41 * 10^{-3} M_n^{-0.8} (1 - 6.36 M_n^{-0.17} \phi)} \tag{7.21}$$

Dosage form diameter
$$D_{G,min} < D_G < D_{G,max} \tag{7.22}$$

Dosage form thickness
$$H_{0,min} < H_0 < H_{0,max} \tag{7.23}$$

7.4.2 Solution of the Optimization Problem

The system of equations is solved for every individual objective function using the *fmincon* solver of the optimization toolbox of MATLAB. Since mixing time and the amount of excipient required are both functions that monotonically decrease with increasing drug volume fraction, there must be a design point that optimizes these measures simultaneously. The solutions obtained for a drug content of 0.5 mg, 5 mg, 50 mg, and 500 mg are presented in Table 7.3 and Table 7.4.

The optimal design point together with the design space can also be illustrated graphically, as shown in Fig. 7.6 and Fig. 7.7. Graphical visualization of the problem provides a better engineering intuition, and hence allows to identify opportunities for further improvement. The figures comprise the frame of D^2 versus H, which allows visualization of the geometric constraints on diameter and thickness as horizontal and vertical lines, respectively. Also the constraint on dissolution time can, by rewriting Eq. (7.16), be represented by a vertical line: it says that the maximum thickness of the dosage form must be smaller than the thickness that is eroded during the maximum specified dissolution time as:

$$H_0 < \frac{1.41*10^{-3} M_n^{-0.8}\left(1-6.36M_n^{-0.17}\phi\right)}{t_{d,\max}} \tag{7.24}$$

Here, the specified maximum dissolution time, $t_{d,max}$, is considered to be 30 minutes. The magnitude of this constraint on maximum dosage form thickness (determined by the maximum erosion rate), as given in Eq. (7.24) depends on drug volume fraction and PEG molecular weight, hence the position of the vertical line of this constraint can be changed by changing these parameters. Finally, the constraint on drug mass given by Eq. (7.11) can be re-written as the following inversely proportional function:

$$D_G^2 = \frac{4M_{d,\infty}}{H_0 \pi \rho_d \phi} \tag{7.25}$$

This constraint is represented by the blue lines in Figs. 7.6 and 7.7. It is evident that also this constraint is a function of drug volume fraction. Therefore, the shape of such inversely proportional curves is changed by changing drug volume fraction.

The objective functions can be reduced to two objectives. The first one is to maximize drug volume fraction, which allows minimization of mixing time and excipient mass, and the second one is to minimize dosage form thickness, which allows to minimize cooling time.

The optimal design point depends on drug content. For highly-potent and potent drugs, at a drug content of 0.5 mg and 5 mg, respectively, it is shown in Fig. 7.6 that the maximum drug volume fraction is constrained to a value of 0.034 and 0.34 by the minimum volume of the dosage form (i.e., the minimum diameter and the minimum thickness). Therefore, the design point that maximizes drug volume fraction is also the design point that minimizes dosage form thickness in this case, giving a design point that is optimal in terms of all the objective functions. This solution is valid for a PEG excipient with M_n < 20,000 at 0.5 mg drug content, and for a PEG excipient with M_n < 8,000 at 5 mg drug content (i.e., the design point is not limited by the erosion rate if excipient of such molecular weight is used).

If the drug content is increased to 50 mg, the optimal design point is at a drug volume fraction of 0.5, limited by the constraint on minimum thickness and the constraint on erosion rate (i.e., the constraint on maximum thickness) using PEG 4,000 as excipient (Fig. 7.7a). Because this design point is determined by the maximum erosion rate, the fastest eroding excipient available, PEG 4,000, is required to erode the 1.5 mm thick dosage form in 30 minutes at a drug volume fraction of 0.5.

At a drug content of 500 mg, the constraint on the maximum dosage form diameter, together with the constraint on erosion rate (i.e., the constraint on maximum thickness) determine the optimal design point. The maximum drug volume fraction is 0.35 using PEG 4000 as excipient at a dosage form thickness of 3 mm (Fig. 7.7b). Even though this thickness is considerably larger than the minimum thickness constraint, it still resembles the minimum thickness to produce the dosage form in specification. Therefore, the observation made above that maximization of drug volume fraction implies minimization of dosage form thickness applies also to the case of 500 mg drug content.

Table 7.3: Design point that minimizes the mass of excipient required and mixing time.

Parameter	0.5 mg	5mg	50 mg	500 mg
t_m/τ_m	2.97	2.58	2.3	2.56
H_0 (mm)	1.5	1.5	1.5	3
D_G (mm)	3	3	7.8	21
φ	0.03	0.34	0.5	0.35
M_n (g/mol)	[1,500 20,000]	[1,500 8,000]	4,000	4,000

Table 7.4: Design point that minimizes cooling time.

Parameter	0.5 mg	5mg	50 mg	500 mg
t_{cool} (s)	1.8	1.8	1.8	7.3
H_0 (mm)	1.5	1.5	1.5	3
D_G (mm)	3	3	7.8	21
φ	0.03	0.34	0.5	0.35
M_n (g/mol)	[1,500 20,000]	[1,500 8,000]	4,000	4,000

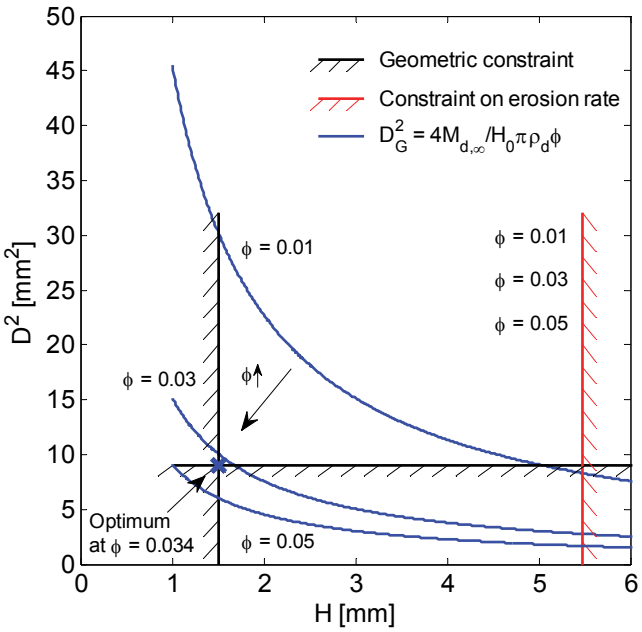

(a)

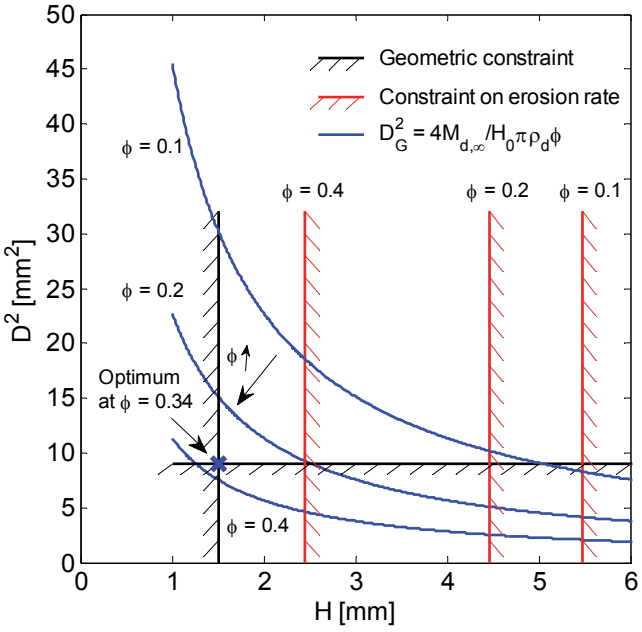

(b)

Figure 7.6: Design space and the design point where drug volume fraction is maximal and dosage form thickness is minimal with a minimum thickness constraint of 1.5 mm and a minimum diameter constraint of 3 mm. The drug content is (a) 0.5 mg and (b) 5 mg.

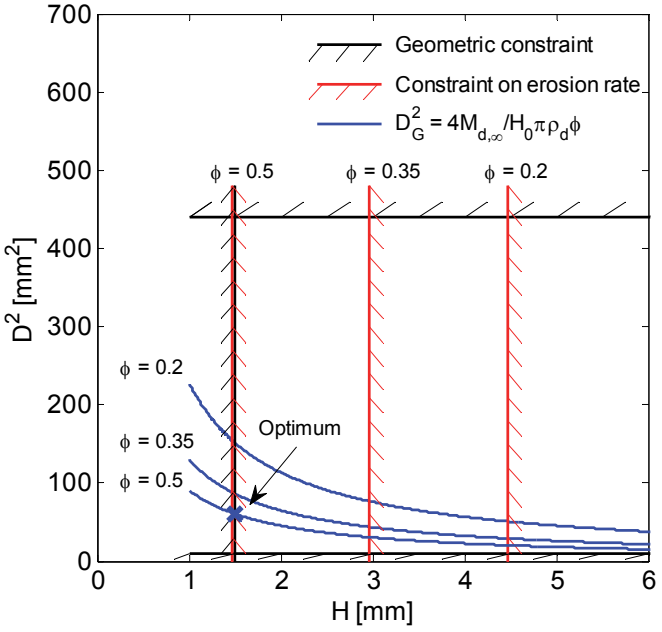

(a)

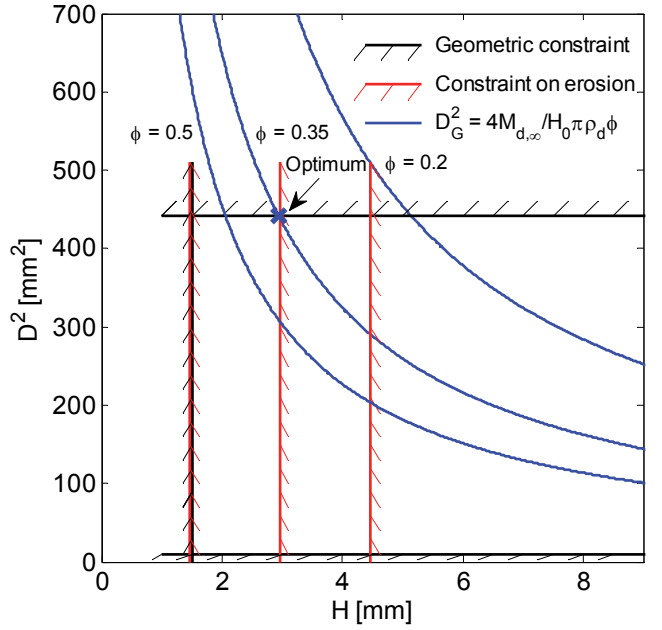

(b)

Figure 7.7: Design space and the design point where drug volume fraction is maximal and dosage form thickness is minimal with a minimum thickness constraint of 1.5 mm and a maximum diameter constraint of 21 mm. The drug content is (a) 50 mg and (b) 500 mg.

The optimal design point, if limited by the constraint on erosion rate, can also be presented within the curves of erosion rate versus drug volume fraction and drug release flux versus drug volume fraction.

If the optimal design point is limited by the constraints on maximum erosion rate and minimum thickness, as it is the case if the drug content is 50 mg, then the minimum required erosion rate (i.e. the erosion rate to erode the initial dosage form thickness within the maximum dissolution time) can be derived by the constraints on minimum thickness and dissolution time. The optimum is in this case, as shown in Fig. 7.8, given by the point with the maximum drug volume fraction that achieves this erosion rate. This point is where drug volume fraction is maximal and dosage form thickness is minimal.

Similarly, if the optimal design point is limited by the maximum diameter, as it is the case if the drug content is 500 mg, then the maximum surface area together with the constraints on drug mass and dissolution time can be combined to give a constraint for the required drug release flux. Therefore, for the case of 500 mg drug content, the optimum is at the maximum drug volume fraction at which the required drug release flux can be achieved (Fig. 7.9). Maximization of drug volume fraction implies minimization of the thickness of the dosage form, as the volume of excipient, and consequently also the total volume of the dosage form, is so minimized for a given drug volume.

7.4.3 Alternative Geometric Designs Based on Non-Porous Material

It is evident, based on the above analysis, that manufacturing performance to produce the disk-shaped solid dosage form design as conceptualized in Fig. 7.5 is limited by such design constraints as minimum thickness and diameter, and maximum diameter. Therefore, if the design could be modified such that performance-limiting constraints are stretched, it may be possible to further improve manufacturing performance.

For example, in case of potent drugs (at a drug content of 0.5 mg and 5 mg), manufacturing performance of such dosage forms as presented in Fig. 7.5 or Fig. 7.11 case A is limited by the constraints on minimum diameter and minimum thickness. Changing these performance-limiting constraints to, for example, a minimum diameter of 1 mm and a

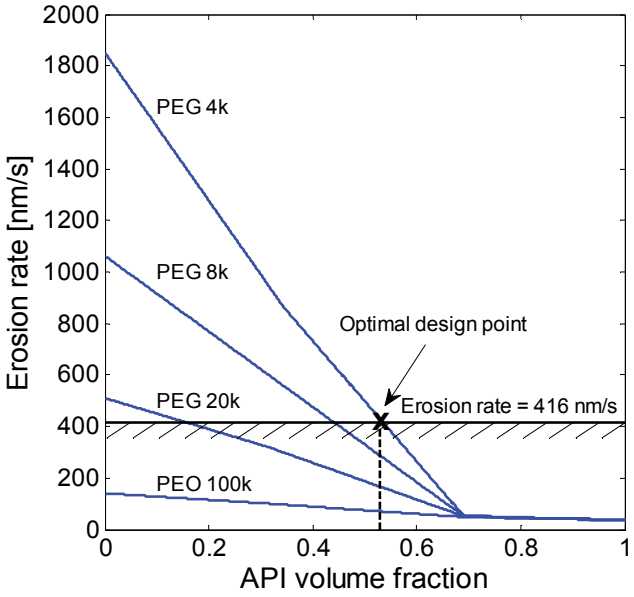

Figure 7.8: Erosion rate versus API volume fraction for selected PEG-aspirin systems derived by combining the model in chapter 4 with the empirical equations shown in section 7.3.1. The curves further indicate the optimal design point for the case with 50 mg drug content given a minimum thickness constraint of 1.5 mm and a maximum dissolution time of 30 minutes (i.e., a minimum erosion rate of 416 nm/s).

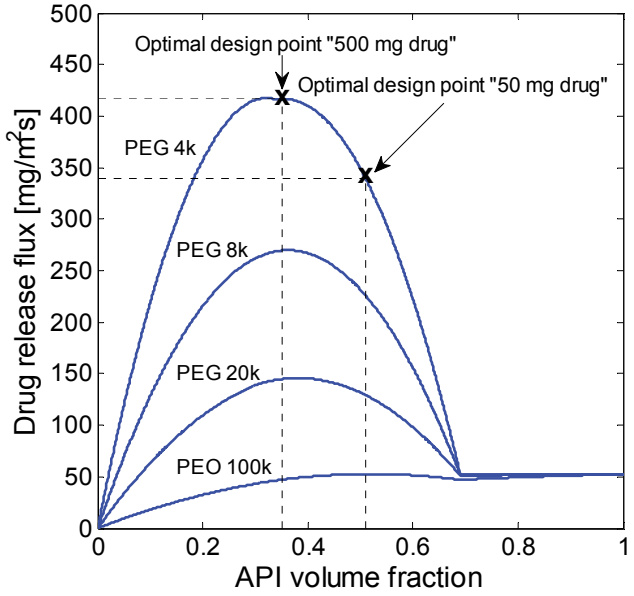

Figure 7.9: Drug release flux versus API volume fraction for selected PEG-aspirin systems derived by combining the model in chapter 4 with the empirical equations shown in section 7.3.1. The curves further indicate the optimal design point for the cases with 50 mg drug content and 500 mg drug content.

minimum thickness of 0.2 mm, would make further improvement of manufacturing performance possible. Fig. 7.10 shows design space and optimal design point of such systems with 0.5 and 5 mg drug content. The maximum drug volume fraction is limited to about 0.6 by the constraint on minimum thickness and the constraint on erosion rate using PEG 4,000 as excipient. At such high drug volume fractions, the minimum thickness of 0.2 mm is eroded in 30 minutes if the fastest eroding excipient considered here, PEG 4,000, is used.

Clearly, such a geometry with only 0.2 mm thickness may not be acceptable, as such dosage forms may not be easy to handle by the consumer. A design solution that would, however, provide an acceptable dosage form size with high local values of drug volume fraction, is a multi-structure design as illustrated in Fig. 7.11, case B. The dosage form consists of two compartments, one compartment of the dosage form is filled with pharmaceutical material at high drug volume fraction, and the other compartment is just a low-cost filler that does not contain any drug. Such a design offers opportunities to reduce mixing time of potent drugs significantly, whereas the dosage form still can be made at patient-compliant size. However, a two-shot injection-molding process is required to produce such a design. Hence, the potential reductions in mold cycle time due to the reduction in thickness of the structures are limited. Also, no reduction in the amount of excipient material required can be achieved.

On the other hand, in case of low potency drugs (for example, at a drug content of 500 mg), the manufacturing performance to produce the design as shown in Fig. 7.11, case A, is limited by the maximum diameter and the erosion rate. For such cases where the constraints on maximum diameter and erosion rate limit manufacturing performance, a dosage form designed for increased drug release flux could potentially reduce such measures as mixing time, cooling time, and excipient mass required. Drug release flux can be increased by: (a) using a faster eroding excipient and (b) increasing the characteristic surface area. The characteristic surface area can, for example, be increased by a design which comprises a thin base on which thin posts are standing. Fig. 7.12 illustrates the design space of such a design, and it is shown that the drug volume fraction in such a design could be increased. Also such a design with thin posts on a thin base disk, however, may not be practical.

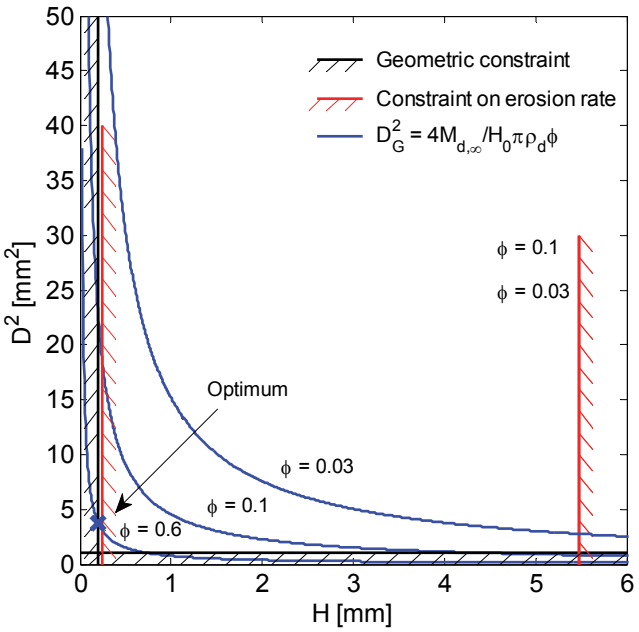

(a)

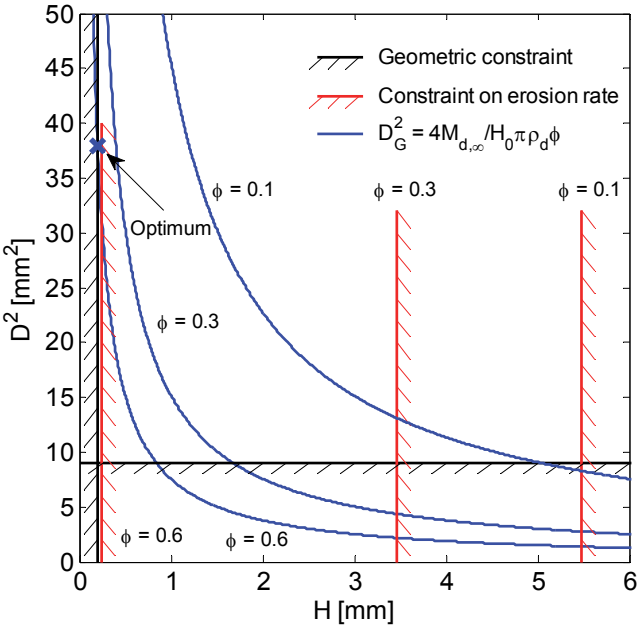

(b)

Figure 7.10: Design space and the design point where drug volume fraction is maximal and dosage form thickness is minimal with a minimum thickness constraint of 0.2 mm and a minimum diameter constraint of 1 mm. The drug content is (a) 0.5 mg and (b) 5 mg.

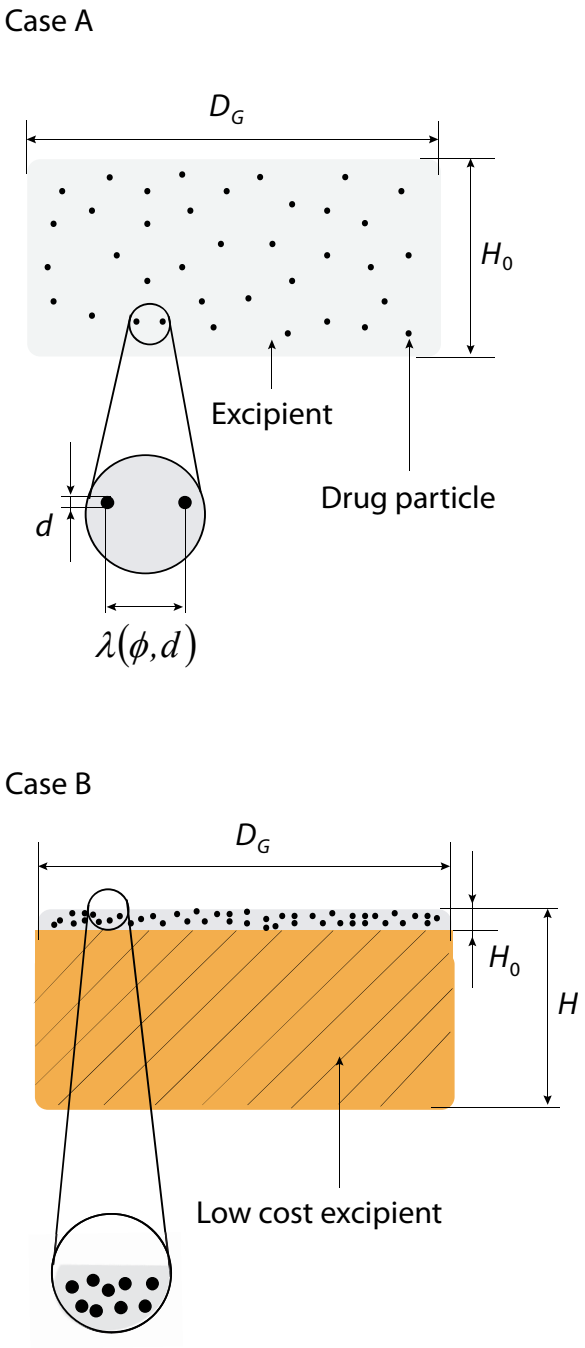

Figure 7.11: Design examples: case A and case B suitable for non-porous immediate-release dosage forms at various drug content.

It is possible, though, to integrate such a design into a consumer-compliant dosage form. For example, the dosage form can again be comprised of two material structures, one structure that contains the drug, the other structure simply consisting of a very fast eroding, inexpensive excipient such as PEG 4,000 with sucrose. The part that contains the drug is equipped with thin posts, as illustrated in Fig. 7.13 case C, whereas the part that does not contain any drug is surrounding these posts. The excipient that surrounds the posts is rapidly eroded, such that erosion of the posts can occur soon after the dosage form is put into the dissolution medium. Since both the characteristic thickness for erosion and for heat transfer can be reduced by such a design, opportunities for optimization of both mixing time (i.e. drug volume fraction in the drug containing compartment) and cooling time are offered. The requirement on the amount of excipient material required, however, cannot be reduced substantially.

Another design that increases the characteristic eroding surface area is a hollow shell design as presented in Fig. 7.13 case D. This dosage form can, for example, be equipped with so-called “dissolution indents”. The dissolution indents allow the core of the dosage form to be filled with dissolution medium soon after the dosage form is put into it. Erosion can, in this case, occur from outside and inside of the dosage form, resulting in the eroding surface area to be increased by a factor greater than 2. The hollow shell design, however, is associated with the additional constraint that the shell material must satisfy mechanical requirements for the dosage form to be structurally stable under the loads during handling. Low molecular weight PEG, which is comparably brittle and has low compressive strength, as well as material with high drug volume fraction where drug particles show a high level of connectivity, may hence not be suitable for such a design.

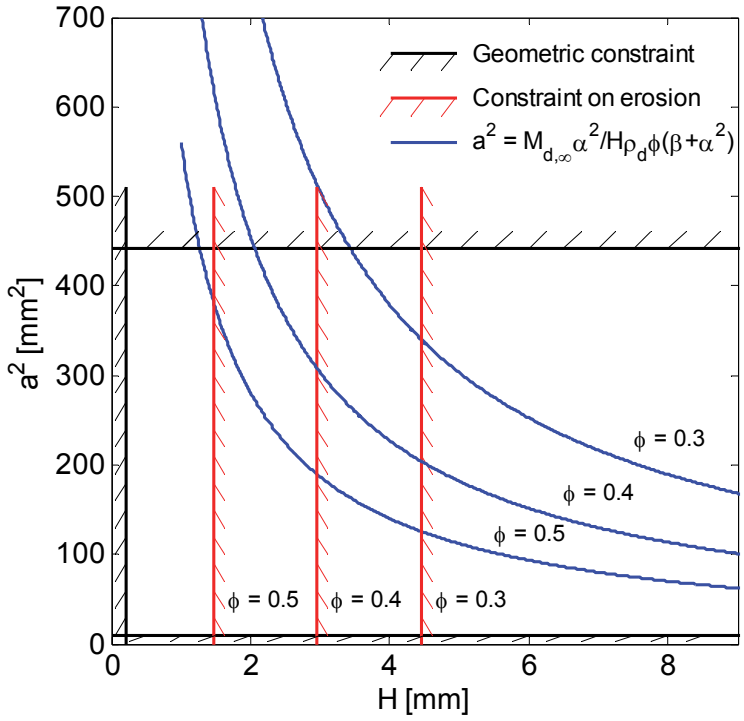

Figure 7.12: Design space for a dosage form design with thin posts or fins on a square plate with maximum edge length 19 mm according to the structure of case C shown in Fig. 7.13 with $\alpha = 1.3$ and $\beta = 1$.

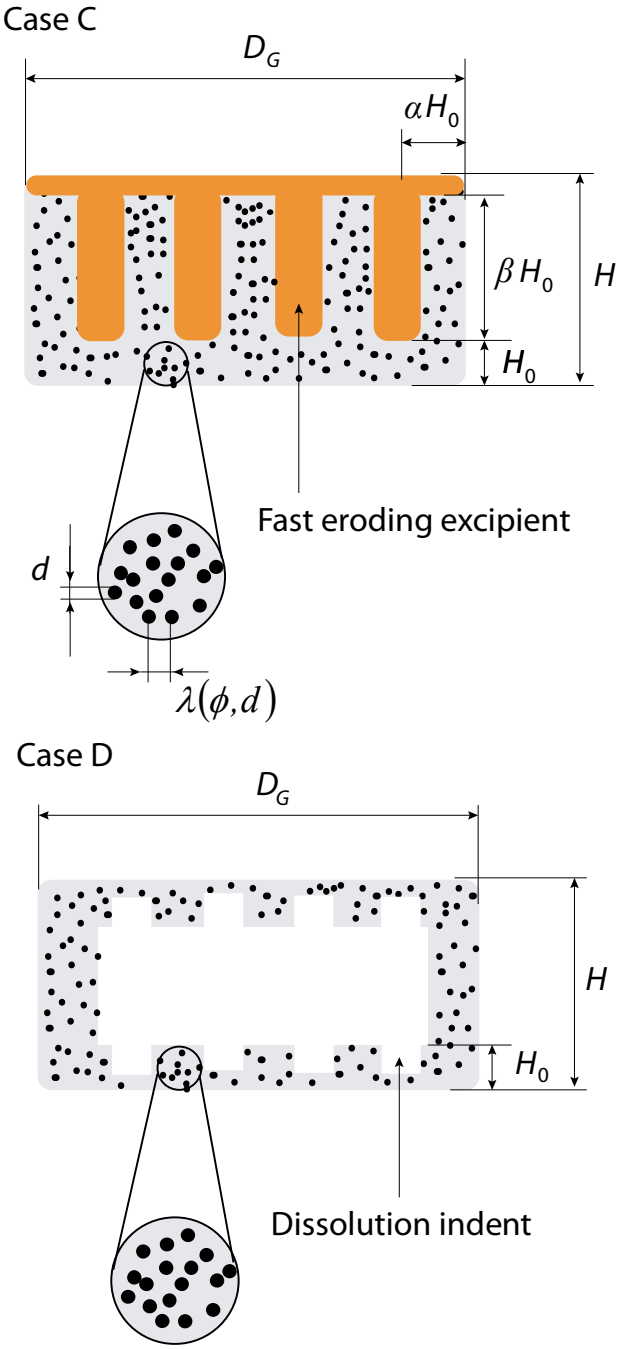

Figure 7.13: Design examples: case C and case D suitable for non-porous immediate-release dosage forms at various drug content.

7.5 Cellular Dosage Forms

It is evident that the general specifications of immediate-release solid dosage forms given by the regulator, to dissolve 80% of the drug content in 30 minutes, can be met with non-porous dosage forms. Still non-porous dosage forms lag behind their porous counterparts in drug release rate and dissolution time. This may be problematic in some specific cases. For example, even using the techniques presented in previous sections of adjusting drug volume fraction, excipient and geometry to achieve rapid drug release, it is difficult to produce non-porous dosage forms at conventional geometries that are dissolved very rapidly, in less than 2-3 minutes. A design concept is therefore desired that allows to increase drug release rate, and to decrease dissolution time for such specific cases.

Further, the above analysis shows that a considerable amount, typically at least about half of the volume of the non-porous dosage form, must consist of excipient for the non-porous dosage form just to meet the specifications of immediate-release given by the regulator (i.e., 80% drug content dissolved in 30 minutes). Excipient material costs, however, can make up a significant share of downstream manufacturing costs, even in the state-of-the-art powder-based designs where drug mass fractions up to 0.8 are achieved. Therefore, reduction of the amount of excipient material beyond the limitations of non-porous designs is desired.

A design concept that achieves both, faster drug release and reduced excipient requirements, is to introduce voids into the microstructure of the excipient material, which decreases the density of the excipient. In such a design, the drug mass fraction can be increased and the amount of excipient material can be decreased, without changing the overall drug volume fraction in the dosage form. This allows the excipient phase, consisting of excipient material and void, to be interconnected, even though the mass of excipient is reduced. Hence, dissolution properties of the composite pharmaceutical material are, even though the mass fraction of excipient is reduced, still to a large extent determined by the properties of the excipient.

It is evident that the properties of such materials comprising drug particles, excipient, and voids, depend on material microstructure, and very importantly, the structure of the voids. Three configurations of voids are differentiated: closed voids that are self-standing, partially open voids where part of the voids are connected with a neighboring void, and open voids where all the voids are connected with a neighboring void. It can be inferred from Fig. 7.14a, which shows a closed-cell excipient structure, that closed voids do not allow rapid passage of fluids into the core of the material. The dissolution mechanism of such materials is therefore similar to the non-porous case, with comparably slow penetration of fluids into the dosage form. If the excipient is surface-eroding, introduction of voids, even if un-connected, does, however, have an impact on the erosion rate of the excipient. The cell walls are eroded in series in direction of erosion, and as derived in chapter 4, the erosion rate of such pure excipient can be written as:

$$\frac{dH}{dt} = \frac{1}{\rho_s}\frac{dm}{dt} = \frac{M_n c_0 D^{\frac{2}{3}}}{\rho_s}\sqrt{\left(\left(\frac{\rho_f}{\mu_f}\right)^{\frac{1}{3}}\frac{v_\infty}{3L}\right)} \tag{7.26}$$

It may be noted that by incorporating voids in the material structure, the effective density of the excipient phase, ρ_s, is reduced. This reduces the amount of excipient material to be removed from the dosage form, and hence increases the average erosion rate of the excipient. For example, a two-fold increase in excipient erosion rate is expected due to a two-fold reduction in excipient density.

On the other hand, a 2-d excipient structure, where about 10%-20% of the hexagonal cell walls are removed such that every void is connected with at least another void, is presented in Fig. 7.14c. If, in 3 dimensions, the open voids form connected pores enabling passage of fluids, the dissolution medium penetrates rapidly into the core of the dosage form provided that the fluid exhibits the property of wetting the open voids. This causes the dissolution mechanism of such material structures to be substantially different from the non-porous case. If all the voids are fully filled with dissolution medium, the cell walls simultaneously erode into the fluid-filled voids. Therefore, the entire structure

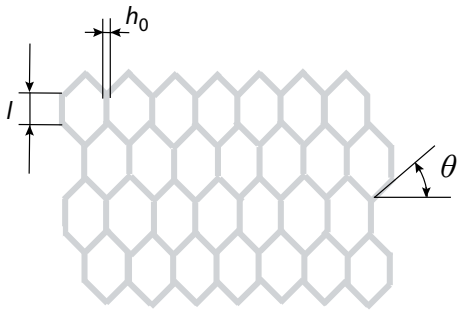

(a)

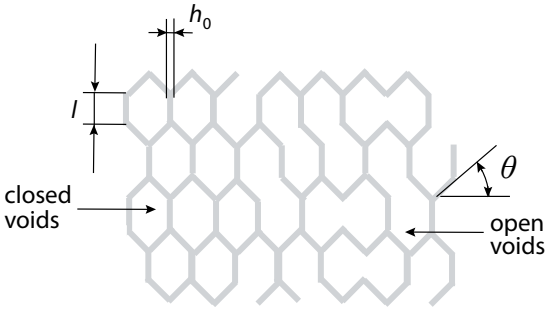

(b)

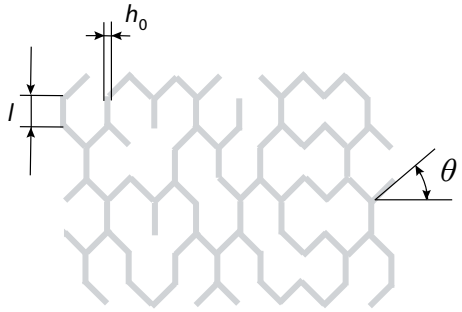

(c)

Figure 7.14: Schematic of structural configurations of cellular excipient in 2-D. The hexagonal shape of the cells is for illustrative purposes only. The configurations shown are: (a) closed-cell structure, (b) partially open cell structure, and (c) open cell structure.

can be eroded in the time of erosion of one single cell wall. Because one cell wall may be shared by multiple voids, as in the case of 2-d hexagons where one cell wall is shared by 2 voids, erosion may occur from both sides of the cell wall. Erosion of cell walls is assumed to happen into a standing fluid, with fluid velocity $v = 0$. This mass-transfer problem has, in reverse direction, extensively been studied in electrochemical systems with the Cottrell equation describing current of species in an infinitely large tank to an electrochemical electrode. Applied to the current problem, the mass flux can be described as:

$$\frac{dm}{dt} = \frac{M_n c_0 \sqrt{D}}{\sqrt{\pi t}} \tag{7.27}$$

Hence, for the erosion rate and the dissolution time of such a single wall it is written:

$$\frac{dh}{dt} = \frac{1}{\rho_s}\frac{dm}{dt} = \frac{1}{\rho_s}\frac{M_n c_0 \sqrt{D}}{\sqrt{\pi t}} \tag{7.28}$$

$$t_d = \frac{h_0}{2\dot{h}} \tag{7.29}$$

where h_0 is the initial thickness of the wall. Clearly, rapid dissolution of the structure is favored in such an open-cell structure. For example, the dissolution time of a wall with 10 μm half thickness is calculated to be about 25 seconds with mannitol as excipient (note: the dissolution time of PEG 8,000 is of the same order of magnitude). This gives a significantly faster dissolution time than with any other non-powder-based designs presented so far. It must be noted, however, that the model assumes that the concentration of the eroding excipient in the fluid-filled voids is well-below the solubility limit. This assumes that the total solid excipient mass is much smaller than the excipient mass that can be dissolved in the fluid-filled voids, i.e. $\rho_e V_e << c_{e,s} V_v$ where ρ_e is the density of the non-porous solid excipient, V_e is the volume occupied by excipient material, $c_{e,s}$ is the solubility of excipient in the dissolution fluid, and V_v is the total void volume.

Molded micro-cellular dosage forms with closed pores at drug mass fractions of 0.1-0.5 have been suggested previously as gastro-retentive dosage forms. Such micro-cellular material can be produced at a density lower than the one of gastric fluids, and because that fluid cannot rapidly penetrate inside the dosage form, the lower density of the dissolving dosage form may be maintained for a prolonged time in the gastric system [22].

The present goal, however, is not necessarily to produce gastro-retentive devices. Rather, it is aimed at providing a design that allows to achieve faster dissolution and to minimize the amount of excipient material required in immediate-release solid dosage forms. This implies that the excipient phase must be well-interconnected, and account for at least 20%-50% of the total volume of the dosage form such that properties of the dosage form can be controlled by the excipient. Also the voids, which are part of the excipient phase, are preferably interconnected, to allow penetration of fluid into the dosage form and provide faster drug release. Illustrations of such structures are given in Fig. 7.15

Fig. 7.15a shows a design with drug particles randomly dispersed in excipient, all integrated in the structure of the cell walls with the particle size being smaller than the thickness of the cell wall. At large drug loadings, as desired here, the cell walls consist to a large extent of the drug phase in this design. Therefore, the drug phase may form interconnected clusters and greatly affect the properties of the wall material. For example, most drugs are significantly less soluble than the rapidly eroding excipients considered here. Therefore, if a slowly eroding drug phase considerably determines the properties of the cell walls, dissolution of the structure is considerably delayed. Further, because void space between drug particles in the cell walls is to be filled with excipient in such a design, it may be difficult to achieve very high drug mass fractions if the drug and the excipient solid phase have about the same density. This is particularly the case if the drug particles are uniformly sized and spherical, having a maximum packing density of 0.74.

An alternative design is shown in Fig. 7.15b, where drug particles are placed into the voids of the excipient structure. In such a design, after complete disintegration of the cells consisting purely of excipient with controllable properties, the drug particles are released and subjected to a moving fluid where they can dissolve rapidly provided that they are small enough. Therefore, such a design allows not only rapid disintegration of the structure, but also rapid drug release. It must be noted, however, that since drug particles are

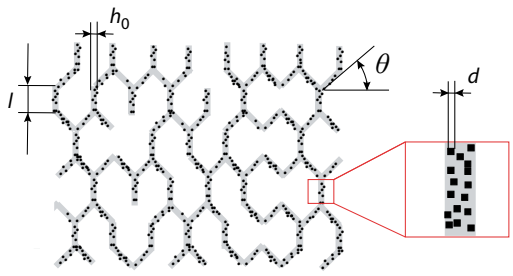

(a)

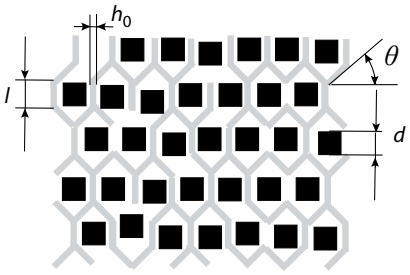

(b)

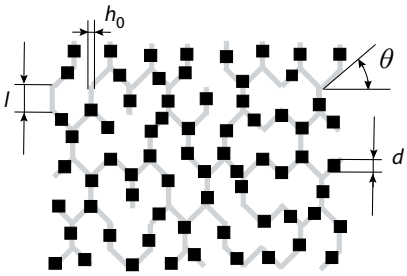

(c)

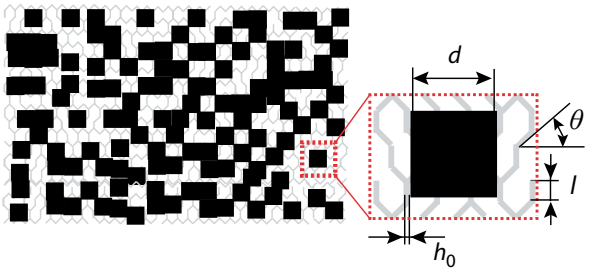

(d)

Figure 7.15: Schematic of arrangement of the drug particles in the dosage form: (a) particles inside the walls of the cellular structure with $d < h_0$, (b) particles inside the voids of the cellular structure, (c) particles inside the walls of the cellular structure with $d > h_0$, $l > d$, and (d) particles inside the walls of the cellular structure with $d > h_0$, $l < d$.

not fixed within the structure, they may move and agglomerate to form clusters that may cause an increased dissolution time. Further, such structures are difficult to produce using typical injection-molding equipment.

Designs that allow both -- disintegration of the structure to be determined by the properties of the excipient, and manufacturing using typical injection-molding equipment are illustrated in Fig. 7.15c and Fig. 7.15d. In Fig. 7.15c, the size of the voids is larger than the particle size, whereas in Fig. 7.15d the size of the voids is smaller than the particle size. In both designs, the drug particles are integrated in the excipient walls, but the wall thickness is of the order of, or smaller than the particle size. Therefore, if void and/or excipient phase are sufficiently well interconnected (i.e. the drug volume fraction is less than about 0.5-0.6) such a design allows disintegration of the cell walls to be controlled by the properties of the excipient. Once the excipient structure is eroded, the drug particles are subjected to rapid release into a moving fluid, allowing to achieve rapid drug dissolution. Further, such structures are advantageous, because they are relatively easy to manufacture using a typical injection molding process. This is therefore a preferred structure for the present purpose.

In consideration of the above arguments, schematics of dosage forms with cellular excipient structure are presented in Fig. 7.16. The dosage forms have a drug volume fraction of about 0.55, a void volume fraction of about 0.4, and an excipient volume fraction of about 0.05. Therefore, even though the drug volume fraction is just 0.55, the volume occupied by excipient accounts for less than 10% of the volume occupied by the drug due to the voids in the excipient structure in these embodiments. The ratio of the characteristic width of the voids to the width of the solid excipient, l/h_0, is about 10. If the size of the void is designed to be about 50 μm – 200 μm (of the order of the drug particle size), the width of the solid excipient is less than about 5 μm – 20 μm. Such a structure allows rapid disintegration and drug release if a fast eroding excipient is used (and the cells are at least partially open).

A high density skin as illustrated in Fig. 7.16a and Fig. 7.16b, consisting either of the same composition as the core or of a different composition, can be applied to all the dosage form designs presented for better mechanical stability and appearance of the dosage form.

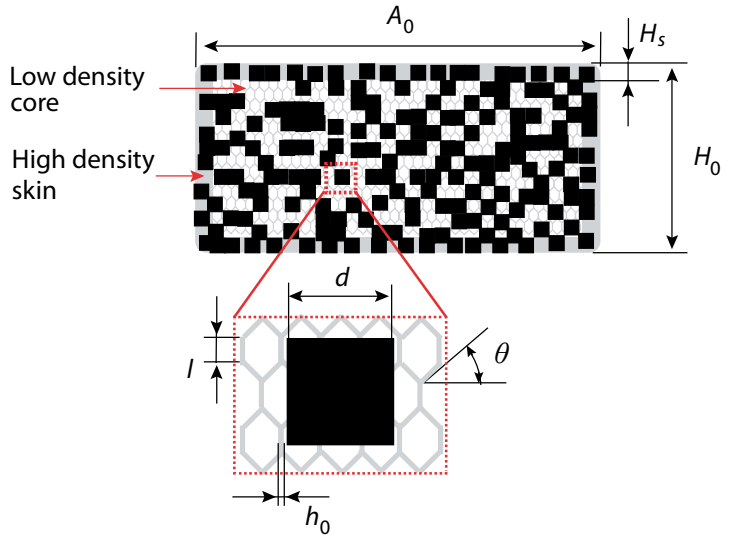

(a)

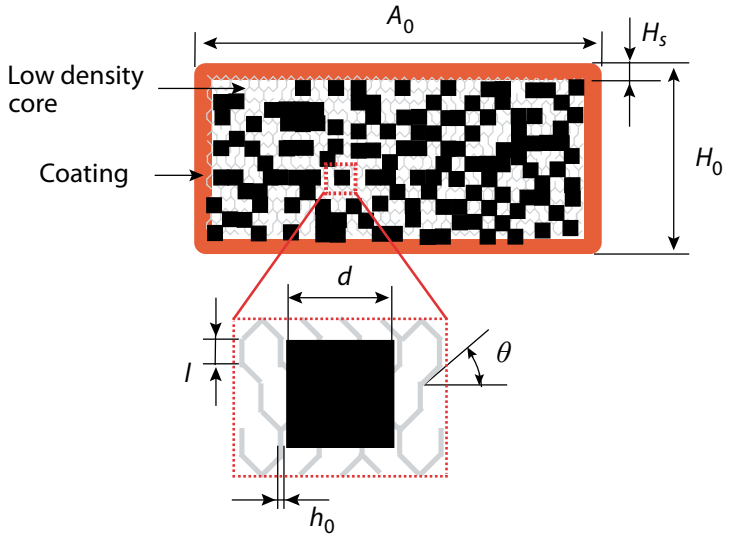

(b)

Figure 7.16: Schematics of melt-processed, optimal solid dosage forms with a drug volume fraction of about 0.55, a void volume fraction of about 0.4 and an excipient volume fraction of about 0.05: (a) a high density skin with thickness H_s comprises the dosage form surface with the same composition as the core material, and (b) a coating with different composition than the core at thickness H_s comprises the dosage form surface.

The excipient material of cellular dosage form designs can generally be chosen by applying similar principles to the ones for typical melt-processed dosage forms, particularly in terms of the excipient's melt processability and physical and chemical stability. For example, to avoid excessive degradation of the drug during the time-scale of melt-processing, an excipient is desired that plasticizes below this drug degradation temperature to enable melt-processing without excessive drug degradation. Further, if rapid drug release is the goal, it is still favorable to use a rapidly eroding excipient, even if the voids are open and interconnected. Cellular dosage forms with such low excipient content as presented above may, however, have slightly increased mechanical requirements on the excipient compared with non-porous designs. Because the elasticity of the cellular excipient is reduced significantly compared with the bulk material, as further discussed in Appendix A, it may be appropriate to use an excipient that shows some ductility. Higher molecular weight polyethylene glycols or low molecular weight polyethylene oxides are good such candidate excipients that further show rapid erosion. A non-inclusive list of candidate excipients that may serve as plasticizers for melt processing and provide rapid drug release includes polyethylene glycols, polyethylene oxides, polymethacrylates, polyols, polyvinylpyrrolidones, poloxamers, etc.

Finally, the designs presented, and in particular the design in Fig. 16b comprising a coated dosage form, can be well-used to produce controlled-release and sustained-release dosage forms by choosing the proper excipient and coating materials.

7.6 Manufacture of Optimal Solid Dosage Forms

7.6.1 Concepts for the Manufacture of Non-Porous Dosage Forms

Both mixing and injection-molding equipment have been developed for decades, and it is aimed here to use these highly optimized technologies for the current process. An overview of continuous mixers has been published by Pernenkil and Cooney [23], and insights into injection molding machines and technologies can be found in Refs. [24-26]. The molding concept, comprising the geometry of mold cavities, the sequence of injec-

tions, and the automation concept must, however, be customized to a specific product. Fig. 7.17 illustrates examples of how the injection sequence and mold cavity can be designed to produce the designs that have been introduced above. For the production of a design according to case A, only single injection into a mold cavity is required. The design cases B and D can be made by two injections, where either the drug containing material or the excipient material is injected first.

Core pull-back, rotary molding, or cube-stack molding technologies are examples of how such a process could be automated. Core pull-back technologies simply require movement of a particular geometric boundary of the mold cavity. The advantage of core pull-back is that it can be done rapidly, typically in less than 0.5 second, and it further does not consume any space by additional cavities on the mold surface. However, core pull back can usually only be applied if the shape of the initial surface and the shape of the overmolded surface do not have the same shape. Core pull-back is therefore well suited for manufacture of a dosage form according to the design case B. In case D, however, the initial surface and the overmolded surface are not identical. Two different mold geometries may be required for manufacturing the initial surface and the final surface. This may make it necessary to use either a mold rotation or a stack molding technology for this case. A summary of the molding steps together with estimated cycle times per cavity to produce the dosage forms is shown in Tables 7.5 and 7.6.

Since injection-molding process rate is the inverse of cycle time per cavity multiplied by the number of cavities, it is critical to design the mold in such a way that the number of cavities can be maximized for a given mold surface area and machine size. A concept to multiply the number of cavities without increasing the total mold surface area is to use a stack mold, which comprises multiple mold parting surfaces in series. Stack molds with 128 cavities per parting surface and 4 parting surfaces resulting in 512 cavities have so far been applied for the manufacture of high-volume products. However, it is difficult to integrate the concept of rotary molding into a stack mold. Therefore, multi-shot technologies using single-cavity or core-pull molds are favored for stack mold systems with increased number of cavities and fast process rates.

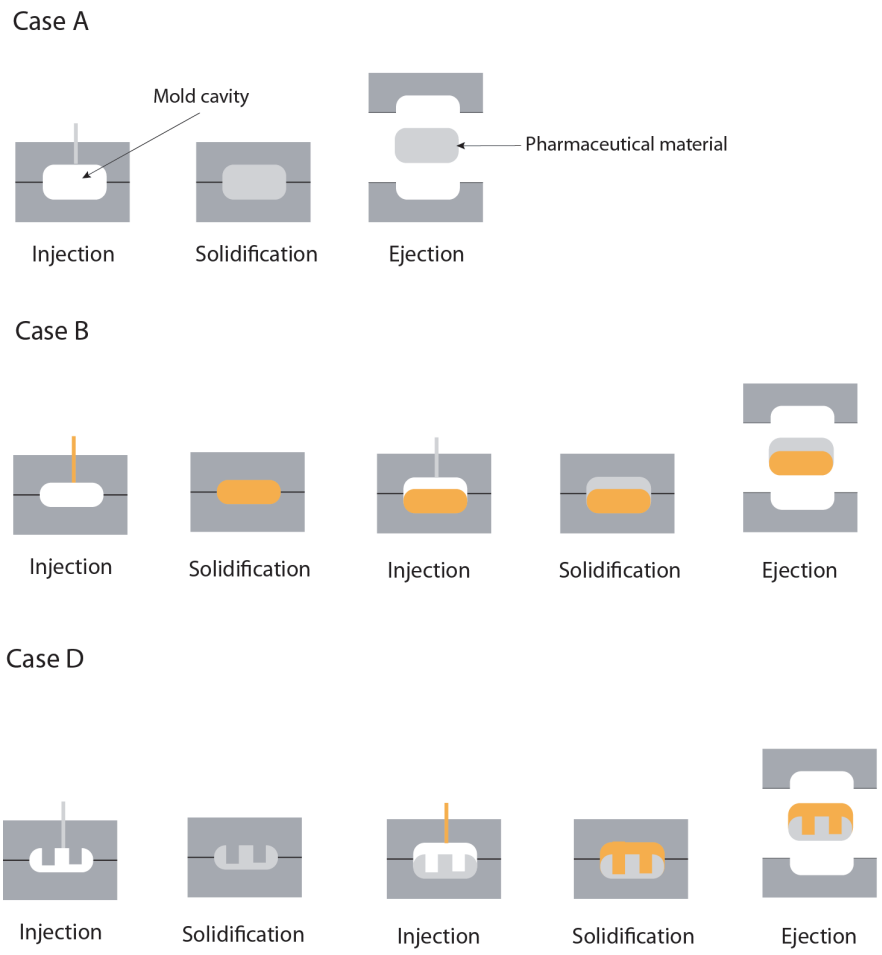

Figure 7.17: Illustration of manufacturing concepts to produce the design examples suitable for non-porous immediate-release dosage forms at various drug content.

7.6.2 Concepts for the Manufacture of Cellular Dosage Forms

Cellular dosage forms can also be manufactured by mixing and injection-molding. In contrast to conventional injection molding, a foaming agent, for example in the form of a gas or supercritical fluid, can be introduced into the melt to generate voids. The equipment to integrate such foaming technologies into an injection-molding machine has been widely used in industry, and a description of injection-molding machines used, for example, to produce micro-cellular foam structures is given in Ref. [27]. Microcellular foams are typically produced by dissolving a gas or supercritical fluid in the polymer melt under pressure to form a homogeneous solution. Upon release of pressure in the mold cavity, the gas nucleates and cells are formed. The cells grow either until the material is solidified, or until the supply of gas or supercritical fluid from the melt is exhausted.

The present process, however, differs from the conventional concept in that a mixture of molten excipient and solid drug at high drug volume fraction is to be processed. Rheology of such fluid-solid mixtures has been widely studied, and it is generally accepted that the liquid phase must have a volume fraction of at least the packing density of the solid phase for the system to be well fluid-processable. The packing density of the solid phase depends on shape and size distribution of the solid particles. For example, in case of regularly packed, hard spheres at uniform size, the packing density is about 0.74. Irregularly packed spheres have a packing density of about 0.64. Non-uniformly sized particles may exhibit a larger packing density than their uniform counterparts. Small particles may fill the empty space between large particles that touch each other. However, even though drug particles are typically non-uniform in size and shape, a system as desired here, with about 5%-10% molten excipient and 90%-95% solid drug by volume, may not be well fluid-processable.

By injecting gas into the two-phase molten excipient – solid drug system, however, a three-phase system may be formed consisting of molten excipient, pressurized gas, and solid drug. The pressurized gas can fill the space between the solid drug particles, and therefore contribute to the fluid phase volume fraction to improve fluid processability. As soon as the pressure is released in the mold cavity, the gas bubbles can nucleate and expand, and they together with the cells originating from nucleation in the excipient, form

the cellular structure. Injection temperature, mold temperature, and dosage form geometry must be adjusted, not only to maximize process rate, but also to obtain the desired microstructure, preferably a microstructure with at least partially open voids.

Finally, also the mold cycle time to produce cellular structures is to a large extent determined by the cooling time. Cellular structures produced by using a gas or supercritical fluid as foaming agent do typically allow to reduce the cycle time compared with the non-porous material if the part thickness is less than about 4 mm. If the part thickness is larger than this thickness, the cycle time of the cellular material may be larger than the one of the non-porous material.

7.6.3 Integration of the Coating Step into Molding

The ease to implement production of multi-component products by injection-molding further allows integration of both non-porous and cellular dosage form coating into the molding process. An example of a sequence of how coated dosage forms according to the concept of overmolding could be produced is given in Fig. 7.18. Also such tablet molding with integrated coating process by overmolding could be done by core pull-back, rotary molding, or cube-stack molding technologies. A schematic of an example of a stack-molding and core pull-back based multi-component injection-molding machine to produce coated dosage forms is illustrated in Fig. 7.19. Tables 7.5 and 7.6 summarize the molding steps and cycle times to produce such coated dosage forms. The first coating half is produced using the first top mold geometry on the side with a single injection unit. The mold is then rotated to the side where the API-containing material as well as the second coating layer can be produced. API-containing material is injected and solidified, and subsequently, by core pull-back, the second coating layer is produced.

The advantage of coating by overmolding is that the flexibility to produce even complex material structures and part geometries is large using that process. However, it may be difficult to use mold stacks and multiply the number of cavities to achieve high process rates. An alternative process that allows the manufacture of a coated dosage form in

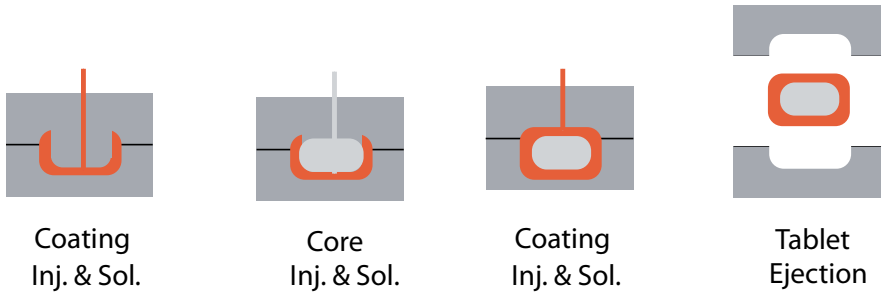

Figure 7.18: Illustration of an injection-molding sequence to produce a coated solid dosage form by the concept of overmolding.

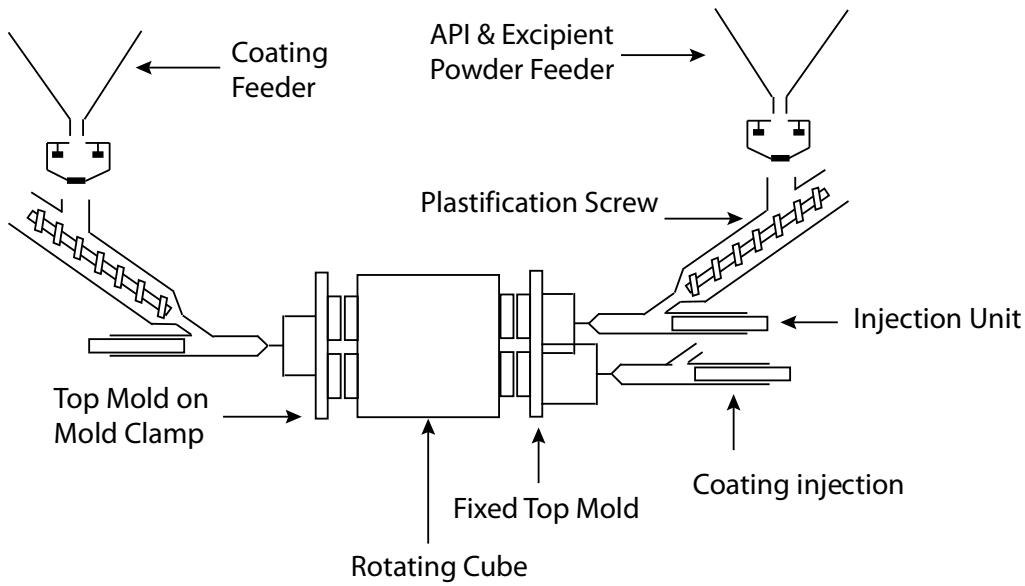

Figure 7.19: Schematic of a multi-component injection-molding machine to produce coated dosage forms by overmolding. Coating injection on the left is considered side 2, whereas API and coating injection on the right is considered side 1 of the machine.

Table 7.5: Molding steps to produce uncoated (uc) and coated dosage forms according to the various design concepts co-injection molding (co-im) and overmolding (om).

Design case	Molding steps
Case A/Cellular (uc)	API & excipient injection -> Solidification -> Mold opening -> Part ejection -> Mold closing
Case B (uc)	Excipient injection -> Solidification -> Mold pull back -> API & excipient injection -> solidification -> Mold opening -> Part ejection -> Mold closing
Case D (uc)	API & excipient injection -> Solidification -> Mold opening -> Mold rotation -> Mold closing -> Excipient injection -> solidification -> Mold opening -> Part ejection -> Mold rotation -> Mold closing
Case A/Cellular (co-im)	API & excipient injection -> Coating injection -> Solidification -> Mold opening -> Part ejection -> Mold closing
Case A & B (om)	Coating injection -> Solidification -> Mold opening -> Mold rotation -> Mold closing -> API & excipient injection -> solidification -> Mold pull back -> Coating injection -> solidification -> Mold opening -> Part ejection -> Mold rotation -> Mold closing
Case D (om)	API & excipient injection -> Solidification -> Mold opening -> Mold rotation -> Mold closing -> Coating injection -> solidification -> Mold pull back -> Coating injection -> solidification -> Mold opening -> Part ejection -> Mold rotation -> Mold closing

Table 7.6: Estimated mold cycle times to produce uncoated (uc) and coated dosage forms by to the concepts of co-injection molding (co-im) and overmolding (om). Estimates are based on the molding steps and the respective times shown in Table 7.5 and Table 7.2.

Design case	Mold Cycle Times
Case A (uc)	$\left(3.5\ s + \sum t_{cool}\right)$
Case B (uc)	$\left(4.5\ s + \sum t_{cool}\right)_{side\,1}$
Case D (uc)	$\max\left(\left(3.5\ s + \sum t_{cool}\right)_{side\,1}, \left(4.5\ s + \sum t_{cool}\right)_{side\,2}\right)$
Case A/Cellular (co-im)	$\left(4\ s + \sum t_{cool}\right)$
Case A & B (om)	$\max\left(\left(5.5\ s + \sum t_{cool}\right)_{side\,1}, \left(3.5\ s + \sum t_{cool}\right)_{side\,2}\right)$
Case D (om)	$\max\left(\left(3.5\ s + \sum t_{cool}\right)_{side\,1}, \left(5.5\ s + \sum t_{cool}\right)_{side\,2}\right)$

one single step is co-injection molding. In co-injection molding, the coating and core material are injected into the same mold cavity in such a way that the coating material forms a skin over the core. Stack molding technologies can be applied using that process; however, the flexibility in the design of the material structure is reduced compared with the overmolding process.

7.6.4 Comparison of Manufacturing Performance of Specific Design Examples

The manufacturing performance of the individual designs is compared for selected cases in terms of the unit operations, mixing time, cycle time per cavity, excipient mass fraction, and solvent mass fraction, and results are summarized in Table 7.7, Table 7.8, and Fig. 7.20. The cooling times for calculation of the mold cycle times are calculated based on Eq. (7.9) with $\alpha = 0.1$ mm^2/s, $T_0 = 75$°C, $T_{max} = 45$°C, and $T_w = 5$°C. This gives cooling times equal to 0.03 seconds, 0.66 seconds, and 1.8 seconds for dosage form thicknesses of 0.2 mm, 0.9 mm, and 1.5 mm, respectively. A maximum ejection temperature, $T_{max} = 65$°C, is assumed for a part of 3 mm thickness giving a cooling time of 3.6 seconds. Further, the coating, largely sugars or polyols, is assumed to dissolve rapidly and not affect dissolution time of the API. Finally, a value of 512 is assumed for the number of mold cavities for calculation of the cycle time per cavity.

Clearly, the cellular design outperforms both the current powder-based, porous design and the non-porous design in most performance measures. Compared with the current continuous downstream processes to produce standard solid dosage forms, the process to manufacture cellular designs allows to reduce the number of unit operations from 6 to 2, reduce process time from 20 minutes to 5 minutes, reduce the amount of excipient material required by more than 50%, and eliminate solvent requirements. With 512 cavities per mold, about 250,000 – 400,000 tablets can be produced per hour with the new process. This is about three times larger than the process rates achieved by injection molding conventional uncoated dosage forms with thicknesses above 5 mm. Finally, the new process can be further optimized. For example, due to the high drug volume fractions, it may be possible to integrate the mixing process into the injection-molding unit to eliminate another unit operation.

Table 7.7: Comparison of process performance for the manufacture of potent and highly potent drugs.

Parameter	Current standard	Case A (non-porous)	Case B (non-porous)	Cellular Design
0.5 mg				
Excipient	-	PEG 8k	PEG 8k	PEG 20k
API volume fraction	0.03	0.03	0.03 (0.6)[b]	0.03
Void volume fraction	0.05	0	0	0.8
Excipient volume fraction	0.92	0.97	0.97	0.17
Diameter (mm)	3	3	3 (1.95)[b]	3
Thickness (mm)	1.5	1.5	1.5 (0.2)[b]	1.5
# Unit operations	5-6	2	2	2
Mixing time (t_m/τ_m)	2.96	2.97	2.08	2.83
Mold cycle time (s)	-	5.3 (5.8)[a]	6.3	5.3 (5.8)[a]
Cycle time/ # cavities (ms)	2-20	10 (11)[a]	12.3	10 (11)[a]
Solvent mass fraction	0.2-1.2	0	0	0
5 mg				
Excipient	-	PEG 8k	PEG 4k	PEG 20k
API volume fraction	0.34	0.34	0.36 (0.6)[b]	0.34
Void volume fraction	0.05	0	0	0.56
Excipient volume fraction	0.61	0.66	0.66	0.1
Diameter (mm)	3	3	3	3
Thickness (mm)	1.5	1.5	1.5 (0.92)[b]	1.5
# Unit operations	5-6	2	2	2
Mixing time (t_m/τ_m)	2.55	2.58	2.2	1.51
Mold cycle time (s)	-	5.3 (5.8)[a]	6.3	5.3 (5.8)[a]
Cycle time/ # cavities (ms)	2-20	10 (11)[a]	12.3	10 (11)[a]
Solvent mass fraction	0.2-1.2	0	0	0

[a] Value in parentheses refers to a coated product manufactured by the co-injection molding process.

[b] Value in parentheses refers to the characteristics of the drug containing layer.

Table 7.8: Comparison of process performance for the manufacture of low potency drugs.

Parameter	Current standard	Case A (non-porous)	Cellular Design
50 mg			
Excipient	-	PEG 4k	PEG 20k
API volume fraction	0.8	0.5	0.55
Void volume fraction	0.05	0	0.4
Excipient volume fraction	0.15	0.5	0.05
Diameter (mm)	-	7.4	7.06
Thickness (mm)	-	1.5	1.5
# Unit operations	5-6	2	2
Mixing time (t_m/τ_m)	1.15	2.3	0.51
Mold cycle time (s)	-	5.3 (5.8)[a]	5.3 (5.8)[a]
Cycle time/ # cavities (ms)	2-20	10 (11)[a]	10 (11)[a]
Solvent mass fraction	0.2-1.2	0	0
500 mg			
Excipient	-	PEG 4k	PEG 20k
API volume fraction	0.8	0.35	0.6
Void volume fraction	0.05	0	0.35
Excipient volume fraction	0.15	0.65	0.05
Diameter (mm)	-	21	16
Thickness (mm)	-	3	3
# Unit operations	5-6	2	2
Mixing time (t_m/τ_m)	1.15	2.56	0.43
Mold cycle time (s)	-	7.1 (7.6)[a]	7.1 (7.6)[a]
Cycle time/ # cavities (ms)	2-20	13.9 (14.8)[a]	13.9 (14.8)[a]
Solvent mass fraction	0.2-1.2	0	0

[a] Value in parentheses refers to a coated product manufactured by the co-injection molding process.

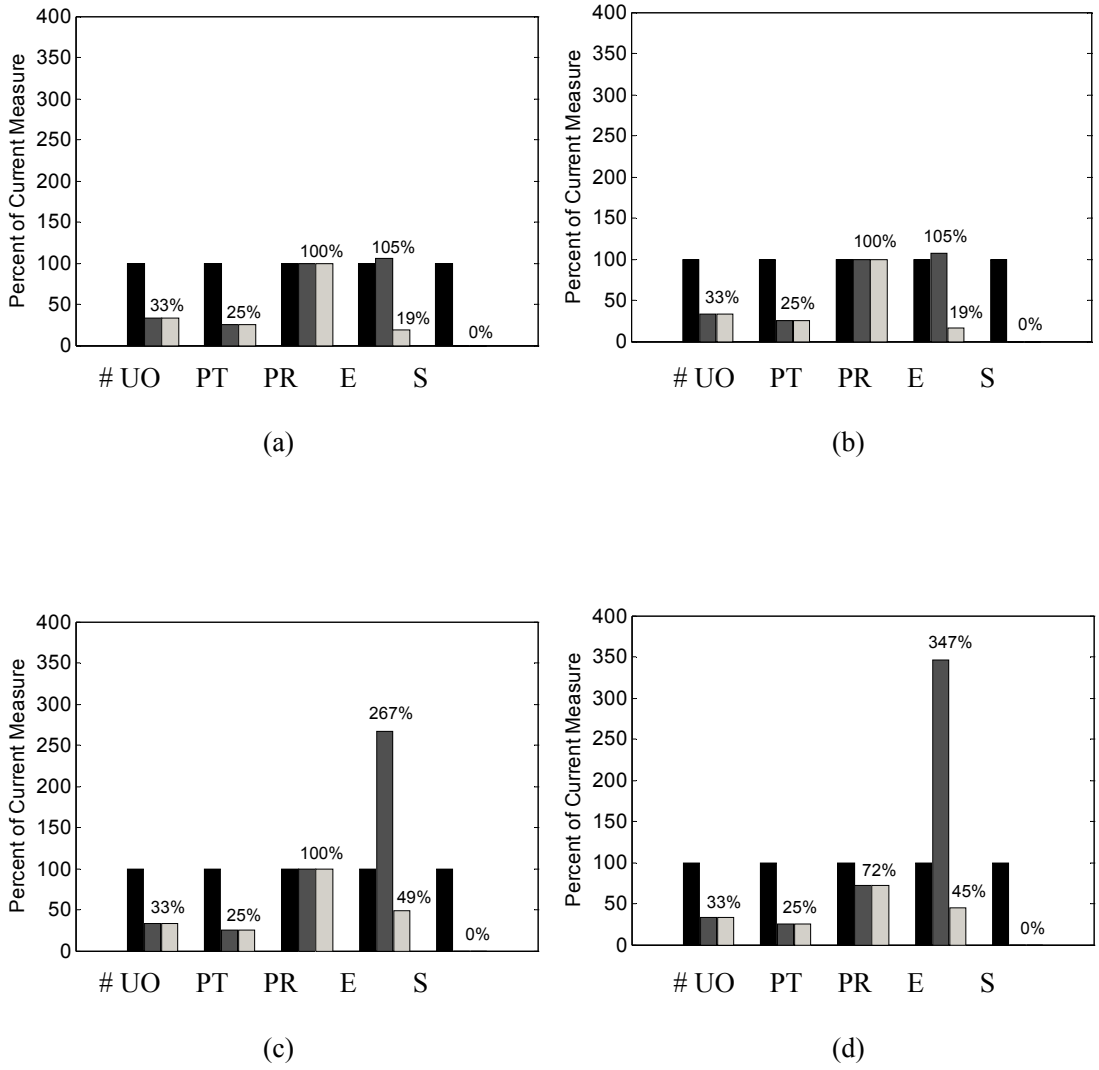

Figure 7.20: Comparison of manufacturing performance measures of the state-of-the-art continuous downstream processes (black) with the injection-molding process to manufacture non-porous dosage forms (dark gray) and the cellular molding process to produce cellular dosage forms (light gray). (UO) number of unit operations, (PT) process time, (PR) process rate, (E) amount of excipient required and (S) amount of solvent required.

7.7 Summary

The present design guidelines for the manufacture of non-porous immediate-release dosage forms by a hot-melt process are expanded in this work. It is shown, based on the dissolution model developed in previous chapters, that the drug volume fraction as well as the product geometry in the form of the eroding surface area and the dosage form thickness further play important roles.

Because multiple solutions exist that potentially satisfy the requirements of immediate-release dosage forms, a design that allows manufacturing optimization as minimization of material cost, mixing time, and mold cycle time is proposed. Material cost and mixing time can be minimized if the drug volume fraction is maximized, whereas the mold cycle time can be minimized if the thickness of the dosage form is minimized. Further, if the dosage form is a disk with diameter D_G and thickness H_0, the design with maximum drug volume fraction is the same as that with minimum dosage form thickness, as erosion rate and dosage form volume decrease with increasing drug volume fraction.

Because the dosage form must be of a certain size to be patient compliant, the minimum thickness characteristic to the manufacturing performance can be circumvented if the material structure is changed. For example, the dosage form can comprise a thin layer of API-containing material attached to a disk of bulk excipient. Or, if the dosage form must satisfy certain requirements on diameter and thickness/diameter ratio, thin sheets or posts of API containing material surrounded by a fast eroding pure excipient can form the material structure of the dosage form. But even though such designs may improve performance slightly, the maximum drug volume fraction in non-porous designs is limited to a value of about 0.5-0.6. This means that excessive amounts of excipient are required to produce such dosage forms.

A cellular design is therefore proposed, which allows fast dissolution at up to 10-fold reduced excipient mass. The cellular forms can be manufactured by an injection molding process that only slightly differs from the conventional process. Due to the large drug mass fraction that is achieved, it may even be possible to integrate the mixing unit into the injection-molding machine to save another unit operation. The molding process to

manufacture the proposed dosage forms further allows the coating step to be integrated in it. It is shown that, for a mold with 512 cavities, a cycle time per mold cavity of 10 ms-14 ms can be achieved to produce such a coated product. This cycle time per cavity is a factor of 3 lower than the cycle time that can be achieved to injection mold conventional dosage form geometries with thicknesses above 5 mm. Consequently, the dosage form designs proposed here that can be manufactured by the 1-2 step, solventless, continuous injection-molding process at short mold cycle times with reduced amounts of excipient required, offer great opportunities for improvement of the manufacture of solid dosage forms.

Nomenclature

A_0	initial projected surface area of the disk-shaped dosage form [m^2]
c	constant determining the effect of surface roughness on excipient erosion rate
c	concentration of a particular species in dissolution medium [mol/m^3]
c_0	concentration of a particular species at solid-medium interface [mol/m^3]
c_{deg}	concentration of degradation products in the dosage form [mol/m^3]
c_e	excipient cost per unit [USD/kg]
c_s	solubility of a particular species in dissolution medium [mol/m^3]
CV	coefficient of variation
D	diffusion coefficient [m^2/s]
D_G or D	diameter of the dosage form [m]
d	drug particle size [m]
E	Young's modulus [GPa]
H	thickness of the dosage form [m]
H_0 or H	initial characteristic thickness of the dosage form [m]
H_s	initial thickness of the surface skin of a cellular dosage form [m]

dH/dt	erosion rate of the sample [m/s]
$dH_{d,0}/dt$	erosion rate of pure drug phase [m/s]
$dH_{e,0}/dt$	erosion rate of pure excipient phase [m/s]
h_0	initial thickness of a single wall in the cellular structure [m]
dh/dt	erosion rate of a single wall in the cellular structure [m/s]
L or L_0	characteristic length of eroding surface [m]
l	length of a single wall in the cellular structure [m]
M_n	number averaged molecular weight [kg/mol]
M_e	excipient content in the dosage form [kg]
$M_{d,\infty}$	drug content in the dosage form [kg]
dM_d/dt	drug release rate [kg/s]
dm/dt	mass flux [mg/m^{2}s
dm_d/dt	drug release flux [kg/m^{2}s]
P	fluid pressure [Pa]
RH_{crit}	critical relative humidity for water sorption
Re	Reynolds number
s	standard deviation in drug content
s_0	initial standard deviation in drug content
t	time [s]
t_{cool}	cooling time
t_{cycle}	mold cycle time [s]
t_d	dissolution time of the dosage form [s]
t_{inj}	injection time [s]
t_m	mixing time to achieve the desired coefficient of variation [s]
t_r	mold resetting time [s]

T	temperature
T_0	injection temperature [°C]
T_m	melting temperature of the underlying material [°C]
T_{max}	maximum ejection temperature [°C]
T_p	injection-molding process temperature [°C]
T_w	mold wall temperature
v	fluid velocity [m/s]
v_∞	maximum fluid velocity [m/s]
α	constant to characterize the geometry of the posts/rips in design case C
α	thermal diffusivity [m^2/s]
β	constant to characterize the geometry of the posts/rips in design case C
δ_c	concentration boundary layer thickness [m]
δ_e	concentration boundary layer thickness of excipient component [m]
ε	strain at fracture
ρ_d	solid densidy of drug [kg/m^3]
ρ_e	solid density of excipient [kg/m^3]
ρ_f	fluid density [kg/m^3]
ρ_s	density of the solid phase [kg/m^3]
σ_y	yield strength [MPa]
σ_c	compressive strength [MPa]
τ_m	mixing time constant [s]
μ	viscosity [Pa·s]
μ_f	viscosity of dissolution medium [Pa·s]
v	Flory exponent
φ	drug volume fraction

φ^* drug volume fraction below which there is no interconnected drug cluster

φ^{**} drug volume fraction above which there is no interconnected excipient cluster

References

[1] ICH Working Group, Specifications: Test Procedures and Acceptance Criteria for New Drug Substances and New Drug Products: Chemical Substances Q6A, 1999, International Conference on Harmonisation of Technical Requirements of Pharmaceuticals for Human Use.

[2] The U.S. Pharmacopeial Convention, US Pharmacopeia, USP 35-NF 30.

[3] Y. Sugimori, K. Kusunoki, F. Cho, S. Uchikawa, 1997, Toyota production system and Kanban system Materialization of just-in-time and respect–for-human system, Int. J. Prod. Res., 15, 553-564.

[4] J.P Womack, D.T. Jones, 1996, Lean Thinking Banish Waste and Create Wealth in your Corporation, Free Press, New York, NY.

[5] J. R. Couper, D.W. Hertz, F.L. Smith, Process Economics, in D.W. Green, R.H. Perry, 2006, Perry's Chemical Engineers' Handbook, 8th Edition, McGraw-Hill, New York, NY.

[6] G. Cuff, F. Raouf, 1998,A preliminary evaluation of injection molding as a technology to produce tablets, Pharmaceut. Tech., 22, 96-106.

[7] R.C. Rowe, P.J. Sheskey, S.C. Owen, 2006, Handbook of Pharmaceutical Excipients, Fifth Edition, Pharmaceutical Press, London, UK.

[8] K. Kolter, M. Karl, A. Gryczke, 2012, Hot-Melt Extrusion with BASF Pharma Polymers, BASF extrusion compendium, second edition.

[9] The Dow Chemical Company, Carbowax Polyethylene Glycol, Technical Data Sheets, as of February 4, 2014.

[10] J.A. Baird, R. Olayo-Valles, C. Rinaldi, L.S. Taylor, Effect of molecular weight, temperature, and additives on the moisture sorption properties of polyethylene glycol, J. Pharm. Sci., 2010, 99, pp. 154-168.

[11] C. Zhang, I.D. Moore, 1997, Nonlinear Mechanical Response of High Density Polyethylene. Part I: Experimental Investigation and Model Evaluation, Polymer Engineering and Science, 37, 404-413.

[12] J.T. Carstensen, 2001, Advanced Pharmaceutical Solids, Marcel Dekker, New York, NY.

[13] H.A. Lieberman, L. Lachman, 1981, Pharmaceutical Dosage Forms: Tablets, Volume 2, Marcel Dekker, New York, NY.

[14] G. Boothroyd, P. Dewhurst, W.A. Knight, Design for Injection Molding, in G. Boothroyd, P. Dewhurst, W.A. Knight , 2011, Product Design for Manufacture and Assembly, Third Edition, CRC Press, Boca Raton, FL.

[15] H.S. Carslaw and J.C. Jaeger, 1959, Conduction of Heat in Solids, Oxford University Press, Oxford, UK.

[16] L.L. Augsburger, S.W. Hoag, 2008, Pharmaceutical Dosage Forms: Tablets, Volume 1: Unit Operations and Mechanical Properties, Third Edition, Informa Healthcare, New York, NY.

[17] L.L. Augsburger, S.W. Hoag, 2008, Pharmaceutical Dosage Forms: Tablets, Volume 2: Unit Operations and Mechanical Properties, Third Edition, Informa Healthcare, New York, NY.

[18] L.L. Augsburger, S.W. Hoag, 2008, Pharmaceutical Dosage Forms: Tablets, Volume 3: Unit Operations and Mechanical Properties, Third Edition, Informa Healthcare, New York, NY.

[19] H.A. Lieberman, L. Lachman, 1981, Pharmaceutical Dosage Forms: Tablets, Volume 1, Marcel Dekker, New York, NY.

[20] H.A. Lieberman, L. Lachman, 1981, Pharmaceutical Dosage Forms: Tablets, Volume 3, Marcel Dekker, New York, NY.

[21] S.S. Rao, 2009, Engineering Optimization: Theory and Practice, fourth edition, John Wiley & Sons, New York, NY.

[22] A.J. Clarke, Novel Pharmaceutical Dosage Forms and Method for Producing Same, U.S. Pat. Pub. No. 20050202090A1, September 15, 2005.

[23] L. Pernenkil, C.L. Cooney, A review on the continuous blending of powders, Chem. Eng. Sci., 2006, 61, 720-742.

[24] I.I. Rubin, 1972, Injection Molding Theory and Practice, John Wiley & Sons, Hoboken, NJ.

[25] T. Osswald, L.S. Turng, P. Gramann, 2008, Injection Molding Handbook, Second Edition, Carl Hanser Verlag, Munich, Germany.

[26] Z. Tadmor, C.G. Gogos, 2006, Principles of polymer processing, John Wiley & Sons, Hoboken, NJ.

[27] K. Okamoto, 2003, Microcellular Processing, Carl Hanser Verlag, Munich, DE.

This page is intentionally left blank.

CHAPTER VIII

CONCLUSIONS

The manufacture of current powder-based, porous immediate-release solid dosage forms is inefficient, because a large number of unit operations and long process times are required to produce such products. Changing the design from the current porous structure to a non-porous one allows integration of the entire downstream manufacturing into just two operations: blending and solvent-less injection-molding. Such an integration enhances manufacturing efficiency by reducing the number of process steps, solvent requirements, and process time. Non-porous dosage forms, however, do not allow rapid penetration of the dissolution medium. Because drug release is a mass transfer problem, this appears problematic as non-porous dosage forms cannot rely on a large surface area-to-volume ratio for immediate drug release.

A major contribution of the present work is a new analytical model describing drug release by surface erosion from a two-phase system, comprising randomly distributed drug particles in an excipient matrix. Because a rapidly-eroding excipient is used in the present case to give fast drug release, the erosion rate of drug particles is comparatively slow. Two microstructural effects that depend on drug volume fraction can be distinguished: blockage of excipient erosion by isolated, slowly eroding drug particles, and by interconnected particle clusters. If the drug volume fraction is below the first percolation threshold, φ^*, the drug particles are isolated in the excipient matrix. the excipient erodes around the particles and releases them. The erosion rate of the dosage form is modeled to follow the erosion rate of the excipient phase, but taking into account that excipient surface area is blocked by the isolated particles. On the other hand, if the drug volume fraction is so large that the drug phase forms an interconnected cluster (i.e., the drug volume fraction is above the second percolation threshold, φ^{**}), the erosion rate of the dosage form is modeled to follow the harmonic mean of the individual phase's erosion rates. If the drug volume fraction is between the first and the second percolation threshold, the erosion rate is linearly interpolated between the values at φ^* and φ^{**}.

Model validation by dissolution tests on the PEG-aspirin system shows reasonably good agreement between the calculated and measured values. An average error of 3% is obtained at a standard deviation of 21.9% and linear regression yielded an R^2-value of 0.9. Further, an average error of measured versus calculated drug release flux of 3.1% was obtained at a standard deviation of 22%. Differences in calculated versus measured values are attributed to such effects as: (a) protrusion of slowly eroding drug particles affecting fluid flow conditions in the vicinity of the eroding excipient surface, increasing the excipient concentration boundary layer thickness, and hence decreasing the erosion rate of the excipient phase, (b) differences in the time assumed to wash off slowly eroding drug particles and (c) differences in the percolation thresholds of the real system compared with the idealized, infinite system used for the model.

Furthermore, dissolution kinetics and mechanical properties of PEGs are studied. PEGs are rapidly eroding polymers with a melting temperature below 70°C. They are well suited to serve as excipients of melt-processed immediate-release dosage forms. Tests show that the erosion rate of pure PEG follows $dH_{e,0}/dt \sim M_n^{-0.8}$. A Flory exponent of 0.492 is obtained if Zimm's model for the polymer diffusion coefficient in dilute solution is applied. This confirms that erosion of PEG can be well estimated by such a model, as the predicted Flory exponent is about 0.5.

Compression tests on PEGs and PEO at various molecular weights show that the mechanical properties of PEGs, with the exception of elastic modulus, highly depend on molecular weight. PEG at low molecular weight is a brittle material with comparatively low strength, whereas PEG at high molecular weight is ductile with high mechanical strength. Additionally, nanoindentation tests were conducted on the Kollicoat IR-mannitol composite system. It is also shown that the mechanical properties highly depend on the volume fraction of the individual components. If the volume fraction of mannitol, which is the stiffer and harder material, is kept below 0.3, the elastic modulus and hardness values of the composite material follow the lower-bound. On the other hand, if the volume fraction of mannitol is above 0.7 the elastic modulus and hardness of the composite follow the upper-bound.

Based on the dissolution model developed, it is shown that, in addition to the microstructural effects, the surface area and the thickness of the dosage form play significant

roles in releasing the desired drug mass within the dissolution time A design point that allows manufacturing optimization by minimizing material cost, mixing time, and mold cycle time is identified. Material cost and mixing time are minimized if the drug volume fraction is maximized, whereas the mold cycle time is minimized if the thickness of the dosage form is minimized. For a disk-like dosage form, the design point with maximum drug volume fraction is the same as that with minimum dosage form thickness, for erosion rate and dosage form volume decrease with increasing drug volume fraction. However, the maximum drug volume fraction in non-porous designs is limited to a value of about 0.5-0.6 for fast drug release. This means that excessive amounts of excipient are unavoidable.

Finally, a cellular design that overcomes the limitations of non-porous dosage forms by providing fast dissolution rates and up to 10-fold reduction in excipient mass, is proposed. Cellular dosage forms can be manufactured by the standard injection-molding equipment. Due to the large drug volume fraction, it may even be possible to integrate the mixing unit into the injection-molding machine to save another unit operation. The molding process to manufacture the proposed dosage forms further allows the coating step to be integrated with it. It is shown that, for a mold with 512 cavities, a cycle time per mold cavity of 10 -14 ms can be achieved to produce such a coated dosage form. This cycle time per cavity is a factor of 3 lower than the cycle time that can be achieved to injection mold conventional dosage form geometries with thicknesses above 5 mm. Consequently, the dosage form designs proposed here that can be manufactured by the 1-2 step, solventless, continuous injection molding at short mold cycle times with reduced amounts of excipient required, offer great opportunities for improvement of the manufacture of solid dosage forms.

This page is intentionally left blank.

APPENDIX A

MECHANICAL PROPERTIES OF CELLULAR DOSAGE FORMS

The introduction of voids into the excipient structure together with the configuration of the voids do, noticeably, also affect mechanical properties of the material. For example, the density as well as the in-plane and out-of-plane elastic moduli in a hexagonal structure, as shown in the book of Gibson et. al [1], for example, are:

$$\frac{\rho^*}{\rho_s} = 1.15\frac{h_0}{l} \tag{A.1}$$

$$\frac{E^*}{E_s} = 2.31\left(\frac{h_0}{l}\right)^3 \tag{A.2}$$

$$\frac{E^*}{E_s} = 1.15\frac{h_0}{l} \tag{A.3}$$

Also, the elastic modulus of a cellular material with open cells can be described as:

$$\frac{E^*}{E_s} = C_1\left(\frac{\rho^*}{\rho_s}\right)^2 \tag{A.4}$$

where ρ^* and ρ are the densities of cellular and non-porous material, E^* and E are the elastic moduli of cellular and non-porous material, h_0 is the wall thickness of a hexagon, and l is the length of an edge in the hexagonal structure. C_1 is a constant which has, by experiment, been determined to be $C_1 = 0.3$. Therefore, if the void fraction in the excipient material reaches 80%-90%, the elastic modulus of the cellular excipient may be reduced by two to three orders of magnitude compared with the non-porous, bulk material. For example, if higher molecular weight PEG with a bulk elastic modulus of about 0.25 GPa is transformed into a cellular structure with open voids at 90% void volume

fraction, the elastic modulus becomes about 0.75 MPa. Such flexible material can be considerably deformed by the forces of the order of 1-10 N that may be applied during handling. The elastic modulus of the pharmaceutical material, however, is not only determined by the properties of the excipient. At a drug volume fraction of about 50% or higher, also the properties of the drug phase determine the properties of the composite to a large extent. As it is shown in chapter 6, the values of mechanical properties of such composite materials generally lie in between the volume-based arithmetic mean of the properties of the individual phases and the volume-based harmonic mean of the properties of the individual phases. For example, if the pharmaceutical material consists of 50% cellular PEG with an elastic modulus of 0.75 MPa and 50% aspirin with an elastic modulus of 7.5 GPa by volume, the elastic modulus of the composite is expected to be in the range 1.5 MPa – 3.75 GPa.

However, because the elasticity of the cellular excipient is reduced significantly compared with the bulk material, it may be appropriate to use an excipient that shows some ductility. Higher molecular weight PEGs or low molecular weight PEOs are good such candidate excipients.

References

[1] L.J. Gibson, M.F. Ashby, B.A. Harley, 2010, Cellular materials in nature and medicine, Cambridge University Press, Cambridge, UK.

APPENDIX B

THE EXPERIMENTAL SETUP

Figure B.1: Illustration of the injection-molding machine for preparation of injection-molded samples

This page is intentionally left blank.